Synchronisation for terrestrial mobile radio systems

Pulley, D. R.

Award date:
1993

Awarding institution:
University of Bath

SYNCHRONISATION FOR TERRESTRIAL MOBILE RADIO SYSTEMS

Submitted by

Douglas Roger Pulley

for the degree of Ph.D. of the University of Bath

1993.

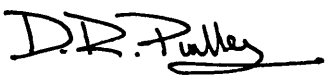

ProQuest LLC
789 East Eisenhower Parkway
P.O. Box 1346
Ann Arbor, MI 48106-1346

To my mother and father

Summary

The adverse effects of terrain and buildings on mobile radio propagation limit the extent and intensity of coverage of a single base station transmitter. Co-channel operation of multiple geographically-separated transmitters offers maximum spectral efficiency in covering large areas. However, areas of coverage overlap between transmitters suffer severe received distortion without costly matching in modulation and carrier frequency of each transmitter and thus coverage overlap must be kept to a minimum, particularly in the more distortion-prone frequency-modulated schemes. This thesis considers a novel approach to the accurate matching of the modulation and carrier frequency of remote F.M. transmitters in order that received distortion in due to coverage overlap is minimised. Coverage overlap can then be used to improve not only the extent, but also the intensity of coverage with the scheme - particularly important in the provision of hand-portable coverage in urban environments.

Digital transmission of the modulating audio to remote transmitters allows accurate matching of the signal delivered to each transmitter input. A novel all-digital modulation technique for the conversion of the digital samples to conventional frequency modulation is presented and the effects of pre-modulation sampling, quantisation and zero-order hold of the modulated phase are derived and quantified. Manufacturing variation in post-modulation filter characteristics results in co-channel distortion considerably less severe than that due to modulating signal misequalisation in conventional quasi-synchronous schemes. The modulator is implemented in an F.M. transmitter architecture which is entirely synchronous with a single reference input - the recovered clock of the digital audio transmission.

To determine phase lock and phase noise performance due to timing jitter in the recovered clock, a new, more realistic model for the accumulation of pattern-dependent jitter in repeatered P.C.M. lines is proposed that does not assume complete correlation of the jitter added at each repeater. The model is applicable to both bandpass and phase-lock timing extraction since both are shown to exhibit partial correlation of pattern-dependent jitter. The model is illustrated by reference to optical fibre repeaters employing surface acoustic wave filter timing extraction, though the principles apply to all forms of self-timed repeater chains. Direct calculation of jitter sequences is used to show the variation of jitter

correlation with the variation of repeater parameters and the spread of partial correlation coefficients in chains of repeaters with random spread parameters due to manufacturing tolerances. The partial correlation of pattern-dependent jitter provides a far better fit to published measurements than existing theory based on Chapman's model. Further still, the constraints on jitter peaking to avoid exponential jitter growth are tightened since partial correlation of pattern-jitter accelerates the runaway growth and will dominate over similar growth of noise-dependent jitter.

Using the model, the growth of transmitter output phase noise and phase-tracking errors due to accumulation of jitter is examined for synchronous transmitters phase-locked to a repeatered digital line. The relative carrier phase stability of transmitters locked to different points of the line that cover the same service area is determined to gauge residual carrier interference effects. It is demonstrated that both the lock performance of the transmitters and the relative carrier phase stability of the transmitters is adequate for the proposed scheme when using 2.048Mbit digital transmission lines, but that the transmitter lock performance is the limiting factor that prohibits use of lower bit rates such as 192kbit standard lines.

Acknowledgements

The author would like to express thanks to Dr. R.J. Holbeche for his supervision of this project.

The author would also like to thank the Science and Engineering Research Council and Vodafone Ltd. for their financial support which made this work possible.

Contents

Chapter 1: Introduction

1.1. Usage of Mobile Radio 1-1
1.2. The Land Mobile Radio Environment 1-1
1.3. Area Coverage Schemes 1-3
1.4. References 1-5

Chapter 2: Synchronous Area Coverage

2.1. Introduction 2-1
2.2. Mobile reception in a single transmitter field 2-1
2.3. A brief review of frequency modulation and its reception 2-4
2.4. Mobile reception in a multi-transmitter field 2-7
2.5. Distortion of demodulated signal in a multi-transmitter field 2-10
2.7. Reduction of F.M. Threshold Noise 2-17
2.8. Conclusions 2-20
2.9. References 2-22

Chapter 3: Precise Phase Modulation

3.1. Introduction 3-1
3.2. Conventional generation of angle modulation 3-1
3.3. Audio preprocessing for indirect F.M. 3-4
3.4. The Precise Phase Modulator 3-6
3.5. A theoretical model of the Precise Phase Modulator 3-10
3.6. Spectral effects due to zero-order hold of phase 3-12
3.7. In-band distortion due to multi-component carrier 3-25
3.8. Constraints on modulator sampling frequency 3-27
3.9. Baseband distortion due to zero-order hold 3-38
3.10. Distortion due to phase quantisation 3-44
3.11. Distortion due to variation in transmitter characteristics 3-54
3.12. Conclusions 3-66
3.13. References 3-70

Chapter 4: A synchronous F.M. transmitter

4.1. Introduction 4-1
4.2. Synchronous transmitter architecture 4-3
4.3. Prototype transmitter 4-7
4.4. Control site processing 4-7
4.5. Precise phase modulator 4-10
4.6. The spectral output of the prototype modulator 4-11
4.7. Measurement of modulator constant 4-13
4.8. Frequency translation and I.F. R.F. alias filtering 4-15
4.9. Transmitter audio response 4-16
4.10. Transmitter linearity 4-18
4.11. Frequency synthesis 4-19
4.12. Synthesized frequency stability 4-21
4.13. Audio delay equalisation 4-22
4.14. Transmitter phase noise model 4-23
4.15. Conclusions 4-28
4.16. References 4-28

Chapter 5: Transmitter Synchronisation

5.1. Introduction 5-1
5.2. Baseband digital transmission 5-1
5.3. P.C.M. reception 5-3
5.4. Line coding 5-5
5.5. Jitter in timing extraction 5-7
5.5.1. Timing extraction 5-7
5.5.2. Timing recovery filters 5-9
5.5.3. Jitter calculation 5-12
5.5.4. Jitter power spectral density 5-17
5.6. Accumulation of jitter in a chain of repeaters 5-23
5.6.1. A model for jitter accumulation 5-23
5.6.2. Jitter transfer functions 5-26
5.7. Partial accumulation of jitter 5-33
5.7.1. A partial correlation model of jitter accumulation 5-33

5.7.2. Determination of correlation coefficient in bandpass extraction 5-38

5.7.3. Variation of correlation coefficient with parameter variation in SAW filter timing extraction 5-40

5.7.4. Correlation of pattern-dependent jitter in PLL timing extraction 5-45

5.8. Effects of partial correlation of on pattern-dependent jitter accumulation 5-49

5.9. Effects of accumulating jitter on synchronous transmitters and coverage scheme performance 5-59

5.10. Conclusions 5-64

5.11. References 5-68

Chapter 6: Conclusions 6-1

Appendix A:

Calculation of distortion in the output of an ideal F.M. receiver by Fast Fourier Transform

A.1 Determination of Received Phase A-1

A.2 Audio distortion factor and the Discrete Fourier Transform A-3

A.3 Implementation of D.F.T. distortion analysis A-8

A.4 References A-10

Appendix B:

Circuit diagrams

Appendix C:

The Bessel function

Chapter 1:
Introduction

1.1. Usage of Mobile Radio

Historically, most radio schemes have tended to consist of a single base station and a number of mobile and/or portable equipments. This is particularly true of public sector emergency services such as the Police, Fire and Ambulance and increasingly true of utility organisations such as the regional Gas, Water and the Electricity boards. These organisations generally require radio coverage over large geographical areas containing regions of difficult terrain and built-up areas.

In a great many of these cases, the required coverage must be good enough to give reliable, high quality communications for U.H.F. hand portable equipments in the middle of built-up areas. This is a technically demanding requirement compounded by the great pressure on the available radio spectrum that leaves the various authorities with very few radio channels allocated to them. Thus there exists a great need for area coverage systems that provide this level of radio coverage in the most spectrally efficient manner.

1.2. The Land Mobile Radio Environment

Land Mobile Radio (L.M.R.) is arguably the most demanding environment in telecommunications. The technical problems posed by radio wave propagation over a huge diversity of terrains are compounded by the demands of a rapidly increasing number of users for reliable, high quality communication between mobile stations. The propagation of radio waves in L.M.R. gives rise to two types of degradation in the received signal strength. First, the propagation of waves over terrain obstacles such as hills and buildings results in considerable path losses due to diffraction and absorption effects. A number of propagation models

for the prediction of these losses for known terrain have been developed over the years such as those put forward by Edwards and Durkin [1], Egli [2] and Okumura [3]. These models vary in suitability depending on the frequency of operation and radio link range.

The other main degradation of the received signal strength results from the multipath transmission to the mobile station. In an urban environment, for example, the line-of-sight propagation path between the transmitter and receiver is usually shadowed by surrounding buildings and obstacles. Thus, radio waves arrive at the mobile via many indirect paths, each path resulting from reflection or diffraction around the terrain. The waves combine to set a spatially-fluctuating standing-wave field or diffraction pattern due to differences in the transmission path length of the received signals. Hence, as the mobile moves through the resulting field pattern, it will experience random fluctuations in the received signal strength or "fades".

Fades of up to 20dB in depth are common and deeper fades in excess of 30dB are not uncommon. Ossana [4] first offered a model to explain this phenomenon which works well for rural and suburban areas. Clarke [5] subsequently proposed a scattering model more applicable to urban areas and considerable effort has been applied in the modelling of multipath reception in urban areas since. Both the effects described are more prevalent at V.H.F. and U.H.F. frequencies where most L.M.R. frequencies have been allocated under the pressure of the increasing number of users and the subsequent demand for radio bandwidth to accommodate them.

Taking the propagation aspects into account, it is clear that to provide a reliable, high quality L.M.R. scheme, a certain minimum level for the line-of-sight received signal strength is required, which must be maintained over the entire coverage area of the scheme.

1.3. Area Coverage Schemes

The propagation models mentioned above allow a radio scheme designer to predict with varying degrees of accuracy the area covered by a single base station transmitter at a known site over known terrain. Area coverage is largely a function of transmitter power, antenna efficiency and transmitter siting (particularly height relative to the surrounding terrain). Broadly speaking, as each of these parameters are increased, the line-of-sight received signal strength at any point is increased and thus the size of area covered is also increased.

However, improving radio scheme coverage is not purely a matter of increasing peak range. Over hilly terrain, ensuring a minimum level of received signal strength over the entire area is a far greater problem. Also, it may be desirable to extend coverage in one direction in preference to another, to allow the re-use of a frequency in a neighbouring county, for example. Indiscriminate increase in transmitter power is not the solution in these cases and careful tailoring of antenna radiation patterns to suit the terrain may give better results. However, there is clearly a limit to the ability of a single transmitter to cover a large, hilly area without leaving "pockets" of poor coverage by varying these parameters of a single base station.

Brinkley [6] first proposed schemes using a number of base station transmitters to improve coverage. Transmitters are sited so that all parts of the required coverage area are covered to the minimum required received signal strength by at least one of them. Gosling [7] draws the distinction between two types of area coverage. Those schemes intended to increase the extent of coverage only are configured such that individual transmitter coverage overlap is minimised. The signal strength in the total coverage area will be statistically distributed in a manner similar to that within the service area of a single transmitter. These are referred to as *extensive* area coverage schemes, where the variance of the

received signal strength is not significantly less than that from a single transmitter.

The other type of scheme is referred to as *intensive* area coverage where satisfactory signals are received in areas of individual transmitter coverage overlap. In these overlap areas the variance of the received signal strength from two or more transmitters can be much less than that from a single transmitter.

Multi-transmitter schemes can be operated as either multi-channel or co-channel systems. In multi-channel schemes, each base station radiates on a different frequency, but uses the same modulation. These schemes suffer from two fundamental drawbacks. Firstly, as the mobile moves through the coverage area, it must monitor the signal strength on each channel in order to select the strongest signal making radio operation very cumbersome to the untrained user and secondly, the use of a number of radio channels to cover one area with one modulation is highly wasteful in radio spectrum.

Co-channel schemes overcome these two difficulties. If the transmitters all operate on the same frequency, the spectral requirement is much less and the need for frequent channel changing by the mobile is eliminated. However, if more than one transmitter radiates at any one time, the received signal in areas of coverage overlap between two base stations will be a combination of the two and will result in interference effects. These will be considered later.

Basic co-channel systems ensure that only one transmitter radiates at any one time. To achieve this, the system operator needs to know the location of the mobile in order to select which base station to use. This requires some form of selective calling and return path assessment in the system in order that each base station may selectively call the mobile in turn and from the signal strength of the mobile's reply gauge which base station to use. The complexity of the system and its operation limits its usefulness to little more than message

handling systems.

Co-channel systems with continuous transmission by all base stations is clearly desirable as it would eliminate the need to know the position of the mobile and channel changing would not be necessary. However, in coverage overlap areas, the resulting signal from two carriers will beat at a frequency equal to the difference in actual carrier frequencies.

Early Police A.M. schemes [8] used spaced carrier such that the beat frequency was greater than the upper audio limit of the receiver response. This resulted in a large channel bandwidth with three carrier schemes operating on 50kHz channel spacing systems. The alternative to this is to try and match the carrier frequencies so that any beating is at a low (sub-audible) frequency. Such a "quasi-synchronous" system can thus operate in the channel spacing of the original single base station system and allows both the extent and the quality of area coverage to be enhanced over that of a single transmitter. This type of system, although it maximises spectral utilisation, poses a range of technical difficulties to overcome. These are discussed in the next chapter.

1.4. References

[1] Edwards R., Durkin J., "*Computer prediction of service areas for V.H.F. mobile radio networks*" Proc. I.E.E. 1969, Vol. 116, No. 9, pp 1493-1500.

[2] Egli J.J., "*Radio propagation above 40Mc over irregular terrain*" Proc. I.R.E. 1957, pp 1383-1391.

[3] Okumura Y., Ohmori E., Kawano T., Fuduka K., "*Field strength and its variability in V.H.F. and U.H.F. land mobile service*" Rev. Elec. Commun. Lab., 1968, Vol. 16, pp 825-873.

[4] Ossana J.F., "*A model for mobile radio fading due to building reflections:*

Theoretical and experimental fading waveform power spectra" Bell Sys. Tech. Journ. Nov. 1964, Vol. 43, pp 2935-2971.

[5] Clarke R.H., "*A statistical theory of mobile radio reception*" Bell Sys. Tech. Journ. July-August 1968, Vol. 47, pp 957-1000.

[6] Brinkley J.R., "*A method of increasing the range of V.H.F. communication systems by multi-carrier amplitude modulation*" J.I.E.E. 1946, Vol. 93, Part III, pp 159-166.

[7] Gosling W., Petrovic V., "*Area coverage in mobile radio by quasi-synchronous transmissions using double-sideband diminished carrier modulation*" Proc. I.E.E., 1973, Vol. 120, No. 12, pp 1469-1476.

[8] Holbeche R.J., (Ed.), "*Land Mobile Radio Systems*", I.E.E. Telecommunications Series, Vol. 14, Peter Peregrinus Ltd., ISBN 0-86341-049-9, 1985.

Chapter 2:
Synchronous Area Coverage

2.1. Introduction

As discussed in chapter 1, a single transmitter is often unable to provide adequate coverage of a desired mobile radio scheme service area both in terms of the area covered and the quality and consistency of coverage within that area. The use of transmitter diversity to improve the extent and intensity of coverage within a scheme has optimum spectral efficiency when the geographically separated transmitters are co-channel operated. This chapter examines the difficulties in co-channel operation of such transmitters with particular reference to frequency modulated schemes whose performance is more sensitive to system parameters than amplitude modulated schemes. Specifically, the advantages of a fully synchronous F.M. scheme are considered over the conventional quasi-synchronous schemes.

2.2. Mobile reception in a single transmitter field

In order to discuss the potential advantages of a synchronous area coverage scheme and the technical requirements to achieve them, a brief review of the characteristics of mobile reception is necessary. If a modulated carrier signal is transmitted at a frequency f_o, then the radiated electric field $E_z(t)$ may be written as:

$$E_z(t) = E_o A(t) e^{j[2\pi f_o t + \varphi(t)]} \qquad (2.1)$$

where $A(t)$ is the amplitude modulation and $\varphi(t)$ the phase modulation of the signal (E_o is the amplitude of the unmodulated carrier). Thus $E_z(t)$ could be any form of modulated signal. For a stationary receiver, the field experienced will generally be the sum of a number of delayed and attenuated waves. Depending

on the terrain between the transmitter and the mobile receiver and the environment in which both are sited, there may be a line-of-sight wave considerably stronger than the other components. However, for many portable and mobile situations of interest this is unlikely. The field at the mobile $E_m(t)$ with N incident component waves is:

$$E_m(t) = \alpha \sum_{i=1}^{N} a_i E_z(t - \tau_i) \qquad (2.2)$$

where a_i and τ_i are the attenuation and propagation delay of the i^{th} component and α is the overall propagation loss and is less than unity. The total power of the components is normalised to the power of the transmitted wave i.e.:

$$\sum_{i=1}^{N} a_i^2 = 1 \qquad (2.3)$$

The time delays τ_i will be spread around a mean value of delay $\bar{\tau}$, where:

$$\bar{\tau} = \frac{1}{N} \sum_{i=1}^{N} \tau_i \qquad (2.4)$$

and so $\bar{\tau}$ is purely a shift in time reference for $E_m(t)$ and can be neglected. However, the spread of τ_i about $\bar{\tau}$ is important and is highly dependent on the propagation environment with typical figures of *0.1* to *10*μs [1]. In narrowband radio schemes, $A(t)$ and $\varphi(t)$ are generally lowpass processes with maximum frequency components considerably smaller than the reciprocal of delay spread, so the effect of delay spread on them is negligible, i.e.:

$$A(t - \delta\tau_i) = A(t), \quad \varphi(t - \delta\tau_i) = \varphi(t) \qquad \textit{for all } i \qquad (2.5)$$

where:

$$\delta\tau_i = \tau_i - \bar{\tau} \qquad (2.6)$$

and so the field at the stationary receiver is:

$$E_m(t) = \alpha A(t) e^{j[2\pi f_o t + \varphi(t)]} \sum_{i=1}^{N} a_i e^{j2\pi f_o \delta\tau_i} \qquad (2.7)$$

The angle $2\pi f_o \delta\tau_i$ due to the spread in propagation delay is uniformly distributed from 0 to 2π radians providing the carrier period is significantly smaller than the delay spread (certainly valid at mobile radio frequency allocations at V.H.F. and above). The summation is equivalent to a time in-variant complex quantity with amplitude and phase that modifies the received signal, but does not affect the demodulated signal (providing there is no excessive overall propagation loss).

Extending this to the case of the mobile receiver moving at a velocity v, each incident wave will receive an apparent frequency offset by virtue of the Doppler effect [1]. The magnitude will depend on the direction of motion relative to the incoming direction of the incident wave. The theory developed can be modified to take account of this by including an extra phase term with the i^{th} component wave of $\beta v t \cos\Phi_i$, where Φ_i is the angle of wave arrival of the i^{th} component wave and β is given in terms of the wavelength of the transmitted signal λ_o as:

$$\beta = \frac{2\pi}{\lambda_o} \qquad (2.8)$$

The effective time-shift that Doppler causes is negligible at the speeds of interest for the modulation processes $A(t)$ and $\varphi(t)$. Thus the field at the mobile receiver is:

$$E_m(t) = \alpha A(t) e^{j[2\pi f_o t + \varphi(t)]} \sum_{i=1}^{N} a_i e^{j[2\pi f_o \delta\tau_i + \beta v t \cos\Phi_i]} \qquad (2.9)$$

The summation of N complex vectors can be represented as a single complex envelope applied to the modulated signal $R(t)e^{j\Psi(t)}$. The amplitude (and thus instantaneous signal strength) $R(t)$ is Rayleigh distributed [1] provided N is large enough (it has been shown that if $N>6$ then the distribution conforms very closely to Rayleigh [12]) and is characterised by its mean and variance. This gives the quality of the received signal since the noise at the receiver can be assumed locally constant (neglecting other forms of interference) and hence the mean and variance of the received signal-to-noise ratio are directly related. The

most important characteristic that the field exhibits is the rapid fluctuations in signal strength as the mobile passes through it. The succession of signal strength troughs or "fading" that the receiver experiences results in rapid fluctuations in the instantaneous signal-to-noise ratio. The severity of fading can be qualified by the "fading rate", i.e. the number of times per second that the receiver experiences the field dropping by more than 20dB (say) below its local mean value.

The phase of the random complex envelope $\Psi(t)$ is referred to by its time derivative $\dot{\Psi}(t)$ known as *random F.M.* This is a lowpass process whose power spectral density has a cut-off frequency at twice the maximum Doppler shift of any incident wave [1]. At speeds of up to 60mph at U.H.F. frequencies this is still sufficiently below the lower audio cut-off of 300Hz used in most narrowband mobile radio receivers to not significantly affect the demodulated signal. The precise effects of $R(t)$ and $\Psi(t)$ on the demodulated signal depend on the mode of modulation used so the next section reviews F.M. reception.

2.3. A brief review of frequency modulation and its reception

In order to discuss the distortion mechanisms critical to the performance of an area coverage scheme, it is necessary to briefly review basic concepts behind the modulation mode of interest and its reception. This thesis is primarily concerned with frequency modulation though its results and conclusions can be extended to all forms of angle modulation both analogue and digital.

The general form of an angle modulated signal $e(t)$ is:

$$e(t) = E_o \cos(2\pi f_o t + \varphi(t)) \qquad (2.10)$$

where f_o is the carrier frequency, E_o the constant carrier amplitude and $\varphi(t)$ the phase variation caused by the modulating signal $m(t)$. In the case of F.M. the time differential of the carrier phase $\varphi(t)$, is directly proportional to the

modulating signal $m(t)$, and if $|m(t)| \leq 1$ then:

$$\dot{\varphi}(t) = 2\pi\Delta f m(t) \qquad (2.11)$$

where the constant of proportionality is $2\pi\Delta f$, and Δf is the maximum frequency deviation. Thus for the simple case of a sinusoidal modulating signal of frequency f_m, i.e.:

$$m(t) = \cos 2\pi f_m t \qquad (2.12)$$

then:

$$e_{fm}(t) = E_o \cos(2\pi f_o t + \frac{\Delta f}{f_m} \sin 2\pi f_m t) \qquad (2.13)$$

The maximum phase deviation of the carrier is known as the modulation index β, where:

$$\beta = \frac{\Delta f}{f_m} \qquad (2.14)$$

Methods of generating F.M. are considered in the next chapter, but its reception is briefly described here. Figure 2.1 shows the form of a basic F.M. receiver from the intermediate frequency (I.F.) stage.

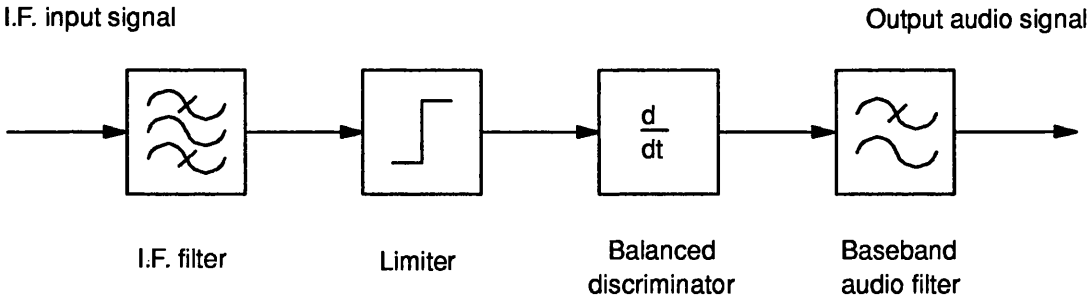

Figure 2.1: *Basic features of a simple F.M. receiver*

To arrive at the I.F. stage of the receiver, the signal will have been subject to a number of amplification, mixing and filtering processes. The stages shown in the block diagram are those most important to the demodulation of the signal. The I.F. filter provides the receiver selectivity and hence its demodulation equivalent

noise bandwidth. This bandwidth depends on the bandwidth of the modulated signal which is discussed in the next chapter. The hard-limiter attempts to remove all amplitude variations caused by the transmission of the signal: both fading and area coverage scheme effects to be discussed later. The balanced discriminator effectively differentiates the signal and envelope detects the audio prior to baseband lowpass filtering to remove out-of-band components.

A full treatment of the noise performance of the F.M. discriminator receiver is given in [1], but the essential features are shown in the graph of output audio signal-to-noise ratio (SNR) against I.F. carrier-to-noise ratio (CNR). An F.M. signal of modulation index β will show an improvement in output SNR over ideal coherent demodulation of amplitude (linear) modulation for the same I.F. carrier-to-noise ratio. As β is increased so is this improvement and thus the reduction of receiver output noise for the same I.F. CNR.

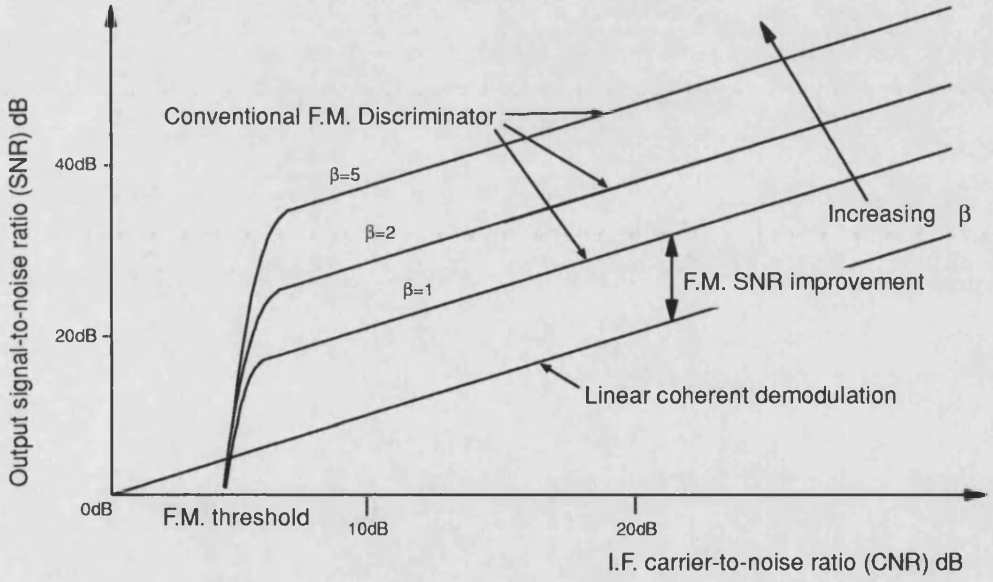

Figure 2.2: *Graph of Output SNR against I.F. CNR of an F.M. receiver*

However, this improvement is only maintained for high CNR. It is found experimentally that as the I.F. CNR is reduced, the output audio begins to deteriorate. At first individual clicks are heard and as the CNR is reduced

further, the clicks rapidly merge into a crackling noise. Near this point of breakdown, theoretical predictions of output SNR begin to considerably overestimate the actual SNR. This is known as the *Threshold effect* and the *threshold* is defined as the minimum CNR at which the F.M. SNR improvement is not significantly less than that for higher CNR (approx. 9dB CNR). As the I.F. CNR reduces further, the output SNR degrades rapidly until the noise eventually "captures" the receiver in much the same way that the signal captures the receiver for high carrier-to-noise ratios. This contrasts with the more gentle degradation of linear modulation systems and the high level of output noise from an F.M. receiver at low CNR is considerably more distracting than that for an A.M. receiver.

2.4. Mobile reception in a multi-transmitter field

As discussed in the introduction to this thesis, co-channel operation of a number of base station transmitters is a spectrally efficient way of extending and/or intensifying the coverage area of a mobile radio scheme. Historically, such schemes have been designed to extend coverage and avoid areas of coverage overlap between transmitters, since considerable distortion was experienced in these areas. The primary objective of a synchronous area coverage scheme is to minimise this distortion so that a number of transmitters can radiate over a common area with improvement in the quality of coverage. To examine this distortion the field at a mobile receiver due to a number of transmitters will be considered. Gosling [2] has shown that when assessing multi-transmitter fields, analysis of the two transmitter case is sufficient. This is because the effects of a multi-transmitter field on the received signal are most prominent when the signals received from each transmitter are of similar strength: a situation that will be rare for three or more transmitters. The two station case is a useful guide to the three station case where theoretical analysis becomes highly complex.

For the case of two base station transmitters, the field at the mobile receiver is the sum of the fields due to each transmitter:

$$E_m(t) = E_{mA}(t) + E_{mB}(t) \qquad (2.15)$$

where:

$$E_{mA}(t) = \alpha_A E_o e^{j[2\pi f_{oA}t + \varphi_A(t)]} \sum_{k=1}^{N_A} a_{kA} e^{j[2\pi f_{oA}\delta\tau_{kA} + \beta_A vt\cos\Phi_{kA}]} \qquad (2.16)$$

and:

$$E_{mB}(t) = \alpha_B E_o e^{j[2\pi f_{oB}t + \varphi_B(t)]} \sum_{i=1}^{N_B} a_{iB} e^{j[2\pi f_{oB}\delta\tau_{iB} + \beta_B vt\cos\Phi_{iB}]} \qquad (2.17)$$

For simplification, the amplitude modulation has been dropped since angle modulation is the subject of this thesis, although a similar analysis can be performed for linear modulation modes [5]. If the complex fading envelopes of transmitters A and B are $R_A(t)e^{j\Psi_A(t)}$ and $R_B(t)e^{j\Psi_B(t)}$ respectively, and if the carrier frequencies and angle modulations are identical (f_o and $\varphi(t)$ respectively) then:

$$E_m(t) = E_o e^{j[2\pi f_o t + \varphi(t)]}\left\{\alpha_A R_A(t)e^{j\Psi_A(t)} + \alpha_B R_B(t)e^{j\Psi_B(t)}\right\} \qquad (2.18)$$

By their very nature, the fading envelopes from the two transmitters are independent and consequently the probability of a simultaneous fade in both paths is extremely remote as demonstrated in figure 2.3. It can be seen that the variance of the field is considerably reduced and the local mean signal strength is increased providing identical signals are radiated from each transmitter. However, this is practically impossible to achieve with geographically separated transmitters and in general the signals radiated from each transmitter will differ in output carrier frequency and modulation. A characteristic of F.M. reception is that in the presence of two signals, the stronger of the signals will dominate the receiver and suppress the weaker providing it is only a few dB greater [1].

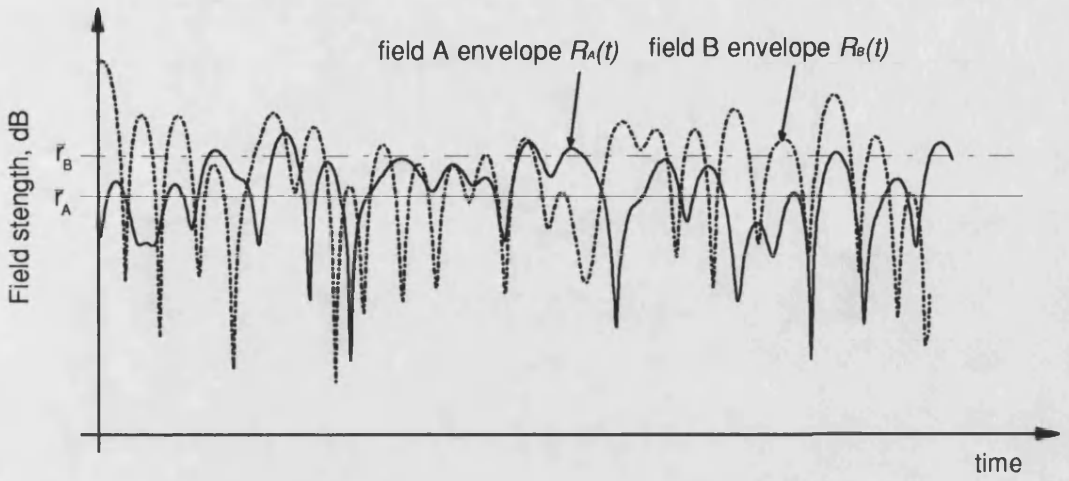

Figure 2.3: *Uncorrelated fading signals*

This *capture effect* would indicate that the receiver would naturally switch from receiving the signal from one transmitter to the other as the relative instantaneous signal strengths vary. However, the degree of capture is dictated by the modulation index and what little capture effect that exists in low deviation narrowband F.M. schemes is insufficient for the receiver to be captured by one or other transmitter for a wide range of similar signal strengths. In these circumstances the receiver responds to the sum of the received signals.

From figure 2.3 it can be deduced for a range of similar relative mean signal strengths $\bar{r}_A$, $\bar{r}_B$ that for a significant proportion of the time the mobile receiver experiences very similar instantaneous signal strengths from the two transmitters. The areas of the service area where this may occur is not limited to areas of coverage overlap equidistant for both transmitters and the immediate vicinity. It can be shown [2] that in a mobile radio environment even with a 3:1 difference in range in the two transmitters (a 10dB median nominal difference in signal strength) signals differ by less than 2dB for nearly 10% of the time and by 4dB for nearly 20% of the time. For correct operation of an intensive area coverage scheme, the reception performance in the presence of nearly equal

signal strengths in critical. If the complex fading envelopes of the two fields shown in figure 2.3 are assumed to vary slower than the modulating signal processes of the radiated signals then the two transmitter field for two arbitrary radiated F.M. signals is:

$$E_m(t) = r_A e^{j[2\pi f_{oA}t+\varphi_A(t)+\psi_A]} + r_B e^{j[2\pi f_{oB}t+\varphi_B(t)+\psi_B]} \qquad (2.19)$$

where r_A and r_B are the respective field strengths and ψ_A and ψ_B the phase shifts. This assumption is not always valid, but necessary to show the distortion mechanisms at work. The above equation can be rewritten as a single vector:

$$E_m(t) = r_m(t)e^{j\theta_m(t)} \qquad (2.20)$$

where the instantaneous envelope $r_m(t)$ is given by:

$$r_m(t) = r_A\sqrt{1+k^2+2k\cos\delta\theta(t)} \qquad (2.21)$$

and the instantaneous phase $\theta_m(t)$ is given by:

$$\theta_m(t) = 2\pi f_{oA}t + \varphi_A(t) + \psi_A + \tan^{-1}\left\{\frac{k\sin\delta\theta(t)}{1+k\cos\delta\theta(t)}\right\} \qquad (2.22)$$

where k is the ratio of the signal strengths due to each transmitter, i.e.:

$$k = \frac{r_B}{r_A} \qquad (2.23)$$

and $\delta\theta(t)$ the instantaneous phase difference is:

$$\delta\theta(t) = 2\pi(f_{oB}-f_{oA})t + \varphi_B(t) - \varphi_A(t) + \psi_B - \psi_A \qquad (2.24)$$

2.5. Distortion of demodulated signal in a multi-transmitter field

The additional time-variation of instantaneous envelope and phase implied above (beyond that due to modulation or conventional fading) will cause additional distortion in reception and demodulation. Taking the envelope $r_m(t)$ first, the fluctuation of the envelope below the threshold level γ, will cause an intolerable increase in the noise output of an F.M. receiver as previously discussed. In short

the following condition must be avoided (suitably scaling γ with reference to r_A):

$$\sqrt{1+k^2+2k\cos\delta\theta(t)} \leq \gamma \qquad (2.25)$$

Figure 2.4 shows the normalised depth of fade that may result from relative signal strengths of up to 2dB. Thus significant depth of fade can result from relative field strengths of up to ±2dB and hence significant time-varying phase $\delta\theta(t)$ can cause significant threshold noise beyond that due to conventional fading.

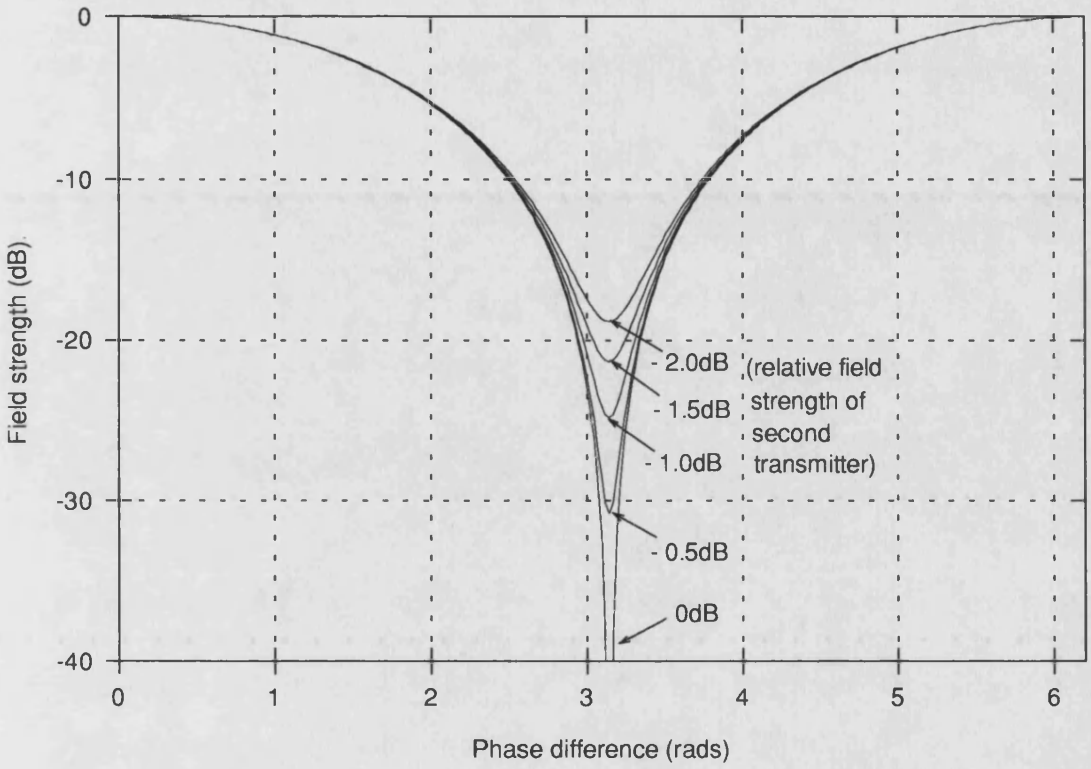

Figure 2.4: *Depth of fade produced from a two-transmitter field*

Examination of equation 2.24 shows that this can result if there is frequency offset between transmitter carrier frequencies (phase offsets are of no consequence) or time-varying difference in the modulation of each transmitter. Both this threshold-related distortion and the distortion terms of the received phase are functions of the time-varying component of the instantaneous phase difference between the transmitted signals. This results from carrier frequency

offset and modulation mismatch. The fundamental objective of an area coverage system is to radiate one modulating signal over a wide area. The modulating signal must be conveyed in some manner from its point of generation to each transmitter site. Traditionally, this has been done by analogue landlines (as first suggested by Brinkley [4]). For the type of communications that area coverage schemes have been used for, the audio quality of conventional telephone bandwidth speech is sufficient. Thus the audio modulating signal is bandlimited to *300Hz-3.4kHz* at source.

From the expressions for the field at the mobile, variation in the amplitude and phase of the modulating signal at each transmitter after transmission from the control site will result in distortion, whether amplitude or angle modulation is employed. Even if the transmitters all behave identically, they will only radiate the same signal if the same modulating signal is presented at the input to each transmitter. If the modulating signal is $g(t)$ at source and the landline (or other medium) has a transmission characteristic $H(f)$, then the input to the transmitter at site $m(t)$ is given by:

$$m(t) = \boldsymbol{F}^{-1}\{\boldsymbol{F}\{g(t)\}H(f)\} \qquad (2.26)$$

where $\boldsymbol{F}$ denotes the Fourier transform and $\boldsymbol{F}^{-1}$ its inverse. The inputs to each transmitter will only be identical if the transmission characteristics of the lines between each transmitter and the source of the modulating signal $H(f)$, are the same. The transmission characteristic may distort the modulating signal, but no further distortion will result at the mobile receiver from synchronous or quasi-synchronous operation if the transmission characteristics of all lines are equalised. In practice, the matching of analogue lines is a complicated and time consuming process and cannot be achieved and maintained exactly [6]. Instead of exact matching, the lines are equalised to within set tolerances as shown in figure 2.5. The amplitude and delay tolerances of the system are determined by

the maximum tolerable distortion that misequalisation may produce. The degree of equalisation required depends on whether amplitude or angle modulation is used, since different distortion mechanisms result in the reception of the field.

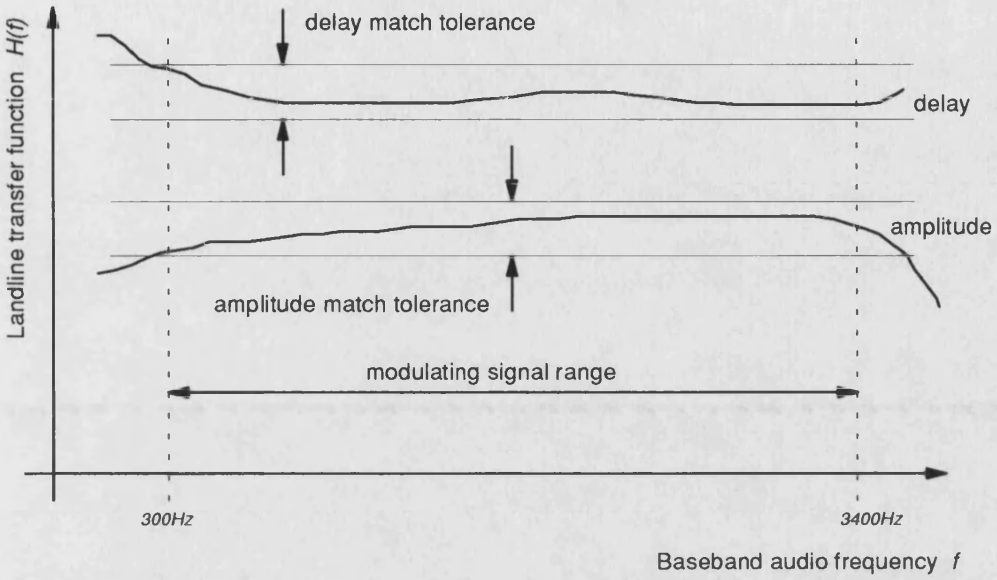

Figure 2.5: *Audio path matching for area coverage schemes*

Returning to threshold-related distortion, the effect of carrier frequency offset is simply to add a phase ramp to the instantaneous phase difference term so that phase difference passes through π radians (and odd multiple thereof) at the frequency of the offset. This 'beating' results in noise bursts from the receiver at the offset frequency with significant degradation of the received audio. This is particularly distracting if at the offset is around 7Hz since this is the syllabic rate of speech and can render the speech unintelligible [7]. Carrier offsets of less than 5Hz are thus highly desirable with respect to this distortion mechanism. The effects of modulation mismatch were considered in terms of a sinusoidal modulating signal. The threshold-related distortion effects of modulation equalisation (due to amplitude and delay mismatch in the audio path to one transmitter relative to the other) was considered by calculating the onset of nulls in the resultant signal in terms of the mismatched modulating audio parameter

at various frequency deviations. Figures 2.6 and 2.7 show contours of the onset of carrier zeroes for a range of audio frequencies (as marked) at equal field strengths.

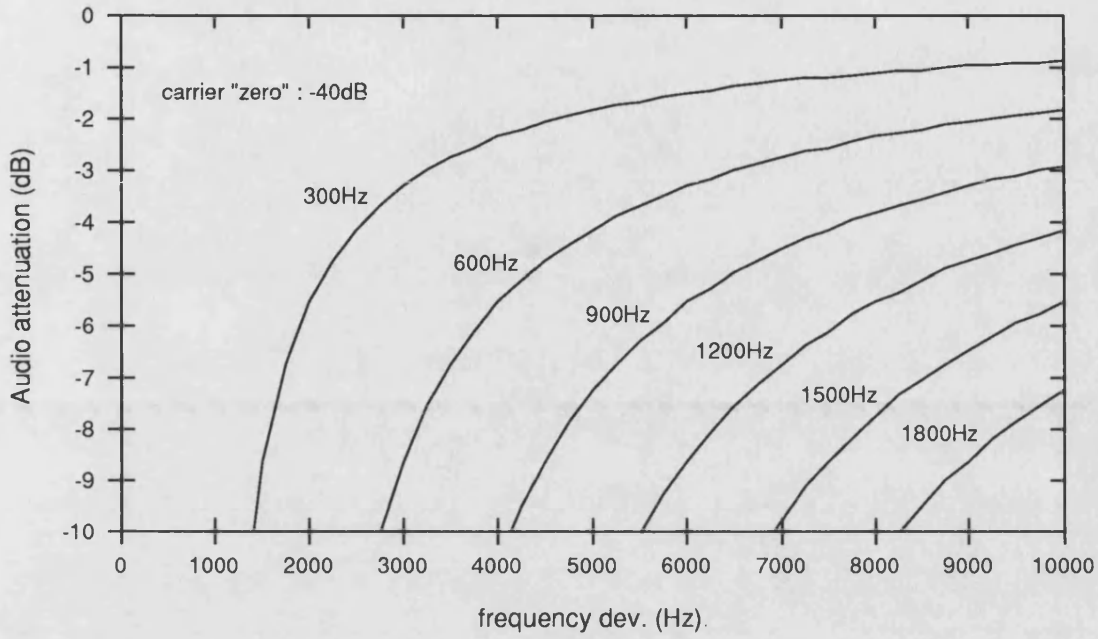

Figure 2.6: *Minimum audio path attenuation resulting in carrier nulls*

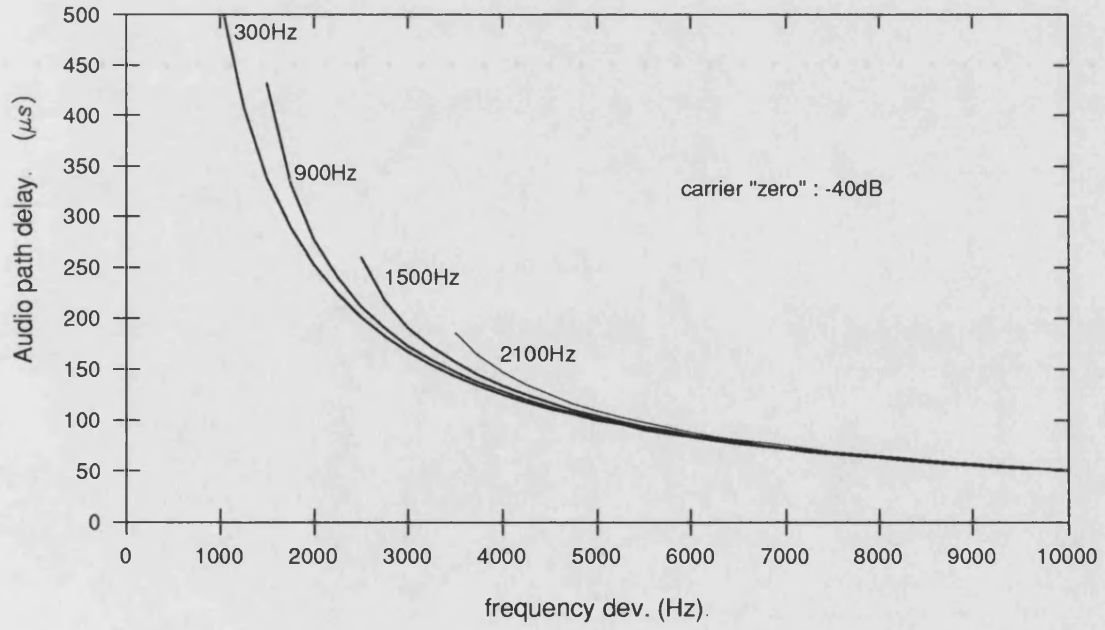

Figure 2.7: *Minimum audio path delay resulting in carrier nulls*

For the purposes of this calculation a carrier null was taken as occurring if the instantaneous resultant field amplitude dipped below -40dB relative to the field of a single transmitter. As can be seen from the two graphs, the lower frequency components are more sensitive to audio path misequalisation in both amplitude and delay. This is significant since in speech signals, most energy is concentrated below 1kHz. For both amplitude and delay, at low deviation the difference between different audio frequencies is most marked with convergence in behaviour as deviation increases. Of greatest interest are the figures for the most commonly used land mobile radio standards: 12.5kHz and 25kHz channel spacing with 2.5kHz and 5kHz deviation respectively. Taking the worst case for both (i.e. 300Hz audio frequency), at 2.5kHz deviation, the onset of threshold-related distortion is at an attenuation of 3.5dB and delay of around 200μs and at 5kHz deviation, an attenuation of 2dB and delay of around 100μs. These figures correlate well with reported figures as discussed later in this chapter. Outside these tolerances, modulation-correlated noise will significantly degrade the received signal.

The other distortion mechanism in the demodulated signal is due to the additional phase terms in the received phase. An F.M. receiver responds to the time differential of the received phase, i.e. $\dot{\theta}_m(t)$ the instantaneous frequency. If $e_{af}(t)$ is the audio output from an ideal receiver with a demodulation constant of $1Vs/rad$ then:

$$e_{af}(t) = 2\pi f_{oA} + \dot{\varphi}_A(t) + \frac{d}{dt}\left\{\tan^{-1}\left(\frac{k\sin\delta\theta(t)}{1+k\cos\delta\theta(t)}\right)\right\} \qquad (2.27)$$

The first term is constant and can be neglected. The second term is the modulating signal of transmitter A as required. The third term is a distortion. Using the identity:

$$\frac{d}{dt}\left\{\tan^{-1}\left(\frac{\alpha}{\beta}\right)\right\}=\frac{\dot{\alpha}\beta-\alpha\dot{\beta}}{\alpha^2+\beta^2} \qquad (2.28)$$

then the distortion term can be shown to be:

$$\frac{d}{dt}\left\{\tan^{-1}\left(\frac{k\sin\delta\theta(t)}{1+k\cos\delta\theta(t)}\right)\right\}=\delta\dot{\theta}(t)\left(\frac{k^2+k\cos\delta\theta(t)}{1+k^2+2k\cos\delta\theta(t)}\right) \qquad (2.29)$$

Thus the removal of time varying components from $\delta\theta(t)$ removes the distortion component. Again this is only possible if there is no frequency offset between transmitter carrier frequencies (phase offsets are of no consequence) and no time varying difference in the modulation of each transmitter. From tables [11] the following identity can be used to express the distortion term as a Fourier series in order to evaluate the distortion in the received signal:

$$1+\sum_{n=1}^{\infty}(-k)^n\cos n\phi=\frac{1+k\cos\phi}{1+k^2+2k\cos\phi} \qquad (k<1) \qquad (2.30)$$

and thus the distortion term is the following Fourier series of the instantaneous phase difference $\delta\theta(t)$:

$$\delta\dot{\theta}(t)\sum_{n=1}^{\infty}(-k)^n\cos n\delta\theta(t) \qquad (2.31)$$

The general expression may be simplified to that of the particular case considered by Al-Nuaimi [7] of sinusoidal modulation via a more involved route. His analysis of the harmonic distortion in the simple sinusoidal case yields a number of conclusions. In contrast with an A.M. quasi-synchronous system [5], the harmonic distortion is significantly reduced when there is at least 3dB difference in the two carrier levels. However for smaller differences the harmonic distortion is much greater. This is borne out in practice with the results of simulated bench tests for speech intelligibility carried out by Al-Nuaimi. A maximum value of audio delay difference of 200μs and 2Hz maximum carrier offset are recommended for good quality speech in areas of more than 3dB

relative signal strengths. However, for intensive coverage schemes (<3dB relative signal strength for much of the time), audio delay equalisation of better than 50μ s is needed to avoid excessive distortion by this mechanism. Al-Nuaimi does not consider amplitude equalisation, but assumes identical deviation at each transmitter. Other authors such as Langseth [3] have shown this to have a less severe contribution to the total distortion. A figure of 2dB maximum amplitude misequalisation across the audio passband is given by Gray [6].

2.7. Reduction of F.M. Threshold Noise

Reduction of modulation-correlated noise bursts and carrier 'beating' threshold noise in the receiver output should improve the intelligibility of the message signal. Threshold extension is one possibility. Clarke and Hess [10] first described F.M. demodulation by a frequency-locked loop which achieves a lowering of the threshold level (*threshold extension*) and click attenuation (see earlier). However, the improvement in output signal-to-noise ratio at signal levels in the threshold region is only around 3-4dB and the threshold effects still exist even if they occur at lower carrier-to-noise ratios.

It was been shown earlier that the R.F. signal strength can drop close to zero and so it is still possible to have noise bursts in the audio output, even if the coverage area over which they can occur is reduced. the following receiver modification first suggested by Al-Nuaimi [8] almost eliminates threshold effects with improvements of around 13dB in output signal-to-noise in the "old" threshold region and suppresses the noise bursts associated with R.F. signal strength zeros. The receiver chain of the previously described practical receiver is broken after the I.F. filter and the modification shown in figure 2.8. inserted. The threshold amplifier passes the I.F. signal from the receiver I.F. stage to the phase-locked loop only when the I.F. signal is larger than a certain preset threshold level. Below this level, the amplifier gives a near-zero output by

blanking out the noisy I.F. signal thus preventing the loop from responding to the I.F. noise.

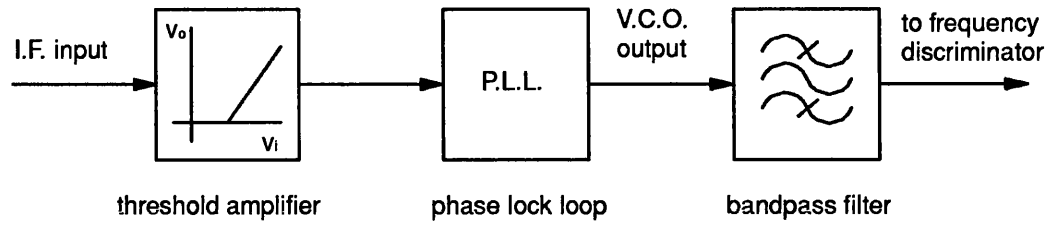

Figure 2.8: *F.M. receiver modifications to reduce threshold noise*

The P.L.L. generates an output in phase coherence with the I.F. signal. This ensures that the phase information contained in the I.F. carrier is transferred faithfully to the P.L.L. output, except in the case of a weak radio field. The bandpass filter ensures that the discriminator is subsequently presented with a harmonic-free input so that it can still faithfully reproduce the modulating signal.

This modification to the receiver supplies the discriminator with exactly the same I.F. signal as usual providing the radio field is sufficiently strong. If the signal drops below the preset threshold by one of the mechanisms described previously, then the discriminator is supplied with a signal that although it contains no modulating signal information, has very little noise content. By suitable design, this modification can be made to allow the periodic loss of information to have little effect on the intelligibility of the received signal. Any loss of information is more than offset by the reduction in the level of noise bursts in the audio.

Modification of large numbers of existing equipments is not an ideal solution however. Modifying the transmitter architectures and system implementation is preferable in order that existing mobile receivers may be used. This requires new approaches to minimising the variation in the signal radiated by each transmitter. A true synchronous scheme has been reported using a signal modulated with the intended audio sent across R.F. links to frequency-

translating, non-demodulating repeaters (Holbeche and Morcom [9]). In this scheme, the carriers of the service transmitters were all phase-locked to the incoming link signal carrier and the link signal was translated to the desired re-radiation frequency without demodulating the audio. Since each repeater used the same R.F. feed signal, both the carrier frequency and the modulation radiated at each site were accurately matched. This gave substantial improvement in mobile and portable coverage within the intended service area, though at the cost of the spectrum required for the R.F. link frequency used.

Alternatively, digital transmission of the audio modulating signal over landlines between the point of generation and the transmitter sites would allow considerably more accurate modulation matching than possible with analogue lines. Firstly, amplitude matching over the line becomes unnecessary as providing the landline operates at a suitably low bit error rate, the digital samples received at each transmitter site will be identical. Secondly, time delay equalisation becomes trivial since the time delay across the audio band of the digital link will be constant with audio frequency and adding delay at each transmitter to account for differences in digital landline delay can be achieved with very simple digital circuitry (provided the delay is fixed and known).

Digital transmission also offers the possibility of fully synchronous transmitter operation since the recovered data stream clock could be used as a frequency standard for each transmitter site allowing accurate matching of transmitter carrier frequencies. The combination of accurate modulation and carrier frequency matching offered by digital audio transmission would eliminate much of the distortion in the received audio discussed in this chapter. However, there remains one area where inaccuracies in modulating signal can occur and that is in the conversion of digital samples to analogue frequency modulation by the original audio. This is the subject of the next chapter.

2.8. Conclusions

Mobile and portable radio receivers in areas covered by a single transmitter experience a great deal of variability in the received signal strength. Attenuation due to obstacles to the radio path such as buildings and reflections resulting in multi-path propagation are the principal causes. Co-channel operation of radio transmitters radiating identical signals can, in theory, offer a substantial increase in the mean signal strength and considerable reduction in the variance of the field allowing increase in both extent and quality of radio coverage.

In practice, the radiation of identical signals from geographically separated sites is impossible due to variation in parameters of transmission lines used to convey modulating audio to each site and the stability of station master oscillators for setting the carrier frequency. Mismatch in the radiated signals from two transmitters results in time variation of the resultant field amplitude and phase. The distortion of the demodulated signal due to this variation dictates the degree of modulation equalisation and carrier frequency matching required to successfully operate co-channel transmitters.

A.M. schemes are more tolerant than F.M. of mismatch in the radiated signal, but many existing mobile and portable radio schemes are based on F.M. The distortion in co-channel operation of F.M. transmitters results from two mechanisms; the high level of audio output noise that results when the instantaneous signal strength drops below the receiver threshold, and the distortion of the instantaneous phase of the resultant field. Both effects are most pronounced when the mean signal strength from each transmitter is similar, which can be shown to be widespread in an intensive area coverage system and so acceptable performance under these conditions is essential.

Both distortion effects are functions of the difference in the instantaneous phase of the F.M. output of the two transmitters. The difference in instantaneous phase

arises from carrier frequency offset and/or mismatch in the frequency modulation of the two transmitted signals. If the instantaneous phase difference between the two F.M. signals is time varying, then for similar signal strengths, ±2dB, the mobile will experience frequent fades in the instantaneous signal strength of 20dB or more in depth. Thus carrier offsets will result in periodic threshold noise bursts at twice the offset frequency and modulation mismatch can result in noise bursts correlated with speech peaks.

The second effect, distortion of the instantaneous phase of the resultant field, contributes more distortion to the output audio even after the audio and carrier frequencies are sufficiently matched to avoid significant threshold-related distortion. The instantaneous phase of the resultant field includes a complex non-linear function of the difference in instantaneous phase that is not easily evaluated, but significant in the received audio output.

Both effects seriously degrade received speech quality and in practice it is found that carrier offsets must be controlled to less than 2Hz and analogue landlines must be equalised to better than 2dB in amplitude and 50μs in delay across the audio bandwidth used. By their very nature, analogue landlines have variable characteristics, both in manufacture and with environmental conditions and require careful equalisation across audio frequency band and frequent monitoring and maintenance. However, digital transmission of modulating audio to remote sites allows exact amplitude matching and easily implemented, accurate delay equalisation across the entire audio range of better than 1μs. Further still, the inherent bit synchronisation signal used in self-synchronising digital line repeaters could be used for carrier frequency synchronisation by suitable phase-lock techniques.

2.9. References

[1] Jakes W. C., (Ed.) "*Microwave mobile communications*" John Wiley & Sons, Inc 1974 New York ISBN 0-471-43720-4

[2] Gosling W., Petrovic V., "*Area coverage in mobile radio by quasi-synchronous transmissions using double-sideband diminished-carrier modulation*" Dec. 1973 Proc. I.E.E. 120, 12, pp.1469-1476.

[3] Langseth R.E., "*Some effects of delay and modulation-index mismatch on co-channel F.M. Interference*" I.E.E.E. Trans. on Vehicular Technology vol. vt-20 No.4 Nov. 1971.

[4] Brinkley J.R., "*A method of increasing range of V.H.F. communication systems by multi-carrier amplitude modulation*" J.I.E.E. 1946, 93, Part III, pp.159-166.

[5] Al-Nuaimi M.O., "*Response of an A.M. receiver to a quasi-synchronous multi-transmitter field*" March 1978 Proc. I.E.E. 125, 3, pp.190-194.

[6] Gray D.G., "*The Simulcasting Technique: An approach to Total-Area radio coverage*" I.E.E.E. Trans. on Vehicular Technology Vol. vt-28 No.2 May 1979 pp.117-125.

[7] Al-Nuaimi M.O., "*Analysis of response of an F.M. mobile receiver to a quasi-synchronous field*" Oct. 1981 Proc. I.E.E., 128, Part.F, 5, pp.317-322.

[8] Al-Nuaimi M.O., "*Reduction of threshold noise in F.M. receivers operating in quasi-synchronous field*" April 1985 Proc. I.E.E., 132, Pt.F, 2, pp.94-98.

[9] Holbeche R.J., Morcom C., "*Synchronous F.M. area coverage in V.H.F. and U.H.F. mobile and portable radio systems*" 2nd International Conference on Radio Spectrum Conservation Techniques, Birmingham, England 6-8 Sept. 1983 London, England: I.E.E. 1983 pp.103-108.

[10] Clarke K.K., Hess D.T., "*Frequency-lock loop F.M. demodulator*", I.E.E.E. Trans. 1967 COM-15 pp.518-524.

[11] Gradshteyn I.S., Ryzhik I.M., "*Tables of Integrals, Series and Products*" London: Academic Press, 1965 ISBN 0-12-294760-6.

[12] Bennett W.R., "*Distribution of the sum of randomly phased components*", Quart. Appl. Math., 1948, 5, pp.385-393

Chapter 3:
Precise Phase Modulation

3.1. Introduction

As discussed in the previous chapter, severe distortion can be experienced in co-channel operation of F.M. area coverage schemes irrespective of the degree of carrier frequency alignment. This is caused by mismatch in the modulation of transmitters used for a particular service area, and can arise for two reasons: mismatch of the transmission characteristics of lines used to convey the modulating signal to each transmitter site, and mismatch in the modulator characteristics of each transmitter.

As proposed in the previous chapter, digital transmission of the modulating audio signal allows accurate (if not almost exact) matching of the transmission characteristics between the control site and each transmitter site and eliminates one reason for modulation mismatch. The other source of mismatch, variation in transmitter modulator characteristics, can only be removed by a modulator whose characteristics can be identically repeated in each transmitter. This chapter considers a novel technique for generating frequency modulation from the digital signal samples arriving at each transmitter. The effects on the demodulated signal of pre-modulation sampling and quantisation and the effects of variation in transmitter filter characteristics are considered.

3.2. Conventional generation of angle modulation

There exist a number of techniques for producing angle modulated signals, particularly frequency modulation as it is more commonly used. They effectively fall into one of two categories: direct and indirect techniques.

Direct frequency modulators work by causing the natural frequency of an

oscillator to fluctuate in sympathy with the modulating signal. There are a large number of implementations and variations on this theme, but the principle is best illustrated by a simple LC oscillator. The natural frequency of an LC oscillator is given by:

$$f_o = \frac{1}{2\pi\sqrt{LC}} \qquad (3.1)$$

i.e., f_o depends on the values of inductance L and capacitance C in the oscillator circuit. If either the inductance or capacitance of the oscillator can be made voltage-variable, then the frequency of the oscillator can be controlled. From equation 3.1, by differentiation:

$$\frac{\partial f_o}{\partial X} = -\frac{f_o}{2X} \qquad (3.2)$$

where X is either reactance L or C. For a small variation of f_o about its natural value:

$$\frac{\partial f_o}{f_o} = -\frac{\partial X}{2X} \qquad (3.3)$$

and so the fractional change in f_o is directly proportional to a fractional change in reactance X. Voltage-variable reactance can be achieved by means of varactor diodes (variable capacitance) or reactance devices [1], but the relation between the capacitance and voltage is firstly non-linear and secondly subject to device manufacturing tolerance spread. Other direct methods exist such as "serrasoid" modulators. These are low-frequency (<10MHz) voltage controlled oscillators that can be made from sawtooth generator circuits. They are easily fabricated in integrated circuit form and are highly linear although they are limited by their maximum operating frequency [1].

Indirect frequency modulators use the relationship between phase and frequency modulation by preceding a phase modulator with an integrator. The most famous

of these is the Armstrong modulator [2] which exploits mathematical approximations that can be made about angle modulation. If the general form of an angle modulated signal is:

$$e(t) = E_o \cos(2\pi f_o t + \varphi(t)) \tag{3.4}$$

then expanding:

$$e(t) = E_o(\cos 2\pi f_o t \cos \varphi(t) - \sin 2\pi f_o t \sin \varphi(t)) \tag{3.5}$$

If the phase deviation is sufficiently small then the approximations $\cos\varphi(t) \approx 1$ and $\sin\varphi(t) \approx \varphi(t)$ can be made and so:

$$e(t) \approx E_o(\cos 2\pi f_o t - \varphi(t) \sin 2\pi f_o t) \tag{3.6}$$

So, in the Armstrong phase modulator where the instantaneous modulated phase is proportional to the modulating signal $m(t)$:

$$e(t) \approx E_o(\cos 2\pi f_o t - \Delta\theta m(t) \sin 2\pi f_o t) \tag{3.7}$$

where $\Delta\theta$ is the peak phase deviation and $|m(t)| \leq 1$. This equation represents the sum of a carrier component and the product of a quadrature carrier mixed with the inverted modulating signal and can be implemented as the block diagram shown in figure 3.1.

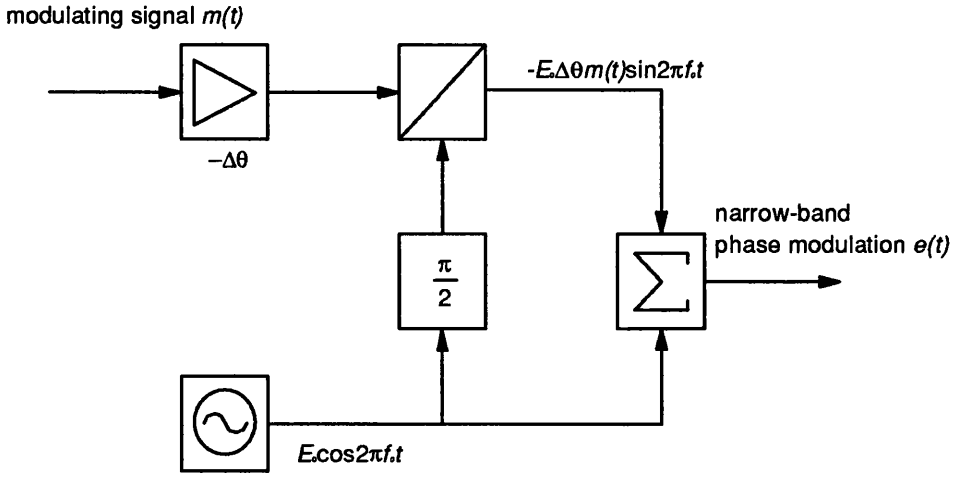

Figure 3.1: *The Armstrong phase modulator*

This form of modulator is often used as a means of generating F.M. by preceding the modulator with suitable audio preprocessing discussed later. The phase deviation is severely limited by the approximation used which is valid up to around *0.1* to *0.3* radians before excessive envelope distortion occurs. Thus the maximum frequency deviation obtainable from a frequency modulator based on an Armstrong modulator is similarly restricted. The deviation can be increased by passing the signal through a non-linear device and extracting the n^{th} harmonic where the n^{th} harmonic is:

$$e_n(t) = E_o \cos(2\pi n f_o t + n\Delta\theta m(t)) \qquad (3.8)$$

and thus the phase deviation (and F.M. modulation index) has been increased by a factor n. However, the carrier frequency has also been increased by a factor of n so the modulated signal must be generated at one n^{th} of the final desired output frequency.

3.3. Audio preprocessing for indirect F.M.

In order to produce a practical F.M. modulator from a phase modulator, a certain amount of audio preprocessing is required. Apart from the bandlimiting of the modulating signal mentioned in the previous chapter, the elements shown in figure 3.2 are required.

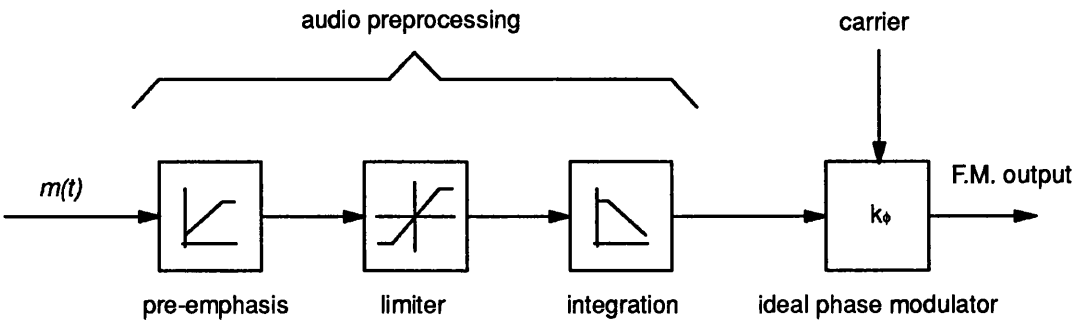

Figure 3.2: *Audio preprocessing for indirect F.M.*

As previously stated, frequency modulation can be obtained from a phase modulator by first integrating the modulating signal. The integrator effectively de-emphasizes the higher frequency components of the modulating signal relative to the lower ones. The transfer function of an ideal integrator is:

$$H_{\text{int}}(f) = \frac{-k_o}{j2\pi f} \tag{3.9}$$

Together, the de-emphasis of the integrator and the phase modulator form a frequency modulator. If the phase modulator constant is k_φ radians per volt, then the frequency modulator constant k_f is:

$$k_f = \frac{k_\varphi k_o}{2\pi} \; HzV^{-1} \tag{3.10}$$

In order to limit the bandwidth of the modulated signal, there must be a limit on the peak frequency deviation, Δf (this is discussed further later in this chapter). Hence the integrator must be preceded by a limiter that amplifies linearly, but clips any excursions in the modulating signal voltage that exceeds the bound for the voltage v_{pk} required to produce a peak deviation of Δf Hz in the frequency of the output signal, i.e.:

$$v_{pk} = \pm\frac{2\pi\Delta f}{k_\varphi k_o} \; volts \tag{3.11}$$

It can be shown that in the reception of F.M. signals by an ideal F.M. discriminator in the presence of white noise that the noise power spectrum of the recovered audio is proportional to f^2 (f is the baseband frequency) for large carrier-to-noise ratios [1]. Since the energy in the higher frequencies of the modulating signal is also likely to be less than at lower frequencies, then the received signal-to-noise ratio at these higher frequencies is degraded.

In order to improve the signal-to-noise ratio at higher audio frequencies, these frequencies are emphasized relative to lower ones prior to modulation. This

requires a pre-emphasis network prior to the amplitude limiter the typical characteristic of which is:

$$H_{PRE}(f) = 1 + j2\pi f\tau \qquad (3.12)$$

where $1/\tau$ is the break frequency of the network. In order to restore the correct energy distribution in the receiver output, a complementary de-emphasis network is required $H_{DE}(f)$ where:

$$H_{DE}(f) = \frac{1}{1 + j2\pi f\tau} \qquad (3.13)$$

3.4. The Precise Phase Modulator

In the previous chapter, the desirability of digital audio transmission to transmitter sites was highlighted. The F.M. signal must then be derived from digital samples of the modulating signal, hence some form of recovery of the analogue signal is required if any of the techniques so far mentioned are to be used. Figure 3.3 shows a possible transmitter site interface.

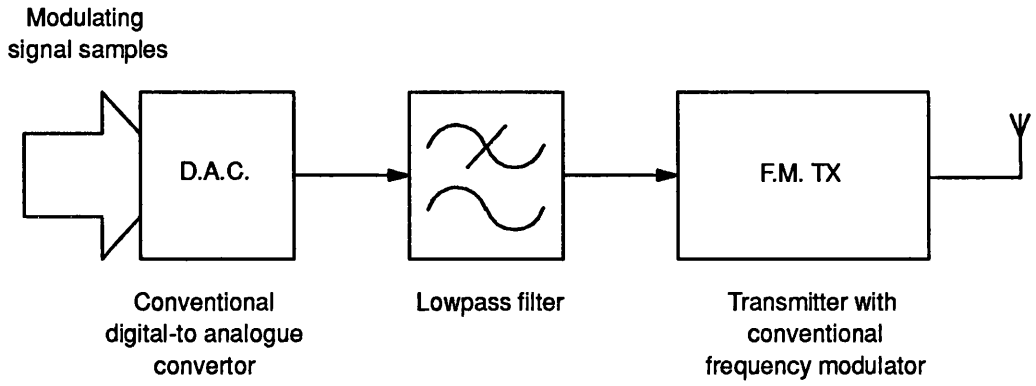

Figure 3.3: *Transmitter site interface for conventional modulators*

However, all the methods of angle modulation generation described so far are sensitive to the spread of manufactured device parameters. Even if the modulating signal at each transmission site were accurately matched by using

digital transmission between sites as discussed in the previous chapter, the modulation of the radiated signal from each site will still vary unless very careful matching of conventional modulators is implemented. To avoid this time-consuming, tedious and possibly fruitless process, a digital implementation is required that removes the need for a digital-to-analogue conversion process allowing precise matching of the modulated signal at each site.

The principle behind a technique for directly phase modulating a carrier with digital samples of the modulating signal is shown in figure 3.4.

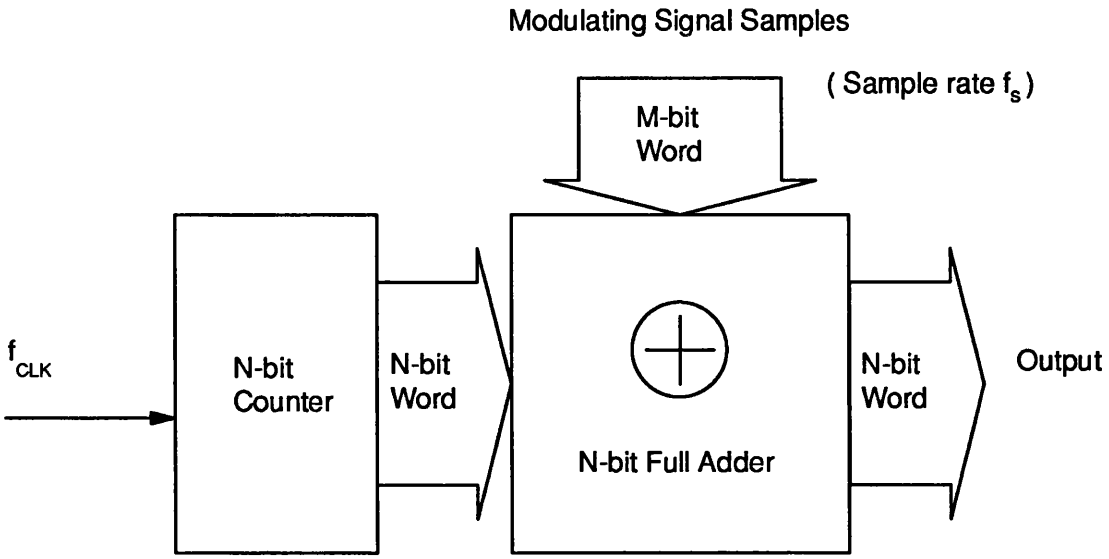

Figure 3.4: *The principle of the precise phase modulator*

An N-bit counter is clocked at a frequency f_{CLK} such that the counter output word cycles from 0 to 2^N-1 at a frequency f_o given by:

$$f_o = \frac{f_{CLK}}{2^N} \qquad (3.14)$$

This frequency f_o is also the frequency of the square wave formed by the Most Significant Bit (*M.S.B.*) of the counter (i.e. *M.S.B.*$= 0$ for counter output words 0 to $2^{N-1}-1$ and *M.S.B.*$= 1$ for counter output words 2^{N-1} to 2^N-1). This is the

unmodulated intermediate carrier frequency and is thus directly dependent on the counter clock frequency only.

If an M-bit word of magnitude x, is added to the counter output word, the M.S.B. of the adder output word will be advanced in time relative to the M.S.B. of the counter output word as shown in figure 3.5.

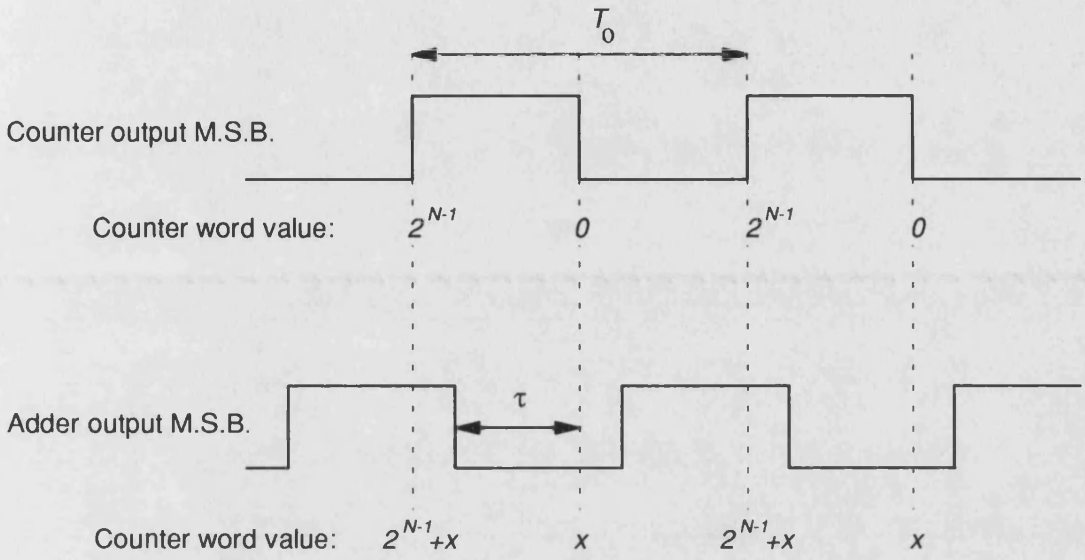

Figure 3.5: *Phase advance by addition of modulating signal samples*

The time advance τ, caused by a modulating sample word x is:

$$\tau = \frac{x}{2^N} T_o \quad seconds \qquad (3.15)$$

or similarly the phase advance θ is:

$$\theta = 2\pi \frac{x}{2^N} = 2^{1-N} \pi x \quad radians \qquad (3.16)$$

Hence the phase advance θ, is proportional to the magnitude of the modulating signal sample x. However, since x is an integer (due to quantisation of the incoming samples), there is a limit to the phase resolution or accuracy due to the number of bits used in the addition, N. The smallest increment or phase

quantisation step size $\delta\theta$ is:

$$\delta\theta = 2^{1-N}\pi \quad radians \; or \; 2^{1-N}180 \; degrees \qquad (3.17)$$

So, for example, an 8-bit modulator would have a resolution of *1.40625* degrees. The number of bits in the modulating word *M* merely limits the maximum cumulative phase shift of the modulator. Once *M*>N, only the *N* least significant bits of the modulating word need be used in the addition, since the phase shift caused a sample word *x* and sample word $x+2^N$ are indistinguishable in isolation: the difference in resultant phase shift is 2π radians. This would indicate that any cumulative phase shift required for the appropriate phase deviation, however large, may be generated by the modulator by continual "wrap-around" from 2^N-*1* to *0* and vice versa. However, there are other limiting factors that are considered further later in this chapter.

The modulating sample word is held at the input to the adder for the duration of the sample period T_s, and then the next sample word is used. The output waveform of the modulator can thus be thought of as a form of phase-shift keying with a large number of finely-quantised phase steps available. The form of the output waveform is shown in figure 3.6.

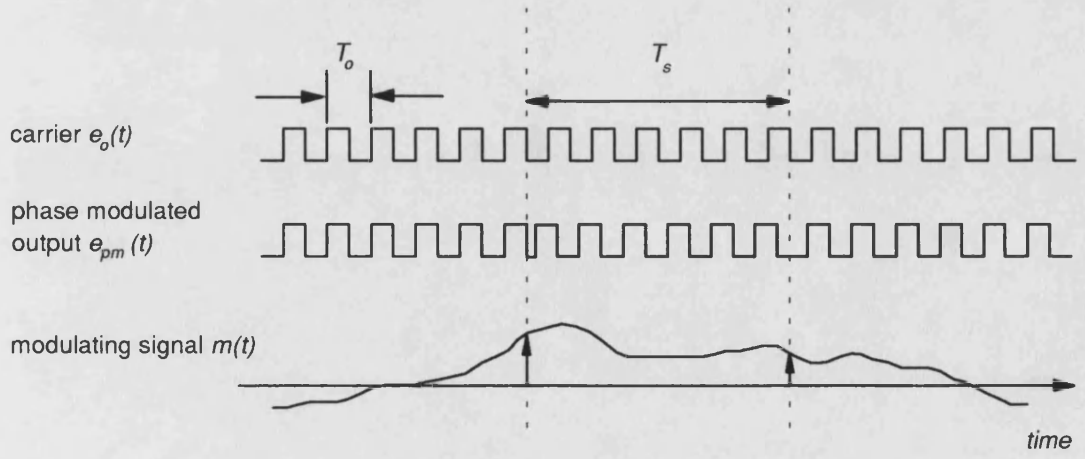

Figure 3.6: *Modulator output waveform*

This modulation technique is a direct conversion from digital samples to phase modulation avoiding any digital-to-analogue conversion and analogue circuitry whose natural spread in manufactured component parameters would automatically introduce inaccuracies between the output from different modulators using the same modulating signal.

However, although the modulator is identically repeatable and the modulation it produces is identical from modulator to modulator, the output of the modulator will differ from that of a conventional modulator in three ways. First, the carrier is a square wave rather than a sinusoid. This at first would seem trivial, but the possible consequences must be considered in the light of the other two differences. Secondly, the modulating signal has been sampled prior to transmission to the modulator and the sampled form is used directly in the modulator. Further still, the effect of constantly adding modulating signal samples to a continually incrementing counter word is to hold the samples for the sampling period T_s prior to modulation. The third factor to consider is that the modulated phase has been quantised in the modulation process.

3.5. A theoretical model of the Precise Phase Modulator

The Precise Phase Modulator described in the previous section is best analysed by considering an equivalent block diagram of its operation as shown in figure 3.7.

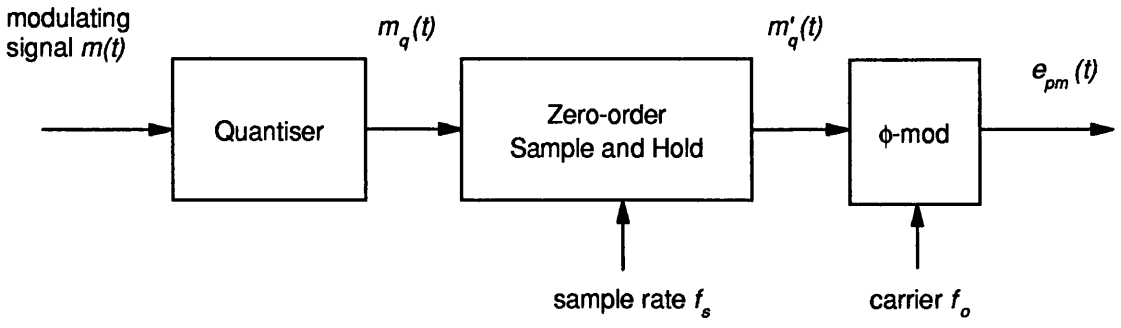

Figure 3.7: *A model of the operation of the Precise Phase Modulator*

The modulating signal input $m(t)$, is quantised to steps defined by the modulator resolution $\delta\theta$. The output of the quantiser $m_q(t)$ is sampled at a rate f_s and that value is held constant for the sampling period T_s. The output of the sample and hold $m'_q(t)$, is then used to modulate a carrier $e_o(t)$ of frequency f_o by an ideal phase modulator. The carrier is actually a square wave, so before the effects of sampling, holding and quantisation are examined, the effect of a non-sinusoidal carrier is considered.

A square wave carrier of peak-to-peak amplitude $2E_o$, frequency f_o and symmetrical about the $t=0$ axis (i.e. an *even* function of time) may be written as a Fourier series of harmonic components:

$$e_o(t) = \sum_{\substack{n=1 \\ oddonly}}^{\infty} \frac{4E_o}{n\pi} \cos 2\pi n f_o t \qquad (3.18)$$

If the input to the phase modulator, $m'_q(t)$, produces a time shift $\tau'_q(t)$ proportional to $m'_q(t)$ as shown in figure 3.5:

$$\tau'_q(t) = k_t m'_q(t) \qquad (3.19)$$

where k_t is a constant. Thus:

$$e_{pm}(t) = e_o(t + \tau'_q(t)) \qquad (3.20)$$

So substituting from equations 3.18 and 3.19 gives:

$$e_{pm}(t) = \sum_{\substack{n=1 \\ oddonly}}^{\infty} \frac{4E_o}{n\pi} \cos 2\pi n f_o \left(t + \tau'_q(t)\right) \qquad (3.21)$$

and then:

$$e_{pm}(t) = \sum_{\substack{n=1 \\ oddonly}}^{\infty} \frac{4E_o}{n\pi} \cos\left(2\pi n f_o t + 2\pi n f_o k_t m'_q(t)\right) \qquad (3.22)$$

If the peak phase deviation of the fundamental, $\Delta\theta$, is written as:

$$\Delta\theta = k_t 2\pi f_o \qquad (3.23)$$

then the output of the modulator can be written as:

$$e_{pm}(t) = \sum_{\substack{n=1 \\ oddonly}}^{\infty} \frac{4E_o}{n\pi} \cos\left(2\pi n f_o t + n\Delta\theta m_q'(t)\right) \qquad (3.24)$$

and thus can be considered as a series of odd harmonics of the fundamental where the n^{th} harmonic has a peak phase deviation n times greater than that of the fundamental and their magnitude relative to the fundamental is $1/n$.

In order to analyze the spectral characteristics of the modulator output, equation 3.24 is too cumbersome to work with. To simplify the analysis, only a single sinusoidal carrier will be assumed, at the fundamental frequency of the carrier, f_o. The results for the single component carrier can be easily extended to the square wave carrier via equation 3.24.

The two factors that influence the possible differences between the output spectrum of the modulator and that of the ideal modulator are the sampling and quantisation of the baseband signal prior to modulation. These two factors will produce different types of spectral distortion and can be considered separately. First, the spectral output of an ideal modulator will be reviewed in order to assess the distortion in the Precise Phase Modulator by comparison.

3.6. Spectral effects due to zero-order hold of phase

With linear modulation techniques such as amplitude modulation, the spectral characteristics of the modulated signal can be easily derived from the spectral characteristics of the modulating signal, i.e. the Fourier transform of the modulated signal $F\{e(t)\}$ and the Fourier transform of the modulating signal

$F\{m(t)\}$ have a simple linear relationship. However, with an angle modulated signal $e(t)$ given by:

$$e(t) = \mathrm{Re}\left[E_o e^{j2\pi f_o t + \varphi(t)}\right] \qquad (3.25)$$

there is no simple relationship between $F\{e^{j\varphi(t)}\}$ and $F\{\varphi(t)\}$ since the exponential $e^{j\varphi(t)}$ is a non-linear function of $\varphi(t)$. However, analytic solutions can be obtained for simple forms of modulating signal. The case where the input to an ideal angle modulator is a sinusoid results in a predictable line spectrum which can be fairly easily evaluated. From previous sections the modulator outputs for P.M. and F.M. can be written as:

$$e_{pm}(t) = \mathrm{Re}\left[E_o e^{j(2\pi f_o t + \Delta\theta \cos 2\pi f_m t)}\right] \qquad (3.26)$$

$$e_{fm}(t) = \mathrm{Re}\left[E_o e^{j(2\pi f_o t + \frac{\Delta f}{f_m}\cos 2\pi f_m t)}\right] \qquad (3.27)$$

By making use of the identities:

$$e^{j\alpha\cos\beta} = \sum_{n=-\infty}^{+\infty} j^n J_n(\alpha) e^{j\beta} \qquad e^{j\alpha\sin\beta} = \sum_{n=-\infty}^{+\infty} J_n(\alpha) e^{j\beta} \qquad (3.28)$$

the expressions can be rewritten as:

$$e_{pm}(t) = \mathrm{Re}\left[E_o \sum_{n=-\infty}^{+\infty} j^n J_n(\Delta\theta) e^{j2\pi(f_o + nf_m)t}\right] \qquad (3.29)$$

$$e_{fm}(t) = \mathrm{Re}\left[E_o \sum_{n=-\infty}^{+\infty} J_n(\beta) e^{j2\pi(f_o + nf_m)t}\right] \qquad (3.30)$$

where $J_n(x)$ is the Bessel function of the first kind of order n. The frequency spectrum can be derived by inspection from these equations and figure 3.8 shows

the magnitude spectrum for F.M. for moderate deviation β.

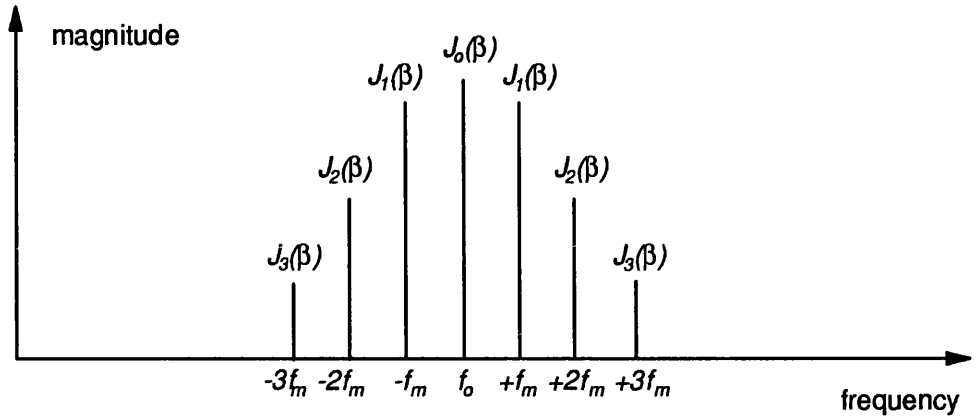

Figure 3.8: *Positive frequency magnitude spectrum for F.M. with a single modulating tone*

Although a single modulating tone has been used, an infinite number of sidebands result, the magnitude of the n^{th} sideband being given by the n^{th} order Bessel function of the first kind and the maximum phase deviation (β or Δθ). The nature of Bessel functions is that the magnitude decreases quite quickly with increasing order for the same deviation and thus although an infinite number of sidebands exist, only a finite number are at all significant. This inherently limits the bandwidth required to transmit the vast majority of the signal power. It should be noted that the *magnitude* spectra for both cases, F.M. and P.M., are the same if β=Δθ and the modulating frequency f_m, is the same. The spectra of angle modulated waveforms of more complex modulating signals can be derived and are discussed later.

In order to compare the performance of the Precise Phase Modulator with that of the ideal modulator, it is necessary to obtain expressions for the output spectra of the precise phase modulator for simple modulating signals like those for the ideal modulator. The effective baseband sampling on the input to the modulator produces well-documented spectral effects in the pre-modulation baseband spectrum [3]. The infinite number of alias components that are produced by the

sampling process mean that even the simplest modulating signal, a single tone, applied to the precise phase modulator is the equivalent to a complex multi-tone input to an ideal modulator. Thus an analytic solution for the output spectrum for an ideal phase modulator is required for a multi-component input. If the modulating signal is now written as:

$$m(t) = \sum_{p=1}^{P} e_p \cos\left(2\pi f_p t + \varepsilon_p\right) \tag{3.31}$$

then from equation 3.26 the output of an ideal phase modulator can be written as:

$$e_{pm}(t) = \mathrm{Re}\left[E_o e^{j\left(2\pi f_o t + \sum_{p=1}^{P} \Delta\theta_p \cos\left(2\pi f_m t + \varepsilon_p\right)\right)} \right] \tag{3.32}$$

where:

$$\Delta\theta_p = \Delta\theta e_p \tag{3.33}$$

Cherry and Rivlin [4] have shown that this can be rewritten as:

$$e_{pm}(t) = \mathrm{Re}\left[E_o e^{j2\pi f_o t} \sum_{k_p=-\infty}^{+\infty} j^k \left(\prod_{p=1}^{P} J_{k_p}(\Delta\theta_p) \right) \sum_{p=1}^{P} k_p (2\pi f_p t + \varepsilon_p) \right] \tag{3.34}$$

where k_p takes all integral values or zero and k is given by:

$$k = \sum_{p=1}^{P} k_p \tag{3.35}$$

The output of the sample and hold before the ideal modulator in the model can be written in the form of equation 3.34 where $P \rightarrow \infty$ and f_p and ε_p can be defined in terms of the modulating frequency f_m, the sampling frequency f_s and p. However, the complexity of the mathematics involved requires exhaustive manipulation of Bessel functions to even approach an analytic solution for a single modulating

tone. Alternatively, an analytic proof for the output spectrum for any modulating signal input may be derived from the following route. Expanding the form of a general angle modulated signal given in equation 3.26 into in-phase and quadrature components:

$$e(t) = E_o\{\cos 2\pi f_o t \cos\varphi(t) - \sin 2\pi f_o t \sin\varphi(t)\} \tag{3.36}$$

The spectrum of $e(t)$ can be determined by taking its Fourier transform $E(f)$:

$$e(t) = E_o\left\{\int_{-\infty}^{\infty}\cos 2\pi f_o t \cos\varphi(t)e^{-j2\pi ft}dt - \int_{-\infty}^{\infty}\sin 2\pi f_o t \sin\varphi(t)e^{-j2\pi ft}dt\right\} \tag{3.37}$$

Since:

$$F\{\cos 2\pi f_o t\} = \frac{1}{2}(\delta(f+f_o)+\delta(f-f_o)) \tag{3.38}$$

$$F\{\sin 2\pi f_o t\} = \frac{j}{2}(\delta(f+f_o)-\delta(f-f_o)) \tag{3.39}$$

then by the convolution theorem of Fourier transforms:

$$E(f) = \frac{1}{2}\left[\left(E_I(f+f_o) - jE_Q(f+f_o)\right)+\left(E_I(f-f_o)+jE_Q(f-f_o)\right)\right] \tag{3.40}$$

where:

$$E_I(f) = F\{\cos\varphi(t)\} = \int_{-\infty}^{\infty}\cos\varphi(t)e^{-j2\pi ft}dt \tag{3.41}$$

$$E_Q(f) = F\{\sin\varphi(t)\} = \int_{-\infty}^{\infty}\sin\varphi(t)e^{-j2\pi ft}dt \tag{3.42}$$

Since the modulated phase $\varphi'(t)$ is sampled and held (as shown in figure 3.9), it can be written as:

$$\varphi'(t) = \sum_{n=-\infty}^{+\infty}h(t-nT_s)\varphi(nT_s) \tag{3.43}$$

where $h(t)$ is a unit amplitude pulse at $t=0$ and of duration T_s.

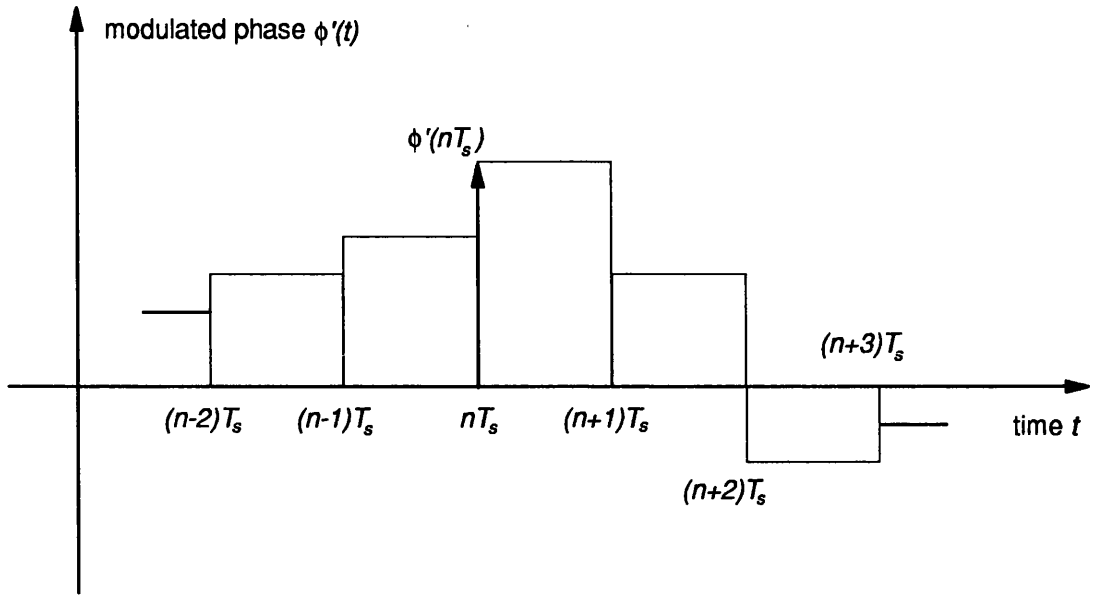

Figure 3.9: *A representation of the sampled and held phase*

In the case of sampled and held modulated phase, the in-phase and quadrature baseband spectra become:

$$E'_I(f) = F\left\{\cos\left(\sum_{n=-\infty}^{+\infty} h(t-nT_s)\varphi(nT_s)\right)\right\} \tag{3.44}$$

$$E'_Q(f) = F\left\{\sin\left(\sum_{n=-\infty}^{+\infty} h(t-nT_s)\varphi(nT_s)\right)\right\} \tag{3.45}$$

Over a period from $t=nT_s$ to $t=(n+1)T_s$, $h(t-T_s)\cos\varphi(nT_s)$ is the same as $\cos(h(t-T_s)\varphi(nT_s))$ and so:

$$\cos\left(\sum_{n=-\infty}^{+\infty} h(t-nT_s)\varphi(nT_s)\right) = \sum_{n=-\infty}^{+\infty} h(t-nT_s)\cos\varphi(nT_s) \tag{3.46}$$

and similarly:

$$\sin\left(\sum_{n=-\infty}^{+\infty} h(t-nT_s)\varphi(nT_s)\right) = \sum_{n=-\infty}^{+\infty} h(t-nT_s)\sin\varphi(nT_s) \tag{3.47}$$

Thus the baseband spectra are:

$$E'_I(f) = \sum_{n=-\infty}^{+\infty} h(t - nT_s)\cos\varphi(nT_s) \qquad (3.48)$$

$$E'_Q(f) = \sum_{n=-\infty}^{+\infty} h(t - nT_s)\sin\varphi(nT_s) \qquad (3.49)$$

Taking the in-phase baseband spectrum $E'_I(f)$, due to the linearity of the Fourier transform:

$$E'_I(f) = \sum_{n=-\infty}^{+\infty} F\{h(t - nT_s)\cos\varphi(nT_s)\} \qquad (3.50)$$

This can be written as:

$$E'_I(f) = \sum_{n=-\infty}^{+\infty} F\{h(t) * \delta(t - nT_s)\cos\varphi(nT_s)\} \qquad (3.51)$$

where * denotes convolution and $\delta(t)$ is the ideal delta function. By the time convolution theorem of Fourier transforms this becomes:

$$E'_I(f) = \sum_{n=-\infty}^{+\infty} F\{h(t)\}F\{\delta(t - nT_s)\cos\varphi(nT_s)\} \qquad (3.52)$$

The Fourier transform of $h(t)$, can be shown to be:

$$F\{h(t)\} = T_s \frac{\sin \pi f T_s}{\pi f T_s} e^{-j\pi f T_s} \qquad (3.53)$$

Rearranging equation 3.52:

$$E'_I(f) = F\{h(t)\}F\left\{\sum_{n=-\infty}^{+\infty} \delta(t - nT_s)\cos(nT_s)\right\} \qquad (3.54)$$

which can equally be written:

$$E'_I(f) = F\{h(t)\}F\left\{\left(\sum_{n=-\infty}^{+\infty} \delta(t - nT_s)\right)\cos\varphi(t)\right\} \qquad (3.55)$$

which by the frequency domain convolution theorem of Fourier transforms is:

$$E'_I(f) = F\{h(t)\}\left\{F\left\{\sum_{n=-\infty}^{+\infty}\delta(t-nT_s)\right\} * F\{\cos\varphi(t)\}\right\} \qquad (3.56)$$

Now $F\{\cos\varphi(t)\}$ is already defined as the in-phase baseband spectrum with continuous phase $E_I(f)$ and by using the standard result [3]:

$$F\left\{\sum_{n=-\infty}^{+\infty}\delta(t-nT_s)\right\} = \frac{1}{T_s}\sum_{n=-\infty}^{+\infty}\delta(f-nf_s) \qquad (3.57)$$

then:

$$E'_I(f) = F\{h(t)\}\left\{\left\{\frac{1}{T_s}\sum_{n=-\infty}^{+\infty}\delta(f-nf_s)\right\} * E_I(f)\right\} \qquad (3.58)$$

which can be shown to be:

$$E'_I(f) = H(f)\sum_{n=-\infty}^{+\infty}E_I(f-nf_s) \qquad (3.59)$$

where:

$$H(f) = \frac{\sin\pi fT_s}{\pi fT_s}e^{-j\pi fT_s} \qquad (3.60)$$

By the same route $E'_Q(f)$ can be shown to be:

$$E'_Q(f) = H(f)\sum_{n=-\infty}^{+\infty}E_Q(f-nf_s) \qquad (3.61)$$

From equation 3.40, the Fourier transform of $e'(t)$ is therefore:

$$E'(f) = \frac{1}{2}\left[\left(E'_I(f+f_o) - jE'_Q(f+f_o)\right) + \left(E'_I(f-f_o) + jE'_Q(f-f_o)\right)\right] \qquad (3.62)$$

which becomes:

$$E'(f) = \frac{1}{2}\left[H(f+f_o)\sum_{n=-\infty}^{\infty}\left(E_I(f+f_o-nf_s) - jE_Q(f+f_o-nf_s)\right)\right]$$

$$+\frac{1}{2}\left[H(f-f_o)\sum_{n=-\infty}^{\infty}\left(E_I(f-f_o-nf_s) - jE_Q(f-f_o-nf_s)\right)\right] \qquad (3.63)$$

This simplifies to that of equation 3.52 for $n=0$, but for the spectral envelope $H(f)$. Thus the output spectrum of a sinusiodal carrier modulated in phase by a sampled and held signal consists of the spectrum of the same carrier phase-modulated by the same signal in its continuous form, plus an infinite number of replicas of that spectrum centred on integer multiples of the sampling frequency f_s either side of the carrier frequency f_o. The *entire* spectrum is scaled by the complex spectral envelope $H(f)$ centred on the carrier frequency. Figure 3.10 illustrates the spectral effects described above, though the effect of the delay of $T_s/2$ due to the linear phase of $H(f)$ has been left out for clarity (the spectrum would twist about the frequency axis linearly with frequency). Considering the simplest form of test modulating signal: a single tone, which for the F.M. case is:

$$\varphi(t) = \beta \sin 2\pi f_m t \qquad (3.64)$$

by using the expansion of equation 3.30, the expression for a single sinusoidal modulating signal is:

$$e_{fm}(t) = \mathrm{Re}\left[E_o \sum_{m=-\infty}^{+\infty} \sum_{n=-\infty}^{+\infty} J_n(\beta) H_{m,n} e^{j2\pi(f_o + mf_s + nf_m)t + \varphi_{m,n}} \right] \qquad (3.65)$$

where:

$$H_{m,n} = \frac{\sin \pi(f_o + mf_s + nf_m)T_s}{\pi(f_o + mf_s + nf_m)T_s} \qquad (3.66)$$

and:

$$\varphi_{m,n} = -\pi(f_o + mf_s + nf_m)T_s \qquad (3.67)$$

The resulting magnitude spectrum for positive frequencies near the carrier frequency assuming $f_o >> f_s$ is shown in the figure 3.11.

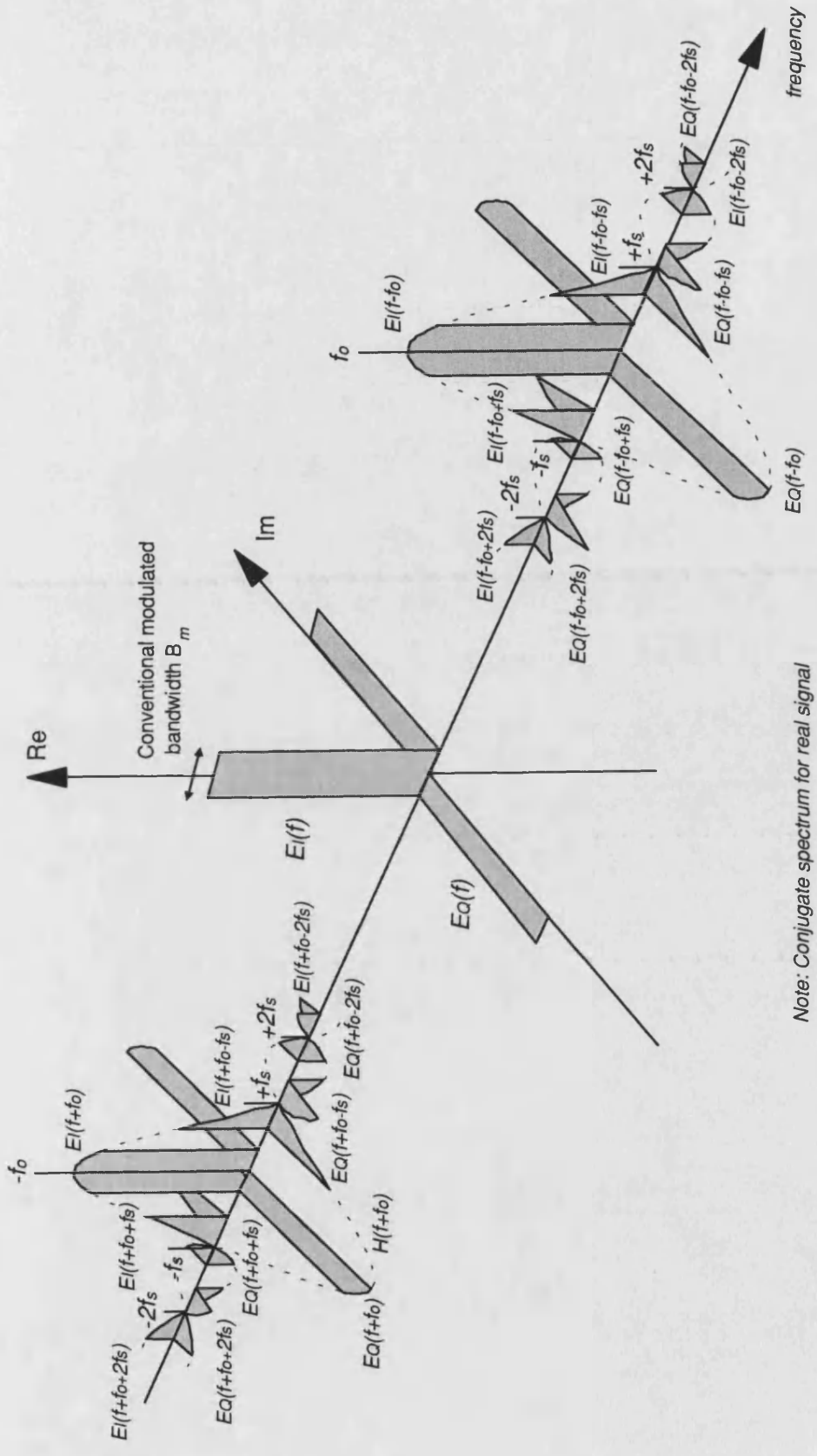

Figure 3.10: *The spectral effect of sampled and held phase by considering quadrature components*

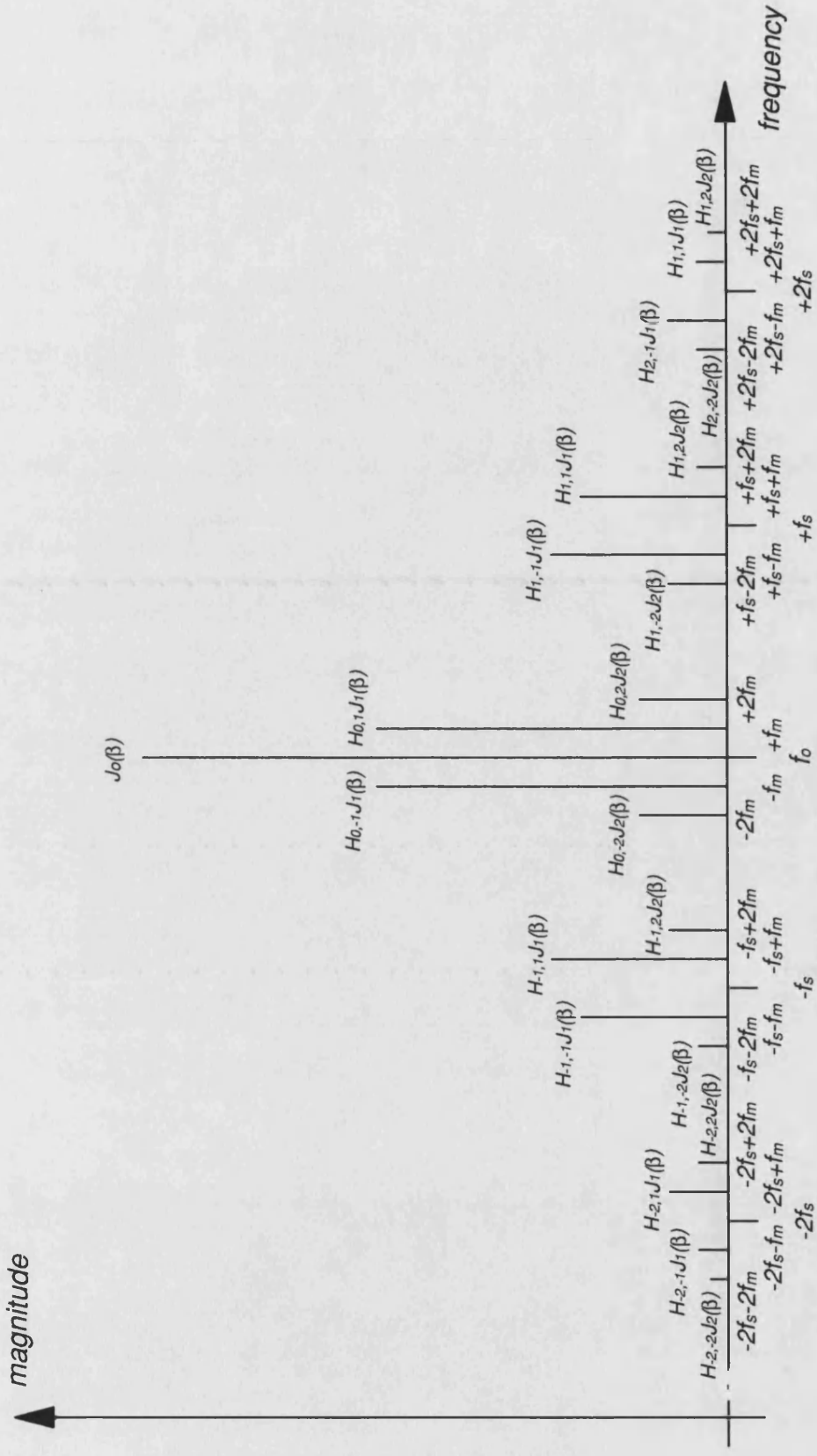

Figure 3.11: *The positive frequency spectrum near the carrier of eqn. 3.65*

Note that the replicas of the carrier components fall on the zeros of $H(f-f_o)$ and thus are canceled out and that $H(f-f_o)$ is unity at f_o and thus the carrier component magnitude is unaffected. Also, the case shown is for small deviations where the magnitude of the higher order Bessel sidebands tails off quickly with increasing sideband order and where the modulating frequency f_m is less than half the sampling frequency, f_o. For higher deviations, even if the modulating signal obeys the Nyquist rule, the higher order sidebands will become significant and overlap between first order components and the aliased higher order sidebands will occur. This is discussed in more detail later.

In order to verify the effect derived above, a sinusoidal signal with sinusoidal frequency modulation where the phase had been sampled and held was simulated by software and its frequency spectrum evaluated by taking the Fast Fourier Transforms of the signal. This was repeated for varying parameters: modulating frequency, frequency deviation and sampling frequency. Two example magnitude spectra are shown in figure 3.12.

The above spectra exhibit the predicted characteristics and thus the complete spectrum of the output of the Precise Phase Modulator can be predicted.

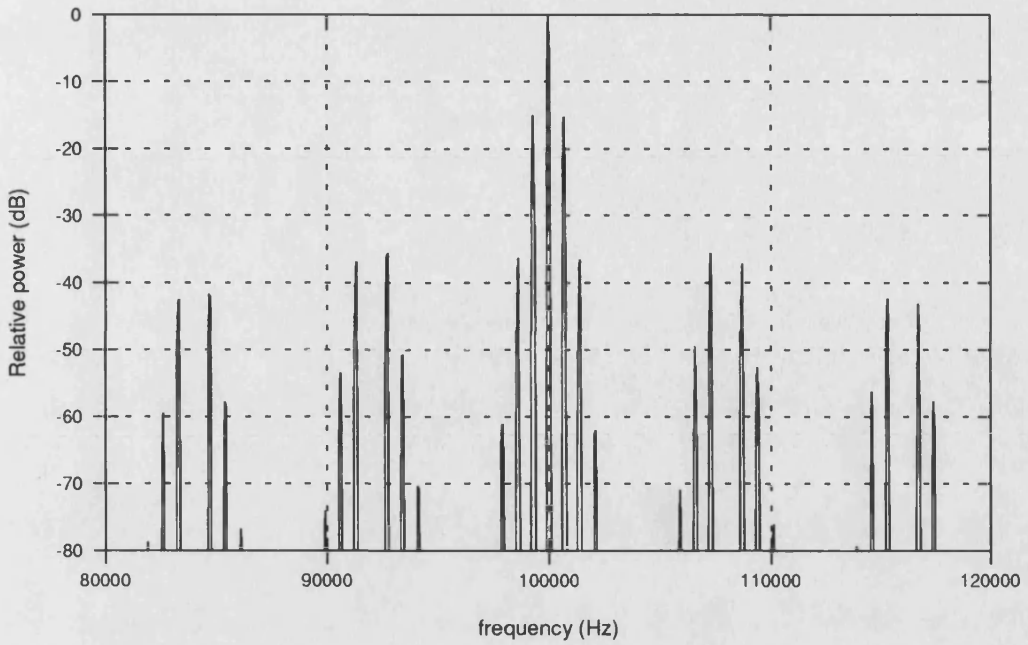

Frequency deviation: 250Hz Modulating Frequency: 700Hz Sampling Frequency:8kHz

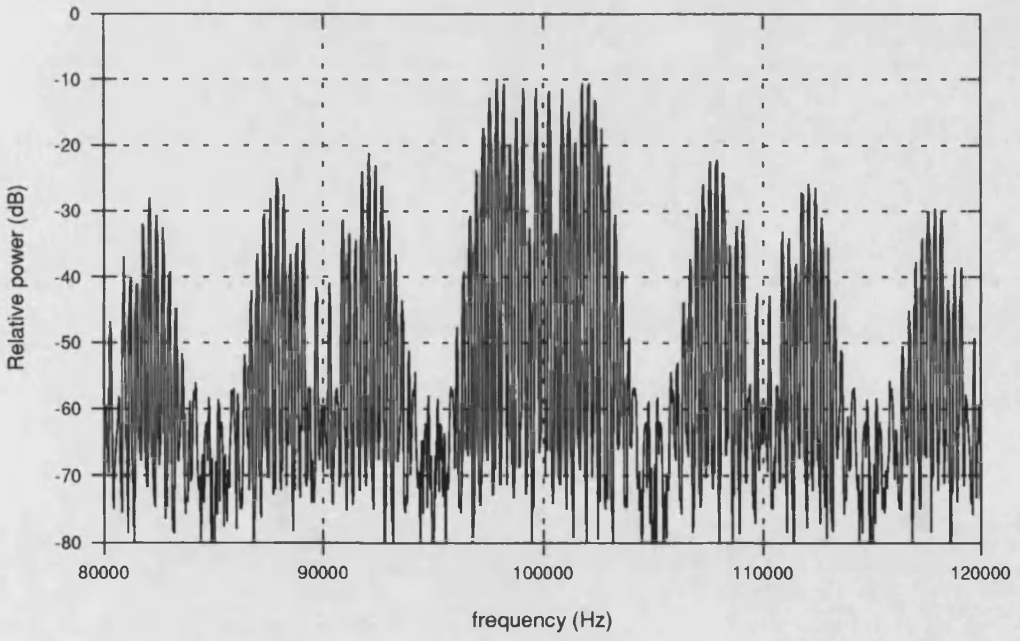

Frequency deviation: 2500Hz Modulating Frequency: 300Hz Sampling Frequency:10kHz

Figure 3.12: *Spectra of a sinusoidal carrier frequency modulated by a sinusoid where the modulated phase is sampled (but not quantised) demonstrating the effects of sampling frequency, modulating frequency and frequency deviation.*

3.7. In-band distortion due to multi-component carrier

The output waveform of the Precise Phase Modulator is a square wave and thus the carrier will consist of an infinite number of components. So far, only a single sinusoidal carrier modulated by a signal that has been sampled and held has been considered. It is thus necessary to assess the possible distortion that will result from the addition of other modulated carrier components. For the purposes of this analysis, the distortion from the third harmonic component of the carrier will be considered first as this component will easily give rise to the greatest amount since it is the largest component in the carrier after the fundamental and is the closest in proximity to the fundamental in the frequency domain. Therefore, from equation 3.24, the modulated two-component carrier can be written as:

$$e_{pm}(t) = \frac{4E_o}{\pi}\cos\left(2\pi f_o t + \varphi'_q(t)\right) + \frac{4E_o}{3\pi}\cos\left(6\pi f_o t + 3\varphi'_q(t)\right) \qquad (3.68)$$

where $\varphi'_q(t)$ is the sampled, held and quantised phase of the fundamental, the third harmonic having three times the frequency deviation. The resultant frequency spectrum of this signal can be examined by superposition of the Fourier transform of the single component case. The frequency spectrum of equation 3.62 can be applied in equation 3.68 to each modulated carrier component separately and summed to give the spectrum though the general case is far too complex to show. Figure 3.13 shows the two spectral envelopes that scale the alias signal power and the relative overlap power due to R.F. aliasing of the third harmonic of the carrier that appears in the passband of the desired signal. If, from the previous chapter, the magnitude of the spectral envelope of the carrier fundamental is:

$$|H(f)| = \frac{\sin \pi(f - f_o)T_s}{\pi(f - f_o)T_s} \qquad (3.69)$$

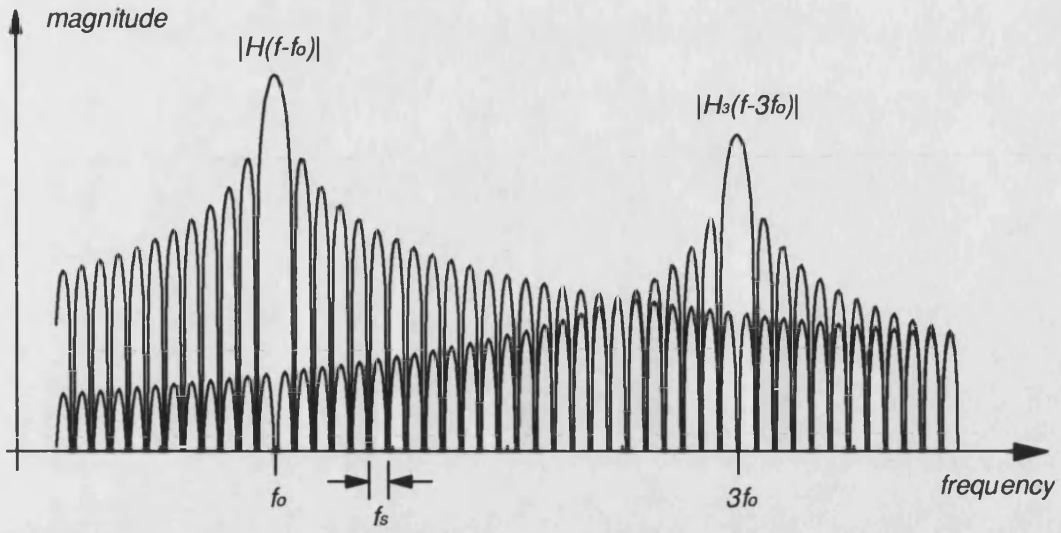

Figure 3.13: *Spectral overlap from the third harmonic of the carrier*

then that of the third harmonic of the carrier is:

$$|H_3(f)| = \frac{1}{3}\frac{\sin \pi(f - 3f_o)T_s}{\pi(f - 3f_o)T_s} \qquad (3.70)$$

The factor of a third is due to the relative magnitude between the fundamental and the third harmonic of a square wave. To assess the level of in-band distortion that may result from the third harmonic spectral overlap, the level of the third harmonic spectral envelope at the carrier frequency, f_o, will give the suppression of third harmonic alias components, i.e.:

$$Distortion\ level = \frac{|H(f)|}{|H_3(f)|} \qquad (3.71)$$

or:

$$Distortion\ level = 20\log_{10}\left|\frac{\sin 2\pi f_o/f_s}{6\pi f_o/f_s}\right| \qquad (3.72)$$

This is plotted against the ratio of carrier frequency to sampling frequency in figure 3.14. If the carrier frequency and sampling frequency are chosen such that the ratio results in a null in $H_3(f)$ occurring at the carrier frequency, then the suppression of signal power (once the signal is modulated) in the band of interest

($f_o - f_s/2 < f < f_o + f_s/2$) is somewhat greater, particularly near f_o. For example, a carrier of 100kHz and a sampling rate of 8kHz yield an f_o/f_s of 12.5. In this case, any alias signal power is reduced by at least 50dB over the range quoted above, and for nearly half of the range it is down by more than 60dB. This should result in negligible distortion in the received signal. However, it must be remembered that since the sampling rate will be fixed by factors involving the modulating signal bandwidth (see later), there will be a minimum carrier frequency at which the modulated signal can be generated (this may conflict with the limits on maximum possible carrier frequency due to hardware speed limitations and the required modulator resolution discussed later).

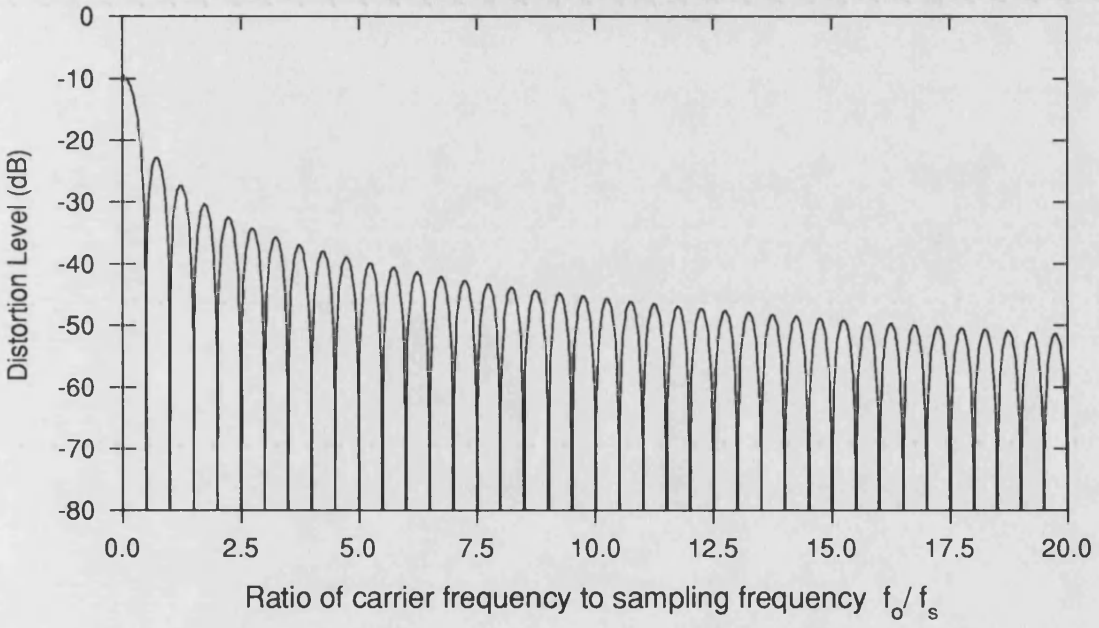

Figure 3.14: *Level of the third harmonic spectral envelope at the carrier frequency with variation in the ratio of carrier fundamental to sampling frequency*

3.8. Constraints on modulator sampling frequency

Neglecting the effects of a square carrier signal and the quantisation of the modulated phase, ideal rectangular bandpass filtering of the output of a frequency modulator based on the precise phase modulator will remove aliased

R.F. spectra leaving a signal of the form:

$$e'_{fm}(t) = \mathbf{F}^{-1}\left\{H(f)\mathbf{F}\left\{e_{fm}(t)\right\}\right\} \qquad (3.73)$$

as the output of an ideal frequency modulator and where *H(f)* is the spectral envelope described in section 3.6. This, however, is only possible if the sampling frequency f_s is such that there is separation between the wanted spectrum and the alias spectra. As is the case with baseband sampling, the spectral distance between the required spectrum and the alias spectra is controlled by the sampling theorem as shown in figure 3.15.

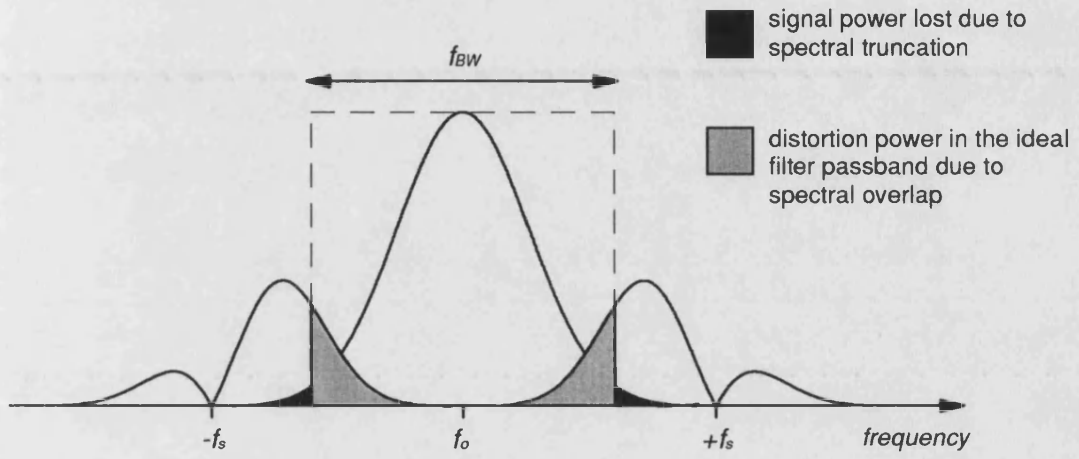

Figure 3.15: *Aliasing of the modulated signal*

For baseband sampling, Nyquist's well-known rule is that, for separation of wanted and aliased spectra to allow an ideal baseband rectangular lowpass filter to reconstruct the original signal, f_s must be greater than twice the highest frequency component of the baseband signal. In the case of the precise phase modulator, ideal bandpass filtering should be able to reconstruct the required signal providing f_s is greater than the modulated bandwidth (Note: not the unmodulated bandwidth), i.e.:

$$f_s \geq f_{BW} \qquad (3.74)$$

where f_{BW} is the bandwidth of the modulated signal. However, in theory the

modulated bandwidth of an angle-modulated signal is infinite, but due to the nature of Bessel functions that dictate sideband amplitude, the modulated spectra tails off both sides of the carrier to an arbitrarily negligible amplitude. It will be necessary for a given modulated spectrum to choose a filter bandwidth to include as much of the modulated spectrum as possible without undue distortion, but constrained by the introduction of greater distortion due to spectral overlap appearing in the filter passband. Choice of baseband sampling frequency is dictated by the tolerable amount of spectral overlap distortion that can be allowed. However, increase in the sample frequency increases the data transmission rate required to convey the modulating signal between transmitter sites and there will be constraints of desirable sampling frequencies, both in terms of cost and compatibility with available systems.

The power spectral density of an F.M. signal has two limiting forms, obtained by considering very small and very large frequency deviations of the carrier. The case for small frequency deviations or *quasi-linear* analysis is best shown from the spectrum of a P.M. signal. As was shown in the case of the Armstrong modulation in the second chapter, if deviation $\Delta\theta$ is low, the approximation can be made that:

$$e_{pm}(t) \approx E_o\{\cos 2\pi f_o t - \Delta\theta m(t)\sin 2\pi f_o t\} \qquad (3.75)$$

where *m(t)* is a general modulating signal (rather than just a sinusoid) and $|m(t)| \leq 1$. If is easily shown from standard results that the Fourier transform of the above is:

$$\boldsymbol{F}\{e_{pm}(t)\} = \frac{E_o}{2}\{\delta(f-f_o)+\delta(f+f_o)+j\Delta\theta(M(f-f_o)+M(f+f_o))\} \qquad (3.76)$$

where:

$$M(f) = \boldsymbol{F}\{m(t)\} \qquad (3.77)$$

Thus the power spectral density (P.S.D.) of the signal is:

$$P(f) = \frac{E_o^2}{4}\left\{\delta(f - f_o) + \delta(f + f_o) + \Delta\theta^2\left(M_p(f - f_o) + M_p(f + f_o)\right)\right\} \qquad (3.78)$$

where $M_p(f)$ is the P.S.D. of $m(t)$. This analysis is then easily modified for the F.M. case by noting that all that is required is the integration (or de-emphasis) of the modulating signal $m(t)$ prior to modulation. This has no effect on the necessary bandwidth required to transmit the signal if the baseband is bandlimited to a frequency f_{max}.

Since the spectrum of the phase-modulated output is effectively that of the baseband (both positive and negative frequency) linearly translated by the carrier frequency f_o, then if the baseband has a unit amplitude rectangular P.S.D. bandlimited to f_{max}, the positive frequency P.S.D. of the modulated signal is shown in figure 3.16.

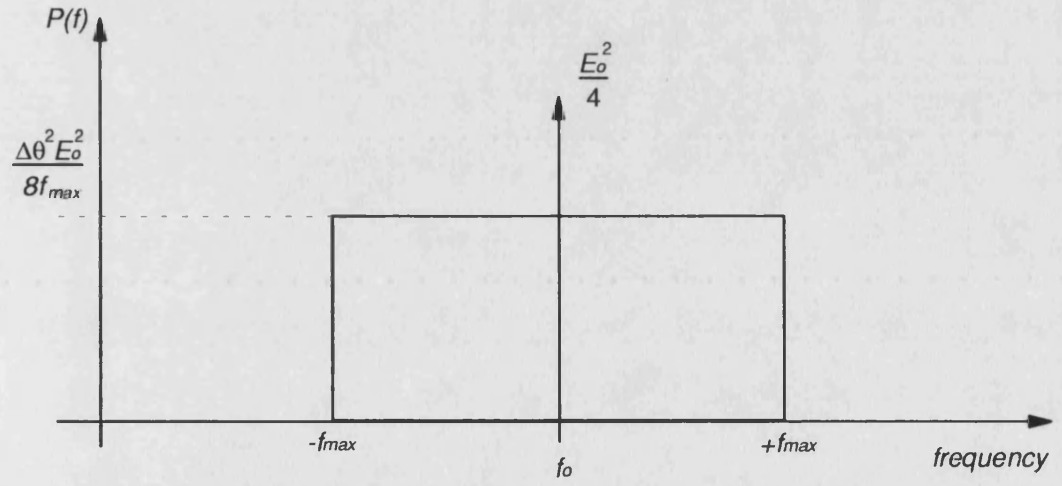

Figure 3.16: *Power spectral density of narrowband phase modulation*

The P.S.D. is thus similar to the A.M. case and thus the required bandwidth is $2f_{max}$. The sampling frequency for recovery of the desired signal by ideal bandpass filtering is then:

$$f_s \geq 2f_{\max} \qquad (3.79)$$

i.e. the baseband Nyquist rate. There are no conditions of frequency deviation

and baseband bandwidth that will allow the use of a lower f_s without introducing a degree of distortion into the recovered signal.

In the case for large frequency deviations (relative to the baseband bandwidth) or *quasi-static* analysis, the power spectral density *P(f)* of the F.M. signal is estimated by considering the carrier as slowly moving in the frequency domain as dictated by the modulating signal. Roughly speaking, the longer the carrier dwells at a particular frequency, the greater the P.S.D. at that frequency. If the mean power measured at a frequency f_1 in a narrowband of δf is p_1, then:

$$P(f_1) \approx \frac{p_1}{\delta f} \qquad (3.80)$$

If a voltage v_1 of the modulating waveform causes a frequency output at a frequency f_1, then the proportion of time that the frequency will be in the narrow band δf around f_1 will be proportional to the amount of time that the modulating signal spends in the voltage range δf around v_1. It follows that the P.S.D. of the *modulated* signal will be proportional to the amplitude probability density distribution of the *modulating* signal and must be scaled such that:

$$\int_{-\infty}^{\infty} P(f)df = \frac{E_o^2}{2} \qquad (3.81)$$

i.e., the total power in the frequency domain must be the same as the total power in the time waveform. In order to assess the bandwidth occupied by a random modulating signal such as speech, assuming a modulating signal *m(t)* of Gaussian noise of power p_i with a probability density function (P.D.F.):

$$P.D.F.\{m(t)\} = \frac{e^{-m^2/2p_i}}{\sqrt{2\pi p_i}} \qquad (3.82)$$

the quasi-static approach implies that the P.S.D. of the F.M. signal is also Gaussian and by analogy:

$$P(f) = \frac{E_o^2}{4} \frac{1}{\sqrt{2\pi\Delta f_{rms}}} \left\{ e^{-(f-f_o)^2/2\Delta f_{rms}} - e^{-(f+f_o)^2/2\Delta f_{rms}} \right\} \qquad (3.83)$$

where f_{rms} is the root mean square frequency deviation of the carrier. Thus the positive frequency P.S.D. is shown in figure 3.17.

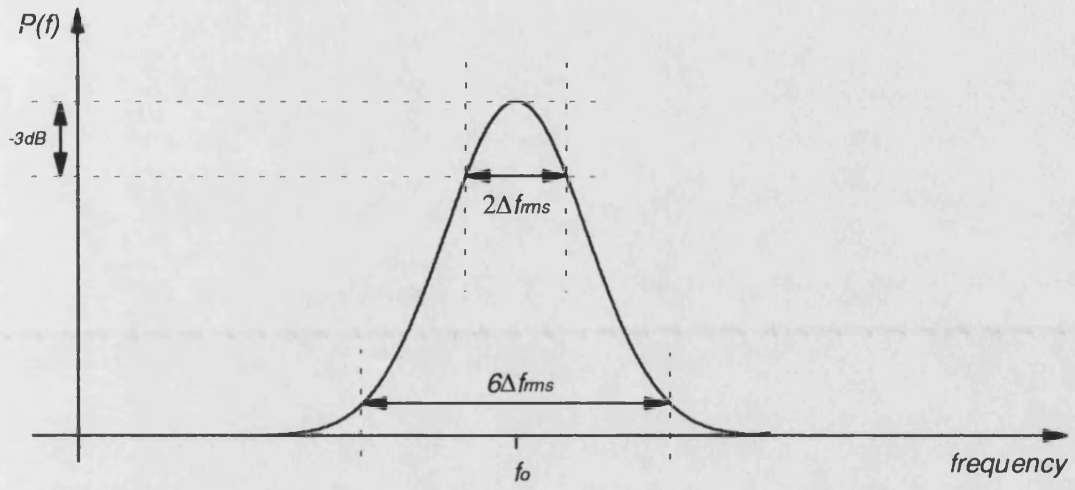

Figure 3.17: *Power spectral density of wideband frequency modulation*

However, as shown in [1] this is only a good approximation to the P.S.D. of the F.M. wave for large frequency deviations. A common choice for the ratio of peak to r.m.s. frequency deviation in F.M. systems is 3. This ratio ensures that the instantaneous frequency deviation only exceeds the bounds $f_o \pm \Delta f$ for 0.1% of the time. Bandlimiting to these constraints results in what is held to be negligible distortion of the signal. Thus, for large frequency deviations a necessary bandwidth of $6\Delta f_{rms}$ or $2\Delta f$ is required and thus the sampling frequency f_s must be bound to:

$$f_s \geq 2\Delta f \qquad (3.84)$$

The combination of the two cases for large and small frequency deviations results in the well-known empirical formula, *Carson's Rule* for the modulated bandwidth f_{BW} where the peak frequency deviation is Δf and modulating signal bandwidth is f_{max}:

$$f_{BW} \geq 2(f_{\max} + \Delta f) \qquad (3.85)$$

and thus an empirical rule for the required sampling frequency is:

$$f_s \geq 2(f_{\max} + \Delta f) \qquad (3.86)$$

or:

$$f_s \geq f_{NYQ} + 2\Delta f \qquad (3.87)$$

where f_{NYQ} is the baseband Nyquist sampling rate (i.e. $2f_{max}$). However, Carson's Rule is only accurate for the extreme cases discussed above and over-estimates the bandwidth for intermediate frequency deviations (i.e. those in most practical F.M. systems) by a significant amount. Thus a better guide is required for the sampling rate required for a particular peak frequency deviation.

Evaluation of the power spectral density for intermediate frequency deviations is possible through calculation of the autocorrelation function of the modulated signal and its relation to the autocorrelation function of the modulating signal. Graphs of the P.S.D. of F.M. by bandlimited Gaussian processes of zero mean are given by Roberts [6] for both conventional F.M. and pre-emphasised F.M.

However, the shape of the P.S.D. is not as important as the power contained in the tails of the P.S.D. at frequencies away from the carrier. This will give a measure of the required bandwidth f_{BW} for transmission without undue distortion and, as required in this case, the amount of distortion power in the filter passband due to the aliased R.F. spectra. If the spectral envelope $H(f)$ is neglected and the filter bandwidth set to the Nyquist rate $f_s/2$ then the power lost in truncation of the required spectrum is the same as the distortion power in the passband due to the R.F. aliasing (assuming the P.S.D. of the required signal is symmetric about f_o and that only a negligible amount of power appears beyond the other edge of the filter cut-off) as shown in figure 3.18.

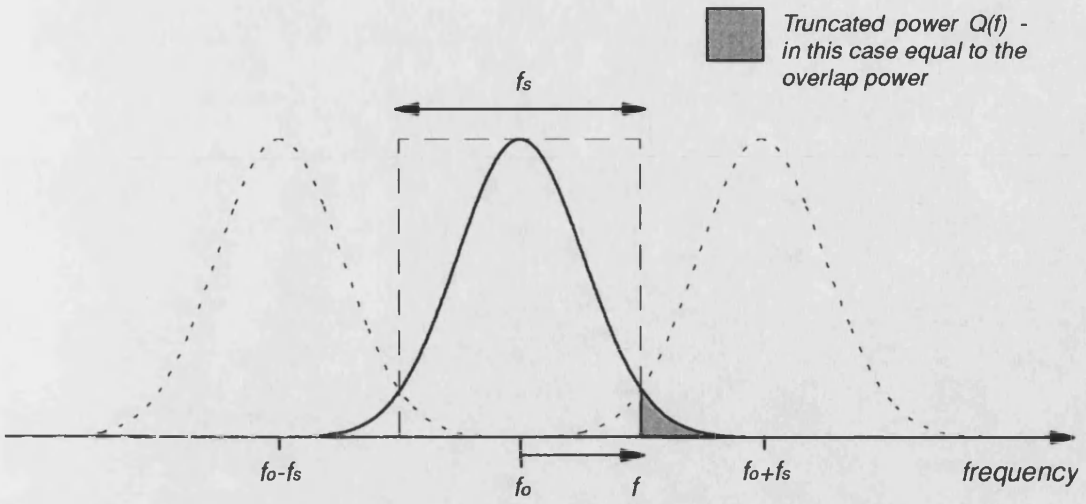

Figure 3.18: *Spectral geometry for the assessment of necessary sampling rate*

Ideally, what is required is an estimate for the fraction of the total power that exists beyond a frequency f away from the carrier as shown. Blachman [7,8] has developed limits on the remaining fraction of the power outside a frequency f in the tail of the P.S.D. of an F.M. signal with bandlimited Gaussian modulation. The bounds are in the form of inequalities due to the nature of their derivation from treating the P.S.D. as a probability distribution function and relating the power in the tail to moments of the spectrum. If $Q(f)$ is the fraction of the total power in the tail beyond frequency f away from the carrier, then rewriting the given spectral bounds from Blachman, the bounds given are the *Chebychev* bound:

$$Q(f) \leq \frac{\Delta f_{rms}^2}{2f^2} \qquad (3.88)$$

the 2^{nd} *moment of spectrum* bound:

$$Q(f) \leq \frac{\Delta f_{rms}^4 + \frac{1}{2}\Delta f_{rms}^2 \Delta f_{\max}^2}{3\Delta f_{rms}^4 + \Delta f_{rms}^2 \Delta f_{\max}^2 - 2\Delta f_{rms}^2 f^2 + f^4} \qquad (3.89)$$

the 4^{th} *moment of spectrum* bound:

$$Q(f) \leq \frac{\left(3\Delta f_{rms}^2 + \Delta f_{rms}^2\right)\Delta f_{\max}^2}{2f^4} \tag{3.90}$$

and the *Chernoff* bound derived by Blachman [7]:

$$Q(f) \leq \left(\frac{e}{2}\frac{\Delta f_{rms}^2}{f f_{\max}^2}\right)^{\frac{f}{f_{\max}}} \tag{3.91}$$

If the bound is set that:

$$Q(f_s/2) \leq \zeta \tag{3.92}$$

then ζ is the fraction of the power outside the filter bandwidth and thus half the total distortion power of the spectral overlap. By normalising the resulting bounds, the following relations between the required normalised sampling frequency (f_s/f_{NYQ}) and the normalised peak frequency deviation ($\Delta f/f_{NYQ}$) are obtained (note that f_s/f_{NYQ} represents the increase relative to the conventional baseband rate, but since $f_{NYQ}=2f_{max}$, $\Delta f/f_{NYQ}$ represents the peak frequency deviation in terms of the baseband bandwidth). From Carson's rule:

$$\frac{f_s}{f_{NYQ}} = 1 + \frac{2\Delta f}{f_{NYQ}} \tag{3.93}$$

from the Chebychev bound:

$$\frac{f_s}{f_{NYQ}} = \sqrt{\frac{2}{9\zeta}}\frac{2\Delta f}{f_{NYQ}} \tag{3.94}$$

from the 4th moment of spectrum bound:

$$\frac{f_s}{f_{NYQ}} = \sqrt[4]{\frac{8}{27\zeta}\left(\frac{2\Delta f}{f_{NYQ}}\right)^4 + \frac{2}{9\zeta}\left(\frac{2\Delta f}{f_{NYQ}}\right)^2} \tag{3.95}$$

and the Chernoff bound:

$$\frac{\Delta f}{f_{NYQ}} = \sqrt{\frac{9}{2e}\left(\frac{f_s}{f_{NYQ}}\right)^4 \zeta^{f_{NYQ}/f_s}} \qquad (3.96)$$

The 2nd moment of spectrum bound does not yield such a workable expression. However, by substitution of the normalised parameters the following is derived which can be evaluated by a software successive approximation method:

$$\zeta = \frac{16\left(\frac{\Delta f}{f_{NYQ}}\right)^4 + 18\left(\frac{\Delta f}{f_{NYQ}}\right)^2}{48\left(\frac{\Delta f}{f_{NYQ}}\right)^4 + 36\left(\frac{\Delta f}{f_{NYQ}}\right)^2 - 72\left(\frac{\Delta f}{f_{NYQ}}\right)^2\left(\frac{f_s}{f_{NYQ}}\right)^4 + 81\left(\frac{f_s}{f_{NYQ}}\right)^4} \qquad (3.97)$$

The above relations are plotted for ζ=1% in figure 3.19.

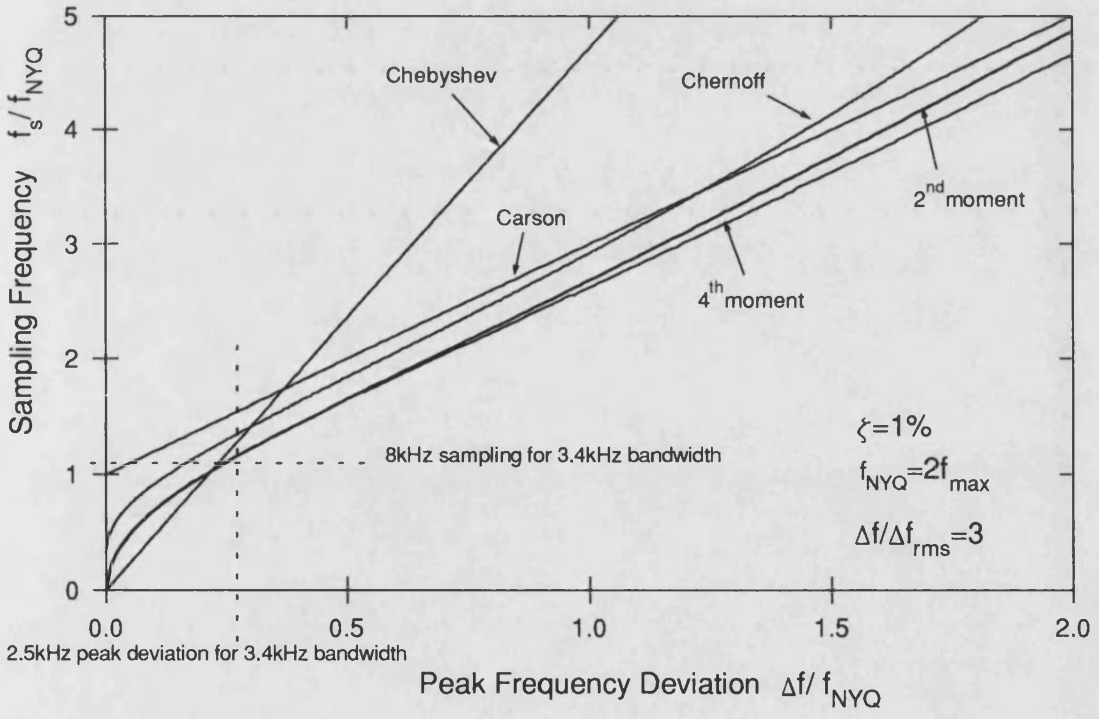

Figure 3.19: *Increase in normalised sampling frequency required by increase in normalised peak frequency deviation*

The Chebychev bound vastly over-estimates the bandwidth expansion beyond

small deviations. Shown on the graph is the operating point chosen for the prototype modulator. By accepting the restriction of operating at the standard speech sampling frequency of 8kHz (in order to maintain compatibility with existing P.C.M. networks) and bandlimiting the audio to 3.4kHz, a peak frequency deviation of 2.5kHz should be possible with only a small degree of in-band distortion. Since I.F. crystal filters are available with suitably sharp cut-offs of bandwidth ±3.75kHz, 2.5kHz will be taken as the maximum peak deviation that can be generated and that increase in deviation must be implemented by frequency multiplication.

However, it is important to note that sinusoidal testing of the modulator will yield distortion results that are in excess of the distortion that would be experienced by a complex modulating waveform (such as speech) since superposition of the sinusoidal performance is not valid unless the deviation is very small. The above results were all derived for random modulating signals where the power spectral density of the modulated signal is a continuous function of frequency. Aliased signal power in the sinusoidal case will result in greater distortion due to the unavoidable folding back of Bessel sidebands into the I.F. filter passband since a greater proportion of the total signal power would be folded back than in the complex modulation case. For example, in the case of a 3kHz modulating tone, the second order Bessel sidebands of the first set of aliased sidebands appear at ±2kHz spacing either side of the carrier and at a deviation of 2.5kHz the magnitude of these aliased components ($J_2(0.83)$) is around 0.08 whereas the first required sidebands at ±3kHz ($J_1(0.83)$) are only four times larger at around 0.36. This neglects the third order alias sidebands that appear at ±1kHz spacing either side of the carrier whose magnitude ($J_1(0.83)$) is about 0.01. The effect of the non-linear combination of the sidebands to form the demodulated signal as is described in the next section is such that

the two sets of sidebands create a set of intermodulation products giving a misleading distortion reading. Thus measurements of transmitter linearity would be expected to rise towards the high frequency end of the baseband frequency range at higher deviations (although within the bounds set in this section) as higher order Bessel sidebands of greater magnitude are unavoidably present in the Nyquist passband.

3.9. Baseband distortion due to zero-order hold

Provided the sampling rate constraints of the previous section are observed, ideal bandpass filtering of the Precise Phase Modulator output will remove all unwanted R.F. components produced by sampling the modulated phase (assuming a single component carrier). However, the remaining signal has the spectrum of the output from an ideal phase modulator modified by a "*sinx/x*" type spectral envelope. Considering the positive frequency envelope only, this spectral function has the form derived in section 3.6:

$$H(f) = \frac{\sin \pi(f - f_o)T_s}{\pi(f - f_o)T_s} e^{-j\pi(f-f_o)T_s} \qquad (3.98)$$

The phase term is linear in frequency and merely represents a delay of $T_s/2$. The magnitude term however could cause distortion in the output signal. Since the sampling frequency f_s must be greater than the modulated bandwidth of the signal to avoid R.F. distortion (see previous section) the range of interest of *H(f)* is small and the departure from a flat response is not great. Figure 3.20 shows that the envelope falls by a small amount at both edges of the ideal rectangular bandpass filtering. The greatest spectral "*droop*" occurs at the edge of the ideal filter bandwidth, i.e. the filter of bandwidth f_{BW} equal to the sampling rate f_s. This maximum droop is given by:

$$|H(f_o - f_s/2)| = 0.6366|H(f_o)| \qquad (3.99)$$

i.e. a drop of just under 4dB. The effect on the resulting signal can be assessed by considering the case of a sinusoidal modulated F.M. signal filtered by *H(f)*, i.e. assuming all alias components removed by ideal filtering). If the ideal signal is:

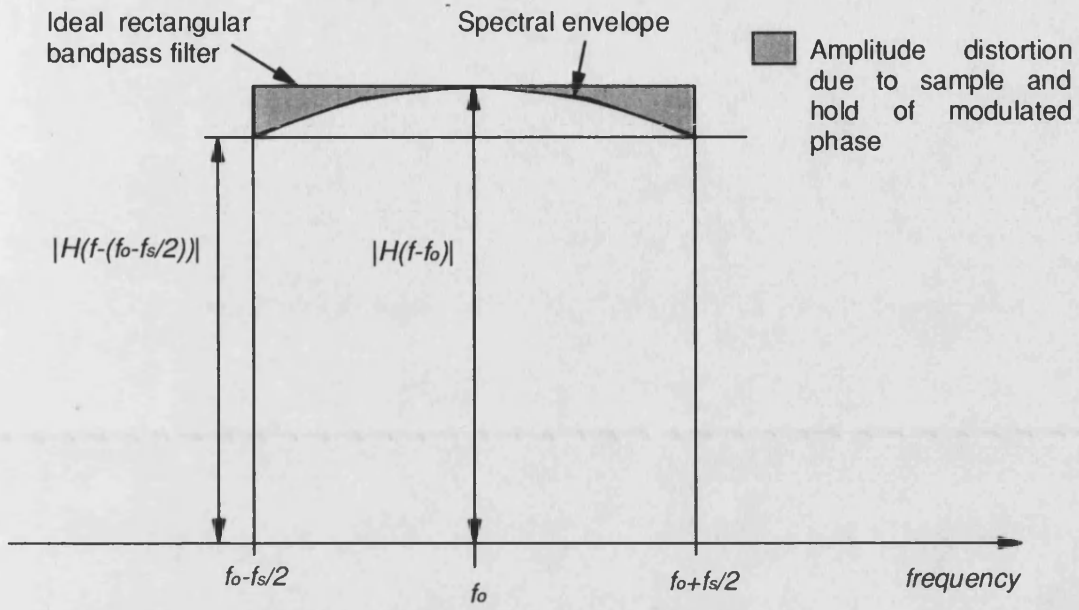

Figure 3.20: *Spectral distortion due to zero-order hold*

$$e_{fm}(t) = \mathrm{Re}\left[E_o e^{j(2\pi f_o t + \frac{\Delta f}{f_m}\sin 2\pi f_m t)} \right] \qquad (3.100)$$

then it can be rewritten (as noted earlier) in the form:

$$e_{fm}(t) = \mathrm{Re}\left[E_o \sum_{n=-\infty}^{+\infty} J_n(\beta) e^{j2\pi(f_o + nf_m)t} \right] \qquad (3.101)$$

The resultant signal $e'_{fm}(t)$ after passing through a filter whose magnitude and phase characteristics are known can easily be obtained by modifying the magnitude and phase of each frequency component by the magnitude and phase of the filter function at that frequency. Thus applying the spectral envelope *H(f)* in this manner:

$$e'_{fm}(t) = E_o \sum_{n=-\infty}^{+\infty} J_n(\beta) \frac{\sin(\pi n f_m T_s)}{\pi n f_m T_s} \cos(2\pi(f_o + n f_m)t - \pi n f_m T_s) \qquad (3.102)$$

Expanding this into frequency components that are in phase and quadrature to the carrier component:

$$e'_{fm}(t) = E_o \left[\cos 2\pi f_o t \sum_{n=-\infty}^{+\infty} J_n(\beta) \frac{\sin(\pi n f_m T_s)}{\pi n f_m T_s} \cos(2\pi n f_m t - \pi n f_m T_s) \right.$$

$$\left. - \sin 2\pi f_o t \sum_{n=-\infty}^{+\infty} J_n(\beta) \frac{\sin(\pi n f_m T_s)}{\pi n f_m T_s} \sin(2\pi n f_m t - \pi n f_m T_s) \right] \qquad (3.103)$$

This can be equated to a signal with the same carrier frequency, but amplitude and phase fluctuations of the form:

$$e'_{fm}(t) = E_o \left[A(t) \cos(2\pi f_o t + \Psi(t)) \right] \qquad (3.104)$$

where the amplitude *A(t)* is given by:

$$A^2(t) = \left(E_o \sum_{n=-\infty}^{+\infty} J_n(\beta) \frac{\sin(\pi n f_m T_s)}{\pi n f_m T_s} \sin(2\pi n f_m t - \pi n f_m T_s) \right)^2$$

$$+ \left(E_o \sum_{n=-\infty}^{+\infty} J_n(\beta) \frac{\sin(\pi n f_m T_s)}{\pi n f_m T_s} \cos(2\pi n f_m t - \pi n f_m T_s) \right)^2 \qquad (3.105)$$

and the phase $\Psi(t)$ is given by:

$$\Psi(t) = \tan^{-1} \left\{ \frac{\sum_{n=-\infty}^{+\infty} J_n(\beta) \frac{\sin(\pi n f_m T_s)}{\pi n f_m T_s} \sin(2\pi n f_m t - \pi n f_m T_s)}{\sum_{n=-\infty}^{+\infty} J_n(\beta) \frac{\sin(\pi n f_m T_s)}{\pi n f_m T_s} \cos(2\pi n f_m t - \pi n f_m T_s)} \right\} \qquad (3.106)$$

Examining the amplitude function first, if the spectral envelope were not present, *A(t)* simplifies very rapidly to unity since the sum of all $J_n(\beta)$ is unity. However, the time varying amplitude that results from the spectral envelope is of the same

form as the modulating signal (i.e. sinusoidal) for small β relative to the sampling frequency. However, its amplitude is found to increase with increasing β and eventually *A(t)* can have zero values. Theoretically, an ideal hard limiter should remove all amplitude fluctuations, but practical limiters will fail for carrier zeros giving rise to distortion in a real receiver similar to that due to carrier zeros resulting from multi-transmitter operation as discussed in Chapter 2. The amplitude function *A(t)* was analysed for varying frequency deviation and modulating frequency and the variation in the resulting peak amplitude ripple is shown for a sampling frequency of 8kHz in figure 3.21 (where normalised ripple of unity indicates an amplitude zero).

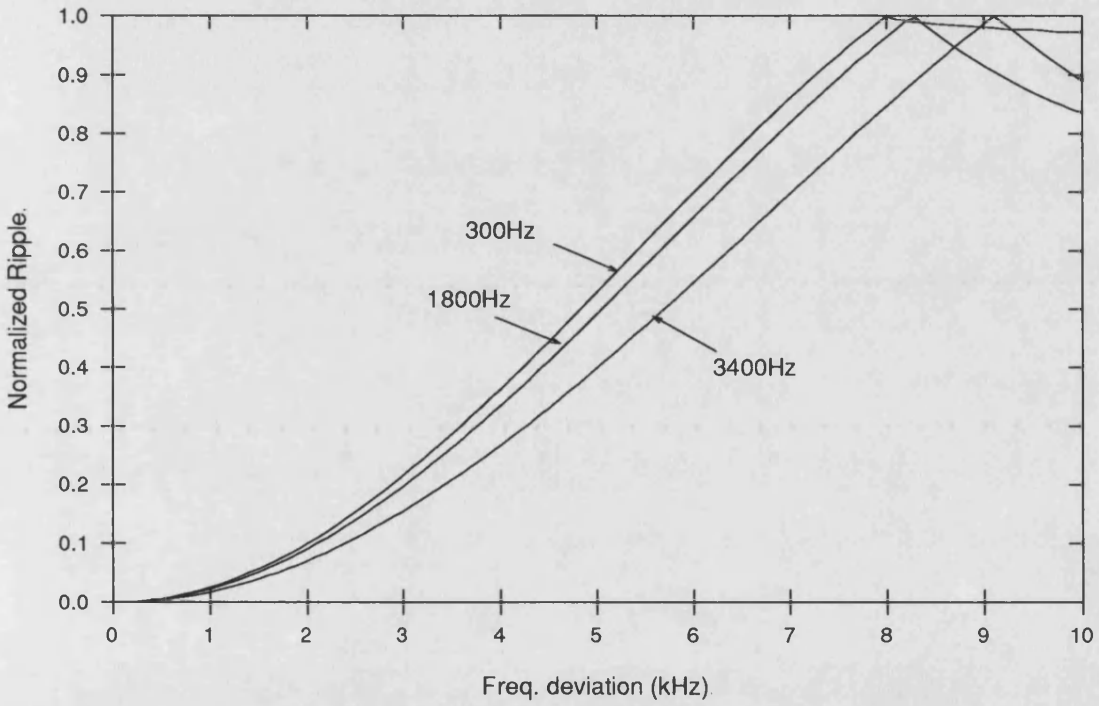

Figure 3.21: *Variation in amplitude ripple with modulating frequency and frequency deviation at an 8kHz sampling frequency*

Thus the amplitude zeros occur at frequency deviations around the sampling frequency f_s, which is in excess of the frequency deviation that can be used for a given sampling frequency if bandpass filtering is to isolate the required signal from alias R.F. components as discussed earlier. Thus practical hard limiting

should remove any amplitude fluctuations that may be encountered.

After demodulation in an F.M. receiver, the normalised output $e_o(t)$ is given by (neglecting the constant term due to the carrier):

$$e_o(t) = \frac{d\Psi(t)}{dt} = \frac{d}{d\left\{\frac{\alpha}{\beta}\right\}}\left\{\tan^{-1}\left\{\frac{\alpha}{\beta}\right\}\right\}\frac{d\left\{\frac{\alpha}{\beta}\right\}}{dt}$$

$$= \frac{\beta\alpha' - \beta'\alpha}{\alpha^2 + \beta^2} \qquad (3.107)$$

where:

$$\alpha = \sum_{n=-\infty}^{+\infty} J_n(\beta)\frac{\sin(\pi n f_m T_s)}{\pi n f_m T_s}\sin(2\pi n f_m t - \pi n f_m T_s) \qquad (3.108)$$

$$\alpha' = \sum_{n=-\infty}^{+\infty} J_n(\beta)\frac{\sin(\pi n f_m T_s)}{\pi n f_m T_s}2\pi n f_m \cos(2\pi n f_m t - \pi n f_m T_s) \qquad (3.109)$$

$$\beta = \sum_{n=-\infty}^{+\infty} J_n(\beta)\frac{\sin(\pi n f_m T_s)}{\pi n f_m T_s}\cos(2\pi n f_m t - \pi n f_m T_s) \qquad (3.110)$$

$$\beta' = -\sum_{n=-\infty}^{+\infty} J_n(\beta)\frac{\sin(\pi n f_m T_s)}{\pi n f_m T_s}2\pi n f_m \sin(2\pi n f_m t - \pi n f_m T_s) \qquad (3.111)$$

Further algebraic manipulation does not reduce the complexity of the above expressions, however, since the magnitude of $H(f)$ is an even function of n, i.e.:

$$|H(f - nf_m)| = |H(f + nf_m)| \qquad (3.112)$$

and the phase of $H(f)$ is an odd function of n, i.e.:

$$\arg\{H(f_o - nf_m)\} = -\arg\{H(f_o + nf_m)\} \qquad (3.113)$$

then it can be shown that [5] equation 3.106 reduces to:

$$\Psi(t) = \tan^{-1}\left\{\frac{2\sum_{n=0}^{+\infty} J_n(\beta)\frac{\sin(\pi n f_m T_s)}{\pi n f_m T_s}\sin(2\pi n f_m t - \pi n f_m T_s)}{J_o(\beta) + 2\sum_{n=1}^{+\infty} J_n(\beta)\frac{\sin(\pi n f_m T_s)}{\pi n f_m T_s}\cos(2\pi n f_m t - \pi n f_m T_s)}\right\}^2 \qquad (3.114)$$

by changing the variable $2\pi f_m t$ to $2\pi f_m t+\pi$ it can be shown [5] that:

$$\Psi(2\pi f_m t) = -\Psi(2\pi f_m t + \pi) \qquad (3.115)$$

and thus the output of the F.M. receiver will contain only odd harmonics of the modulating signal as distortion terms (differentiation of the phase merely emphasizes higher order components). The effect of these may not be serious since the departure of *H(f)* from a flat magnitude response over the range of interest is not excessive and the worst areas are those near the edge of the filter passband where the magnitude and significance of the sidebands are reduced due to the nature of Bessel functions that define their magnitude.

To assess the distortion, the receiver output $e_o(t)$ was calculated by computer as further analytical simplification is complex and probably fruitless. The distortion of the simulated signal was determined by Fast Fourier Transform techniques (see Appendix A) for various values of the principal parameters: sampling rate, peak deviation and modulating frequency as shown in figure 3.22. With the maximum usable frequency deviation of 2.5kHz for 8kHz sampling the amount of distortion is small and can be neglected. The distortion shown in figure 3.22 is calculated without baseband lowpass filtering described in appendix A and in practice, harmonics of the higher frequencies (particularly approaching the maximum audio frequency) would fall outside the filter passband resulting in

less output distortion. Amplitude equalisation of the form $1/H(f)$ is difficult to implement in this narrow bandpass situation and misequalisation of the I.F. path from transmitter to transmitter results in further distortion as examined later (whereas the spectral envelope is identical at every transmitter).

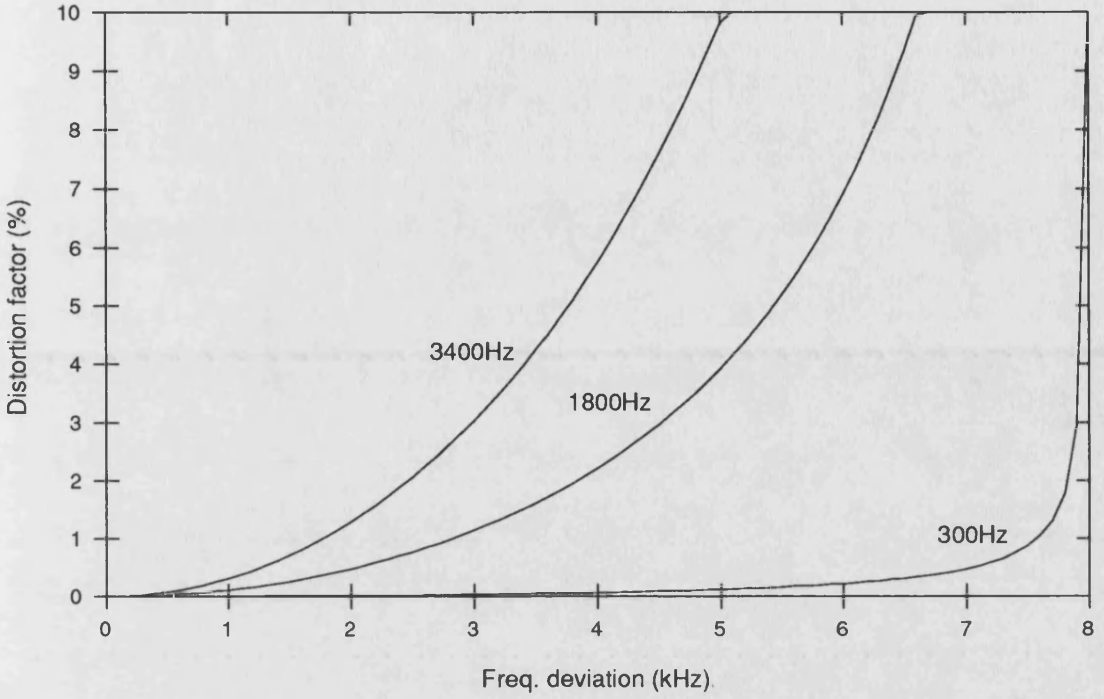

Figure 3.22: *Distortion in the received signal due to the spectral envelope at various modulating frequencies and frequency deviation at an 8kHz sampling rate*

3.10. Distortion due to phase quantisation

In all the previous analysis the effect of quantising the modulated phase has been neglected. As discussed in section 3.4, the phase-shift produced by the modulator can only take a finite number of values (2^N, where N is the number of bits used in the modulation process). Since the modulator can produce phase-shifts of between 0 and 2π radians, this fixes the smallest possible phase-shift to $\delta\theta$ given by:

$$\delta\theta = \pi 2^{1-N} \ radians \qquad (3.116)$$

The quantisation steps are linearly spaced from *0* and 2π radians and thus if decision levels for quantisation are chosen midway between quantisation levels, there will exist errors in the modulated phase in the range of $\pm\delta\theta$. This is no different to conventional analogue-to-digital conversion of signals, but the precise phase modulator effectively has no constraint on input signal range. As discussed earlier, the phase difference between *0* and 2π radians is indistinguishable in isolation and thus the phase shift of the modulator is not limited to 2^N quantisation levels as would signals in conventional analogue-to-digital conversion. By using modulating signal samples of *M* bits and ignoring the most significant *M-N* bits in the modulation process any peak phase deviation can be achieved: the maximum phase shift θ_{max} available from M-bit modulating samples and an N-bit modulator is therefore:

$$\theta_{\max} = 2^{M-N} 2\pi \ radians \qquad (3.117)$$

This is in contrast to conventional analogue-to-digital conversion where the conversion range and the conversion resolution are both limited by the number of bits used in the converter, *N*. In this case, range and resolution can be independently set.

Considering the effect of phase quantisation noise on the modulated output, an angle modulated signal with quantised (but not sampled) phase can be written:

$$e_q(t) = E_o \cos\left(2\pi f_o t + \varphi(t) + \varepsilon_q(t)\right) \qquad (3.118)$$

where $\varepsilon_q(t)$ represents the instantaneous phase quantisation error. Expanding the above:

$$e_q(t) = E_o\left[\cos\varepsilon_q(t)\cos\left(2\pi f_o t + \varphi(t)\right) - \sin\varepsilon_q(t)\sin\left(2\pi f_o t + \varphi(t)\right)\right] \qquad (3.119)$$

Now, both sine and cosine can be expanded as power series as:

$$\cos\theta = 1 + \sum_{n=1}^{\infty}(-1)^n \frac{\theta^{2n}}{(2n)!} \qquad \sin\theta = \sum_{n=1}^{\infty}(-1)^{2n-1} \frac{\theta^{2n-1}}{(2n-1)!} \tag{3.120}$$

Thus equation 3.119 can be written as:

$$e_q(t) = E_o \cos(2\pi f_o t + \varphi(t)) + E_o \sum_{n=1}^{\infty}(-1)^n \frac{\varepsilon_q^{2n}(t)}{(2n)!} \cos(2\pi f_o t + \varphi(t))$$

$$+ E_o \sum_{n=1}^{\infty}(-1)^{2n-1} \frac{\varepsilon_q^{2n-1}(t)}{(2n-1)!} \sin(2\pi f_o t + \varphi(t)) \tag{3.121}$$

This represents the original signal without distortion plus a series of in-phase distortion terms plus a series of quadrature distortion terms. Without quantisation of phase both series vanish. If phase quantisation error $\varepsilon_q(t)$ is small, any power of $\varepsilon_q(t)$ will be very small if not negligible. In assessing the amount of distortion present in the modulated signal, by far the most significant terms are the first terms in each series, since the powers of $\varepsilon_q(t)$ quickly become negligible. Thus equation 3.121 becomes (neglecting powers of $\varepsilon_q(t)$of two or more):

$$e_q(t) = E_o \cos(2\pi f_o t + \varphi(t)) - E_o \varepsilon_q(t) \sin(2\pi f_o t + \varphi(t)) \tag{3.122}$$

i.e. the ideal modulated signal plus the quadrature of the ideal modulated signal multiplied by the quantisation noise. The mean square quantisation distortion is thus:

$$N_q = \overline{\{E_o \varepsilon_q(t) \sin(2\pi f_o t + \varphi(t))\}^2} \tag{3.123}$$

which gives:

$$N_q = \overline{\varepsilon_q^2(t)} \frac{E_o^2}{2} \tag{3.124}$$

It is a well known result for fine linear quantisation of a signal that the mean square quantisation error is given by [1]:

$$\overline{\varepsilon_q^2(t)} = \frac{\Delta^2}{12} \qquad (3.125)$$

where Δ is the quantisation step size: in this case $\delta\theta$ as defined in equation 3.116. Thus N_q becomes:

$$N_q = \frac{E_o^2}{2} \cdot \frac{\delta\theta^2}{12} = \frac{\pi^2 E_o^2}{3.2^{2N+1}} \qquad (3.126)$$

The power spectral density of N_q, $P_n(f)$, will be basically broadband in nature though centred on the carrier frequency f_o, and satisfies the relation:

$$N_q = \int_{-\infty}^{\infty} P_n(f)df \qquad (3.127)$$

If this quantisation distortion is subjected to ideal impulse sampling the resulting aliased quantisation distortion spectrum is shown in figure 3.23.

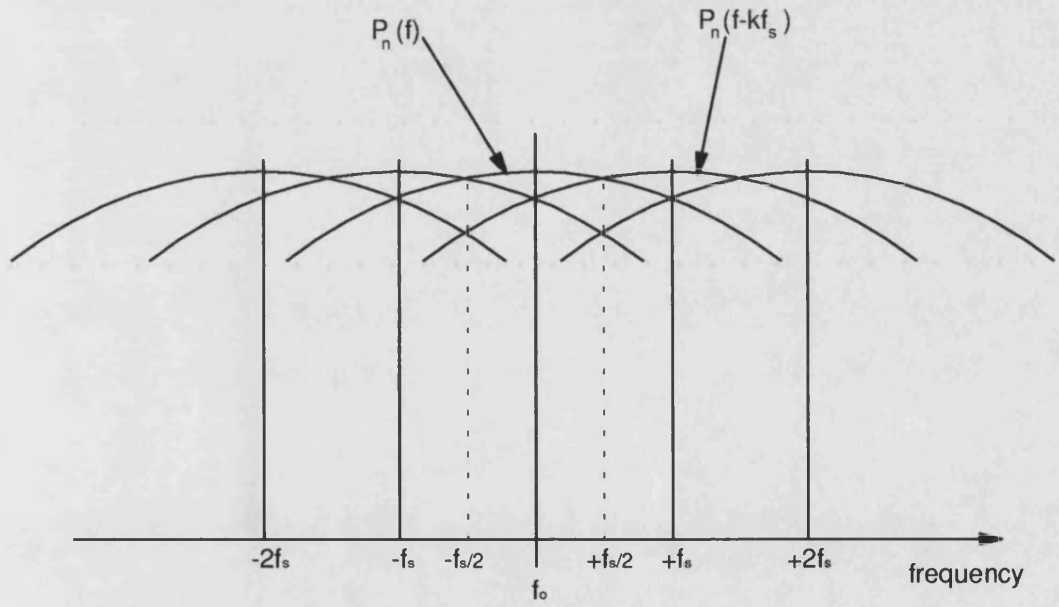

Figure 3.23: *Aliased quantisation distortion power spectral density*

The mean squared quantisation distortion output of an ideal bandpass filter of Nyquist bandwidth centred on the carrier frequency is then:

$$N'_q = \int_{f_o+f_s/2}^{f_o-f_s/2} P'_n(f)df \qquad (3.128)$$

However, since:

$$P'_n(f) = \sum_{k=-\infty}^{\infty} P_n(f - kf_s) \qquad (3.129)$$

then:

$$N'_q = \sum_{k=-\infty}^{\infty} \int_{f_o+f_s/2}^{f_o-f_s/2} P'_n(f - kf_s)df \qquad (3.130)$$

The symmetry due to aliasing allows the above to be rewritten as:

$$N'_q = \sum_{k=-\infty}^{\infty} \int_{kf_s+f_o+f_s/2}^{kf_s+f_o-f_s/2} P_n(f)df = \int_{-\infty}^{\infty} P_n(f)df \qquad (3.131)$$

and hence after sampling, the output mean square quantisation distortion after the bandpass filter is the same as the mean square quantisation distortion without filtering or sampling. Thus the effect of sampling and quantising the modulated phase of the carrier is to immerse the ideal modulated signal in random noise (providing the quantisation step size or modulator phase resolution is sufficiently fine) of approximately flat power spectral density, but bandlimited by the bandpass signal reconstruction filter. After transmission the signal will be subject to further channel noise which can also be thought of as bandlimited white noise and since it is entirely independent of the quantisation distortion the channel noise is additive to it. For now, the channel noise will be set to zero; its effects were considered earlier. If the bandlimited quantisation distortion is modelled by in-phase and quadrature noise components, the received I.F. signal is (without modulation):

$$e_{IF}(t) = E_o \cos 2\pi f_o t + n_I(t)\cos 2\pi f_o t + n_Q(t)\sin 2\pi f_o t \qquad (3.132)$$

No modulation is included in the above expression to reduce the complexity, but it should be noted that $n_I(t)$ and $n_Q(t)$ are only present with modulation. This expression is rewritten as:

$$e_{IF}(t) = \sqrt{(E_o + n_I(t))^2 + n_Q^2(t)} \cos\left(2\pi f_o t - \tan^{-1}\left\{\frac{n_Q(t)}{E_o + n_I(t)}\right\}\right) \qquad (3.133)$$

The amplitude fluctuations are removed by pre-discriminator limiting, the noise induced phase modulation is the quantity of interest:

$$n_\varphi(t) = \tan^{-1}\left\{\frac{n_Q(t)}{E_o + n_I(t)}\right\} \qquad (3.134)$$

It is a reasonable assumption for fine quantisation that $E_o > n_I(t)$ and $n_Q(t)/E_o$ is small, thus:

$$n_\varphi(t) \approx \frac{n_Q(t)}{E_o} \qquad (3.135)$$

If an F.M. discriminator is taken as a two stage process, i.e. first phase detection of the modulated signal and then ideal differentiation after detection, and the detector has a constant of *1 volt rad^{-1}*, the mean squared input to the differentiator is:

$$\overline{n_{\varphi o}^2(t)} = \frac{\overline{n_Q^2(t)}}{E_o^2} \quad volt^2 \qquad (3.136)$$

It can be shown that $\overline{n_Q^2(t)} = N_q'$, and since the power spectral density of the quantisation distortion prior to differentiation is taken to be flat:

$$P_n''(f) = \eta \qquad (3.137)$$

where:

$$\eta = \frac{N_q'}{E_o^2 BW_{IF}} \quad volts^2 Hz^{-1} \qquad (3.138)$$

A pure time differentiator has a transfer function given by:

$$H_{diff}(f) = j2\pi f \tag{3.139}$$

so the output power spectral density of the quantisation distortion from the discriminator is:

$$P_{no}(f) = \left|H_{diff}(f)\right|^2 P_n''(f) = 4\pi^2 f^2 P_n''(f) \tag{3.140}$$

Thus if the power spectral density of the quantisation distortion at the input to the discriminator is flat then the output quantisation distortion power spectral density is parabolic as shown in figure 3.24.

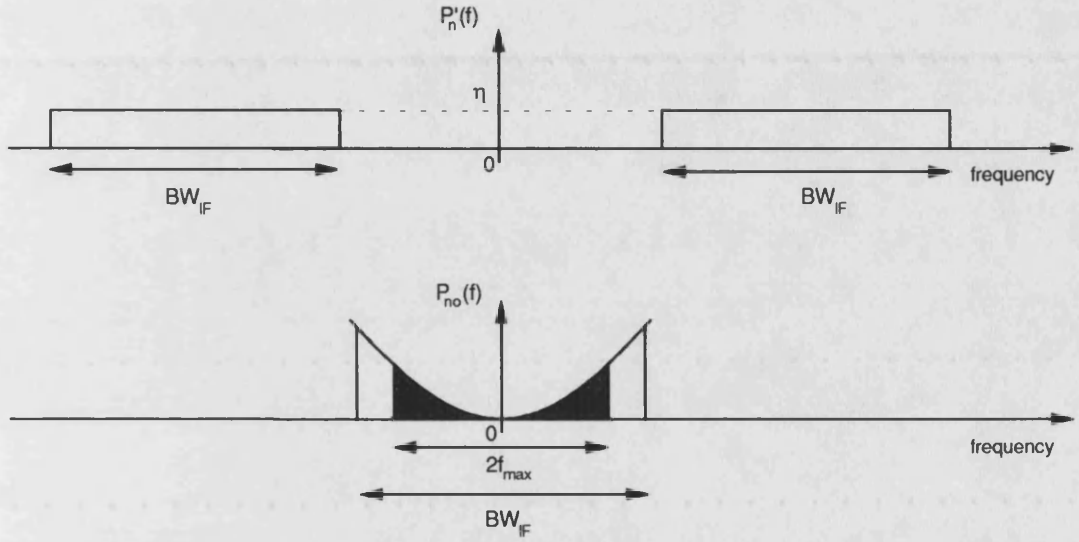

Figure 3.24: *Power spectral density of quantisation distortion in the receiver*

The mean-square quantisation distortion at the output of the discriminator can be found from (any lower cut-off of the receiver output audio is neglected due to parabolic shape of the power spectral density):

$$N_{qo} = \int_{-f_{max}}^{f_{max}} P_{no}(f)df = \frac{4\pi^2 N_q'}{E_o^2 BW_{IF}} \int_{-f_{max}}^{f_{max}} f^2 df \tag{3.141}$$

i.e.:

$$N_{qo} = \frac{8\pi^2 N'_q f_{\max}^3}{3E_o^2 BW_{IF}} \qquad (3.142)$$

The mean squared output signal from the F.M. discriminator is the mean squared frequency deviation from the carrier frequency. The case of sinusoidal modulated phase of the form $(\Delta f/f_m)\sin 2\pi f_m t$ the mean squared output is:

$$S_o = 2\pi^2 \Delta f^2 \qquad (3.143)$$

So the output signal to quantisation distortion ratio *SQDR* of the received signal is:

$$SQDR = \frac{S_o}{N_{qo}} = \frac{3\Delta f^2 E_o^2 BW_{IF}}{4 f_{\max}^3 N'_q} \qquad (3.144)$$

However, from earlier, the mean squared phase quantisation distortion is given by:

$$N'_q = N_q = \frac{E_o^2}{2} \cdot \frac{\delta\theta^2}{12} = \frac{\pi^2 E_o^2}{3.2^{2N+1}} \qquad (3.145)$$

Thus:

$$SQDR = \frac{9\Delta f^2 2^{2N-1} BW_{IF}}{\pi^2 f_{\max}^3} \qquad (3.146)$$

If $\Delta f/f_{\max}$ is the phase deviation β, then:

$$SQDR = 2^{2N} \frac{9\beta^2}{\pi^2} \left(\frac{BW_{IF}}{2f_{\max}} \right) \qquad (3.147)$$

where the term $BW_{IF}/2f_{max}$ represents the F.M. non-linear bandwidth expansion of the modulating signal. This expansion is related to β as shown earlier when considering the necessary sampling rate for a fixed frequency deviation and baseband bandwidth. Increased transmission bandwidth can be exchanged for improvement in signal-to-quantisation distortion ratio and figure 3.25 shows this. However, this is limited for a fixed sampling frequency by the maximum

allowable frequency deviation before excessive in-band sampling distortion occurs. Figure 3.25 shows the quantisation performance after reception with frequency deviation using the *fourth moment of spectrum* bound as the non-linear expansion term.

If pre-emphasis and de-emphasis are used in the transmitter and receiver respectively, then the mean-square quantisation distortion at the output of the discriminator is:

$$N_{qo} = \frac{4\pi^2 N_q'}{E_o^2 BW_{IF}} \int_{-f_{max}}^{f_{max}} |H_{DE}(f)|^2 f^2 df \qquad (3.148)$$

where $|H_{DE}(f)|^2$ is the de-emphasis characteristic. If over the range of interest the de-emphasis characteristic is:

$$H_{DE}(f) = \frac{1}{1 + jf/f_b} \qquad (3.149)$$

where f_b is the break frequency of the characteristic, then:

$$N_{qo} = \frac{4\pi^2 N_q'}{E_o^2 BW_{IF}} \int_{-f_{max}}^{f_{max}} \frac{f^2}{1 + f^2/f_b^2} df \qquad (3.150)$$

From tables [9], the indefinite integral in the above equation is:

$$f_b^2 \int \frac{f^2/f_b^2}{1 + f^2/f_b^2} df = f_b^3 \left(\frac{f}{f_b} - \tan^{-1}\left(\frac{f}{f_b} \right) \right) \qquad (3.151)$$

Thus:

$$N_{qo} = \frac{8\pi^2 N_q'}{E_o^2 BW_{IF}} f_b^3 \left(\frac{f_{max}}{f_b} - \tan^{-1}\left(\frac{f_{max}}{f_b} \right) \right) \qquad (3.152)$$

Hence with pre-emphasis and de-emphasis of the audio, the signal-to-quantisation distortion ratio at the receiver output is:

$$SQDR_{PRE/DE} = \frac{3\Delta f^2 2^{2N-1} BW_{IF}}{\pi^2 f_b^3 \left(\frac{f_{max}}{f_b} - \tan^{-1}\left(\frac{f_{max}}{f_b} \right) \right)} \qquad (3.153)$$

Figure 3.25 also shows $SQDR_{PRE/DE}$ with a break frequency of 100Hz. This allows emphasis of the full audio bandwidth from 300Hz to 3.4kHz. A useful improvement in *SQDR* results and thus the performance of an 8-bit modulator for narrowband systems of interest (2.5kHz and 5kHz deviation) is adequate in terms of the signal-to-quantisation ratio performance of 65-70 dB.

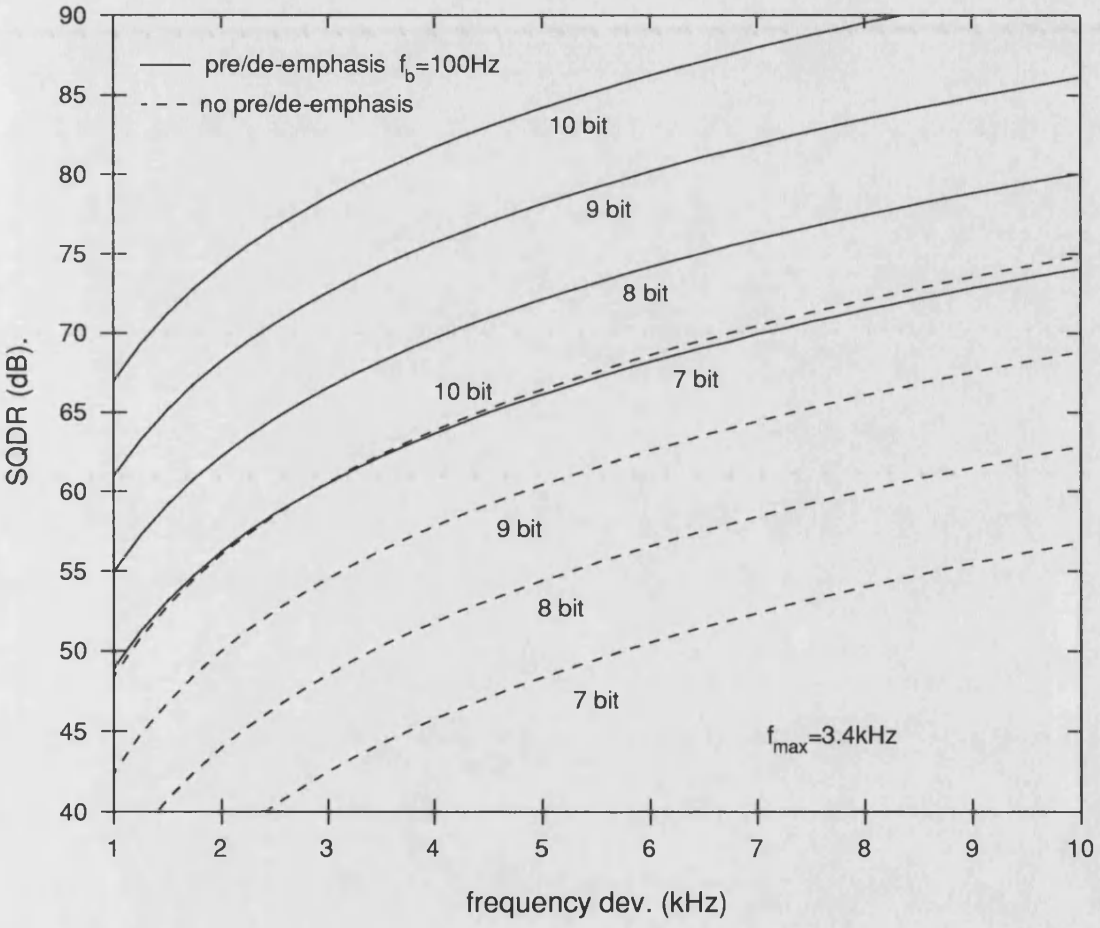

Figure 3.25: *Variation of signal-to-phase quantisation distortion ratio with frequency deviation and pre/de-emphasis*

3.11. Distortion due to variation in transmitter characteristics

The use of a Precise Phase Modulator should allow exact matching of the modulation of any number of F.M. transmitters. However, variability in the characteristics of circuits through which the modulated signal passes after the modulator, but before radiation, will cause variation in the radiated field from transmitter to transmitter. The most likely cause of variation is the I.F. filter used in each transmitter to remove alias R.F. components. In order to assess the variation allowable in the transmission characteristics of the I.F. filtering and other circuits and filters in the transmitter, the synchronous field at the mobile due to transmitters with different characteristics must be examined. The distortion that will result in the mobile receiver output can then be assessed. Figure 3.26 shows the response of a typical I.F. crystal filter.

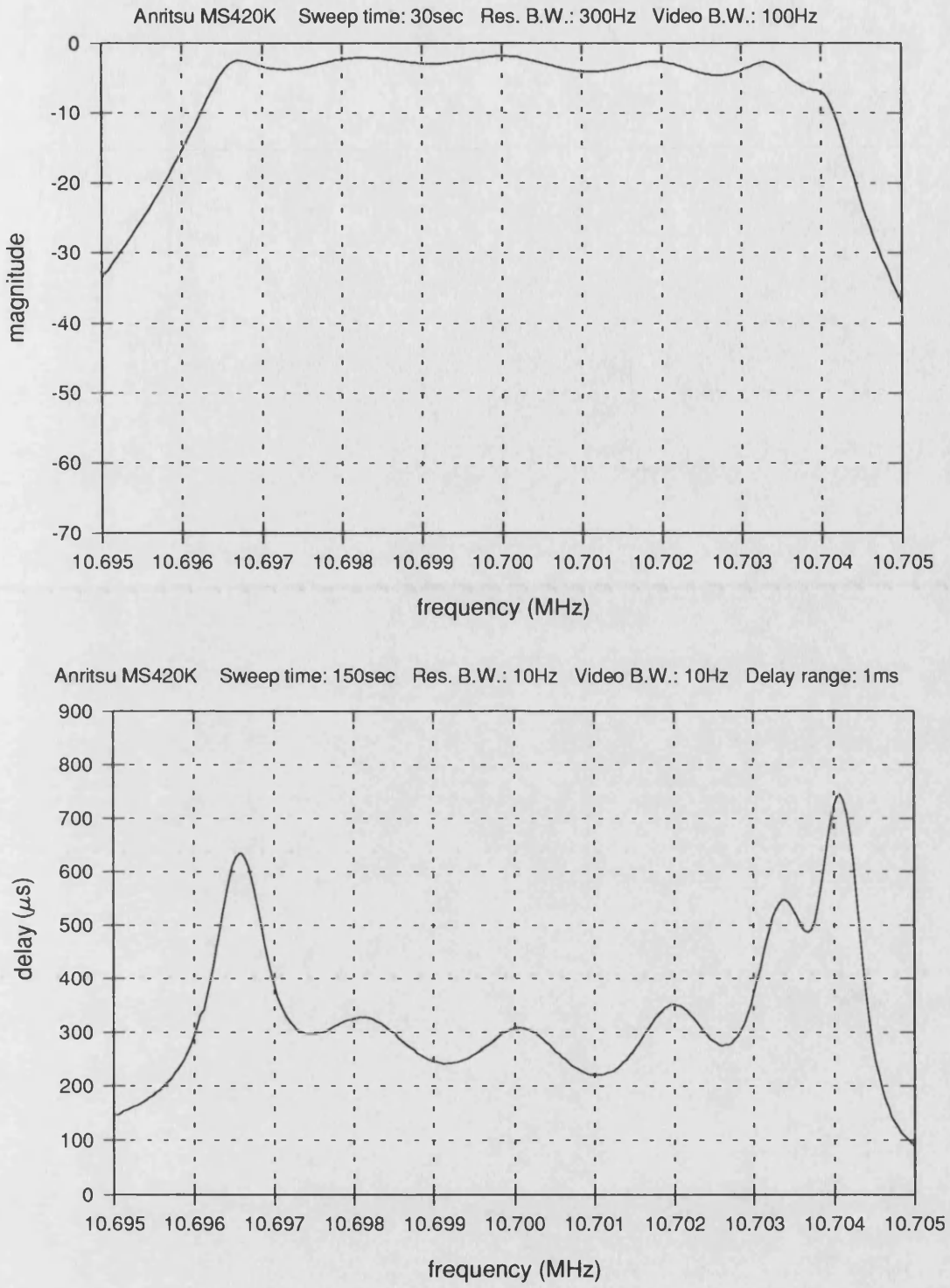

Figure 3.26: *Passband response of a IF crystal filter IQD 10.7H7.5A*

Consider two transmitters, A and B whose amplitude and delay characteristics are shown in figure 3.27.

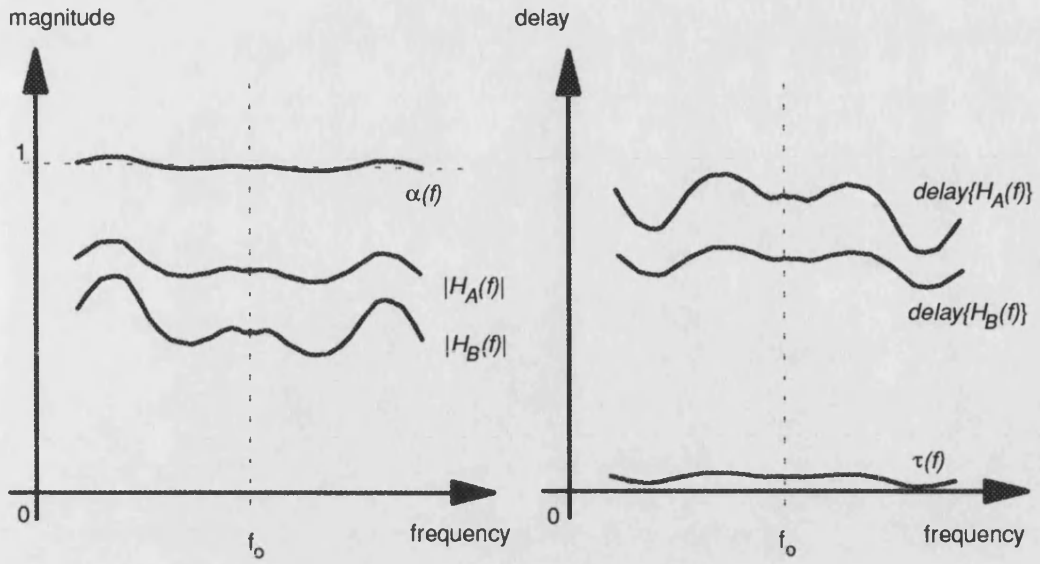

Figure 3.27: *Differential characteristics of IF crystal filter passband response*

The synchronous field resulting from the two transmitters can be assessed more simply by considering one transmitter to be ideal and the other to have differential characteristics, i.e. the ideal modulated signal after transmission through a network of amplitude $\alpha(f)$ and delay $\tau(f)$ where:

$$\alpha(f) = \frac{|H_A(f)|}{|H_B(f)|} \qquad (3.154)$$

and:

$$\tau(f) = delay[H_A(f)] - delay[H_B(f)] \qquad (3.155)$$

If the synchronous field at the mobile is $e(t)$ for the case where there is no relative propagation delay and matched carrier frequencies and sinusoidal modulation then:

$$e(t) = e_{FM}(t) + ke'_{FM}(t) \qquad (3.156)$$

where k is the relative propagation loss ($0 \le k \le 1$) and:

$$e_{FM}(t) = E_o \cos(2\pi f_o t + \beta \sin 2\pi f_m t) \qquad (3.157)$$

The term $e'_{FM}(t)$ is $e_{FM}(t)$ modified by the transmission parameters $\alpha(f)$ and $\tau(f)$.

Since (as discussed earlier) $e_{FM}(t)$ can be rewritten as:

$$e_{FM}(t) = E_o \sum_{n=-\infty}^{\infty} J_n(\beta)\cos(2\pi(f_o + nf_m)t) \qquad (3.158)$$

Thus if:

$$\alpha(f_o + nf_m) = \alpha_n \qquad (3.159)$$

and:

$$\tau(f_o + nf_m) = \tau_n \qquad (3.160)$$

then by modifying the amplitude and phase of each sideband as for the spectral envelope analysis:

$$e_{FM}(t) = E_o \sum_{n=-\infty}^{\infty} \alpha_n J_n(\beta)\cos(2\pi(f_o + nf_m)t + \gamma_n) \qquad (3.161)$$

where the phase γ_n is given by:

$$\gamma_n = 2\pi(f_o + nf_m)\tau_n \qquad (3.162)$$

By the same vector combination method as used earlier in this chapter the magnitude of the resultant field at the mobile is:

$$|e(t)|^2 = \left(E_o \sum_{n=-\infty}^{+\infty} \sqrt{1 + 2\alpha_n k\cos\gamma_n + \alpha_n^2 k^2}\, J_n(\beta)\sin(2\pi n f_m t + \Psi_n) \right)^2$$

$$+ \left(E_o \sum_{n=-\infty}^{+\infty} \sqrt{1 + 2\alpha_n k\cos\gamma_n + \alpha_n^2 k^2}\, J_n(\beta)\cos(2\pi n f_m t + \Psi_n) \right)^2 \qquad (3.163)$$

where:

$$\Psi_n = \tan^{-1}\left\{ \frac{\alpha_n k \sin\gamma_n}{1 + \alpha_n k\cos\gamma_n} \right\} \qquad (3.164)$$

This amplitude fluctuation can be removed by hardlimiting in the receiver provided $|e(t)| = 0$ has no solutions for the range of interest of system parameters such as f_m, β, k, α_n and γ_n. However, the phase of the two transmitter field is:

$$\Phi(t) = \tan^{-1}\left\{\frac{\sum_{n=-\infty}^{+\infty}\sqrt{1+2\alpha_n k\cos\gamma_n+\alpha_n^2k^2}\,J_n(\beta)\sin(2\pi nf_m t+\Psi_n)}{\sum_{n=-\infty}^{+\infty}\sqrt{1+2\alpha_n k\cos\gamma_n+\alpha_n^2k^2}\,J_n(\beta)\cos(2\pi nf_m t+\Psi_n)}\right\} \quad (3.165)$$

The output of an ideal receiver is, as noted earlier, the time differential of the field phase, $\dot{\Phi}(t)$.

To examine the possible spread in transmission characteristics, three I.F. crystal filters (type *IQD10.7H7.5A* centre frequency *10.7MHz*, bandwidth *7.5kHz* and passband ripple *2dB*) were tested. The input /output impedances were matched to *50*Ω with single LC "L" network and the transmission characteristics of each filter were measured using the same matching components for each filter (in practice, the value of the matching components would also be subject to manufacturing tolerances). If the filter transmission characteristics of the filters are $H_A(f)$, $H_B(f)$ and $H_C(f)$, then normalizing to filter *A* the variation of characteristics are shown in figure 3.28, i.e., the magnitude ratios:

$$\frac{|H_B(f)|}{|H_A(f)|} \quad and \quad \frac{|H_C(f)|}{|H_A(f)|} \qquad (3.166)$$

and differential delays:

$$delay[H_B(f)] - delay[H_A(f)] \quad and \quad delay[H_C(f)] - delay[H_A(f)] \qquad (3.167)$$

To try and assess the level of distortion that varying degrees of mismatch produce, the mismatch of both amplitude and delay responses can be modeled by sinusoidal ripple on the mismatched filter, i.e. the amplitude responses:

$$|H_A(f-f_o)| = 1 \qquad (3.168)$$

$$|H_B(f-f_o)| = 1+\delta_{amp}\cos\frac{2\pi f}{\lambda} \qquad (3.169)$$

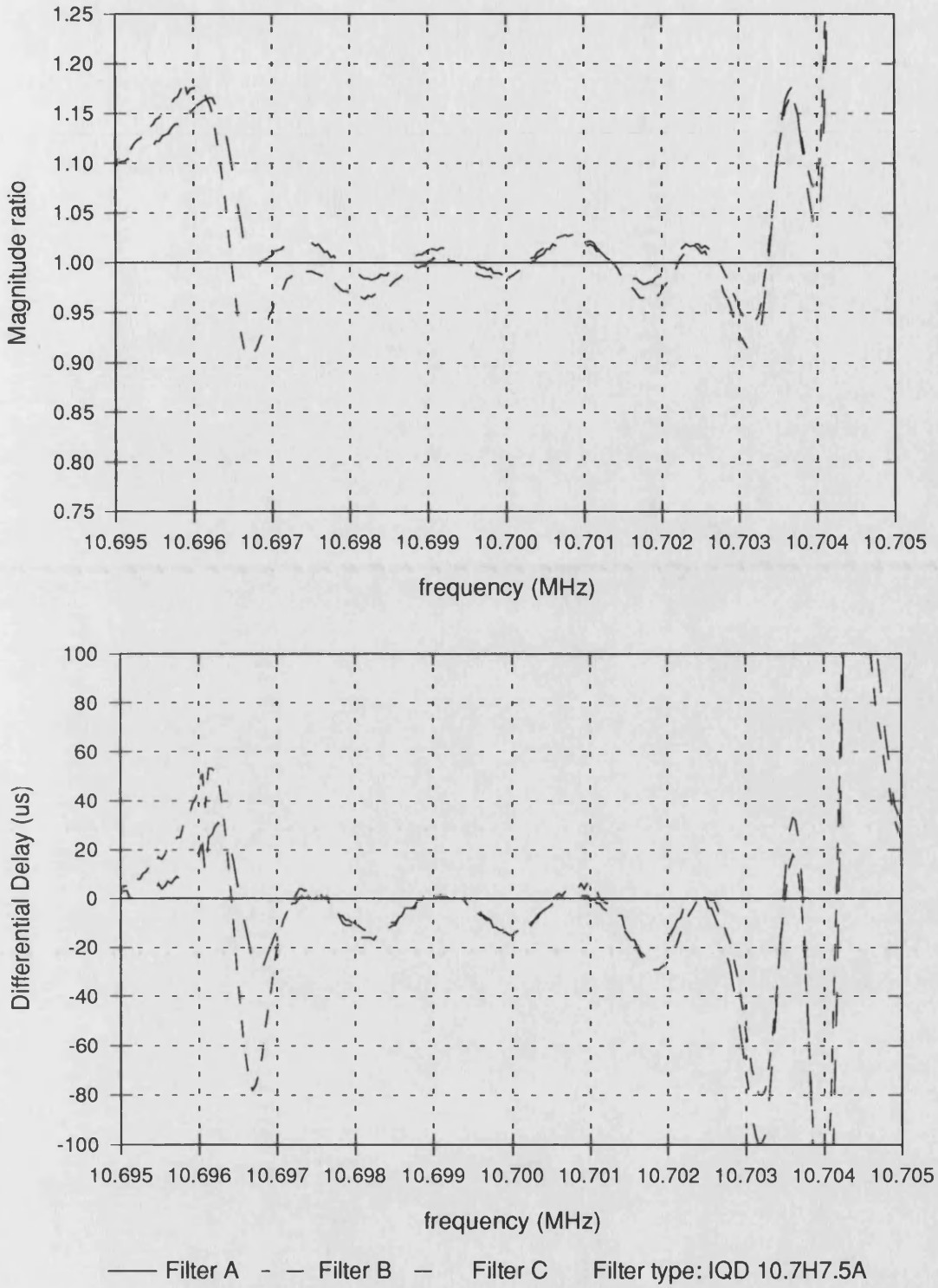

Figure 3.28: *Differential characteristics of three IF crystal filters*

where δ_{amp} is the peak amplitude of the ripple and λ is the ripple "*wavelength*" in

hertz. Similarly, the delays become:

$$delay\{H_A(f-f_o)\}=0 \qquad (3.170)$$

$$delay\{H_B(f-f_o)\}=\delta_{del}\cos\frac{2\pi f}{\lambda} \qquad (3.171)$$

where δ_{del} is the peak delay ripple.

From the measured variation in transmission characteristics, the variations can be characterized by two choices of ripple wavelength: one to model small variations over the passband of the filter and one to model the variations due to passband ripple of shorter wavelength characteristic to narrowband I.F. filters (note that any mean delay or amplitude difference will be indistinguishable from propagation loss and delay). For the filters used, suitable values of λ were taken as 16kHz and 1.8kHz. Thus, α_n and γ_n in equation 3.165 can be written as:

$$\alpha_n = 1+\delta_{amp}\cos\frac{2\pi n f_m}{\lambda} \qquad (3.172)$$

$$\tau_n = \delta_{del}\cos\frac{2\pi n f_m}{\lambda} \qquad (3.173)$$

The audio output $e_{af}(t)$ was calculated and the audio distortion factor calculated (see appendix A) for both values of λ across the audio band for the cases where there is amplitude mismatch and no delay mismatch, and no amplitude mismatch and delay mismatch, for varying amounts of ripple (δ_{amp} and δ_{del}). These results are shown in the following figures.

Comparison of figure 3.28 and the results in figures 3.29-3.33 shows that noticeable distortion may result from spread on filter characteristics and certainly the use of different manufacturer's filters is undesirable unless accurately specified. The short "wavelength" ripple due to the mismatch in passband ripple of the filter is the major cause of distortion with delay ripple mismatch causing more distortion than amplitude ripple mismatch. Thus in specifying and implementing the post-modulation anti-alias filtering, the short

"wavelength" delay ripple mismatch is the parameter most likely to causes excess distortion in the near equal field strength scenario.

However, the graphs presented give the worst case - that of equal carrier magnitudes - and is considerably better than that in existing quasi-synchronous F.M. schemes.

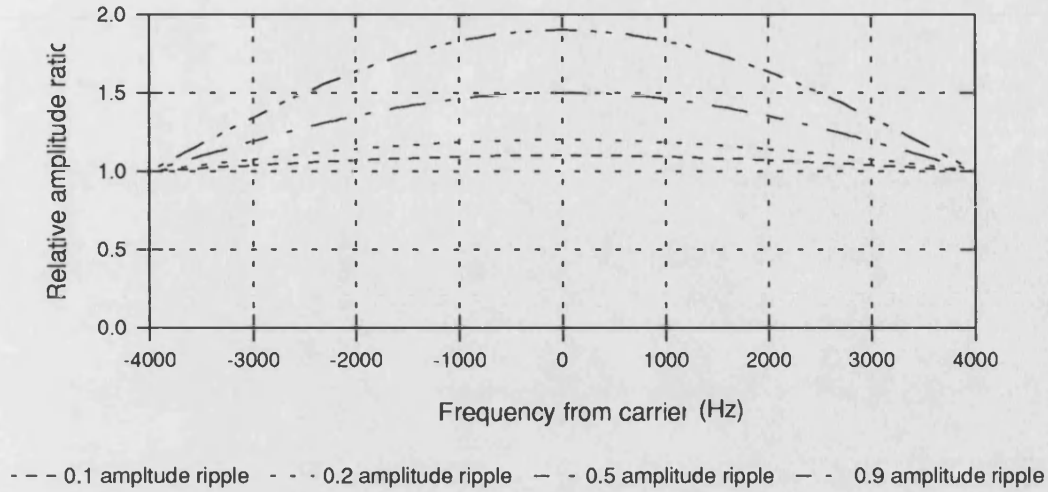

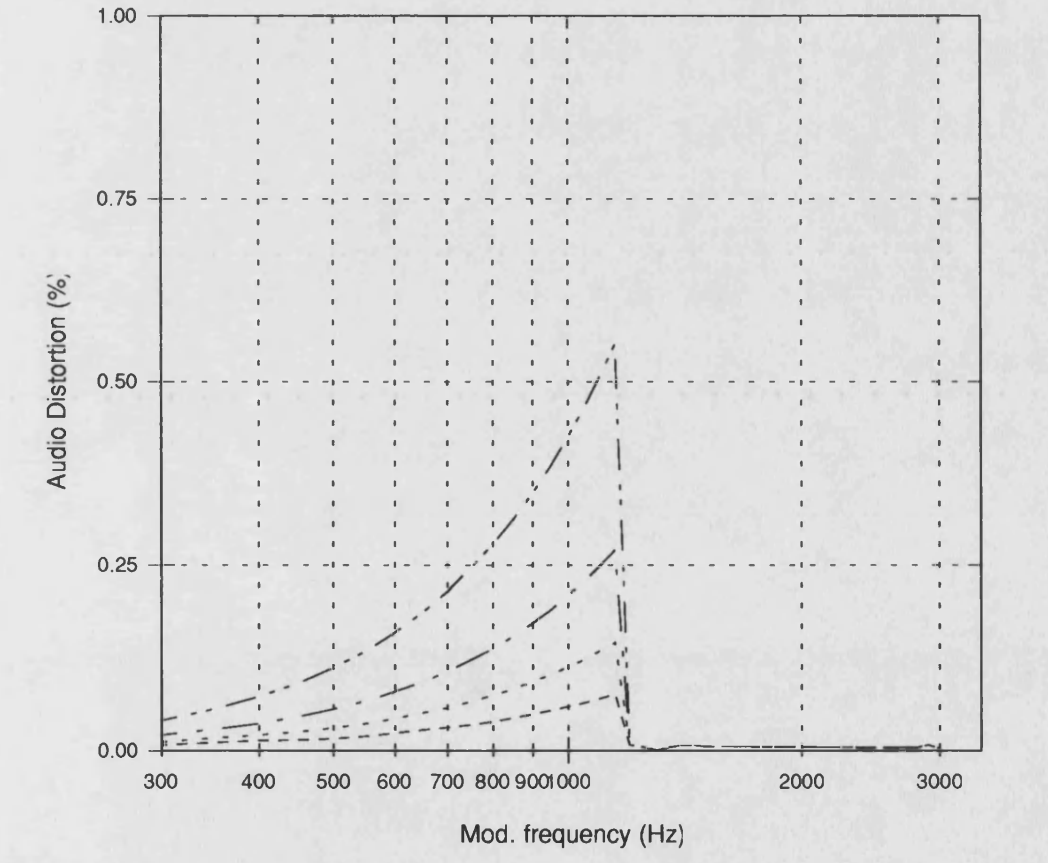

Figure 3.29: *Audio distortion in an ideal receiver due to amplitude mismatch*

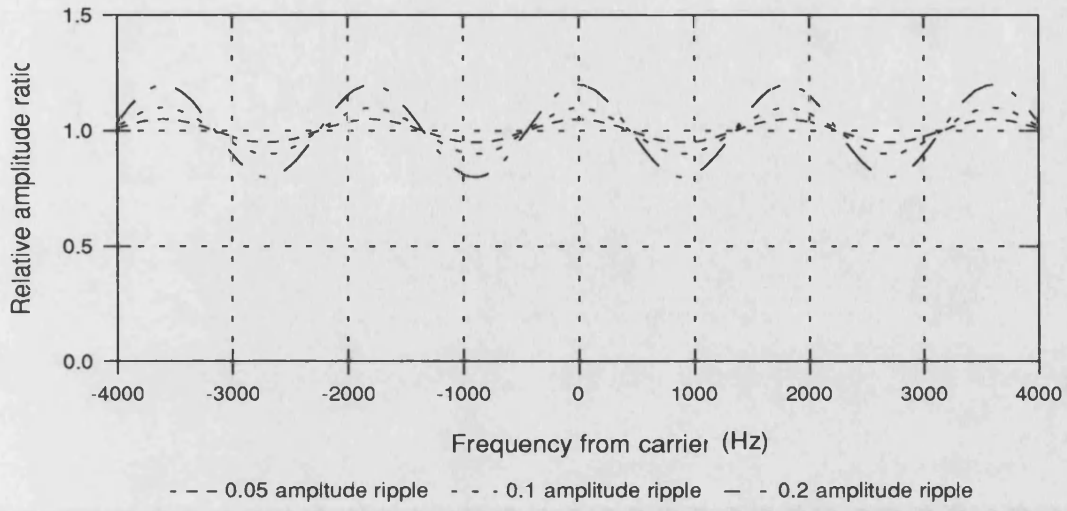

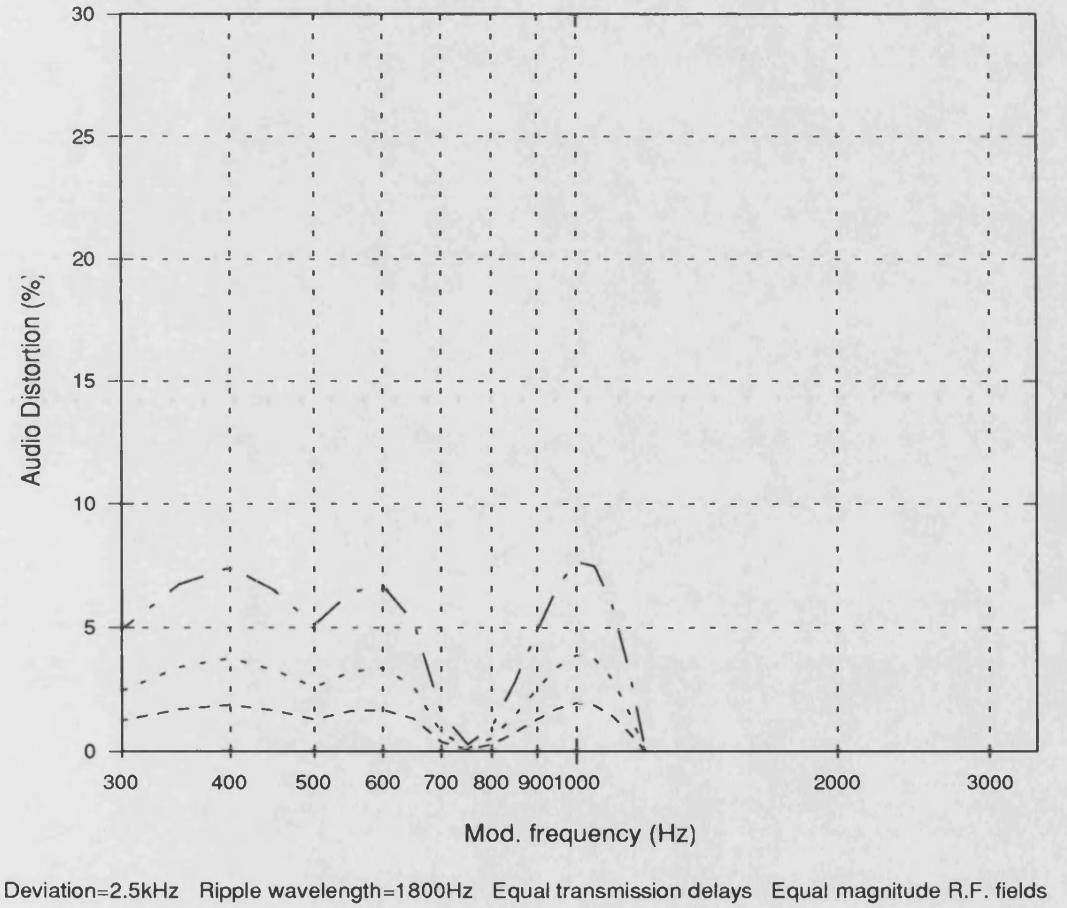

Figure 3.30: *Audio distortion in an ideal receiver due to amplitude mismatch*

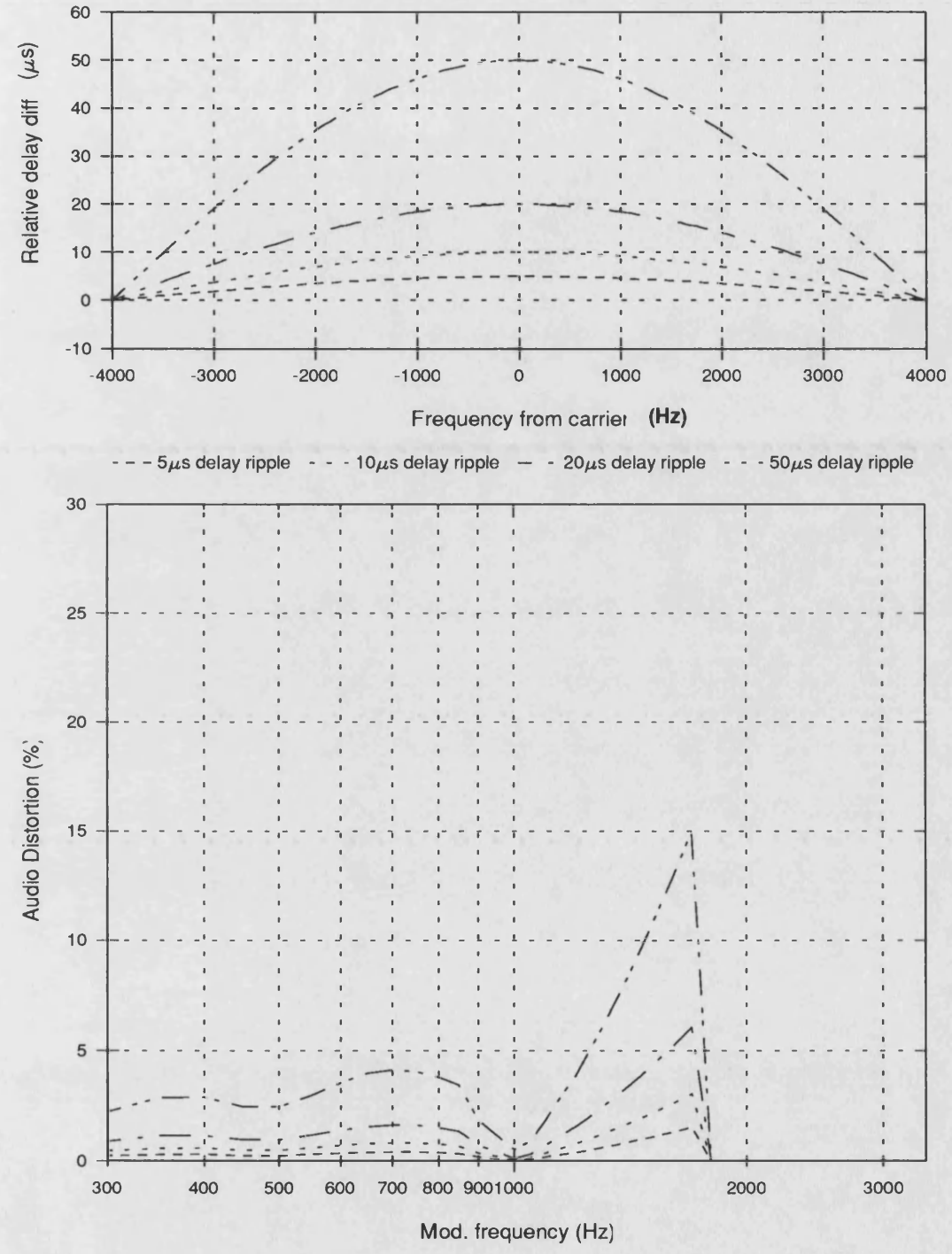

Figure 3.31: *Audio distortion in an ideal receiver due to delay mismatch*

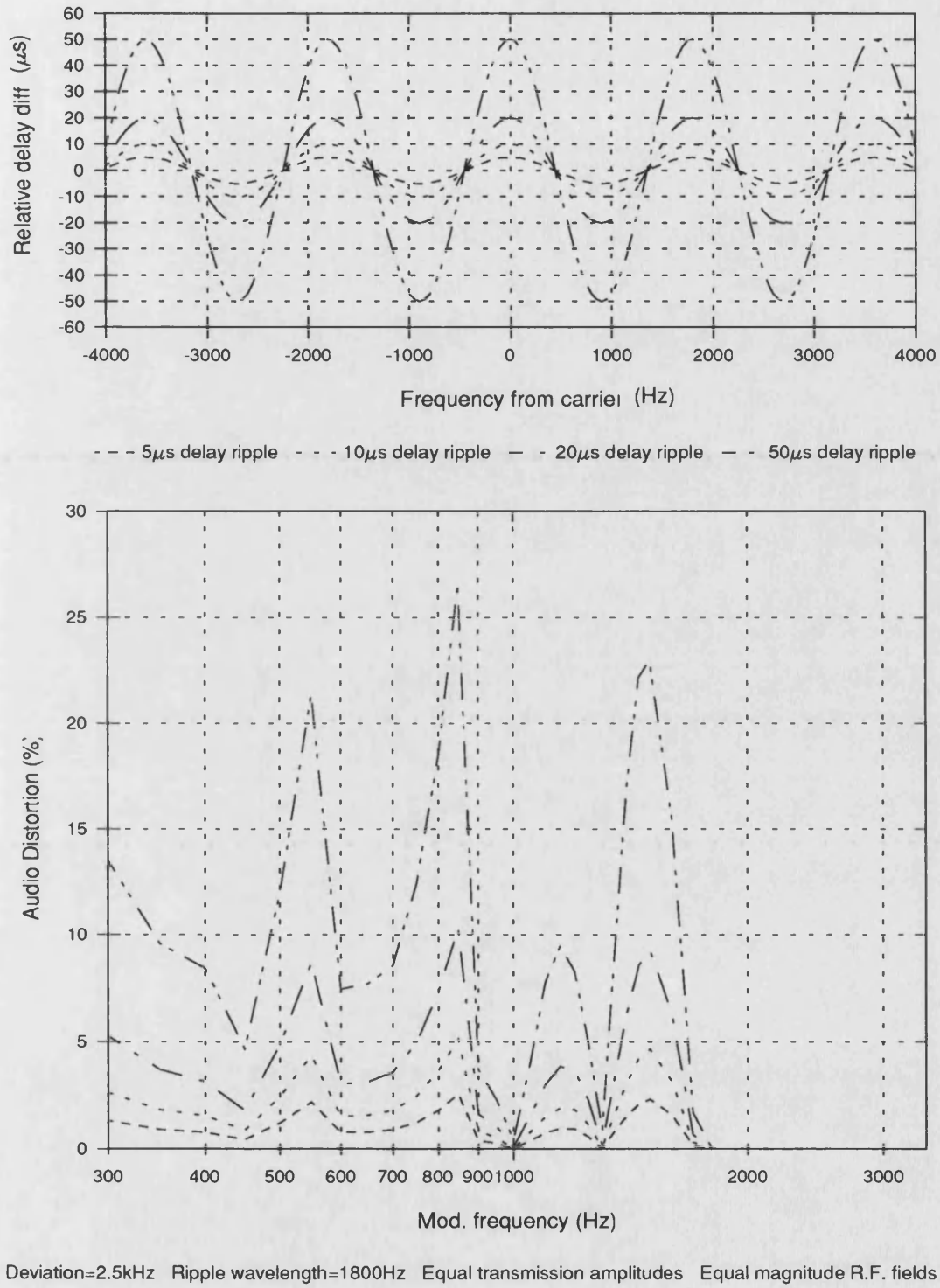

Figure 3.32: *Audio distortion in an ideal receiver due to delay mismatch*

3.12. Conclusions

In order to reduce distortion of the received signal in a multi-transmitter field, the radiated modulation of each transmitter must be accurately matched. To achieve this, the audio must be conveyed accurately to each transmitter site and each transmitter should have the same modulator characteristics. The use of conventional analogue lines to convey the audio is complicated by the difficulty in accurately equalising the frequency responses of each line. Digital transmission of the audio overcomes this difficulty, removing the need to equalise the amplitude and allowing easily implemented, accurate equalisation of delay.

However, conventional frequency modulators are all implemented by analogue means and thus are all subject to device parameter variation. Further still, analogue-to-digital converters and anti-aliasing filters required to recover the digital audio are also subject to parameter variation in their manufacture and so digital audio transmission is no guarantee of accurate modulation matching. This chapter has presented a novel phase modulator capable of converting digital samples directly into analogue phase modulation via an all-digital process without going through a conventional analogue-to-digital conversion process. Suitable preprocessing of the modulating audio before digital transmission results in a frequency-modulated output though the modulated phase has been sampled, held for the sampling period and quantised. This results in a number of distortion mechanisms in the received signal, but since the output of each modulator is identical there is no degradation in performance in a multi-transmitter field.

It has been shown that sampling the modulated phase of the carrier signal results in the desired ideal modulated signal spectrum with replicas of that spectrum centred on integer multiples of the sampling frequency either side of the carrier frequency. These post-modulation aliased spectra may be removed by

suitable bandpass filtering around the carrier frequency. However, conventional baseband anti-alias filtering is based on Nyquist's theorem, i.e. providing the sampling frequency is twice the bandwidth of the signal, a filter cut-off at half the sampling frequency will recover the signal by removing all alias components. In this post-modulation case, a sampling frequency greater than the modulated signal bandpass bandwidth is necessary to allow bandpass filtering that cuts off at half the sampling frequency either side of the carrier frequency. Since F.M. is a non-linear process it is not true in general that the same sampling frequency used for the baseband modulating signal can be used to sample the modulated phase without aliasing. Bandwidth expansion caused by F.M. is related to the deviation of the modulation and thus the required sampling frequency used for the modulated phase is also. The nature of the modulating process does not allow for pre-filtering of the modulated signal prior to sampling its phase thus the key parameters sampling frequency, modulating signal bandwidth and frequency deviation must be chosen in order to allow practical post-modulation anti-alias filtering. This filtering must have sufficient bandwidth to pass the desired signal with acceptable distortion due to spectral truncation, but without excessive in-band aliased signal power.

Conventional bandwidth estimates from Carson's rule are fairly accurate for very large and very small frequency deviations, however for existing narrowband mobile radio systems Carson's rule overestimates the bandwidth required and thus the necessary sampling frequency. A number of more accurate rules for choosing the required sampling frequency for a given modulating signal bandwidth and deviation have been developed from statistical bounds on the spectral distribution of power in an F.M. wave with band-limited Gaussian modulation. Blachman's 2^{nd} and 4^{th} moments of spectrum are used as the best of the bandwidth estimators to give around 1% in-band distortion power for a 3.4kHz bandwidth modulating signal sampled at 8kHz and a frequency deviation

of 2.5kHz. This is the deviation used in 12.5kHz channel spacing narrowband F.M. mobile radio systems for which there exists readily available crystal filters suitable to perform the required post-modulation filtering. This is also a practical limit on the deviation possible with standard mobile radio audio bandwidth and 8kHz sampling without introducing excessive in-band post-modulation alias distortion.

The inherent zero-order hold of the sampled phase also introduces some distortion in the received signal. The ideal modulated spectrum is modified by a "sinx/x" type function centred on the carrier frequency. Across the bandwidth of interest (half the sampling frequency either side of the carrier frequency), this amounts to a spectral "droop" with a maximum value of 4dB at the extremes of the post-modualtion filtering passband. This results in a variation in the envelope of the signal and a distortion in the modulated phase. The envelope variation is only severe at deviations in excess of those allowed under the bandwidth constraints already described and is easily removed by a limiter. The distortion in the received signal due to the distorted phase has been calculated by Fast Fourier Transform techniques and has been shown to be sufficiently small in the cases of interest. Since each modulator behaves identically, no extra distortion will result in co-channel operation and the spectral effect of the zero-order hold not compensated for.

Theory has also been developed to calculate the distortion power in the output of an F.M. receiver due to the phase quantisation inherent in the modulation process. If the degree of phase quantisation is such that the phase quantisation errors are small and largely independent of the audio input signal, the quantisation distortion can be treated as broadband white noise accompanying the desired modulated signal. Due to the nature of F.M. detection, the quantisation distortion in the receiver output will have a parabolic power

spectral density rising rapidly with baseband frequency. As with conventional analysis of F.M. reception with channel noise, the signal-to-quantisation distortion ratio (SQNR) at the receiver output is a function of the ratio of modulated signal bandwidth to baseband bandwidth (the F.M. bandwidth expansion) and similarly bandwidth expansion can be traded for increase in SQNR. As noted above, bandwidth expansion is a function of the frequency deviation used and thus increasing the frequency deviation for a fixed modulator resolution gives higher signal-to-quantisation distortion ratio. At a deviation of 2.5kHz with 8kHz sampling, an 8-bit modulator gives around 50dB SQNR, but with the addition of pre-emphasis of the audio prior to analogue to digital conversion and complementary de-emphasis at the receiver output, this is increased to more than 65dB.

Having produced identical modulated signals within each transmitter in a coverage scheme the only possible remaining cause of distortion due to mismatch in the modulation of radiated signals is variation in the transmission characteristics of the post-modulation filtering and amplification of each transmitter. This is likely to be dominated by the use of a narrowband crystal filter as a post-modulation anti-alias filter and several filters of the same type and manufacturer were measured and compared. The measured variation in frequency responses can be characterised by assuming one transmitter to have perfect transmission of the ideal modulated signal and a second having transmission characteristics of the difference between their absolute measured values. The amplitude and delay difference *ripple* across the passband of the filter can be closely modeled as sinusoidal variation with frequency of two "wavelengths". The distortion resulting in the receiver output in the presence of two signals of equal strength but different I.F characteristics has been calculated by Fast Fourier Transform techniques. The mismatch in the shorter wavelength passband ripple of both amplitude and delay results in greater distortion with

the short wavelength delay ripple resulting in the most distortion. It is shown that, within manufacturing tolerances, the degree of distortion attributable to variation in response of a particular filter type will be considerably less than that achieved in co-channel schemes using conventional techniques in the equal signal strengths case.

3.13. References

[1] Coates R.F.W., "*Modern Communication Systems*", 2nd Ed., Macmillan Press Ltd., ISBN 0 333 33344 6 1983.

[2] Black H.S., "*Modulation Theory*" D. Van Nostrand Company Inc., Princeton N.J., ISBN 1953

[3] Haykin, S., "*An Introduction to Analogue and Digital Communications*" John Wiley & sons 1989.

[4] Cherry E.C., Rivlin R.S., "*Non-linear distortion with particular reference to the theory of Frequency Modulated Waves-Part I*" Philosophical Magazine vol.32 no. 213 Oct. 1941 265-281.

[5] Panter, "*Modulation, Noise and Spectral Analysis*", McGraw-Hill 1958

[6] Roberts, J.H. "*Angle Modulation*" Peter Peregrinus Ltd. England I.E.E. Telecommunications series 5. 1977.

[7] Blachman, N.M. "*On the moments and tails of the spectrum of an F.M. wave*" Radio Sci., 1969, 4, pp. 437-439.

[8] Blachman, N.M. "*New bound for the spectrum of an F.M. wave*" Proc. I.E.E. vol.121 no.9 Sept. 1974.

[9] Gradshteyn I.S., Ryzhik I.M., "*Tables of Integrals, Series and Products*" London: Academic Press, 1965 ISBN 0-12-294760-6.

Chapter 4:
A Synchronous F.M. Transmitter

4.1. Introduction

The idea of transmitter synchronisation by P.C.M. lines was introduced in chapter 2, the principle being that the recovered P.C.M. clock signal could be used to derive its output carrier frequency. Any number of transmitters could then in theory operate with the same output frequency if they used the same P.C.M. clock reference. Further still, use of a Precise Phase Modulator in each transmitter will ensure that modulation matching between transmitters is accurate with slight variations in the transmission through filters and transmitter output stages being the only sources of modulation mismatch between transmitters. The final advantage is the ease with which the modulation delay between the point of modulating signal generation and each transmitter can be equalised in digital form by very simple digital circuits. This is the only parameter of the modulating signal transmission that requires equalisation, unlike analogue transmission lines, where the amplitude and delay audio frequency responses require equalisation too. Figure 4.1 shows the proposed scheme.

The audio preprocessing of the modulating signal required prior to a phase modulator to obtain frequency modulated signals from each transmitter is most easily achieved by analogue methods. Digital methods for precise implementation at the transmitter sites have been investigated, but have found to be cumbersome and since this processing is only required once and only at the control site, it cannot cause any modulation mismatch between transmitters.

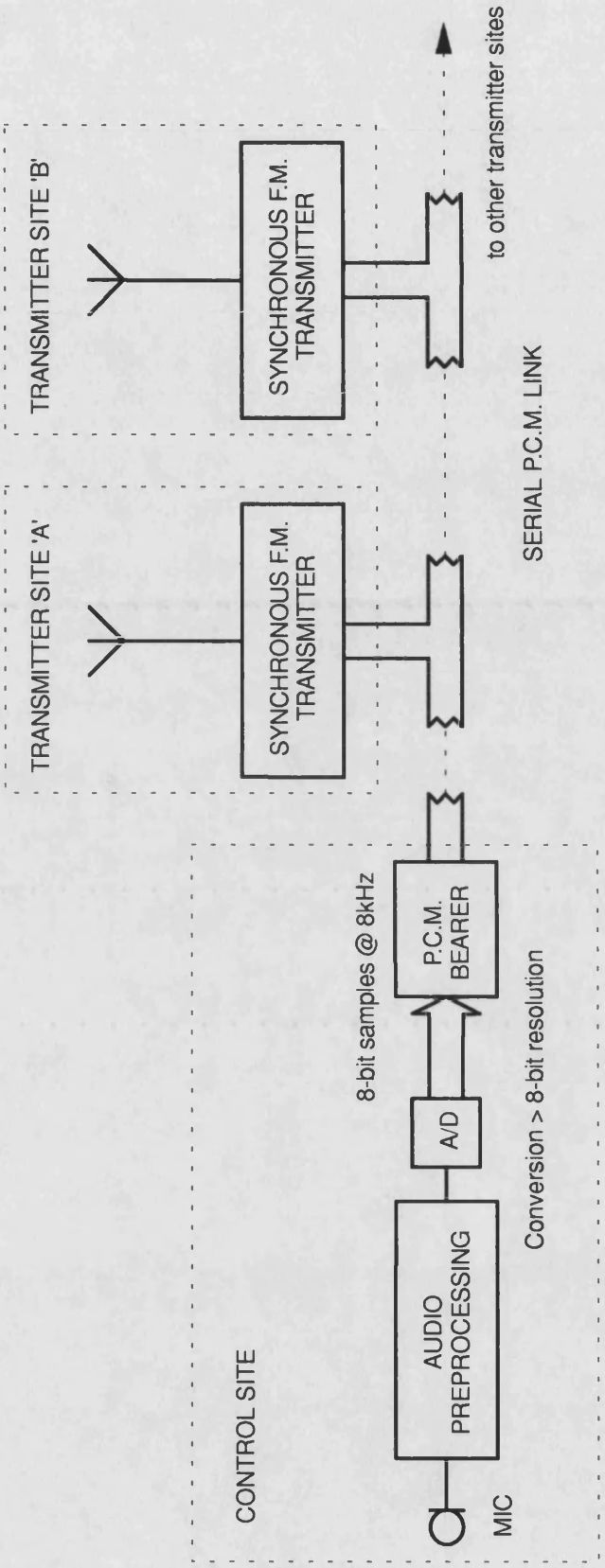

Figure 4.1: *Synchronous F.M. area coverage scheme*

4.2. Synchronous transmitter architecture

The architecture of an F.M. transmitter design to be "driven" from a P.C.M. link is dictated by three main requirements. Firstly, the modulated output from the Precise Phase Modulator must be translated to the required output frequency, since the speed of conventional logic hardware limits the maximum frequency at which the modulated signal can be generated. This translation of the modulated signal must be achieved by mixing with other locally generated signals rather than by frequency multiplication since, as noted earlier, this increases the frequency deviation of the modulation, (although this property can be used to overcome sampling rate limitations). Further still, these locally generated signals must all be derived from the recovered P.C.M. clock to ensure the synchronous nature of the transmitter output frequency: this includes the high frequency clock that drives the phase modulator.

Secondly, the transmitter must provide for the bandpass filtering required to recover the modulated signal from the aliased R.F. components as described earlier. This filtering is required to be of sharp cut-off characteristics to approximate the ideal rectangular frequency response. Intermediate frequency channel filters designed for receiver selectivity are of suitable performance for operation as R.F. anti-alias filters so translation to a standard I.F. frequency of the Precise Phase Modulator output is required to implement this filtering. As shown in chapter 3, the zero-order hold on the modulated phase produces amplitude fluctuations of the modulated signal after filtering and thus the filter must be followed by a limiter to remove these fluctuations.

Finally, the architecture should be arranged so that changing the output frequency of the transmitter requires a minimal change in the transmitter circuitry In this way the same basic transmitter can be used on any V.H.F./U.H.F. frequency band.

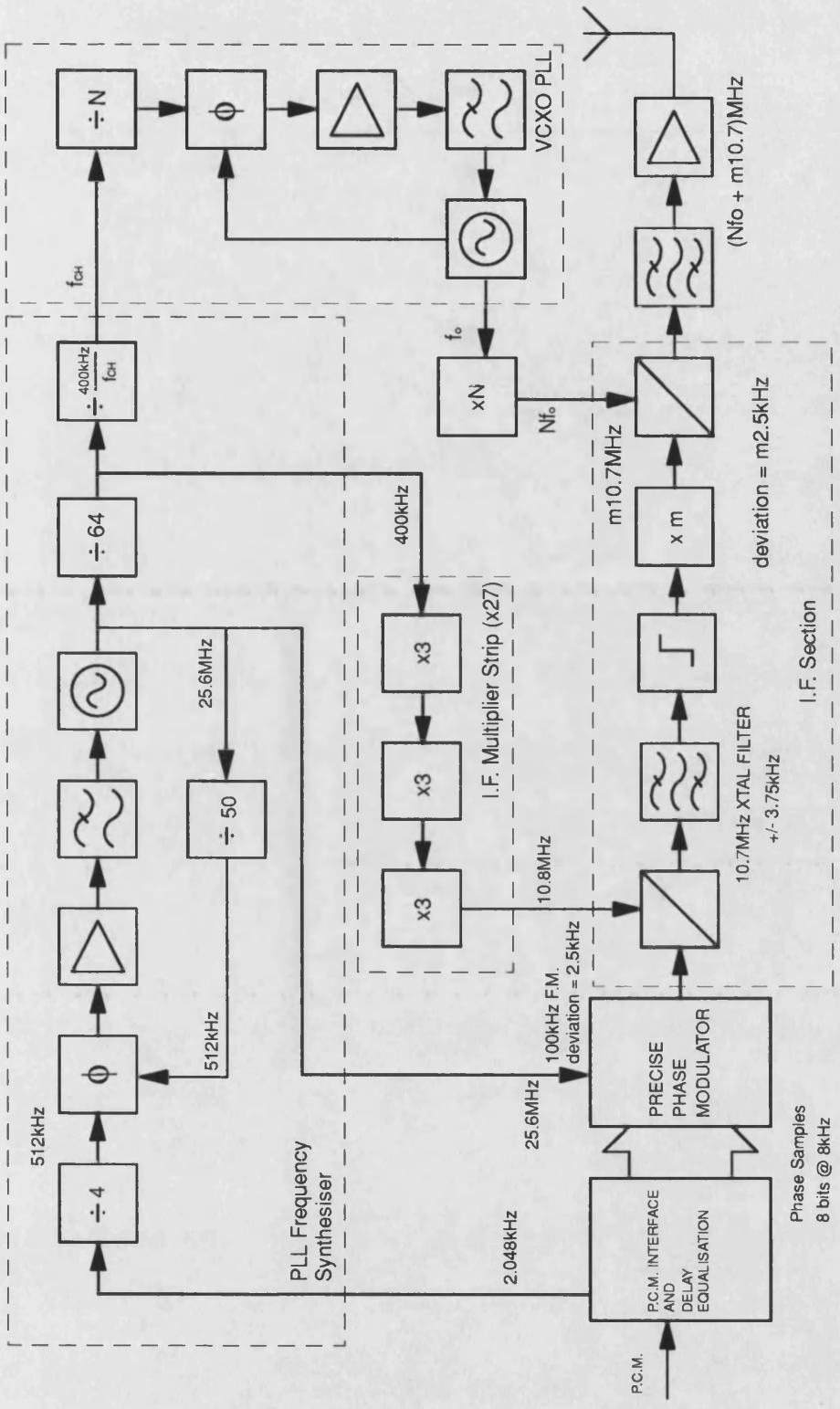

Figure 4.2: *Synchronous F.M. transmitter for 25kHz channel spacing*

The original intention had been to drive the transmitter from a *2.048Mbit/s* multiplex P.C.M. line, using one of the *64kbit/s* channels for the modulating signal samples (i.e. 8 bit by 8kHz). These lines are more expensive to install to remote transmitter sites, particularly if only one channel is required for the audio. However, since available devices intended to decode the audio for single subscriber digital lines or those to multiplex up to trunk line level produce phase lock signals at 2.048MHz anyway, a 2.048MHz signal is used as the input frequency reference to the transmitter from which all other signals are derived. The P.C.M. level interface is not included, the P.C.M. link for testing purposes was "hard wired" direct from the control site circuitry as parallel 8 bit words at a sampling rate of 8kHz which was also derived from the 2.048MHz reference to maintain phase coherence.

The 2.048MHz signal is used as a reference by the phase-locked loop (PLL) frequency synthesizer to produce reference frequencies for the rest of the transmitter. The 2.048MHz signal is divided down to 512kHz and then multiplied to 25.6MHz by a conventional crystal-controlled PLL frequency multiplier. This 25.6MHz signal is used to clock the Precise Phase Modulator. It is also divided down to 400kHz to provide a signal for the I.F. multiplier strip and divided again to produce a reference signal, f_{CH}, for the VCXO (voltage-controlled crystal oscillator) PLL. The 400kHz output is multiplied by a factor of 27 in the I.F. multiplier strip. This consists of a cascade of three frequency triplers that result in an output frequency of 10.8MHz which is still in phase-lock with the 2.048MHz transmitter reference frequency. This signal is used in the I.F. section to mix the 100kHz modulated signal from the Precise Phase Modulator to 10.7MHz. It is then filtered for alias components by a 10.7MHz crystal filter of bandwidth 7.5kHz (the frequency deviation is 2.5kHz at this point). The output is then hardlimited to remove amplitude fluctuations resulting from filtering and the spectral envelope discussed earlier. To increase the

deviation from the generated *2.5kHz*, the signal then passes through a frequency multiplier (*xm*) resulting in a signal of frequency *m10.7MHz* and deviation *m2.5kHz*.

This signal is then mixed up to the final output carrier frequency by a locally generated signal from the R.F. multiplier strip that is phase-locked to the transmitter reference. The R.F. multiplier strip is fed from the output of the VCXO PLL. This loop also performs multiplication of its reference frequency, but allows easy selection of different output channel frequencies without altering much of the rest of the transmitter. The final translational mixer must be supplied with a frequency minus *m10.7MHz* (the modulated signal frequency). This signal must remain locked to the transmitter reference so must be an integer multiple of a lower frequency derived from the PLL synthesizer. In order that all possible channel frequencies at a particular channel spacing can be achieved, this reference, f_{CH}, to the VCXO PLL must be the channel spacing itself as it is the highest factor that can always be guaranteed to be an integer sub-multiple of the required frequency (allowing for the factor of *m10.7MHz*). However, direct multiplication to V.H.F. and U.H.F. frequencies is limited by design considerations of the loop and the maximum frequency at which practical crystal oscillators can be made. Hence, the frequency of the VCXO is reduced by an integer factor (N) and hence the need for the R.F. multiplier strip.

To compensate for the frequency multiplication after the VCXO, the input reference f_{CH} must be divided by the same integer factor, so that all possible integer multiples of f_{CH} are possible in the frequency supplied to the final mixer and thus re-crystalling the VCXO is the only major modification required to change the final output frequency over a particular frequency band (retuning or even redesign of these R.F. stages is required if the required change of output frequency is large).

4.3. Prototype transmitter

A prototype transmitter as shown in figure 4.2 was constructed to prove the precise phase modulator. The output frequency is 84.725MHz and the channel spacing is 25kHz, thus the 400kHz signal is divided by 16 to give a 25kHz reference to the VCXO loop. The VCXO operates at 10.554166MHz requiring multiplication by 6 before the final mixer to give a frequency of 63.325MHz. The deviation of the modulator must be doubled to give 5kHz deviation for 25kHz channel spacing thus a signal of 21.4MHz mixes with 63.325MHz to give the output frequency of 84.725MHz (and image at 41.925MHz which is filtered out).

4.4. Control site processing

The circuit diagram of the control site audio processing is shown in Appendix D, but the block diagram is shown in figure 4.3.

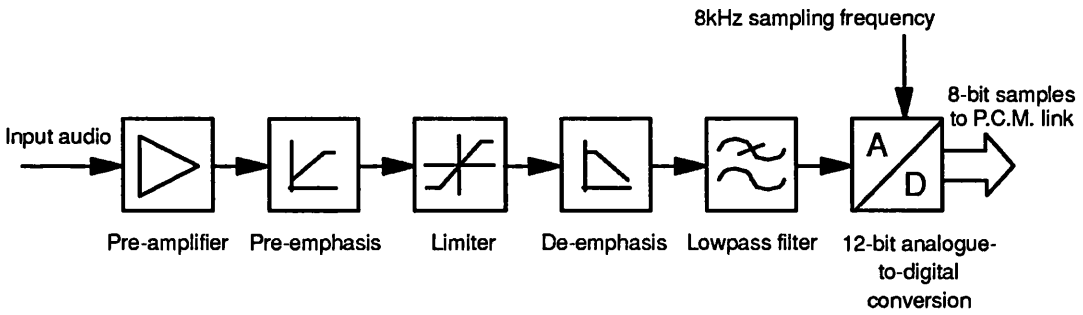

Figure 4.3: *Control site processing*

The input audio, either test tones from a signal generator or recorded speech from a tape recorder, is first amplified by an op-amp preamplification stage. The signal is then pre-emphasized in a further op-amp stage, though the high frequency response is levelled off to avoid high frequency noise and instability. The signal is then symmetrically clipped to limit the peak frequency deviation of the transmitted signal. The signal is then de-emphasized by an op-amp integrator, the low frequency response of which is levelled off to avoid saturation

by d.c. offsets. The signal is then lowpass filtered to 3.4kHz by a 12th order switched capacitor filter to avoid aliasing in the analogue-to-digital conversion.

The signal is converted to digital form by a 12-bit analogue-to-digital convertor. A 12-bit convertor and separate antialias filter are used rather than a conventional P.C.M. CODEC (COder-DECoder, which contains both) to allow the "roll-over" of the phase-shift of the Precise Phase Modulator by more than 2π radians. An 8-bit modulator is used and only the 8 least significant bits of the modulated phase are transmitted from the control site to the transmitter, but if an 8-bit convertor was used, the digital output would clip at 255 or 0 for excursions in the input greater than the 8-bit conversion range. The circuit diagram for the analogue-to-digital conversion used is also shown in Appendix D, the input to the convertor is buffered by a unity gain low-noise op-amp and the clock to the convertor is derived with appropriate duty cycle from a 4-bit counter, thus to sample at 8kHz, an input of 128kHz is required. This signal is derived from the 2.048MHz reference to the transmitter to maintain timing coherence as would be the case in a full synchronous system, but an external clock of variable frequency was also used to verify the theoretical performance of the modulator. The output of the convertor is latched when stable. This output would then be transmitted in serial form over the P.C.M. link, but here is connected to the synchronous transmitter directly.

Since only 8 bits of the 12-bit output are required, the least significant bits may be discarded to improve the rejection of noise at the input to the convertor. If the largest phase shift required ($\pm\beta_{max}$) is for a frequency deviation of 2500Hz at 300Hz, then β_{max} must be at least ± 10 radians. Thus a 10-bit conversion range is sufficient (a total shift of $4\times 2\pi$ radians) and the two least significant bits of the convertor are discarded.

The full scale input for the convertor is ± 3V so the voltage step size at the input

for a single increment in the 10 bits of interest is:

$$\delta v = \frac{6}{2^{10}} = 5.859mV \qquad (4.1)$$

The phase step size for an 8-bit modulator:

$$\delta\theta = \frac{2\pi}{256} = 2.454.10^{-2} radians \qquad (4.2)$$

Then the phase modulator constant k_φ is:

$$k_\varphi = \frac{\delta\theta}{\delta v} = 4.1890\ radians V^{-1} \qquad (4.3)$$

Thus the op-amp integrator that precedes the phase modulator must be chosen to have a suitable gain in order to give a usable overall F.M. modulator constant k_f. If the ideal integrator response is:

$$H_I(f) = \frac{k_I}{j2\pi f} \qquad (4.4)$$

Then the F.M. modulator constant k_f. is:

$$k_f = \frac{k_I k_\varphi}{2\pi} \qquad (4.5)$$

If the maximum frequency deviation allowed without excessive in-band alias distortion at 8kHz sampling is 2.5kHz, then if the peak input voltage is chosen to be 5V for peak deviation:

$$k_I = \frac{2500}{5 \times 0 \cdot 6667} = 750 \qquad (4.6)$$

Thus, the overall modulator constant is:

$$k_f = 500 HzV^{-1} \qquad (4.7)$$

The input to the integrator is clipped by the unity gain limiter preceding it, the zener diodes limiting voltage excursions to ±5V.

4.5. Precise phase modulator

The circuit diagram of the precise phase modulator is shown in Appendix D. The implementation is in T.T.L. logic though it would be easily implemented in practice on a single application-specific device. The input 8-bit samples of modulated phase (since preprocessing has already been performed) are each latched for the sample period, 125ms, to ensure a stable input to the modulator. The input clock signal is used to generate the 8 bit "carrier word" by division by 256 by an 8-bit counter formed by two cascaded 4-bit synchronous counters. The carrier word and sample words are added in an 8-bit full adder formed by two cascaded 4-bit full adders. Both the counter devices and the full adders are of the FAST T.T.L. type in order to work at the required speed.

It should be noted that increase in modulator resolution would require a considerably different implementation. This is demonstrated by considering the case of an increase in resolution of only one bit, i.e. 9-bit arithmetic requiring a 9-bit carrier word and 9-bit modulating sample. Since the output frequency is halved so is the ratio of the output frequency to the sampling frequency, with the possibility of noticeable distortion as the suppression of overlap aliased signal power from the third harmonic of the carrier is reduced (not to mention redesign of the transmitter as the required frequencies that need to be generated from the reference input are much less readily obtained). If the input clock is doubled to compensate, the implementation of 9-bit synchronous counter at 51.2MHz is stretching the capabilities of most T.T.L. logic. Further still, 9-bit full addition at this rate is similarly difficult to achieve and specialized high speed (and high cost) logic devices would be required. Also, the data rate from the P.C.M. link would also have to be uprated, complicating the use of conventional P.C.M. systems and devices.

4.6. The spectral output of the prototype modulator

Figure 4.4 shows the typical output from the Precise Phase Modulator used in the prototype transmitter before any frequency translation or I.F. processing is implemented. The first spectrum shows the effect of the multicomponent carrier as described previously. The modulated signal is "wider" for the higher carrier harmonics indicating the predicted increase in frequency deviation over that of the fundamental (though in order to see the multi-component carrier effects there is insufficient resolution to pick out the individual sidebands).

Both spectra show the effect of the spectral envelope. The nulls of the envelope fall on integer multiples either side of the carrier fundamental and each harmonic. Since the spacing between harmonics is an integer multiple of the sampling frequency, nulls of the envelopes of each harmonic coincide. The effect of aliasing of the third carrier harmonic is clearly seen to reduce rapidly as the fundamental is approached and about half way between third harmonic and the fundamental, the signal power due to the fundamental easily masks any sign of that of the third harmonic.

The second spectrum shows the spectrum around the passband of the I.F. filter. The Bessel sidebands and the quantisation "noise floor" are self-evident, the spectral envelope causing notches in the quantisation noise floor at multiples of 8kHz either side of the carrier frequency.

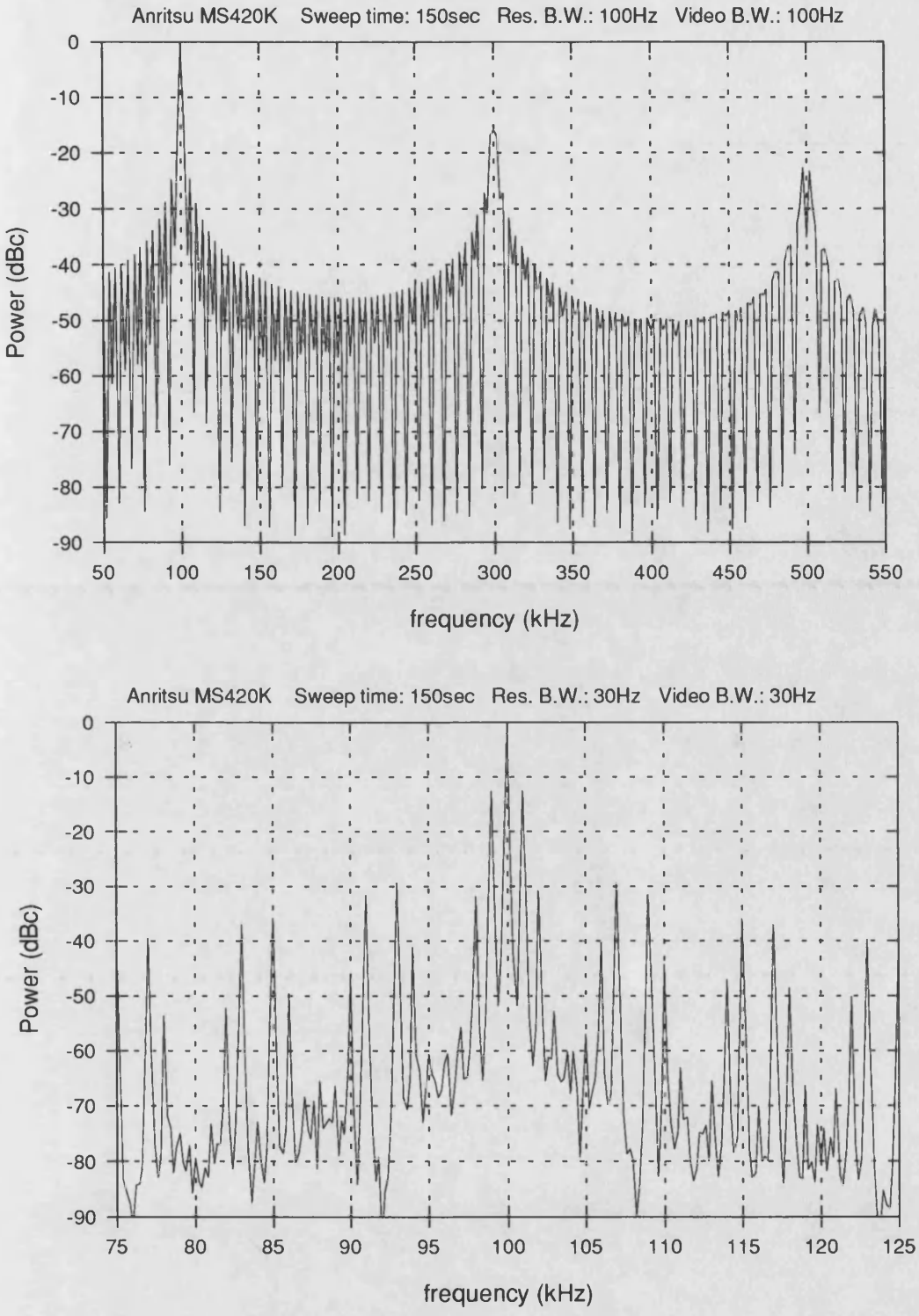

Figure 4.4: *Typical output spectra from the Precise phase modulator used in the prototype transmitter*

4.7. Measurement of modulator constant

Accurate calibration of an angle modulator by static methods (i.e. applying d.c. potential to the modulator and measuring the resulting change in frequency or phase) is often difficult or unreliable. Any a.c. coupling in the modulator will render this unworkable and even if this is not the case, the a.c. and d.c. equivalent circuits may differ giving inaccurate results. Furthermore, the direct measurement of phase difference in the modulator is inherently difficult even allowing that an ambiguous result may occur if the phase difference is greater than 2π radians. To avoid these problems, a dynamic test procedure is usually adopted using a sinusoidal test signal. If a sinusoidal test signal is used, then as previously discussed, the modulated signal is:

$$e_{fm}(t) = E_o \cos(2\pi f_o t + \beta \sin 2\pi f_m t) \qquad (4.8)$$

which can be written as the series expansion:

$$e_{fm}(t) = E_o \sum_{n=-\infty}^{\infty} J_n(\beta) \cos 2\pi (f_o + n f_m) t \qquad (4.9)$$

As is clear from the graphs of $J_n(\beta)$ (the Bessel function of the first kind of order n) shown in Appendix F that since all $J_n(\beta)$ resemble damped sinusoidal oscillations, there are an infinite number of solutions for β of the equation:

$$J_n(\beta) = 0 \qquad \text{for all } n \qquad (4.10)$$

Thus for certain values of β, the carrier component or pair of sidebands may disappear from the frequency spectrum. These values of β can be calculated and Appendix F tabulates values of β for zeros in the carrier and first set of sidebands, i.e. solutions for β of:

$$J_0(\beta) = 0 \text{ and } J_1(\beta) = 0 \qquad (4.11)$$

These points are easily measured on a spectrum analyzer by observing the values of the amplitude of the modulating signal that cause nulls in the carrier and first set of sidebands for a given modulating frequency f_m. Furthermore, this

method is immune to the spectral envelope resulting from the zero-order hold of modulated phase (zero positions are unaffected by any magnitude scaling provided the sideband of interest does not coincide with a zero in the spectral envelope). If a modulating signal of r.m.s. amplitude v_{rms} and frequency f_m causes a zero in $J_n(\beta)$ at β_z, the phase modulator constant can be calculated by:

$$k_\varphi = \frac{\sqrt{2}\beta_z}{v_{rms}} \; radV^{-1} \qquad (4.12)$$

The zeroes were measured for the prototype phase modulator with the input audio directly applied. The measured zeroes in the carrier ($J_o(\beta)$) gave a value of $4.1875radV^{-1}$ for the phase modulator constant k_φ. This value (as would be expected) is subject to negligible variation with frequency and negligible variation over the three zeroes measured. This is easily within experimental tolerances of the calculated value given earlier as $4.1890radV^{-1}$. However, zeroes in the first set of sidebands yield variation in k_φ of $4.2325radV^{-1}$ to $4.1800radV^{-1}$ with increasing β_z (though independent of modulating frequency). The possible causes of this are quantisation noise giving incorrect sideband zeroes, non-linearity in the analogue-to-digital convertor characteristic resulting in the variation in the phase deviation per volt input with increasing input, or incorrect measured zeroes due to alias sidebands from the multicomponent carrier coincident with the sidebands required. Quantisation noise should have exhibited a similar effect on the carrier zeroes, but since no significant variation was measured this is unlikely. Non-linearity would have resulted in incorrect values of deviation for the carrier measurements, too, so is similarly unlikely. However, since the values of sampling frequency and carrier harmonic spacing are such that the zeroes of all carrier harmonic spectral envelopes fall on the carrier fundamental frequency so the only signal power measured at the fundamental is due to phase modulation of the fundamental only. However, zeroes measured at the sideband frequencies of $\pm nf_m$ are in fact zeroes of:

$$\left| \sum_{m=1}^{\infty} \frac{J_n(n\beta)}{m} \frac{\sin \pi(((m-1)f_o \pm nf_m)T_s)}{\pi(((m-1)f_o \pm nf_m)T_s)} e^{-j\pi(((m-1)f_o \pm nf_m)T_s)} \right| \qquad (4.13)$$

This is the more likely reason for a small error in the measured zeroes.

For the frequency modulator, as defined earlier, the frequency deviation Δf can be calculated from a given β from:

$$\Delta f = \beta f_m \qquad (4.14)$$

The modulator constant k_f (the frequency deviation of the carrier per volt modulating signal) can now be found. :

$$k_f = \frac{\sqrt{2}\beta_z f_m}{v_{rms}} \; HzV^{-1} \qquad (4.15)$$

This was used to verify the overall F.M. constant k_f.

4.8. Frequency translation and I.F. R.F. alias filtering

The circuit diagram for the frequency translation and I.F. filtering of the output of the Precise Phase Modulator is given in Appendix D. The 100kHz output of the modulator is buffered in an op-amp stage and suitable level of drive (approx 0dBm) is matched into the 50Ω input impedance of the first double-balanced mixer which also accepts the 10.8MHz output of the I.F. multiplier strip to produce products centred on 10.8MHz ± 100kHz. The lower product at 10.7MHz is selected by the I.F. crystal filter (bandwidth 7.5kHz - normally used for 12.5kHz channel spacing reception) whose input/output impedance (910Ω in parallel with 25pF) is matched to 50Ω by simple LC matching.

The resulting signal is then amplified by the tuned amplifier Q1, and then hardlimited by the linearised HCMOS inverter U1B, to remove all traces of the amplitude fluctuations due to the sample and hold of the modulated phase. The signal is then passed to the transistor frequency doubler Q2 resulting in an output of 21.4MHz and deviation of 5kHz. This is then mixed by the second

double-balanced mixer with the output of the R.F. frequency multplier strip, 63.325MHz, to produce output products at 84.725MHz and 41.925MHz.

The former is selected by the output R.F. filtering, the circuit diagram of which is also shown in Appendix D. For the frequencies used, this is merely a doubled tuned amplifier which provides a measured relative attenuation of about 50dB in the unwanted product. At higher output frequencies (particularly at U.H.F.), or for 12.5kHz channel spacing (a lower deviation of 2.5kHz and thus no doubler is required - the input to the second mixer becomes 10.7MHz), the ratio of the spacing between the wanted and unwanted product of the final mixer and the output frequency itself becomes small and thus filtering off the unwanted component becomes more difficult.

4.9. Transmitter audio response

The audio response is shown in figure 4.5. The magnitude response clearly shows the 6dB per octave rise in response over the band of interest due to the pre-emphasis network employed in the audio preprocessing. This is to compensate for the high frequency noise characteristics of an F.M. receiver as discussed earlier, the receiver possesses a complimentary audio response to restore the energy distribution of the signal. The high frequency roll-off beyond the audio passband is very sharp due to the baseband anti-alias filtering and the narrowband I.F. filter used to remove aliased modulated spectra.

The audio phase response appears reasonably linear though the best way to evaluate this is to measure the distortion response of the transmitter. This is given in the next section.

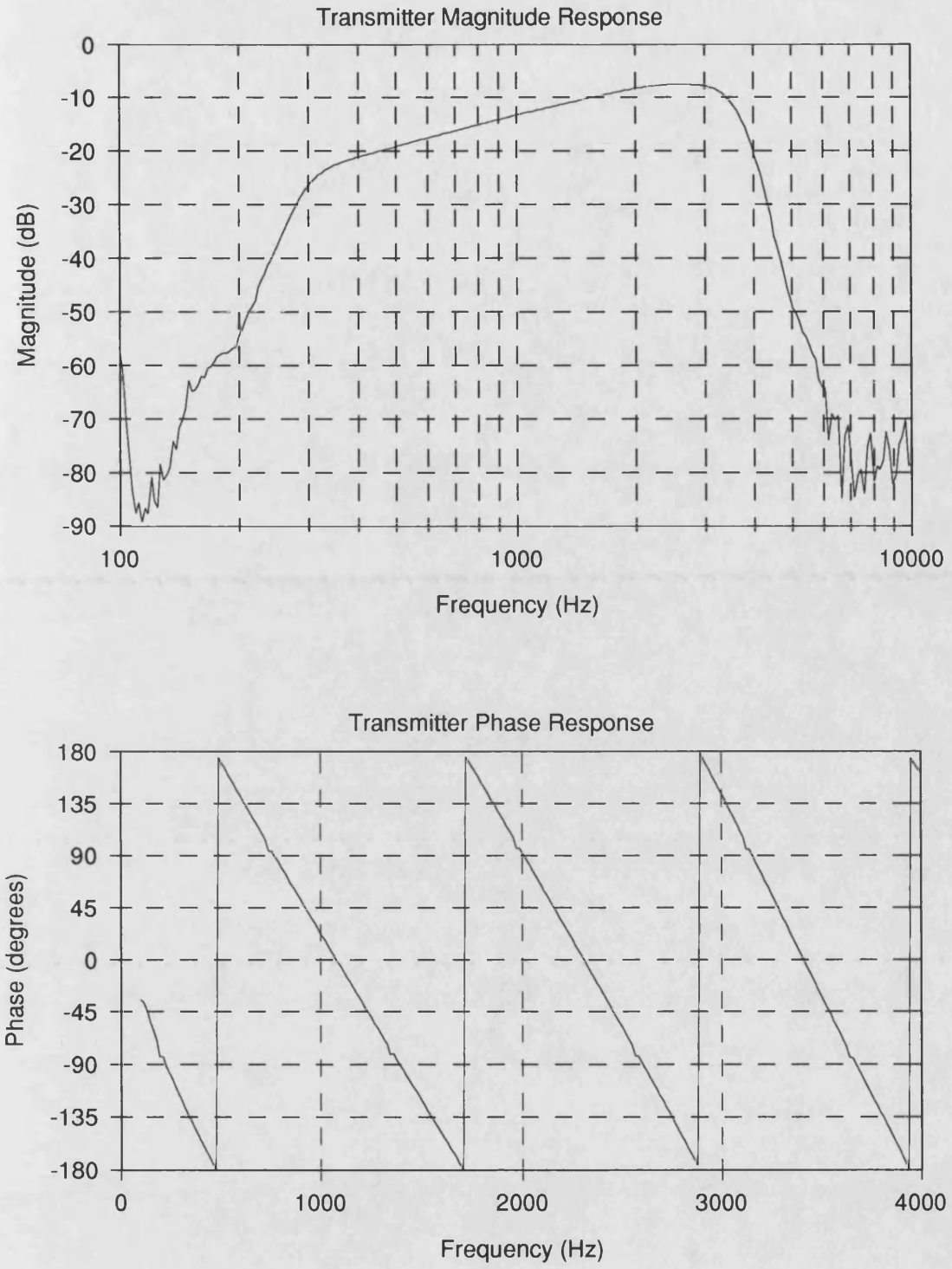

Figure 4.5: *Transmitter audio magnitude and phase response*

4.10. Transmitter linearity

The measured audio distortion response is shown in figure 4.6.

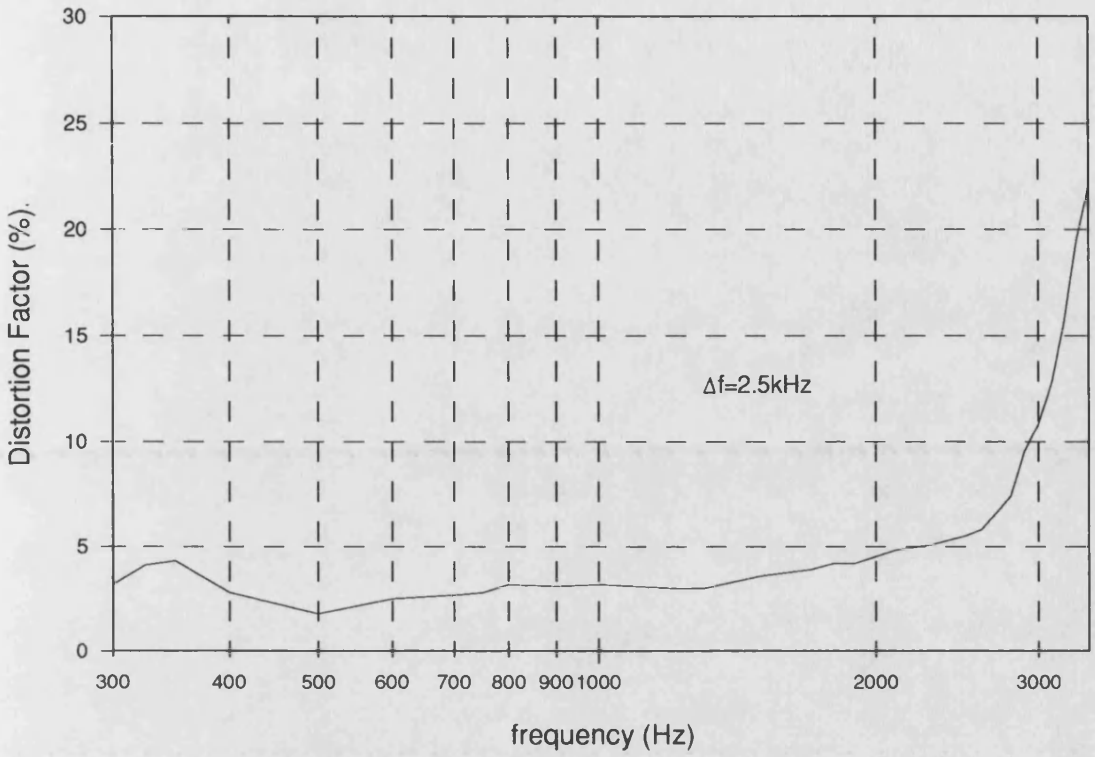

Figure 4.6: *Transmitter audio magnitude and phase response*

For most of the audio frequency band, the distortion is acceptable for narrowband mobile radio equipment. However, for audio frequencies greater than 2.5kHz the distortion level rises rapidly. This is due to two mechanisms, both resulting from the fact that at the deviation used, there is significant power in second and third order sidebands of modulating frequencies above 2kHz. The first mechanism is that this power is truncated from the wanted spectrum by the I.F. filter in the transmit path causing harmonic distortion of the received signal. The second mechanism is that this truncated power from the required spectrum is reflected in-band by the sampling of the modulated phase. The in-band reflected sidebands cause intermodulation products with the required frequency

also raising the measured distortion at higher frequencies.

As noted in chapter 3, the non-linear nature of F.M. is such that superposition of distortion of a single tone to that of a complex modulating signal is not necessarily valid. In fact, as is shown in chapter 3, the overlapped (and truncated) signal power as a percentage of the total signal power is less than in certain sinusoidal cases as the nature of the modulating signal confines the signal power to a narrower band. Thus, the distortion experienced by the higher frequency components of speech signals will not be as severe as that measured for sinusoidal tones.

4.11. Frequency synthesis

The circuit diagram for the main PLL frequency synthesizer is shown in Appendix C. The input reference is at 2.048MHz and the outputs are phase locked at 25.6MHz, 400kHz and 25kHz. The 2.048MHz signal is divided by four to 512kHz and input to the NE564 PLL. The centre frequency is set by a 25.6MHz crystal since the internal VCO has insufficient stability at higher frequencies to design a narrow bandwidth loop whose output is sufficiently stable to lock the VCXO loop. The 25.6MHz of the PLL is output direct to the Precise Phase Modulator and divided down by the synchronous counter chain to give both 400kHz and 25kHz. The loop is completed by dividing the 25.6MHz down by 25 with the preload 8-bit counter chain to 1.024MHz and halved by a 'D'-type latch to 512kHz at a 50% duty cycle signal as the other input to the PLL phase comparator. The loop gain is set by R4 and the loop filter is formed by capacitors C2 and C3.

The circuit diagram for the I.F. multiplier strip is also shown in Appendix C. The 400kHz HCMOS logic signal from the main PLL synthesizer is multiplied by a cascade of three transistor frequency tripler stages to 1.2MHz, 3.6MHz and

finally an output of 10.8MHz. This signal is used to mix the output of the Precise Phase Modulator to 10.7MHz for filtering in the I.F. section.

The 25kHz output of the main synthesizer is the input to the VCXO loop as shown in the VCXO circuit diagram (Appendix C) as described earlier, this is first divided by six to give a reference of 4.166kHz to a frequency of 10.554166MHz (a factor of 2533) without employing a divider in the feedback path of the PLL. This is achieved by effectively making the loop harmonic locking [1]. The 4.166kHz signal is used to trigger a monostable of pulse width of half the period of 10.554166MHz (approx. 50ns). This can be thought of as enhancing the level of the harmonic of 4.166kHz at 10.554166MHz and thus the loop is unity multiplication locking to the harmonic signal.

In practice the short pulse of repetition rate 4.166kHz and the VCXO output of 10.554166MHz are compared by gating the two together producing an output pulse whose width is the overlap between the two or phase difference. The pulse is used to turn on the transistor Q1 and charge the capacitor C1 and between phase error pulses the capacitor discharges through resistor R1. If the ratio of charge time constant and discharge time constant is set to be the same as the ratio of half the reference pulse period, then the output voltage should be centred at half the 5V rail voltage with a small ripple whose amplitude is dictated by C1, when the loop is in lock the phase error pulse is half the width of the reference pulse width (approx. 25ns).

The output voltage of this integrating phase comparator is buffered by the high input impedance of the op-amp and then filtered by the loop filter (d.c. coupled to pass the error voltage to the VCXO) to remove the charge/discharge ripple which would modulate the VCXO causing spurious components in the transmitter output. The VCXO used is a commercially made device, of centre frequency 10.554166MHz with offset adjust (to align the loop). The control voltage range is

0.5 to 4.5V for a ±40ppm variation in the output frequency. The output is buffered by a source follower to the R.F. multiplier strip.

The R.F. multiplier strip (Appendix D) consists of two stages; first a frequency tripler to raise the VCXO to 31.6625MHz and finally a doubler to 63.325MHz which drives the final mixer in the I.F. filtering and translation section.

4.12. Synthesized frequency stability

Since every signal generated within the transmitter is phase-locked to the recovered clock signal of a P.C.M. link, the stability of the final carrier frequency is entirely dependent on the stability of the received clock signal. The clock stability, broadly speaking, divides into two aspects; short term stability or "phase jitter" and long term stability or "drift" in the P.C.M. clock.

The degree of phase jitter in the incoming recovered clock affects the ability of the phase-lock loops within the transmitter to remain in lock. Large amounts of jitter would cause excessive phase modulation of the loops which not only causes unlocking, but leads to excessive output phase noise in the transmitted F.M. signal, since the degree of frequency multiplication (particularly in the case of a U.H.F. transmitter) to reach the required carrier frequency, magnifies the input phase jitter. The effects of phase jitter are considered later in this chapter and chapter 5.

Long term drift in the P.C.M. clock frequency will cause no degradation in system performance due to quasi-synchronous effects as all transmitters in the system should track the variation in frequency together providing they all remain in lock. However, since the frequency multiplication required to achieve V.H.F. or U.H.F. carriers are large, small variations in the input frequency cause larger variations in the output frequency. For example, phase lock of a 500MHz transmitter to a 2.048Mbit/s link requires multiplication of the order of 250 and

2500 from a 192kbit/s link (base level "2B+D" 64kbit/s subscriber line).

The input clock should be accurate enough to avoid the transmitter drifting too far from the allocated channel frequency. It certainly should not drift as much as the channel spacing not only to avoid being outside the I.F. passband of a receiver tuned to the correct frequency, but to avoid excessive adjacent channel interference. For example, Department of Trade and Industry MPT1326 specifications [2] for F.M. Private Mobile Radio stipulate frequency tolerances of range ±1kHz on V.H.F. and U.H.F. bands.

The frequency error in the modulator output at 100kHz is negligible relative to that in I.F. "local oscillator" and certainly that of the R.F. "local oscillator". If the input clock is accurate to ±xppm (parts per million), then the output carrier frequency is also accurate to ±xppm. Thus a carrier at 100MHz is accurate to ± 100xHz and at 500MHz to ±500xHz. The tolerance on the P.C.M. clock frequency is ±10ppm at V.H.F. and ±2ppm at U.H.F. in order to meet these specifications. This may necessitate the installation of a high stability frequency standard to control the P.C.M. link clock frequency if a dedicated digital transmission link is installed, or if a third party digital network is used, then the tolerance of network clocks must provide better than this stability.

4.13. Audio delay equalisation

As discussed in chapter 3, digital transmission of the modulating audio allows simple equalisation of the audio paths to each transmitter in a scheme. Amplitude equalisation is unnecessary by the very nature of digital transmission. Audio delay equalisation is easily achieved by delaying the digital samples of the modulating audio just prior to the precise phase modulator. The recovered digital stream clock (or higher frequency phase-locked to it) can be used to drive a pre-loaded counter such that after a pre-set number of clock periods the modulating

word is latched to the input of the modulator. The smallest delay step is fixed by the clock period, but a clock of 2.048MHz allows 488ns steps in delay, which is at least an order of magnitude of that available previously using analogue landlines.

With fixed digital links between control site and transmitters, scheme installation requires a one-off delay alignment of each transmitter and then should be largely maintenance-free. However, use of a digital network provided by a third party, whose operation is outside the control of the scheme operator introduces further difficulties. Due to the traffic demands on the network, the network operator may elect to switch traffic through whichever route and via whichever network nodes he chooses in order to minimise congestion. In this case delays in the network are not fixed, but variable requiring the constant measurement of delay and adaptive delay equalisation to compensate. The transmitter delay equalisation is easily made remotely variable from the control site, but the magnitude and frequency of variation in network delay is a matter for further investigation if a synchronous area coverage scheme is to be implemented on a third-party digital network. One possible method of measuring delay to up-date the delay equalisation at each transmitter is the use of NAVSTAR global positioning system (G.P.S.) satellites which can give time accuracy of better than 1μs. Time stamping the modulating audio at the control site with G.P.S. time and comparing it with G.P.S. time at the transmitter would give the instantaneous delay, but frequency of measurement would dependant on the function of the network.

4.14. Transmitter phase noise model

The input to the frequency synthesiser of the synchronous transmitter will be a single frequency component at the symbol rate of the transmission line and will

have a random timing phase jitter $\phi(t)$ whose power spectral density is $S_\phi(f)$. The nature and magnitude of this phase jitter is explored in chapter 5.

The propagation of timing jitter as phase noise through the phase-lock circuits of the synchronous transmitter may be considered in terms of the power spectral density and variance of the phase noise assuming any P.L.L.s operate in the linear region. Account can also be made of the likelihood of un-locking of phase-locked loops within the transmitter by monitoring the phase error variance of each loop. If the linear phase transfer function of the transmitter is $H_{TX}(f)$ then the output phase noise spectrum $S_{\phi o}(f)$ is:

$$S_{\phi o} = H_{TX}(f)S_\phi(f) \quad rad^2Hz^{-1} \qquad |f| < 1/2T \tag{4.16}$$

and its variance is:

$$\sigma^2_{\phi o} = \int_{-1/2T}^{1/2T} H_{TX}(f)S_{\phi o}(f)df \quad rad^2 \tag{4.17}$$

The synchronous radio transmitter described in this chapter can be represented as a phase noise transfer function that relates the input phase jitter from a P.C.M. line to the output phase noise of the transmitter. In order to achieve this a number of simplifying assumptions are made:

1. All phase-locked loops can be represented by linear phase transfer functions. This assumes that the loops operate linearly in the area of interest;

2. All frequency multipliers and dividers have constant phase transfer magnitude responses over the Fourier frequency range of interest. (bandpass networks in frequency multipliers will, at high enough Fourier frequencies, attenuate the higher frequency components of the phase variations in their input signals;

3. Noise added in the circuitry such as oscillator phase noise is neglected since that due to input jitter is invariably larger.

Further still, this model also allows for the likelihood of un-locking of the phase-locked loops due to excess phase noise at their inputs. The linearised model is shown in the following figure 4.7.

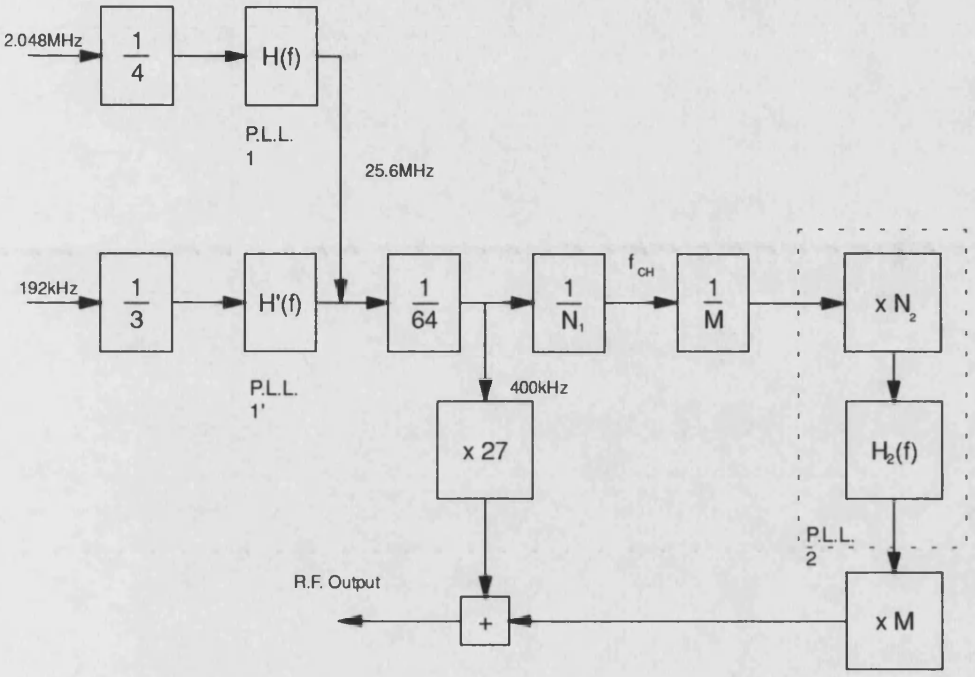

Figure 4.7: *Synchronous transmitter phase transfer model*

The likelihood of the loops within the transmitter un-locking is determined from the magnitude of the phase error at their input (Gardner [3]). It is also shown that the phase error transfer function $H_e(s)$ of a conventional loop with a Laplace transfer function $H(s)$ is given by;

$$H_e(s) = 1 - H(s) \qquad (4.18)$$

and for a loop with a division factor of N in the feedback path;

$$H_e(s) = 1 - \frac{H(s)}{N} \qquad (4.19)$$

Thus the three quantities of interest in the performance of the synchronous transmitter are the output phase noise and the phase errors of the PLLs (both standard deviation and power spectral density). The second PLL is harmonic locking [1] and thus does not have a divider in the feedback path. From the point of view of its phase noise performance, it can be treated as a conventional non-multiplying loop operating at the loop oscillator frequency preceded by a multiplier of factor N_2 - the actual overall frequency multiplication of the loop.

With a given input jitter power spectral density (scaled appropriately for units of phase rather than time), the phase noise power spectral density at the output of the transmitter is;

$$S_{\phi o}(f) = S_{\phi}(f)\left|H_{TX}(f)\right|^2 \qquad (4.20)$$

and the phase error spectral densities of the two P.L.L.s are;

$$S_{\phi e1}(f) = S_{\phi}(f)\left|H_{err1}(f)\right|^2 \qquad (4.21)$$

and

$$S_{\phi e2}(f) = S_{\phi}(f)\left|H_{err2}(f)\right|^2 \qquad (4.22)$$

The transfer functions are obtained by inspection from figure 4.7;

$$H_{TX}(f) = \frac{H_1(f)}{256}\left(27 + \frac{N_2 H_2(f)}{N_1}\right) \qquad (4.23)$$

$$H_{err1}(f) = \frac{H_{e1}(f)}{4} \qquad (4.24)$$

$$H_{err2}(f) = \frac{H_1(f)}{256}\left(\frac{N_2 H_{e2}(f)}{N_1}\right) \qquad (4.25)$$

Assuming second order loops;

$$H_1(f) = \frac{50 f_{n1}^2}{f_{n1}^2 - f^2 + j2\zeta_1 f_{n1} f} \tag{4.26}$$

$$H_2(f) = \frac{f_{n2}^2}{f_{n2}^2 - f^2 + j2\zeta_2 f_{n2} f} \tag{4.27}$$

$$H_{e1}(f) = \frac{j2\zeta_1 f_{n1} f + f_{n1}^2}{f_{n1}^2 - f^2 + j2\zeta_1 f_{n1} f} \tag{4.28}$$

$$H_{e2}(f) = \frac{j2\zeta_2 f_{n2} f + f_{n2}^2}{f_{n2}^2 - f^2 + j2\zeta_2 f_{n2} f} \tag{4.29}$$

The standard deviation of the quantity $\phi_o(t)$ is obtained from;

$$\sigma_{\phi o} = \sqrt{\int_{-\infty}^{\infty} S_{\phi o}(f) df} \tag{4.30}$$

and $\phi_{e1}(t)$ and $\phi_{e2}(t)$ are obtained similarly. The standard deviations of the loop phase errors give the likelihood of loop unlock. The maximum phase error that a loop can withstand providing no other loop components go into saturation first is dictated by the range of the phase detector. Given a multiplying phase detector, the maximum phase error is $\pm\pi/2$ radians before cycle slipping occurs [3]. If the static loop phase errors are assumed negligible and the phase noise is gaussian then the limit on the phase noise standard deviation used by Gardner [3] may be employed to predict loss of lock. From experimental data, Gardner states that the loop does not fall out of lock provided the phase error standard deviation multiplied by a factor of 3.5 does not exceed the loop limit. Thus the σ_{e1} and σ_{e2} must not exceed 0.45 radians. However, should static phase errors exist in either loop (due to a frequency offset between loop input frequency and loop oscillator free running frequency [3]) then these must be subtracted from the limit of 0.45

radians and thus the loop jitter tolerance is reduced.

4.15. Conclusions

A synchronous transmitter architecture designed to phase lock the final output carrier frequency to a recovered data clock has been implemented, arranged around an implementation of the precise phase modulator presented in chapter 3. An 8-bit modulator was used with 8kHz sampling of the modulated phase, to give 2.5kHz deviation F.M. with frequency doubling to increase the deviation to 5kHz for a 25kHz channel spacing. Post-modulation anti-alias filtering was implemented using a conventional I.F. crystal filter and hardlimiting was implemented to remove the amplitude variation (which had been predicted in chapter 3) caused by the spectral envelope that results from the zero-order hold of the modulated phase. The measured audio distortion factor was within that accepted for mobile radio equipment and below 5% for most of the audio spectrum.

A phase noise transfer model has been discussed together with the limits on input phase jitter to the transmitter that allow the phase lock circuitry to remain in lock.

4.16. References

[1] Gardner, F. M. "*Phase lock techniques*" 1979 John Wiley & Sons, Inc. New York ISBN 0-471-04294-3

[2] Department of Trade and Industry Radio Regulatory Division MPT1326 "*Performance Specification - Angle modulated equipment for use at fixed and mobile stations in the Private Mobile Radio service*" Nov. 1985 H.M.S.O. London.

[3] Gardner, F.M., "*Angle modulation limits of a noise-free phase lock loop*"

I.E.E.E. Trans. Comms. vol. COM-26 No. 8 Aug. 1978 pp.1129-1136.

Chapter 5:
Transmitter Synchronisation

5.1. Introduction

The synchronisation of the carrier frequency of a number of geographically separated transmitters is vital for acceptable performance of a mobile radio area coverage scheme in areas of coverage overlap. In quasi-synchronous schemes, high stability oscillators are installed in each base station and aligned as close as possible to the same carrier frequency (within a few hertz in the case of F.M. schemes). The performance of such schemes is thus highly dependent on the drift and ageing performance of these oscillators. Since modulation information must be conveyed to each transmitter via some form of link, this link could also be used to convey synchronization information to each transmitter.

Previously, it has been shown that the use of P.C.M. transmission of the modulating signal to each transmitter allows far greater accuracy in equalising the modulation of each transmitter. The digital transmission of the modulating signal inherently includes bit timing information which could be used as a frequency standard by each transmitter. However, the purity of the timing signal presented to each transmitter may be crucial to the performance of the transmitter: individually and as part of an area coverage scheme.

5.2. Baseband digital transmission

The basic components of baseband transmission are shown in figure 5.1. The binary data stream may be first subject to source coding. This may include scrambling and encryption of the data, or the addition of framing and overhead information in the case of multiplex trunk systems. The resulting binary stream is then subject to line coding to aid transmission across the medium used.

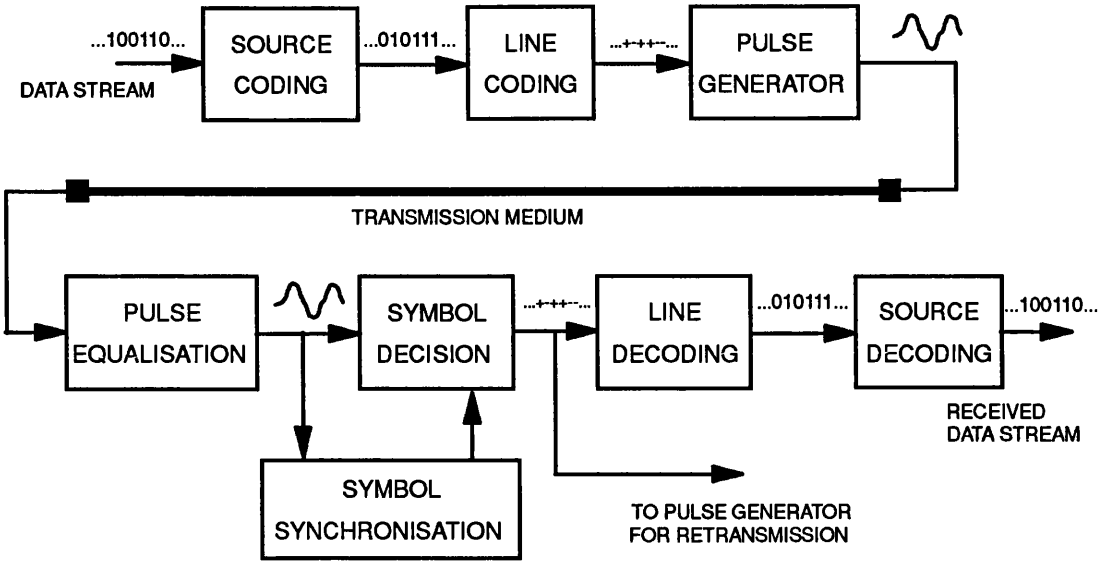

Figure 5.1: *The basic elements of baseband digital transmission*

The resulting symbols are converted to appropriate pulses and, if necessary, from electrical to optical signals if optical media are used. After transmission and opto-electrical conversion as necessary, the received signal is pre-processed to equalise the signal pulse shape to optimise the symbol detection process. A synchronising signal is derived from the processed received symbol stream and used to determine the optimum decision instant for each symbol. After detection the received symbols may either be fed to a pulse generator for retransmission (as in a digital repeater) or decoded for both line and source coding in order to retrieve and/or demultiplex the received data.

Pulse code modulation transmission at baseband has one overriding advantage over analogue landline transmission: the ability to reconstruct at the receiver an identical signal to that transmitted (with a given probability of error). The degradations of the transmission line: attenuation, distortion and noise cannot be removed entirely from an analogue signal, but merely increase the probability of error in regeneration of a digital signal. The limit on transmission distance in a digital system is the probability of error acceptable to the user (error rates of

$<10^{-9}$ are common [1]), thus digital repeaters may be used to extend transmission distance indefinitely if repeater spacing is within this limit.

Repeater spacing varies for the symbol rate and transmission medium used. Transmission media divide into two categories: metallic media such as coaxial cable and twisted pairs and optical media - both single and multi-mode fibres. Optical media, in general, offer lower loss allowing greater repeater spacing and larger bandwidths allowing greater transmission speeds [1]. For this reason they have found favour in trunk line applications, but many digital networks contain a great deal of metallic media and new installations continue to use metallic cables for inexpensive local lines. Repeater spacing for twisted pair, coaxial cable and multi-mode fibres is of the order of a mile, with the more expensive single-mode fibres requiring repeaters only every 25 miles or so [1].

Large regional, national and international digital networks are formed through the interconnection of digital multiplex/demultiplex units and digital switches by digital transmission lines. If a digital network is to support a synchronous area coverage scheme synchronized to timing information conveyed by the digital streams transmitted between network nodes, then any degradation of this timing information introduced by network equipments will accumulate through the network and may degrade the area coverage scheme performance.

5.3. P.C.M. reception

The basic form of a P.C.M. receiver is shown in figure 5.2. These basic elements are present regardless of whether the transmission medium is metallic or optical. In both cases, the transmitted signal is subjected to distortion and attenuation due to transmission characteristics of the medium used and the effects of additive noise. The first elements of processing, amplification and equalisation, are necessary to compensate for these effects.

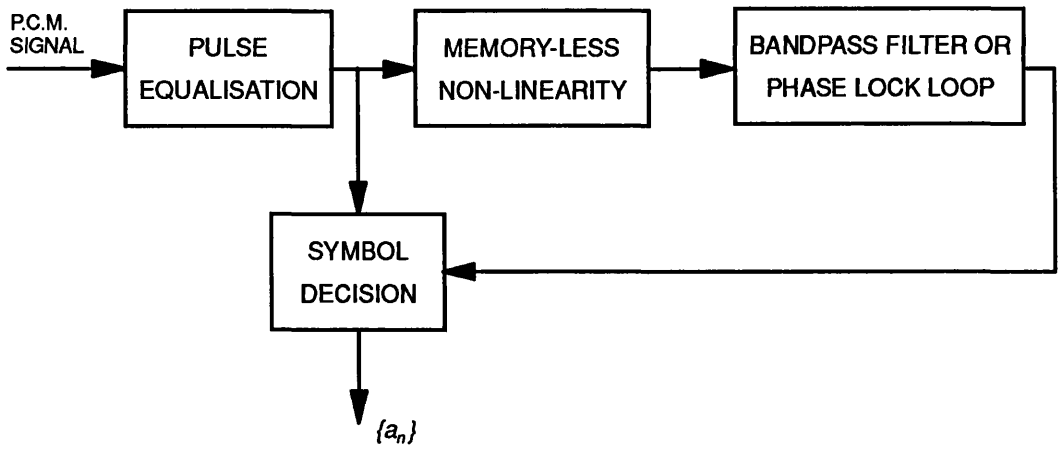

Figure 5.2: *Basic configuration of a P.C.M. receiver*

The general form of the received P.C.M. signal after this initial processing is (assuming no jitter no the input P.C.M. stream - discussed later in this chapter):

$$s(t) = \sum_{n=-\infty}^{+\infty} a_n g(t - nT) + n(t) \qquad (5.1)$$

where $\{a_n\}$ are the transmitted symbols, T is the symbol period, $n(t)$ is additive white Gaussian noise and $g(t)$ is the received pulse shape after equalisation. Pulse shape equalisation maximises the ability of the receiver to determine the symbols, $\{a_n\}$, in the presence of noise and aids accurate clock extraction. Since all channels are inherently bandlimited, the equalisation of the channel is bandlimited and chosen to minimize inter-symbol interference (I.S.I.): i.e. ensuring that at time $t=nT$ that $g(t-mT)=0$ for all m except $m=n$. The raised-cosine channel proposed by Nyquist [2] has a frequency response $G(f)$ defined:

$$G(f) = 0.5 - 0.5\sin\left(\frac{\pi(fT - 0.5)}{\beta}\right) \qquad \frac{(1-\beta)}{2T} < |f| < \frac{(1+\beta)}{2T} \qquad (5.2)$$

$$G(f) = 1 \qquad 0 < |f| < \frac{(1-\beta)}{2T} \qquad (5.3)$$

$$G(f) = 0 \qquad \text{all other } f \qquad (5.4)$$

This results in a pulse response $g(t)$ of [2]:

$$g(t) = \frac{\sin\frac{\pi t}{T}\cos\frac{\pi\beta t}{T}}{\frac{\pi t}{T}\left(1-\left(\frac{2\beta t}{T}\right)^2\right)} \qquad (5.5)$$

where β is the roll-off factor of the channel and $0 \leq \beta \leq 1$ although a fully-raised cosine channel, $\beta = 1$, is most commonly used.

5.4. Line coding

Practical P.C.M. systems do not use uni-polar signalling, i.e. the raw bit stream, but apply some form of line coding or re-formatting prior to transmission. The type of line coding employed is largely dependent on the transmission medium and symbol rate and is used to optimise the transmitted signal to minimise vulnerability to I.S.I. and noise, to guarantee stable and reliable timing recovery, to aid conditioning of the received signal and simplify hardware implementation at the receiver.

The most common family of line codes for baseband digital transmission (particularly for metallic transmission media) are forms of pseudo-ternary coding the most simplest of which is Alternate Mark Inversion (A.M.I.). A.M.I. exhibits a high degree of redundancy in that three levels (positive, zero, negative) are used to code two possible symbols: a binary zero translates to a zero symbol and each binary mark results in a symbol mark of the opposite polarity of the previous symbol mark. However, long runs of consecutive binary zeroes result in no symbol transitions which degrades timing recovery considerably. Consequently, two coding schemes exist for zero substitution of the binary scheme: *BnZS* (Bipolar *n*-Zero Subsitution) and *HDBn* (High Density Bipolar order *n*).

B6ZS and HDB3 are the most commonly used of these families of codes [1]. B6ZS

code replaces a sequence of six consecutive zeroes by "*0VB0VB*" where "*0*", "*V*", and "*B*" indicate a ternary zero, a violation of A.M.I. coding rules, and a mark that obeys A.M.I. rules respectively. HDB3 coding makes a substitution for four consecutive zeroes with a choice of two sequences, "*000V*" and "*B00V*" which are used alternately in order that no net D.C. component exists in the transmitted signal.

For optical fibre transmission, line codes from the *mBnB* code family are popular, particularly 7B8B. In these codes, every m bits of the data stream are converted to n-bit words for transmission, where m<n. The n-bit words used to represent all combinations of m bits are chosen by virtue of the balance of marks and spaces in each word and the number of consecutive marks or spaces in each word. The properties of this family of codes are given in detail by Brooks and Jessop [5]. These codes do have the drawback of increasing the actual bit rate of the transmission.

5.5. Jitter in timing extraction

5.5.1. Timing extraction

Timing extraction by using a single-tuned circuit has been extensively used in the past due to its simplicity and low power consumption - particularly important in digital repeaters fed with power transmitted down the line. The block diagram of such a repeater is shown below.

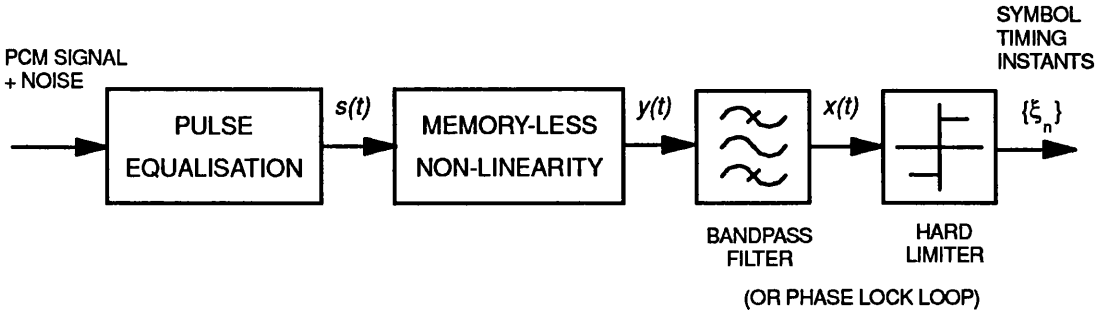

Figure 5.3: *Block diagram of symbol synchronisation process*

This configuration has been studied by a number of authors for perfect equalisation of the pulse shape and a square-law non-linearity, since this allows a tractable mathematical analysis. If $\{a_n\}$ is a wide-sense stationary random process then it can be shown [3] that *s(t)* is a cyclo-stationary random process i.e. its mean and autocorrelation exhibit periodicity of period T. However, *s(t)* does not contain a spectral component at the symbol rate, $1/T$, for synchronization. However, it can also be shown that by passing a cyclo-stationary process through a memory-less non-linearity, *y(x)*, of the form:

$$y(x) = \sum_{m=0}^{M} \alpha_m x^m \qquad \text{where } \alpha_m \text{ are constants} \qquad (5.6)$$

results in a spectral component at the symbol rate which may be extracted by bandpass filtering.

The bandpass filter may be a single-tuned circuit, phase-locked loop or surface acoustic wave filter depending on the performance and symbol rate required. The hard limiter removes amplitude fluctuations in the extracted clock signal and symbol decisions are made on the negative (say) going edges. The edges should correspond to the instants $t=nT$, but in general there will be a small error in the timing signal for each symbol. If the receiver forms part of a repeater and is used to re-time the signal for re-transmission, then the signal received after equalisation at the following receiver is of the form:

$$s'(t) = \sum_{n=-\infty}^{+\infty} a_n g(t - nT - \xi_n T) + n(t) \qquad (5.7)$$

where $\{\xi_n\}$ are the small timing errors or *jitter* in the digital stream. The variable $\{\xi_n\}$ may be treated as a Gaussian random variable with variance σ_ξ^2 and autocorrelation $R_\xi[kT]$ where:

$$R_\xi[kT] = E[\xi_n \xi_{n+k}] \qquad (5.8)$$

and hence the jitter power spectral density, $S_\xi(f)$, is given by the Discrete Fourier transform of $R_\xi[kT]$:

$$S_\xi(f) = \sum_{k=-\infty}^{+\infty} T R_\xi[kT] e^{-j2\pi kfT} \qquad (5.9)$$

and thus its variance is calculated from:

$$\sigma_\xi^2 = \int_{-1/2T}^{1/2T} S_\xi(f) df \qquad (5.10)$$

If the input stream is not jitterless as equation 5.1, but is already jittered as equation 5.7, then the P.C.M. stream is still a cyclo-stationary process provided the jitter sequence $\{\xi_n\}$ is jointly stationary with $\{a_n\}$. However, from the point of view of reception of the signal, a quantity of great importance is then the

alignment jitter, i.e. the difference between the jitter of the input stream $\{\xi_n\}$ and the jitter of the recovered clock $\{\xi'_n\}$:

$$\Delta\xi_n = \xi'_n - \xi_n \qquad (5.11)$$

A repeater could operate with low error rate even if the input and output jitter were large provided the alignment error between the two is small so that bit decisions are made near to the optimum instants for noise immunity.

5.5.2. Timing recovery filters

Three types of timing wave recovery filter are commonly used for symbol synchronisation in P.C.M. reception. These are tuned circuit type bandpass filters, phase lock loops and surface acoustic wave (SAW) filters.

A second order bandpass filter has a transfer function given by:

$$H(s) = \frac{\omega_n s/Q}{s^2 + \omega_n s/Q + \omega_n^2} \qquad (5.12)$$

where Q is the Quality factor of the filter and sets the 3dB bandwidth and ω_n is the natural frequency (*rads* s^{-1}). For high values of Q, ω_n is the centre frequency of the bandpass filter, which for perfect tuning is set to the symbol rate f_b. However, a degree of mistuning is inevitable in a practical system so if the actual centre frequency of the filter is at f_o then the degree of mistuning δ is:

$$\delta = \frac{f_o - f_b}{f_b} \qquad (5.13)$$

So by putting $s=j2\pi f$ and $\omega_n=2\pi f_o$, then the response is:

$$H(f) = \frac{j f f_o/Q}{f_o^2 - f^2 + j f f_o/Q} \qquad (5.14)$$

Since non-linear processing of the P.C.M. signal yields a frequency component in the resulting signal at the symbol rate of the signal, timing extraction can

equally be performed by phase locking an oscillator at the symbol rate to this component. A conventional second order phase lock loop as described in literature (Gardner [9]) can be used for this purpose. The jitter performance is discussed further in the later sections.

At high bit rates, phase lock loop timing recovery becomes more difficult and more expensive to implement. Also, even at lower bit rates, PLL timing recovery requires more power and circuit complexity and thus a reduction in reliability relative to passive timing recovery. Power consumption and reliability are paramount in inaccessible installations (buried or underwater transmission lines) and thus passive timing recovery is often favoured in these situations. The use of SAW filters in timing recovery has become widespread in the range 100Mbit/s to 2Gbit/s [10]. The simplest form of a transversal SAW filter is shown in figure 5.5 [10].

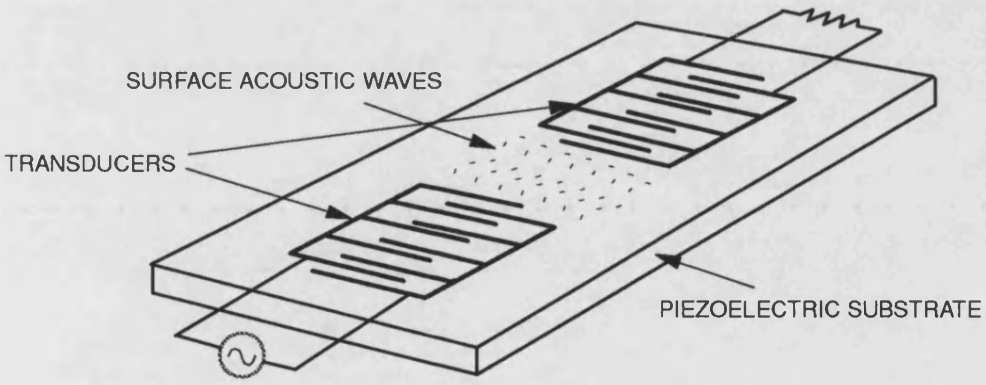

Figure 5.4: *Simple form of a transversal surface acoustic wave filter*

Piezoelectric transducers that convert input voltage into propagating surface acoustic waves and back into output voltage are fabricated as "combs" of metallic film deposited on a piezoelectric substrate. This is usually quartz in the case of narrowband filters used for timing recovery. The voltage applied to the sending transducer causes strong field of alternating sign between successive pairs of

fingers to generate localised alternating strains (acoustic surface waves) in the substrate. The inverse process occurs at the receiving transducer resulting in a voltage at the output.

Chamzas [7] reports a full model for transversal SAW filters related to their electrical and physical characteristics, i.e. number of comb "fingers", distance between transducers, terminating impedances etc. Chamzas uses a simpler model for jitter analysis. If the SAW filter has a bandpass transfer function $H_{SAW}(f)$, then it has an equivalent lowpass function $H_L(f)$ given by:

$$H_L(f) = \frac{H_{SAW}(f + f_b)}{H_{SAW}(f_b)} \qquad (5.15)$$

where f_b is the baud rate (number of symbols per second) of the system. The significance of the lowpass function for jitter analysis is discussed later in this chapter. Chamzas models the lowpass function in the case of a transversal SAW filter as:

$$H_L(s) = \frac{s_1 s_2}{(s - s_1)(s - s_2)} e^{-cs} \qquad (5.16)$$

where:

$$s_i = -a_i + jb_i = -(1 \pm \varepsilon)a + jb_i \qquad i = 1,2 \qquad (5.17)$$

are its two poles, ε is the degree of asymmetry and c is a linear phase slope used to correct the phase of the model, since SAW filters are not minimum phase filters. If BW_{SAW} is the SAW filter bandwidth and f_c its centre frequency then the various parameters of the filter are related to the pole positions by the following equations. The filter mistuning from the baud rate is:

$$2\pi(f_c - f_b) = (b_1 + b_2)/2 \qquad (5.18)$$

The detuning factor α (i.e. relative to the bandwidth is):

$$\alpha = 4\pi(f_c - f_b)/BW_{SAW} \qquad (5.19)$$

The natural frequency ω_n and damping factor ζ of the filter are given by:

$$\omega_n^2 = a^2 + b^2 \qquad (5.20)$$

$$\zeta = a/\omega_n \qquad (5.21)$$

The filter's quality factor Q is given by:

$$Q = \omega_n / BW_{SAW} \qquad (5.22)$$

and the constants a and b are:

$$a = (a_1 - a_2)/2, \quad b = (b_1 - b_2)/2 \qquad (5.23)$$

The natural frequency ω_n can be determined approximately from the bandwidth BW_{SAW} (for $\varepsilon << 1$) by:

$$\omega_n^2 = \left(\frac{BW_{SAW}}{2}\right)^2 \frac{1}{-(1-2\zeta^2) + ((1-2\zeta^2)^2 + 1)^{0.5}} \qquad (5.24)$$

Typical values for these filter parameters are:

$$160kHz < \frac{BW_{SAW}}{2} < 240kHz \qquad \frac{BW_{SAW}}{2} \text{ is the bandwidth of } H_L(s)$$

$$|f_c - f_b| < 50kHz$$

$$0.60 < \zeta < 0.80$$

$$-0.1 < \varepsilon < 0.1$$

$$c = 0.2 \text{deg}/kHz \qquad (5.25)$$

If the baud rate is 300MHz, the above values give values of Q between 625 and 940.

5.5.3. Jitter calculation

A number of authors [13,14,15] have produced theoretical algorithms and analyses of the jitter power spectral density. Most are confined to particular choices of parameters to allow tractable mathematical analysis such as the restriction of square-law non-linearity, choice of line coding, choice of pulse shape

and the assumption of noiseless reception. In order to evaluate and quantify the effects of all system parameters on jitter and compare jitter from repeaters in a chain (discussed later in this chapter), direct simulation of the timing extraction process was employed to calculate jitter sequences.

Live digital traffic conditions are difficult to simulate exactly, though in practice pseudo-random binary sequences (P.R.B.S.) are easily generated and extensively used in the testing and alignment of digital systems [11]. C.C.I.T.T. recommendation O.151 [11] specifies the use of $2^{15}-1$ length sequences based on a 15-bit shift register and $2^{23}-1$ length sequences based on a 23-bit shift register. However, due to the cyclic nature of a P.R.B.S., a $2^{23}-1$ length sequence is used in order that no repetition occurs during long bit sequences. Longer sequences are required to give significant jitter spectral content at low frequencies at the symbol rates of interest. Cyclic sequence repetition results in distortion of the jitter power spectral density by spectral lines across the range of interest spaced at the repetition rate. For example, at $2.048Mbit/s$ the $2^{15}-1$ length sequence has a repetition rate of $62.5Hz$.

Generation of samples of the digital stream given the PRBS, line code and pulse shape is readily achieved in computer simulation. However, in order to implement filtering on non-linearly processed P.C.M. stream samples a F.I.R. (Finite Impulse Response) filter was used to model the timing extraction filter. This is obtained by calculating $N+1$ frequency points of the complex filter frequency response linearly spaced from $f=0$ to:

$$f = \frac{N_s f_b}{2} \qquad (5.26)$$

where N_s is the number of samples per symbol period. Then the complex conjugates of the $N-1$ points from the second point to the N^{th} point are taken, reversed in order and concatenated to the original $N+1$ points to form a $2N$-point

spectrum with the conjugate symmetry of a D.F.T. (Discrete Fourier Transform). A $2N$-point inverse F.F.T. (Fast Fourier Transform) is taken to give a F.I.R. representation of the filter impulse response. This impulse response is convolved with the calculated samples of the incoming equalised P.C.M. stream that have already been processed for the memory-less non-linearity. To increase the speed of this process, an "overlap and save" fast convolution is used [12], i.e. the impulse response is zero-padded to twice its length and a $4N$-point F.F.T. taken which is successively multipled to the F.F.T.s of overlapped $4N$-point blocks of the signal stream samples and inverse transformed to give $2N$ output points and $2N$ discarded points.

Having obtained samples of the timing wave $x(t)$, the timing instant for each symbol decision is determined by the moment that the timing wave crosses a set threshold γ, with a negative gradient (a positive gradient could equally well be used). This amounts to solutions of the conditions:

$$x(t) = \gamma, \quad \dot{x}(t) < 0 \tag{5.27}$$

the solutions $\{\tau_n\}$ being:

$$\tau_n = nT + \xi_n T \tag{5.28}$$

where $\xi_n T$ is the time displacement or "*jitter*" from the ideal sampling instant. This may include a static offset, but this is equalised out in a P.C.M. receiver. Ideally, the threshold γ (normalised to unity post-equalisation pulse amplitude) is zero, but in practice small offsets will exist. Since discrete samples of the timing wave have been calculated the instant of threshold crossing can only be established to occur at some point between two samples. In order to attain sufficient accuracy in the threshold crossing position a great many samples per symbol period would have to be calculated resulting in a prohibitive amount of computation. If N_s samples per symbol period are calculated, then the threshold crossing can be determined to occur between the k^{th} and $k+1^{th}$ samples of that

symbol period. To increase the accuracy further, *L-1* samples of the timing wave can be interpolated between the k^{th} and $k+1^{th}$ samples. This is performed by zero padding with *L-1* zero samples between each calculated sample *x(k)* and applying a F.I.R. interpolation filter to calculate samples *x'(i)* between the two original samples of interest. The filter used has an impulse response given by applying a Hanning window to the brick-wall response of a ideal interpolation filter [8] to give the impulse response *h(n)*:

$$h(n) = (0.5 + 0.5\cos(2\pi n / N))\frac{\sin(\pi n / N)}{\pi n / N} \qquad (5.29)$$

for $-N/2 \leq n \leq N/2$ where N is the length of the F.I.R. response and is assumed to be odd. This filter is easily implemented in the faster polyphase form with L phases of the input signal driving L phases of the impulse response *h(n)* denoted $h_\rho[n]$ where ρ is the phase [8]:

$$h_\rho[n] = \left(0.5 + 0.5\cos 2\pi(n + \rho / L)\right)\frac{\sin\left[\pi(n + \rho / L)\right]}{\pi(n + \rho / L)} \qquad (5.30)$$

The interpolated points are then examined for the threshold crossing conditions giving the crossing instant to occur between two of the interpolated points, the i^{th} and $i+1^{th}$ between the k^{th} and $k+1^{th}$ original points over the given symbol period. The actual instant is then determined as the point on a straight line drawn between the i^{th} and $i+1^{th}$ interpolated points that equals the threshold value γ. Figure 5.4 shows the principle. If the threshold is crossed between the i^{th} and $i+1^{th}$ interpolated samples between the k^{th} and $k+1^{th}$ original samples of the timing wave of a given symbol period, then the timing instant can be readily shown to be:

$$\xi_n T = T_s\left(k + \frac{1}{L}\left(i + \frac{\gamma - x'(i)}{x'(i+1) - x'(i)}\right)\right) \qquad (5.31)$$

where L is the interpolation factor, T_s the sample period and T the symbol period (related by the number of samples per period N_S).

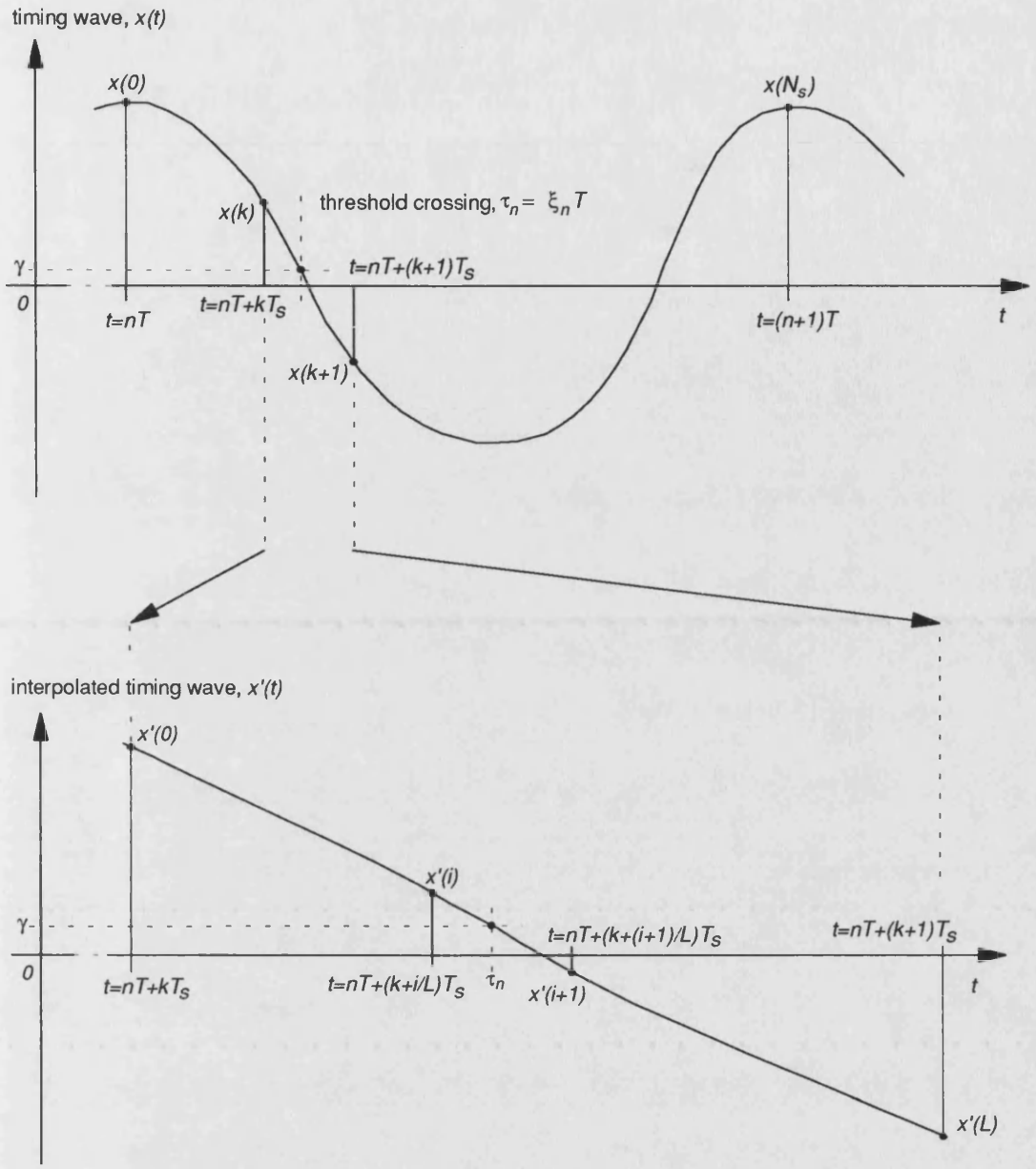

Figure 5.5: *Calculation of timing jitter from the recovered timing wave*

The accuracy of the interpolated samples of the timing wave are the key to the accuracy of this technique. The insertion of zeros causes well-documented effects in the spectrum of the interpolated signal [8], i.e. the sets of alias components of the pre-interpolation spectrum centred on integer multiples of the original sampling frequency. These must be removed or attenuated to an acceptable level by the interpolation filter to yield accurate interpolated samples at the new

sampling frequency. All jitter calculated in this thesis was derived using 32 samples per period (N_s) of the P.C.M. stream and an interpolation factor of 100 (L) with an interpolation filter of 1001 (N) points. Since the spectrum of the timing wave after recovery is narrowband and centred on a frequency 1/16th of the Nyquist folding frequency, the significant spectral power due to the first aliased spectrum produced by interpolation is some distance away in spectral terms, easing the roll-off requirement of the interpolation filter. The filter used gave 100dB of attenuation by the centre of the first aliased spectrum and thus a negligible amount of aliased spectral power appears in the interpolated timing wave.

5.5.4. Jitter power spectral density

Having determined a set of jitter values $\{\xi_n\}$, the jitter power spectral density can be estimated. The definition of jitter power spectral density given earlier in this chapter implies an infinite duration jitter sequence which is not possible in practice. A spectral estimate can be obtained by taking a jitter sequence of N points, windowing the sequence with a Hanning window as used to window the interpolation filter reponse and taking its D.F.T. The power spectral density is then calculated as the square of the magnitude. However, to reduce the variance of the estimate and give a smoother power spectral density and a number of such estimates are calculated from blocks of a longer jitter sequence and the results averaged to give the jitter power spectral density. Thus, if the m^{th} estimate of the jitter power spectral density is $\tilde{S}_{\xi M}[k]$ where:

$$\tilde{S}_{\xi m}[k] = \left| \sum_{n=0+mN}^{N-1+mN} \xi_n e^{-j2\pi kn/N} \right|^2 \qquad (5.32)$$

then the averaged result $\overline{S}_{\xi}[k]$ over M estimates is:

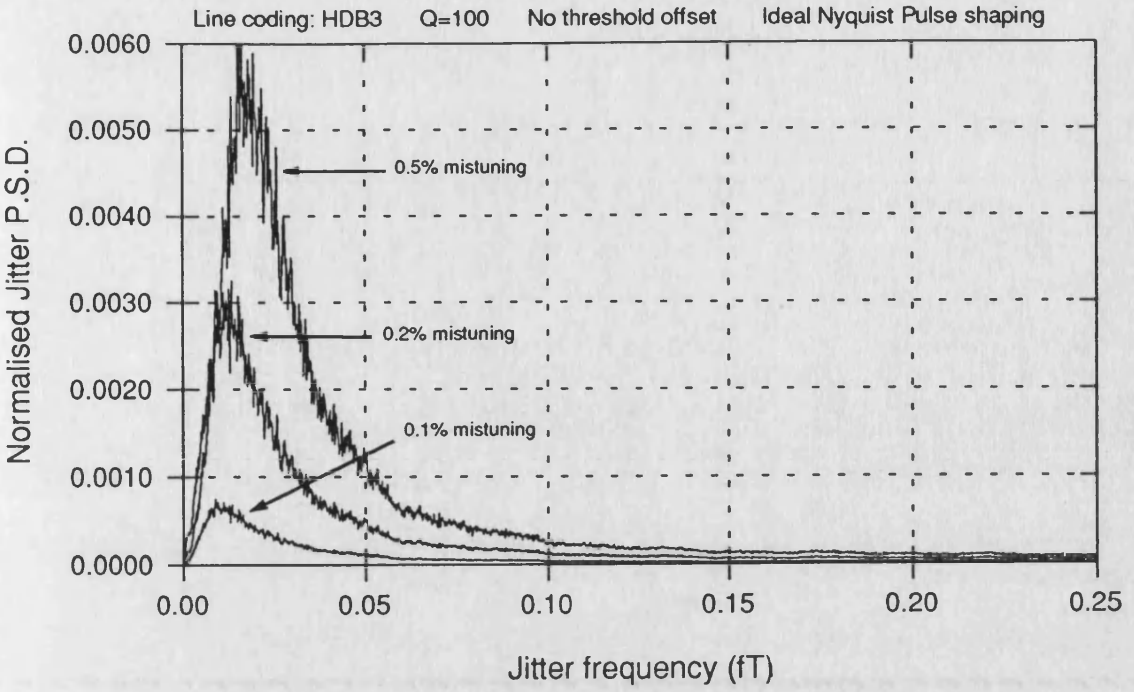

Figure 5.6a: *Jitter power spectral density variation with mistuning: fixed Q, no threshold offset and no noise (pattern-dependent jitter only)*

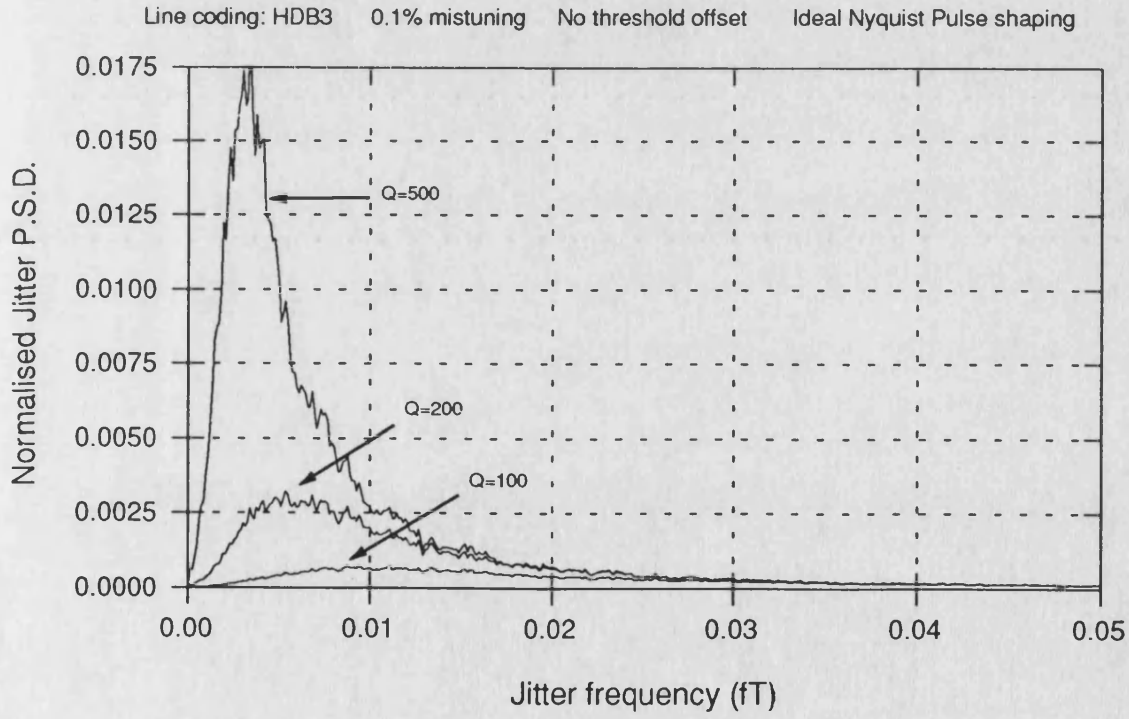

Figure 5.6b: *Jitter power spectral density variation with Q: 0.1% mistuning, no threshold offset and no noise (pattern-dependent jitter only)*

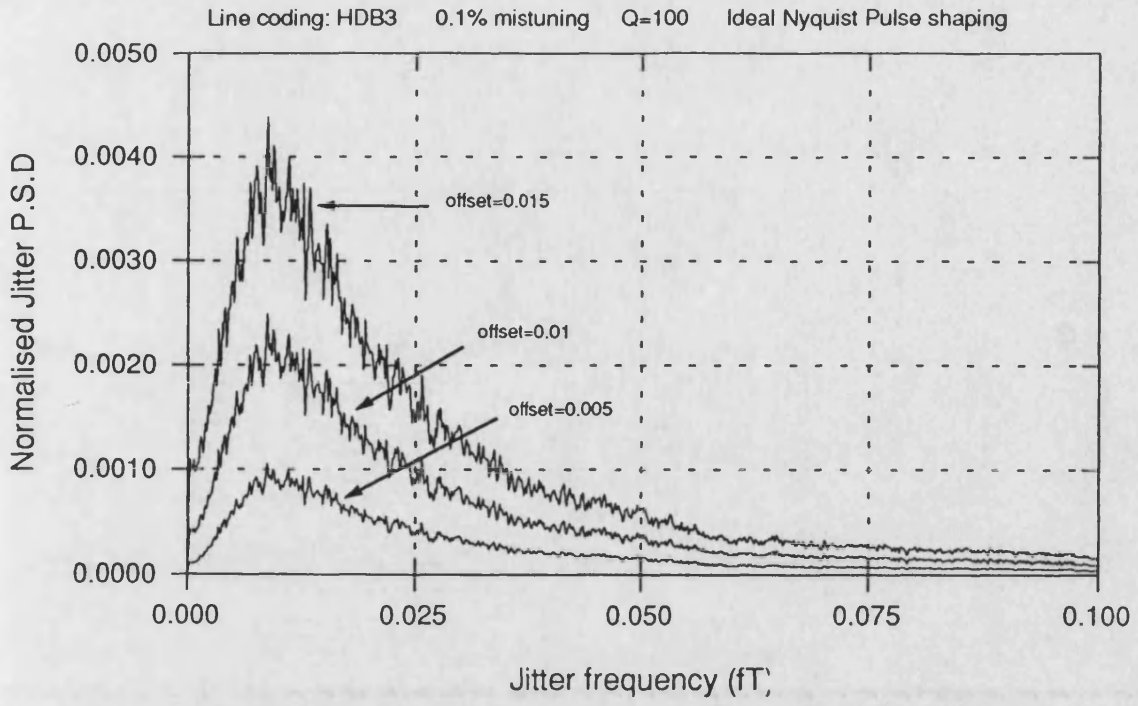

Figure 5.6c: *Jitter power spectral density variation with threshold offset: 0.1% mistuning, Q=100 and no noise (pattern-dependent jitter only)*

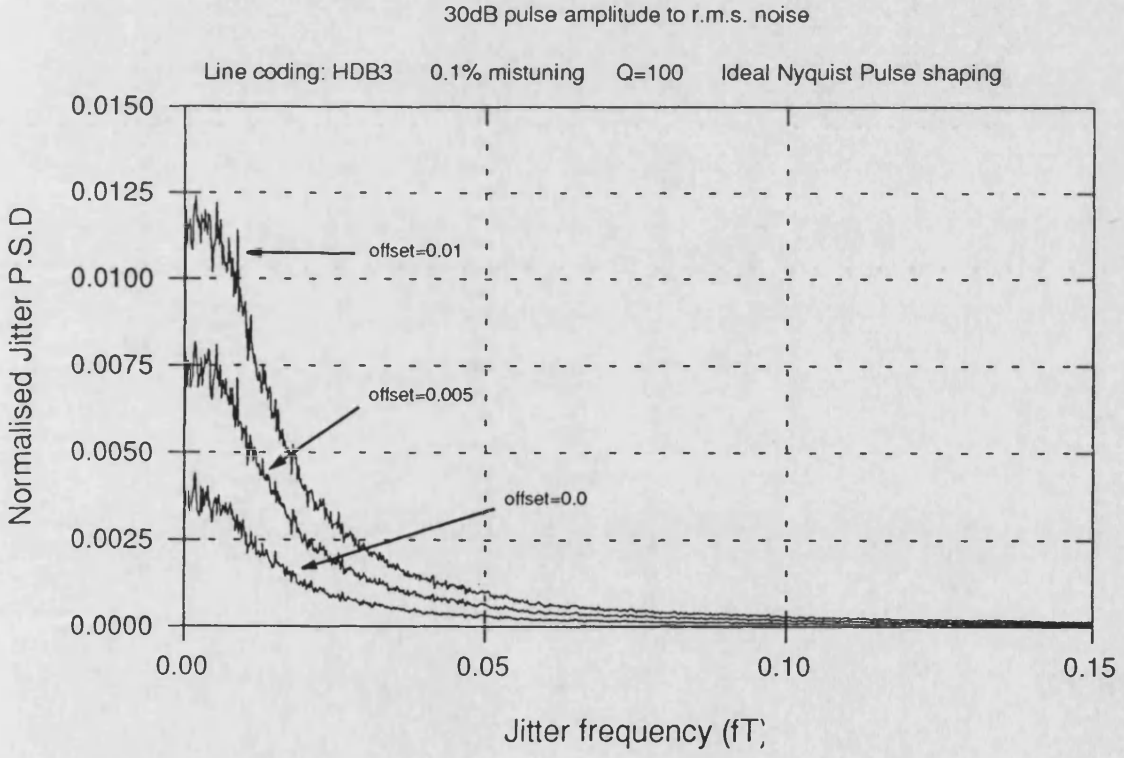

Figure 5.6d: *Jitter power spectral density variation with threshold offset: 0.1% mistuning, Q=100 and white gaussian channel noise*

$$\overline{S}_{\xi}[k] = \frac{1}{M}\sum_{m=1}^{M}\tilde{S}_{\xi m}[k] \qquad (5.33)$$

The jitter power spectral density is calculated for bandpass filter timing recovery using a second order filter and the results are given in figures 5.6a, b, c and d. The parameters examined for their effect on the jitter power spectral density are the bandpass filter Q, the mistuning of the tuned circuit from the symbol rate, δ, the threshold offset of the zero-crossing detector and channel noise The jitter power spectral densities shown are each the result of 150 averaged spectral estimates, each estimate derived from a 8192 point jitter sequence. A square-law non-linearity is used, the channel is fully raised cosine (i.e. β=1) and HBD3 line coding is used. The values of thresholds given are relative to unity peak pulse amplitude and the signal-to-noise figure for figure 5.7d for additive white gaussian channel noise is determined from the ratio of peak pulse amplitude to r.m.s. noise amplitude.

The principle difference in the shapes of the jitter power spectral densities shown is in their behaviour as the frequency approaches zero. Those cases with no trigger threshold offset or channel noise have a jitter power spectral density that approaches zero as the frequency approaches zero. Those with threshold offset or additive channel noise have power spectral densities that approach and level off at a finite non-zero value as they approach zero frequency.

Immediately prior to filtering (whether by bandpass filter or phase lock loop), the significant part of the processed signal $y(t)$ near the symbol frequency can be written as:

$$y(t) = (e_o + I(t))\cos 2\pi f_o t + Q(t)\sin 2\pi f_o t \qquad (5.34)$$

where e_o is the magnitude of the component at the symbol rate and $I(t)$ and $Q(t)$ are the random, zero-mean in-phase and quadrature components of the

disturbance due to the data pattern, pulse shape, intersymbol interference or channel noise. The power spectral densities of *I(t)* and *Q(t)* are difficult to determine analytically and no general solution exists for all pulse shapes and digital coding. Gardner [9] gives the general shape of their spectra:

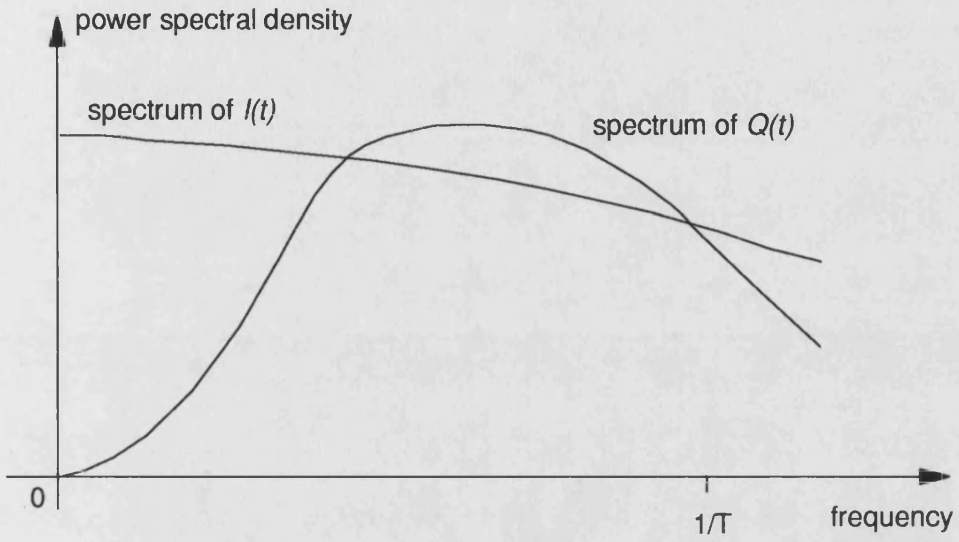

Figure 5.7: *In-phase and quadrature disturbances contributing to jitter*

Bandpass filtering of *y(t)* to give the timing wave *x(t)* imposes a low pass roll-off on both *I(t)* and *Q(t)*, but near zero-frequency their behaviour remains the same. (The exact nature of the phase jitter transfer of a bandpass filter is discussed later, but to a first approximation it performs a low-pass filtering action on the modulating components of a signal to which it is tuned) The filtered in-phase disturbance *I(t)* does not contribute to the jitter unless ampltude-to-phase conversion resulting from trigger threshold offsets exist. The filtered quadrature disturbance *Q(t)* always results in jitter whether threshold offsets exist or not. This accounts for the shapes of the jitter power spectral densities shown: the *Q* of the bandpass filter determines the steepness of roll-off of the spectrum, the degree of mistuning determines the position of the peak of the spectrum (see the later treatment of the jitter transfer function of a bandpass filter) and the

threshold offset determines the degree of amplitude-to-phase conversion and thus amount by which the in-phase component *I(t)* of the pattern-dependent disturbance contributes to jitter.

The jitter performance of a phase lock loop can be treated in a similar way, though a rigorous analysis is given be Roza [15]. Ideally, the loop will respond only to *Q(t)* and not at all to *I(t)*. The phase jitter it produes is filtered by the lowpass dynamic response of the loop. If, however, the loop oscillator has a static phase error θ_e, then (if, for example, the loop has a multiplying phase detetctor) the output of the phase detector will contain a term $I(t)sin\theta_e$ as well as a term $Q(t)cos\theta_e$ [9]. The static phase error results from a frequency offset between that of the symbol rate to be tracked and that of the loop oscillator free-running frequency and thus must be minimised to reduce jitter. The effect of static phase errors in PLL recovery is thus analogous to that of threshold offset in bandpass recovery. The principle contributing factors to jitter, *I(t)* and *Q(t)* are independent of timing recovery filter and thus conclusions of the jitter perfomance of both types may be drawn from results of one type.

Takasaki [4] has classified jitter into two types by the behaviour of the jitter power spectral density. Type A has a spectral density that goes to zero at zero frequency and type B has a flat spectral density at zero frequency. It has been shown here and by other authors that Type A jitter is generated by the tuned circuit mistuning and Type B jitter is generated by trigger threshold offset (i.e. amplitude-to-phase conversion) and pulse shape asymmetry. In a practical system all effects will be present to some degree, so most jitter power spectral densities are flat and non-zero at zero-frequency with the characteristic lowpass roll-off.

5.6. Accumulation of jitter in a chain of repeaters

5.6.1. A model for jitter accumulation

To increase the range of a digital transmission link, digital repeaters (regenerators), are placed along the line. The jitter of the recovered clock signal at each repeater will not only be a function of the parameters discussed in the previous section, but of the jitter on the input P.C.M. stream due to previous clock recovery processes. Consider a digital transmission line with regularly spaced digital repeaters fed with a jitterless source as shown in figure 5.8, where $e_k[n]$ is the timing jitter at the output of the k^{th} repeater i.e.: the displacement of the n^{th} re-timed symbol from that repeater (and is also the input jitter to the next repeater).

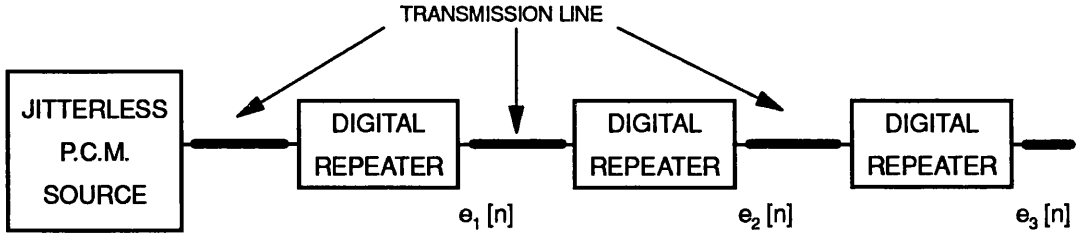

Figure 5.8: *A transmission line with a chain of digital repeaters*

Generalising the model attributed to Chapman by Byrne et al. [6], the k^{th} repeater in the chain may be effectively modeled as an additive jitter source $e_{ik}[n]$, where the jitter added has a power spectral density $S_{ik}(f)$ (assuming the jitter is a stationary random process) and a jitter transfer function $H_k(f)$ dependent on the type of timing filter. The injected jitter arises from both noise and pattern-dependent effects as described in the previous section and thus has two components; a random compoent and a systematic component. The jitter at the output of the k^{th} regenerator is the filtered sum of the jitter injected at the k^{th} and all previous repeaters filtered by each repeater through which it passes.

The jitter power spectral density at the output of the k^{th} repeater is denoted $S_k(f)$. The model is shown in figure 5.9.

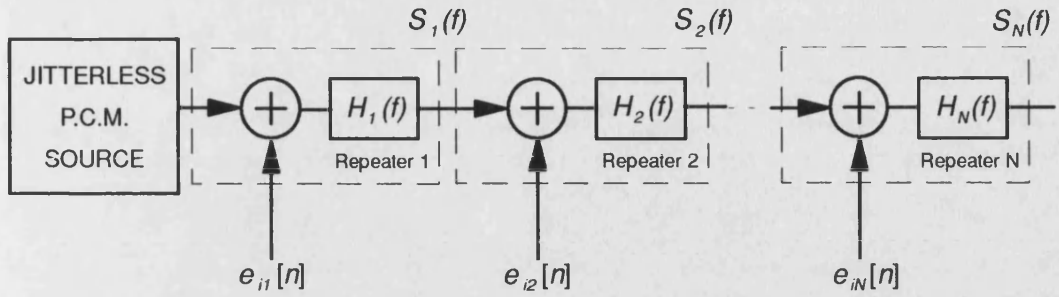

Figure 5.9: *Chapman's model for jitter accumulation*

The following assumptions were made by Chapman:

1. The same systematic jitter is injected at each repeater. Random jitter due to thermal noise is neglected and does not accumulate down the chain (this is a fair approximation in the case of a large amount of systematic jitter being injected at each repeater as was the case with Chapman's system, but not true in general). Systematic jitter is assumed to depend largely on the digital pattern which is the same at each repeater so that small variations in repeater parameters have little effect:

2. Jitter adds linearly from repeater to repeater:

3. All repeaters have identical transfer functions. Chamzas [7] has performed a stocastic analysis on a chain of repeaters whose transfer functions were distributed about a mean transfer function. He found for long chains that the variance in r.m.s. jitter is only 5%, showing that this assumption gives a reliable estimate of r.m.s jitter.

The systematic jitter power spectral density of the jitter injected at each repeater

is denoted $S^S(f)$, but since the systematic jitter is assumed to add coherently from repeater to repeater, the "amplitude" spectral densities due to each repeater ($\sqrt{S^S(f)}$ suitably filtered by *H(f)* the appropriate number of times) add together. Thus the systematic jitter power spectral density after N repeaters due to systematic jitter alone $S_N^S(f)$, is given by:

$$S_N^S(f) = \left| \sqrt{S^S(f)} \prod_{n=1}^{N} H(f) + \sqrt{S^S(f)} \prod_{n=2}^{N} H(f) + \ldots + \sqrt{S^S(f)} H(f) \right|^2$$

$$= S^S(f) \left| \sum_{n=1}^{N} H^n(f) \right|^2 \qquad (5.35)$$

This can be shown to simplify to [6]:

$$S_N^S(f) = S^S(f) |H(f)|^2 \left| \frac{1 - H^N(f)}{1 - H(f)} \right|^2 \qquad (5.36)$$

and thus the variance of the systematic jitter is given by:

$$\left\langle \sigma_N^S \right\rangle^2 = \int_{-1/2T}^{1/2T} S_N^S(f) df \qquad (5.37)$$

If random jitter is examined in the same way, its accumulation mechanism differs in that the jitter power spectral density contributions from all previous repeater add (not the amplitude spectral densities). Thus the jitter power spectral density after *N* repeaters, due to random jitter alone $S_N^R(f)$ (denoting the random jitter power spectral density injected at each repeater as $S^R(f)$) is given by:

$$S_N^R(f) = S^R(f) \prod_{n=1}^{N} |H(f)|^2 + S^R(f) \prod_{n=2}^{N} |H(f)|^2 + \ldots + S^R(f) |H(f)|^2$$

$$= S^R(f) \sum_{n=1}^{N} |H(f)|^{2n} \qquad (5.38)$$

This can be shown to simplify to [6]:

$$S_N^R(f) = S^R(f)|H(f)|^2 \frac{1-|H(f)|^{2N}}{1-|H(f)|^2} \qquad (5.39)$$

and thus the variance of the systematic jitter is given by:

$$\left\langle \sigma_N^R \right\rangle^2 = \int_{-1/2T}^{1/2T} S_N^R(f)df \qquad (5.40)$$

Since, by definition, the random jitter and systematic jitter is uncorrelated, their accumulated power spectral densities add, thus the total jitter at the output of N repeaters has variance:

$$\sigma_N^2 = \left\langle \sigma_N^R \right\rangle^2 + \left\langle \sigma_N^S \right\rangle^2 \qquad (5.41)$$

As discussed previously in this chapter, in many situations the injected jitter (whether random or systematic) can be assumed to have a flat power spectral density and thus $S^R(f)$ and $S^S(f)$ are constant. The quantity of interest is thus the effective jitter *power* transfer functions for random and systematic jitter, $T_N^R(f)$ and $T_N^S(f)$ respectively:

$$T_N^R(f) = |H(f)|^2 \frac{1-|H(f)|^{2N}}{1-|H(f)|^2} \qquad (5.42)$$

and:

$$T_N^S(f) = |H(f)|^2 \left| \frac{1-H^N(f)}{1-H(f)} \right|^2 \qquad (5.43)$$

The nature of both transfer functions are thus heavily dependent on the jitter transfer functions $H(f)$ of the repeaters in the chain.

5.6.2. Jitter transfer functions

The simplest case of the timing recovery filters is that of the phase-locked loop,

the linearised transfer function of the phase-locked loop is the required jitter transfer function *H(f)*, which for a second order loop [9] is:

$$H_{PLL}(f) = \frac{j2\zeta f_n f + f_n^2}{f_n^2 - f^2 + j2\zeta f_n f} \qquad (5.44)$$

The case of bandpass filter extraction (both conventional tuned circuit and SAW filter) is more involved. Chamzas has shown [7] that if a bandpass filter has a transfer function $H_{BPF}(f)$ then by defining a low-pass equivalent function $H_L(f)$:

$$H_L(f) = \frac{H_{BPF}(f + f_b)}{H_{BPF}(f_b)} \qquad (5.45)$$

where f_b is the symbol rate, the jitter transfer function $H(f)$ can be written as:

$$H(f) = \frac{1}{2}\left[H_L(f) + H_L^*(-f)\right] \qquad (5.46)$$

where * denotes complex conjugate. Thus using the form of mistuned second-order bandpass filter from equation 5.13, its jitter transfer function is readily obtained. Figure 5.10 shows the jitter transfer functions of a second order bandpass filter for various degrees of mistuning, δ, and that of a PLL for various values of damping ratio, ζ. Mistuning and low-damping ratios have similar effects on the jitter transfer function in that both result in "peaking" of the jitter transfer function $H(f)$ above unity for some jitter frequencies. In the case of the bandpass filter, increase in mistuning of the centre frequency of the filter relative to the baud rate increases the jitter peaking and in the PLL case, reduction in damping ratio increases peaking. As for other bandpass filters such as SAW filters that may exhibit passband ripple, jitter peaking may exist regardless of factors such as mistuning. For symmetric ripple in the passband, since the shape of the passband is preserved at baseband (equation 5.41) a filter with no mistuning automatically exhibits peaking since the centre of the passband is normalised to unity when translated to d.c. to give the jitter transfer function.

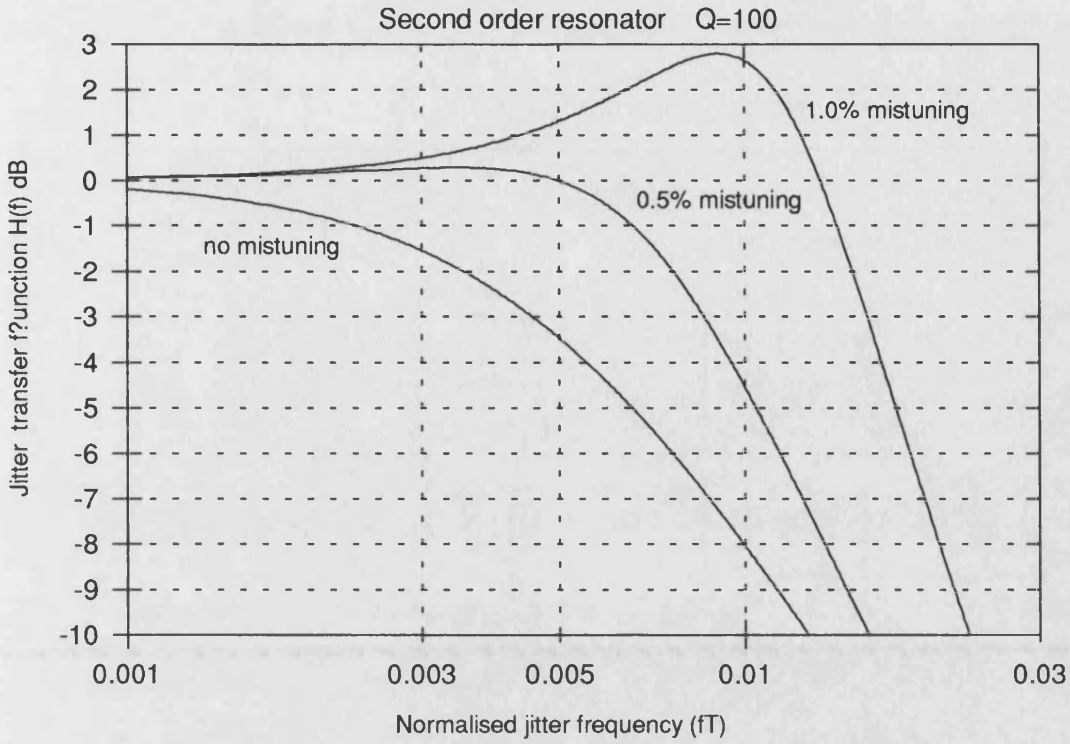

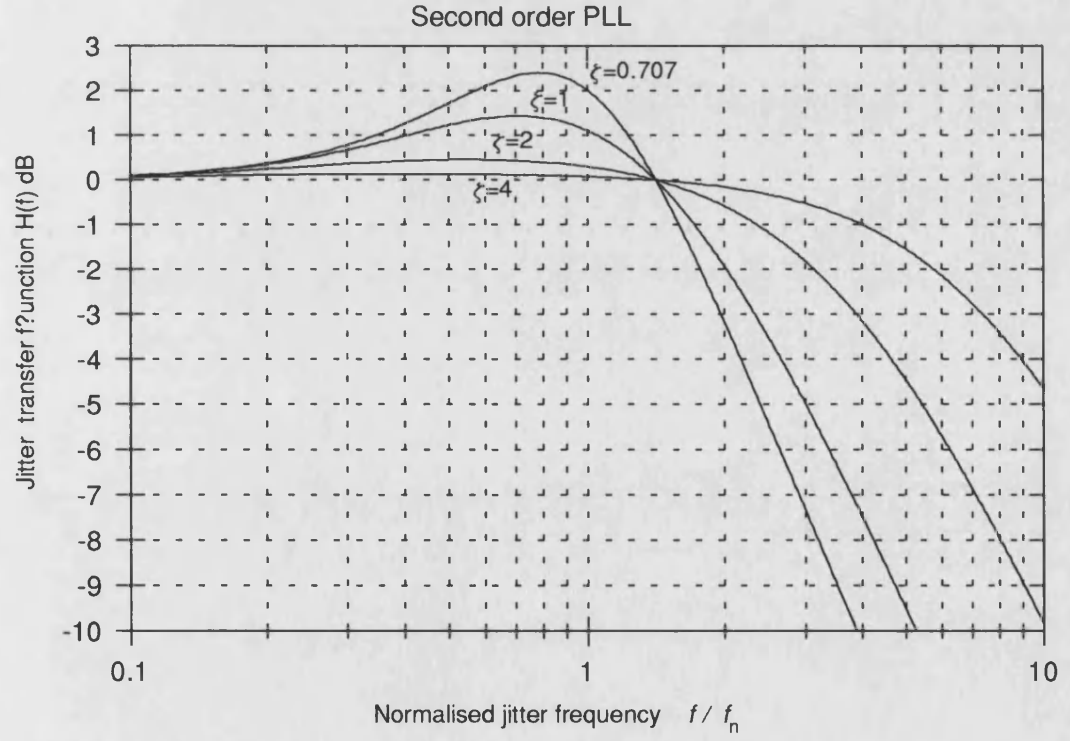

Figure 5.10: *Jitter transfer functions (magnitude)*

The effect of this peaking can be shown by using the equations for cascaded repeaters (equations 5.38 and 5.39), to plot the jitter *power* transfer functions for a chain of N repeaters in figure 5.11. The repeater used has PLL timing recovery, whose jitter transfer function is given by the second order response of equation 5.40 with a well-damped response ($\zeta=4$) which results in 0.115dB peaking (see figure 5.10). The systematic jitter power transfer functions are normalised by the square of the number of regenerators in the chain (N^2), since the jitter power gain goes to N^2 as the jitter frequency is reduced to zero. The random transfer functions are normalised by N, the number of regenerators in the chain, since the jitter power gain goes to N as the jitter frequency is reduced to zero. Thus, as would be expected, the systematic jitter should accumulate faster than the random jitter. This, however is only a valid assumption is the shapes of the transfer functions are not taken into account, i.e. the roll-off and peaking of the functions.

The roll-offs of the systematic jitter power transfer functions are considerably sharper than that of the random jitter transfer functions. As the injected jitter power spectral density is in practice white then proportionately more jitter would result in it were not for the difference in normalisation factors. The effect of peaking is more serious. Intuitively, if no repeater exhibited peaking then no "extra accumulation" results. However, from these graphs it can be seen that in a chain of repeaters exhibiting peaking in the jitter transfer function of the individual repeaters, both the random and systematic jitter power transfer functions for the chain exhibit jitter peaking whose amplitude increases with chain length. This causes amplification of jitter beyond that of a purely accumulative mechanism. The random jitter power transfer function shows greater accumulated peaking.

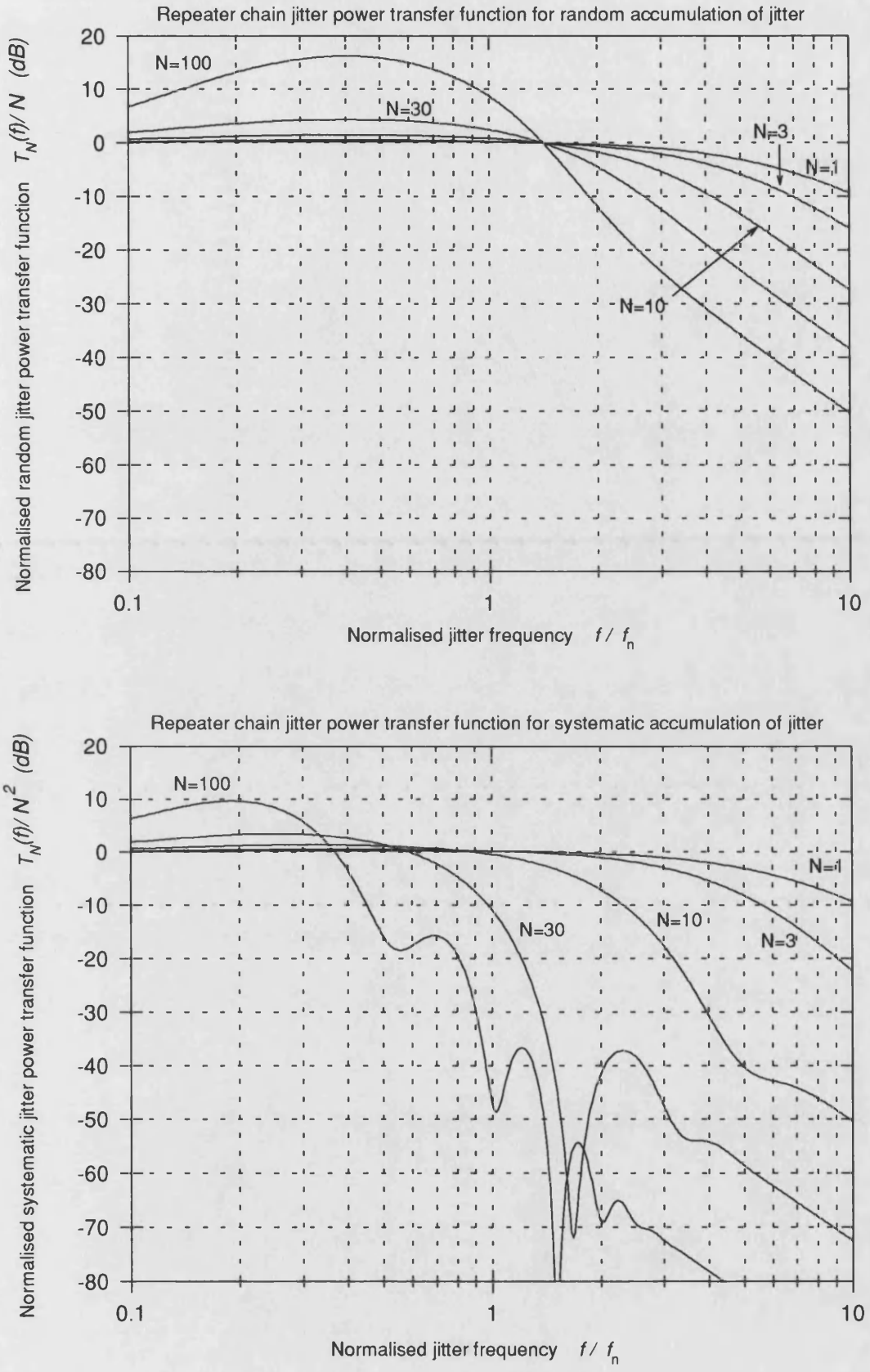

Figure 5.11: *Repeater chain jitter power transfer functions*

To show effect of jitter power transfer function peaking on jitter accumulation in a chain, the growth in r.m.s. jitter down a chain of identical repeaters is required. The defining the growth as the ratio of r.m.s. jitter at the output of the N^{th} repeater to that at the first, the growths for random jitter k_R and systematic jitter k_S are:

$$k_R = \frac{\sigma_N^R}{\sigma_1^R} = \frac{\int_{-1/2T}^{1/2T} S_N^R(f)df}{\int_{-1/2T}^{1/2T} S_1^R(f)df} \quad and \quad k_S = \frac{\sigma_N^S}{\sigma_1^S} = \frac{\int_{-1/2T}^{1/2T} S_N^S(f)df}{\int_{-1/2T}^{1/2T} S_1^S(f)df} \qquad (5.47)$$

These are evaluated by numerical integration and plotted in figure 5.12 for a number of different degrees of peaking in the jitter transfer function ($H(f)$) of a single repeater. In the ideal case of no jitter peaking (0.0dB), the systematic jitter accumulates considerably faster than the random jitter. However, the accumulation of random jitter is far more sensitive to the effects of jitter peaking than systematic jitter with runaway exponential growth occuring with much shorter chains for the same jitter peaking. This excess growth in the jitter along a chain is due to the extra amplification of jitter caused by peaking in the cascaded jitter power transfer function as demonstrated in figure 5.10. Hence the need for the high damping ratio.

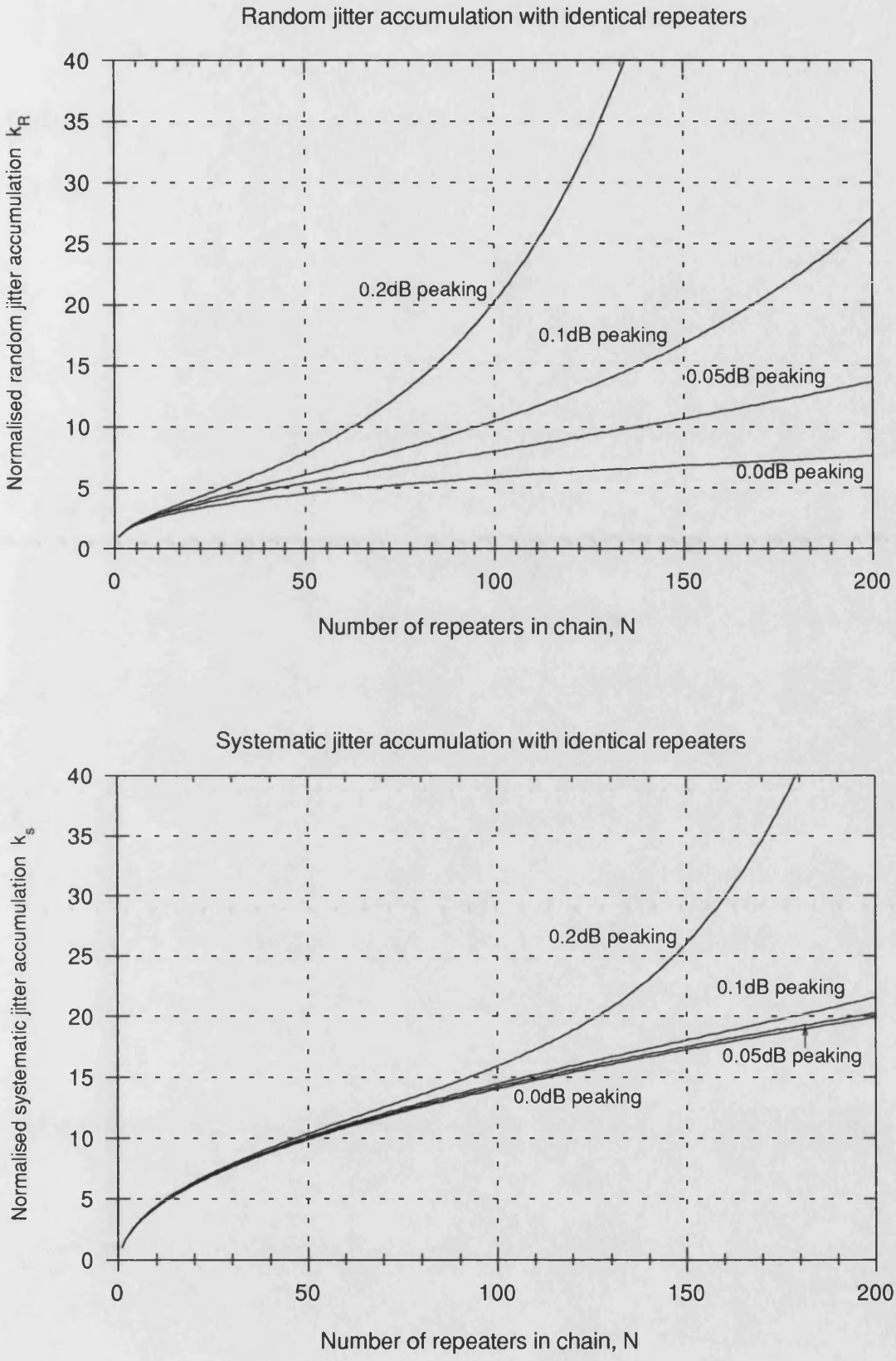

Figure 5.12: *Jitter accumulation in a chain of identical digital repeaters using Chapman's model.*

5.7. Partial accumulation of jitter

5.7.1. A partial correlation model of jitter accumulation

Consider the l^{th} regenerator of the chain in isolation:

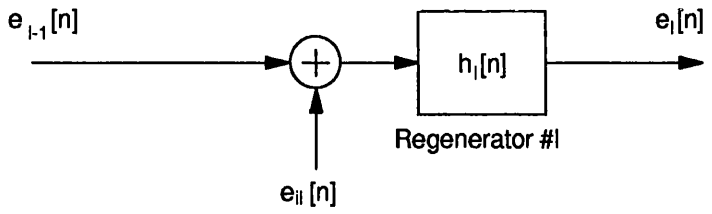

Figure 5.13: *The linear jitter model for the l^{th} regenerator in a chain*

where $e_{l-1}[n]$ is the input jitter, $e_{il}[n]$ is the injected jitter at the l^{th} regenerator and $h_l[n]$ is the jitter unit impulse response of the l^{th} regenerator. The output jitter $e_l[n]$ is given by:

$$e_l[n] = \{e_{il}[n] + e_{l-1}[n]\} * h_l[n] \qquad (5.48)$$

The quantities of interest of $e_l[n]$ are its power spectral density and variance - both of which require the calculation of the autocorrelation of $e_l[n]$ i.e.:

$$R_l[k] = E\{e_l[n]e_l[n+k]\} \qquad (5.49)$$

where $R_l[0]$ gives the variance (assuming $e_l[n]$ is a zero-mean process) and the D.F.T. of $R_l[k]$ gives the power spectral density $S_l(f)$. Some manipulation shows that $R_l[k]$ is given by:

$$R_l[k] = \left[R_{il}[k] + R_{l-1}[k] + R_{il(l-1)}[k] + R_{(l-1)il}[k]\right] * h[-k] * h[k] \qquad (5.50)$$

However, since the D.F.T. of $h[-k]$ is $H^*(f)$ (where * denotes the complex conjugate) and the D.F.T. of $R_{(l-1)il}[k]$ is $S^*_{il(l-1)}(f)$, the power spectral density $S_l(f)$ is thus:

$$S_l(f) = \left[S_{il}(f) + S_{l-1}(f) + S_{il(l-1)}(f) + S^*_{il(l-1)}(f)\right] H^*_l(f) H_l(f) \qquad (5.51)$$

and simplifying further:

$$S_l(f)=\left[S_{il}(f)+S_{l-1}(f)+2\mathrm{Re}\left\{S_{il(l-1)}(f)\right\}\right]\left|H_l(f)\right|^2 \qquad (5.52)$$

By rewriting the above equation in the following form:

$$S_l(f)=\left[S_{ii}(f)+S_{l-1}(f)\right]\left|H_l(f)\right|^2+2\left|H_l(f)\right|^2\mathrm{Re}\left\{S_{il(l-1)}(f)\right\} \qquad (5.53)$$

it is clear that the correlation of the injected jitter at the current regenerator with that injected at previous regenerators results in the second term in the above equation and that the first term gives the jitter output spectral density if there were no correlation at all (i.e. random accumulation). The above equation relating the output jitter to the input jitter and the injected jitter (of arbitrary correlation with input jitter) is in a form that can be applied iteratively to a chain of regenerators. Starting from the first regenerator with no input jitter, its output power spectral density is simply:

$$S_1(f)=S_{i1}(f)\left|H_1(f)\right|^2 \qquad (5.54)$$

Applying equation 5.49 iteratively, it can be verified after some algebra that the jitter power spectral density at the end of a chain of N regenerators is given by:

$$S_N(f)=\sum_{l=1}^{N}S_{il}(f)\prod_{m=l}^{N}\left|H_m(f)\right|^2+2\mathrm{Re}\left\{\sum_{p=1}^{N}S_{ip(p-1)}(f)\prod_{r=p}^{N}\left|H_r(f)\right|^2\right\} \qquad (5.55)$$

It is more desirable to be able to use quantities that can be measured on individual regenerators in isolation, however $S_{ip(p-1)}(f)$ depends on the cascade of jitter transfer functions previous to the p^{th} regenerator and the accumulated jitter. The cross-spectrum $S_{ipiq}(f)$ is the cross-spectrum of the injected jitter at the p^{th} and q^{th} regenerators ($p>q$) and is independent of their absolute positions in the chain. The cross-spectrum $S_{ip(p-1)}(f)$, is the D.F.T. of the cross-correlation:

$$R_{ip(p-1)}[k] = E\{e_{ip}[n]e_{p-1}[n+k]\} \tag{5.56}$$

However, the input jitter to the p^{th} regenerator is:

$$e_{p-1}[n] = \sum_{q=1}^{p-1} e_{iq}[n] * h_q[n] * h_{q+1}[n] * \ldots * h_{p-1}[n] \tag{5.57}$$

Thus it can be shown that $R_{ip(p-1)}[k]$ is:

$$R_{ip(p-1)}[k] = \sum_{q=1}^{p-1} R_{ipiq}[k] * h_q[k] * h_{q+1}[k] * \ldots * h_{p-1}[k] \tag{5.58}$$

where the cross-correlation $R_{ipiq}[k]$ is:

$$R_{ipiq}[k] = E\{e_{ip}[n]e_{iq}[n+k]\} \tag{5.59}$$

Hence the cross-spectrum $S_{ip(p-1)}(f)$ is given in terms of the cross-spectrum $S_{ipiq}(f)$ (the D.F.T. of $R_{ipiq}[k]$) by:

$$S_{ip(p-1)}(f) = \sum_{q=1}^{p-1} S_{ipiq}(f) \prod_{s=q}^{p-1} H_s(f) \tag{5.60}$$

Thus the power spectral density of output jitter of the chain of N regenerators is:

$$S_N(f) = \sum_{l=1}^{N} S_{il}(f) \prod_{m=l}^{N} |H_m(f)|^2$$

$$+ 2\mathrm{Re}\left\{ \sum_{p=1}^{N} \left(\prod_{s=p}^{N} |H_s(f)|^2 \sum_{q=1}^{p-1} S_{ipiq}(f) \prod_{r=q}^{p-1} H_r(f) \right) \right\} \tag{5.61}$$

The variance of the output jitter is the integral of $S_N(f)$ over the Nyquist range as discussed earlier. In order to reduce the above equation to measurable parameters of practical regenerators, the composition of the injected jitter at a regenerator must be considered. As discussed earlier, jitter can be attributed to two sources: one noise-dependent, one digital pattern-dependent. Thus the injected jitter at the l^{th} regenerator can be written as the sum of these

components:

$$e_{il}[n] = e_{il}^{\eta}[n] + e_{il}^{PD}[n] \qquad (5.62)$$

The noise-dependent jitter $e_{il}^{\eta}[n]$ is assumed to be a zero-mean white process and entirely uncorrelated with the noise-dependent jitter generator at any other regenerator in the chain, i.e.:

$$\begin{aligned} E\left\{e_{il}^{\eta}[n]e_{im}^{\eta}[n+k]\right\} &= \mathrm{var}\left\{e_{il}^{\eta}[n]\right\}\delta[k] \quad \text{for } m = l \\ &= 0 \qquad m \neq l \end{aligned} \qquad (5.63)$$

Also, by definition there is no correlation at all between the noise-dependent and pattern-dependent jitter ($e_{il}^{PD}[n]$) at or between any regenerator, i.e.:

$$E\left\{e_{il}^{\eta}[n]e_{im}^{PD}[n+k]\right\} = 0 \quad \text{for all } l,m \qquad (5.64)$$

Applying these relationships the spectral densities $S_{il}(f)$ and $S_{ipiq}(f)$:

$$S_{il}(f) = S_{il}^{\eta}(f) + S_{il}^{PD}(f) \qquad (5.65)$$

$$S_{ipiq}(f) = S_{ipiq}^{PD}(f) \qquad (5.66)$$

This allows the splitting of $S_N(f)$ into noise-dependent and pattern-dependent components:

$$S_N(f) = S_N^{\eta}(f) + S_N^{PD}(f) \qquad (5.67)$$

where:

$$S_N^{\eta}(f) = \sum_{l=1}^{N} S_{il}^{\eta}(f) \prod_{m=l}^{N} |H_m(f)|^2 \qquad (5.68)$$

and

$$S_N^{PD}(f) = \sum_{l=1}^{N} S_{il}^{PD}(f) \prod_{m=l}^{N} |H_m(f)|^2$$

$$+2\mathrm{Re}\left\{\sum_{p=1}^{N}\left(\prod_{s=p}^{N}|H_s(f)|^2\sum_{q=1}^{p-1}S_{ipiq}^{PD}(f)\prod_{r=q}^{p-1}H_r(f)\right)\right\} \qquad (5.69)$$

The quantity $S_{ipiq}^{PD}(f)$ depends by definition on the correlation between the pattern-dependent jitter generated at different regenerators. Previous analyses [6,7,14] have assumed complete correlation such that a direct proportionality exists, i.e.:

$$e_{iq}^{PD}[n]=\alpha_{pq}e_{ip}^{PD}[n] \qquad (5.70)$$

in which case:

$$S_{ipiq}^{PD}(f)=\alpha_{pq}S_{ip}^{PD}(f) \qquad (5.71)$$

Several authors have found that in practice the pattern-dependent jitter (like the noise dependent jitter) is a zero-mean white process and so:

$$S_{iq}^{PD}(0)=\alpha_{pq}^2S_{ip}^{PD}(0) \qquad (5.72)$$

and so for completely correlated pattern jitter, if the magnitude of the power spectral densities are measured then:

$$S_{ipiq}^{PD}(f)=\sqrt{S_{ip}^{PD}(0)S_{iq}^{PD}(0)} \qquad (5.73)$$

However, as noted from the results of a number of authors [16,17], practical chains consistently under-accumulate relative to the individually measured parameters of the regenerators. This leads to the conclusion that the assumption of complete correlation is not always valid. Here it is assumed that only a proportion of the jitter is completely correlated from regenerator to regenerator so that the relation becomes:

$$e_{iq}^{PD}[n]=\alpha'_{pq}e_{ip}^{PD}[n]+\varepsilon_{pq}[n] \qquad (5.74)$$

where $\varepsilon_{pq}[n]$ is the residual jitter of $e_{iq}^{PD}[n]$ that is uncorrelated with $e_{ip}^{PD}[n]$. The coefficient of correlation $e_{ip}^{PD}[n]$ between the processes $e_{ip}^{PD}[n]$ and $e_{iq}^{PD}[n]$ is defined by:

$$\rho_{ipiq}^{PD} = \frac{R_{ipiq}^{PD}[0]}{\sqrt{R_{ip}^{PD}[0]R_{iq}^{PD}[0]}} \tag{5.75}$$

Since each of the correlations in the above equation is that of a stationary, white process, they may all be replaced by their respective power spectral densities, i.e.:

$$\rho_{ipiq}^{PD} = \frac{S_{ipiq}^{PD}(0)}{\sqrt{S_{ip}^{PD}(0)S_{iq}^{PD}(0)}} \tag{5.76}$$

Hence the cross-spectrum is:

$$S_{ipiq}^{PD}(0) = \rho_{ipiq}^{PD}\sqrt{S_{ip}^{PD}(0)S_{iq}^{PD}(0)} \tag{5.77}$$

where $-1 \le \rho_{ipiq}^{PD} \le 1$, and thus the pattern-dependent power spectral density after N regenerators in a chain is:

$$S_N^{PD}(f) = \sum_{l=1}^{N} S_{il}^{PD}(0)\prod_{m=l}^{N}|H_m(f)|^2$$

$$+2\,\mathrm{Re}\left\{\sum_{p=1}^{N}\sqrt{S_{ip}^{PD}(0)}\left(\prod_{s=p}|H_s(f)|^2\sum_{q=1}^{p-1}\rho_{ipiq}\sqrt{S_{iq}^{PD}(0)}\prod_{r=q}^{p-1}H_r(f)\right)\right\} \tag{5.78}$$

The above equation has been derived without the constraints of the key assumptions of Chapman's model, i.e. non-identical repeater transfer functions, differing levels of injected pattern-dependent jitter and arbitrary correlation between the injected jitter at any pair of repeaters.

5.7.2. Determination of correlation coefficient

A technique to compute the jitter at the output of a digital repeater with arbitary parameters was described earlier in this chapter. It can also be used in order to determine the degree of correlation between the pattern-jitter generated by two repeaters with differing parameters. However, to determine the correlation coefficient ρ_{ipiq}^{PD} between the pattern-dependent jitter at two regenerators with different parameters, it is necessary to calculate the effective input jitter, i.e. the output jitter referred to the input of the regenerator. Otherwise, the variation in jitter output due to the variation in the jitter transfer function will distort the result. If no noise or jitter is present on the input stream then the output jitter $e_1[n]$ is:

$$e_1[n] = e_{i1}^{PD}[n] * h_1[n] \qquad (5.79)$$

where $h_1[n]$ is the jitter unit impulse response of the regenerator. In order to determine $e_{i1}^{PD}[n]$, the D.F.T. of equation 5.75 is taken and thus:

$$e_{i1}^{PD}[n] = IDFT\left\{\frac{DFT\{e_1[n]\}}{DFT\{h_1[n]\}}\right\} \qquad (5.80)$$

where I.D.F.T. is the inverse Discrete Fourier Transform. An "overlap and save" algorithm was used to perform equation 5.76 on the simulated output jitter stream as with that used for calculating the timing filter output. The D.F.T. of the jitter impulse response of the repeater timing filter was determined by calculating the jitter transfer function *H(f)* from the bandpass response by the method described in the section 5.6.2. and reflecting it to form the complex conjugate symmetry of a D.F.T. (as with bandpass filtering used to calculate timing recovery wave).

Thus to calculate estimates of the correlation coefficient ρ_{ipiq} with a spread of

regenerator parameters the arrangement shown in figure 5.14 is used.

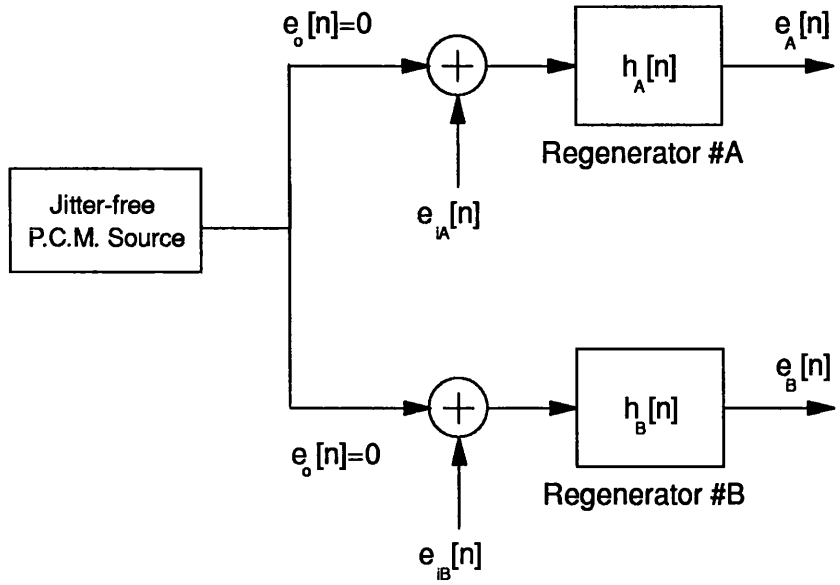

Figure 5.14: *Arrangement used for determination of correlation coefficient*

The correlation coefficient is then given by (having subtracted the mean values from $e_{iA}^{PD}[n]$ and $e_{iB}^{PD}[n]$):

$$\rho_{iAiB} = \frac{\sum_{n=0}^{N-1} e_{iA}[n] e_{iB}[n]}{\sqrt{\sum_{n=0}^{N-1} e_{iA}^2[n] \sum_{n=0}^{N-1} e_{iB}^2[n]}} \qquad (5.81)$$

where N is the number of jitter samples used.

5.7.3. Variation of correlation coefficient with parameter variation

To allow comparison of the partial correlation model of pattern-dependent jitter accumulation with published measurements [16,17], the case of a chain of fibre-optic repeaters using SAW filters for timing recovery was examined to illustrate the model. SAW filter characteristics and a model for their passsband response has already been considered. Jitter sequences of 8192 points were calculated in

the same manner as with the bandpass timing recovery discussed earlier, but with the SAW filter response replacing the second order resonator, and with the use of a 7B8B line code [5]. These jitter sequences were referred to the effective injected input jitter in the manner described in the previous section given the particular SAW filter transfer function (which is easily derived from the frequency response). The variation of the calculated correlation coefficient with the parameters of threshold offset, mistuning and filter Q-factor is shown in the graphs of figure 5.15.

The graph of variation of the correlation coefficient with variation of Q-factor vindicates Chapman's repeater jitter model of an injected jitter source followed by a linear, time-invariant transfer function. Variation of filter Q should only vary the jitter transfer function, not the effective jitter injected at the input to the jitter transfer function. Since the jitter sources (e.g. threshold offset and mistuning) are kept constant, the injected jitter should be the same and the correlation coefficient should be unity. Over the range of interest, the calculated correlation coefficient is greater than 0.95 for most of that range as expected.

Exact mathematical analysis of the variation of correlation coefficient with trigger threshold offset is potentially complex and lengthy. However, the basic behaviour may be characterised as follows. Intuitively, it might be expected that the correlation coefficient of the jitter generated by a repeater with positive threshold offset and a repeater with a negative threshold offset will be negative. However, from the third graph of figure 5.15, this phenomena was not observed. The timing wave $x(t)$ after bandpass filter recovery can be written as:

$$x(t) = a(t)\cos(2\pi f_b t + \varphi(t)) \qquad (5.82)$$

where f_b is the symbol rate, $a(t)$ is the amplitude variation of the timing wave and $\varphi(t)$ the phase variation. The level crossing problem that determines the timing instants (and thus jitter) is shown in figure 5.16.

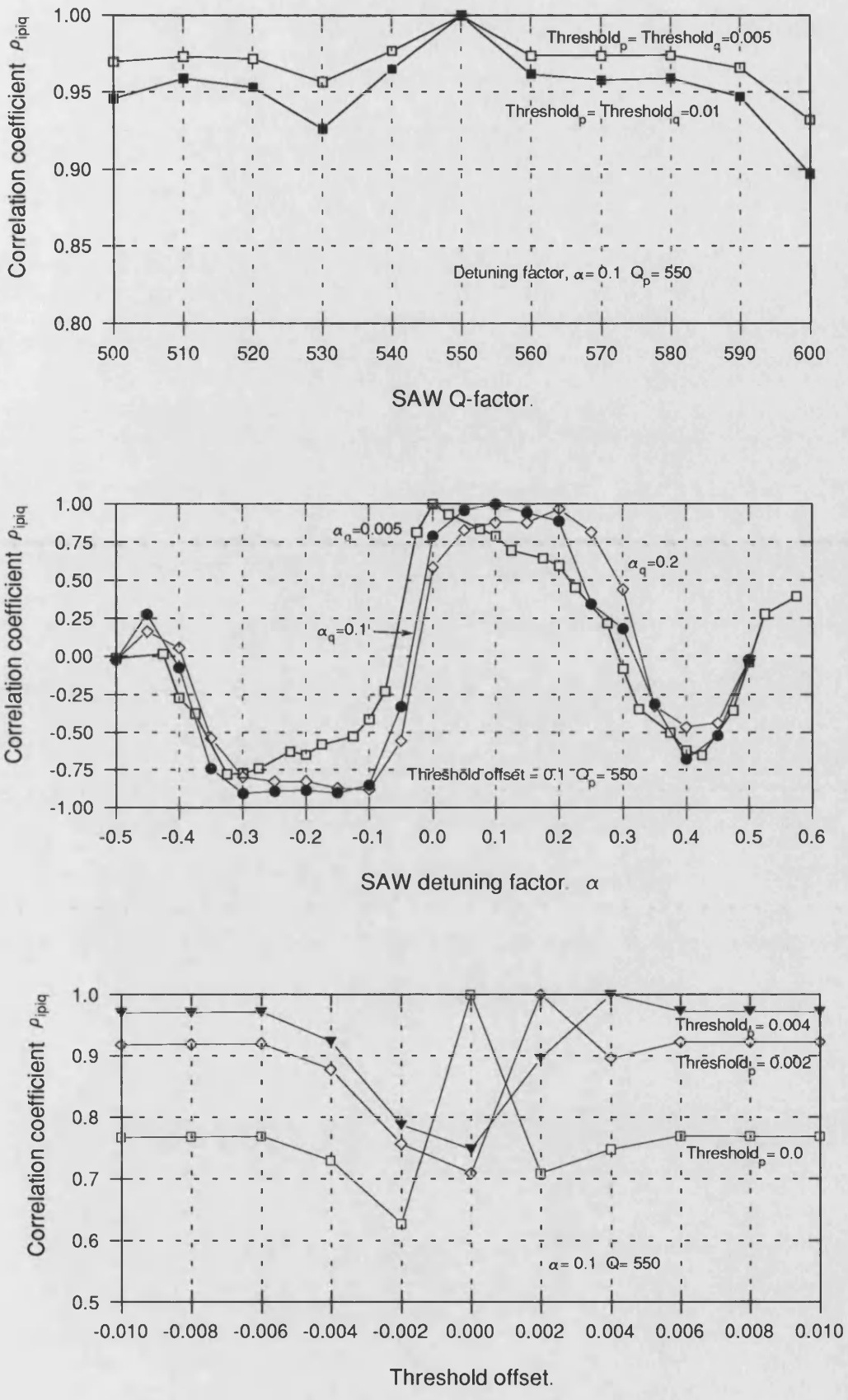

Figure 5.15: *Variation of correlation coefficient with repeater parameters*

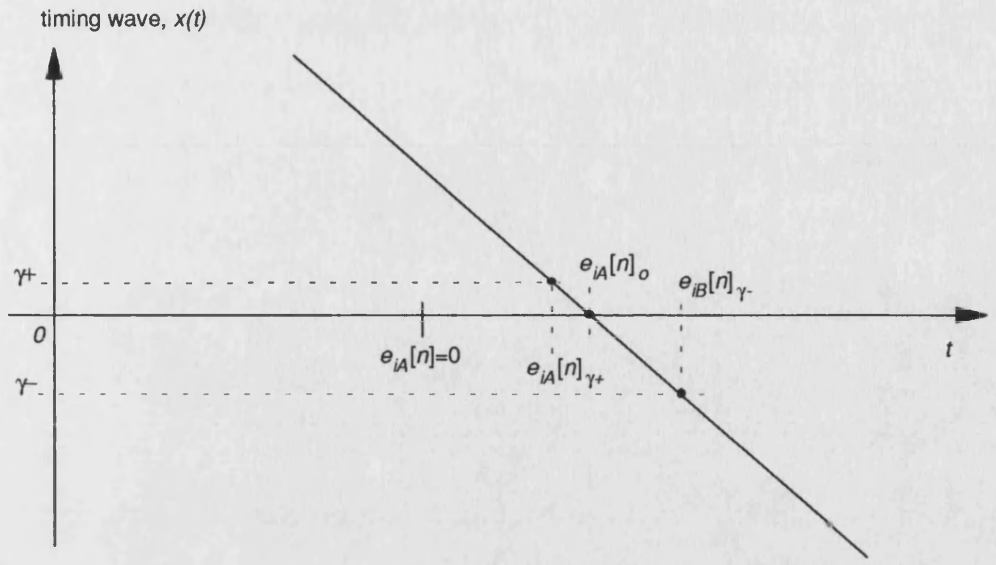

Figure 5.16: *Variation of jitter with threshold offset*

The timing jitter $\{e_{iA}[n]\}$ is assumed zero-mean (shift in time reference achieves this). The reference for $e_{iA}[n]=0$ is shown on the time axis and is the zero-crossing instant for $\varphi(t)=0$. In general, the zero-crossing point will be a point offset from this point in either positive or negative direction, $e_{iA}[n]_o$. Introducing threshold offsets in either negative or positive reduce or increase the magnitude of the jitter, but, in the case shown, not the sense, i.e. the jitter values $e_{iA}[n]_{\gamma+}$ and $e_{iB}[n]_{\gamma-}$ remain positive. Since the numerator of the correlation coefficient is the sum of the product of these jitter values, this particular jitter instant will not contribute towards a negative correlation coefficient.

If the zero-crossing instant of the timing wave was the other side of $e_{iA}[n]=0$ i.e. negative, both positive and negative offsets yield negative jitter of different magnitudes and thus their product is positive and so is the contribution towards the correlation coefficient.

The zero-crossing instant $e_{iA}[n]_o$ is distributed around $e_{iA}[n]=0$ the mean value and for a proportion of the time will be close to $e_{iA}[n]=0$ such that the positive and negative threshold offsets will give positive and negative jitter values,

yielding a negative contribution towards the correlation coefficient. However, unless $e_{iA}[n]_o$ is very close to zero, one of the jitter values will be small and thus the product is small and its negative contribution towards the correlation coefficient will serve only to reduce its magnitude slightly rather than make it negative, since (assuming small threshold offsets), most level crossings will give positive correlation values of greater magnitude.

Apart from the absence of negative correlation coefficients, the threshold offset graph in figure 5.15 shows that the correlation coefficient decreases if the magnitude of the threshold offset is small (<0.002). The amplitude-to-phase conversion of amplitude variation of the timing wave into jitter that threshold offset causes is a non-linear function of threshold offset, thus the jitter that results from small offsets would be expected to have less correlation with that of larger offsets.

The graph of variation in correlation coefficient with variation in mistuning is the most striking of the three in figure 5.15. In contrast with one of the principal assumptions of Chapman's model, i.e. complete correlation of the jitter injected at each repeater, combinations of two repeaters with opposite polarity mistuning yield large negative correlation coefficients. The pattern-dependent jitter injected at the input to the jitter transfer function is highly correlated despite the filter tuning which effectively inverts the jitter depending on the sense of the tuning. The mechanism can be described by considering the impulse response of an ideal resonator which can be approximated by a damped sinusoid whose frequency is the centre frequency of the resonator. The timing recovery process is the excitation of the resonator with a stream of pulses (or impulses if the effect of pulse shape is neglected). These pulses are all positive due to the even-order non-linear processing and thus the timing wave can be considered the sum of damped sinusoids of the frequency of the resonator tuning. Thus a resonator with slight

sinusoids of the frequency of the resonator tuning. Thus a resonator with slight negative mistuning results in an impulse response of frequency slightly lower than the symbol rate and thus the threshold crossings all occur slightly later (positive jitter) and vice versa for positive mistuning. The jitter in both cases is strongly correlated to the digital pattern of pulses, but has different polarity. At extreme mistunings ($|\alpha|>0.25$-0.3), the behaviour of the resonator gives poor jitter performance and a drop in the degree of the magnitude of the correlation of the injected jitter as observed in figure 5.15.

5.7.4. Correlation of pattern-dependent jitter in PLL timing extraction

Partial correlation of pattern-dependent jitter is not confined to bandpass timing extraction, but is also possible and probable in phase-lock loop timing extraction. In a rigorous analysis of pattern-dependent jitter in PLL timing extraction, Roza [15] shows that the jitter at a repeater with no jitter on the incoming stream is:

$$e_l[n] = \sum_{k=0}^{n} b_k h_w[n-k] \tag{5.83}$$

where:

$$b_k = -\left(\frac{c_k - \overline{c_k}}{\underline{c_k}}\right)\theta_\varepsilon - \frac{c_k}{\underline{c_k}}\left(\frac{\overline{c_k\tau_k}}{\underline{c_k}} - \tau_k\right) \tag{5.84}$$

$$c_k = \frac{T}{2\pi}\int_{-T/2}^{T/2} f_o'(\tau)y(kT+\tau)d\tau \tag{5.85}$$

$$c_k\tau_k = \frac{T}{2\pi}\int_{-T/2}^{T/2} f_o(\tau)y(kT+\tau)d\tau \tag{5.86}$$

$y(t)$ is the digital stream after non-linear processing, $f_o(t)$ is the loop oscillator

waveform (periodic in T) and $h_w[n]$ is the normalised pulse response of the weighted closed-loop transfer function of the PLL. Its D.F.T. $H_w(f)$ is hence the jitter transfer function of the repeater, and is related to the actual PLL time-domain response via the open-loop response by:

$$g_w[n] = \overline{c_k} T g[n] \qquad (5.87)$$

where T is the symbol period, $g_w[n]$ is the normalised pulse response of the weighted open-loop transfer function and $g[n]$ is the normalised pulse response of the actual open-loop transfer function of the PLL.

The constant θ_ε is the static phase error of the loop due to mistuning between the bit rate of the digital stream and the free-running centre frequency of the phase lock loop, $\Delta\omega$, and is given by [15]:

$$\theta_\varepsilon = \frac{\Delta\omega}{K_v} \qquad (5.88)$$

where K_v is the velocity constant of the loop [9].

Since there is no input jitter, the b_k is effectively the injected jitter referred to the input of the jitter transfer function of the repeater, i.e. in the notation of the accumulation model, $e_{iI}[n]$. The two constituent terms of equation 5.84 are examined for spectral behaviour by Roza; the first has a flat power spectral density at low frequency and the second is zero at zero frequency and rises with increasing frequency. These are thus the two components discussed earlier in this chapter. Since, as shown by Roza, these two components have negligible correlation with each other, their accumulation in a chain of PLL repeaters can be considered separately. However, due to the nature of their respective power spectral densities, the first term of equation 5.84 (that with flat power spectral density at zero-frequency) will dominate because of the shape of the effective jitter transfer function of a chain of repeaters. As shown earlier the lowpass

response of a chain to systematic jitter (and random jitter to a lesser extent) becomes progressively more narrowband and higher in zero frequency gain as the chain increases in length. The cut-off of the jitter transfer function of a single repeater will be significantly less than the peak of the power spectral density of the second term of equation 5.84 (see figure 5.7) and so the power spectral density of the second jitter term that is within the progressively narrowing jitter transfer function of the chain reduces rapidly as the chain increases. In contrast, the power spectral density of the first term of equation 5.84 is constant for low frequencies and its contribution to accumulated pattern-dependent jitter is significantly larger. This phenomenon was noted for bandpass extraction by Manley [18] where the peak power spectral density of the component of jitter with zero value at zero frequency increases negligibly after the 5^{th} or 6^{th} repeater in the chain and effectively stops accumulating. Thus the principal source of accumulating injected pattern-dependent jitter is the first term of equation 5.84 and thus may be approximated by:

$$e_{il}[n] = b_k \approx -\left(\frac{c_k - \overline{c_k}}{\overline{c_k}}\right)\theta_\varepsilon \qquad (5.89)$$

Since the injected jitter is proportional to the static phase error of the loop, negative correlation of the injected jitter will exist between repeaters with loop static phase errors of opposite polarity (all other parameters being equal, the correlation coefficient will be -1). The effect of negative correlation is to significantly reduce the overall proportion of systematically accumulating pattern-dependent jitter as is discussed later in this chapter. The correlation coefficient is also a function of the series c_k, and thus is a function of variation in the accuracy of pulse equalisation and variation in oscillator waveforms. With widespread use of square wave loop oscillators, significant variation in oscillator waveform between repeaters is very unlikely and pulse equalisation is more

likely to affect the correlation of injected jitter. Whether slight variations in pulse equalisation can result in a reduction in the degree of positive correlation or significant negative correlation is not obvious from the complexity of equation 5.85. Detailed examination is required of the effects of slight misequalisation on pulse shaping, which depends heavily on the transmission medium used and the type of equalisation employed [1]. This is an area for further study.

5.8. Effects of partial correlation on pattern-dependent jitter accumulation

The correlation coefficients for three chains of SAW filter based repeaters were calculated, with random spread in the parameters filter Q, mistuning α and trigger threshold offset. The filter Q of each chain of repeaters had a mean value of 550 and a standard deviation of 10. For a Gaussian distribution the likelihood of a value exceeding three standard deviations from the mean is very small and so the range of filter Q is 520 to 580. The threshold offset of each chain was taken to have zero mean and standard deviation of 0.0025. The mistuning factor α was taken to have zero mean for each chain, but the standard deviation was varied from chain to chain. For chain A the standard deviation was 0.05, for chain B it was 0.025 and chain C, it was 0.01.

The sets of calculated correlation coefficients $\{\rho_{ipiq}\}$ have two properties:

$$\begin{aligned} &\rho_{ipiq} = 1 \quad \textit{for } p = q \\ &\rho_{ipiq} = \rho_{iqip} \end{aligned} \qquad \textit{(5.90)}$$

Thus the subset of unique values of interest are $\{\rho_{ipiq}\}$ for all p, but $q<p$. All references to the statistics of $\{\rho_{ipiq}\}$ in this section refer to this subset. The distribution of values of $\{\rho_{ipiq}\}$ is shown by the Probability Density Functions for each chain of 50 repeaters plotted in figure 5.17. The PDFs were determined by quantising the range of ρ_{ipiq} from -1 to 1 into 0.005 steps and for each quantisation level determining the proportion of all values that fall in that range.

As would be expected, the spread in $\{\rho_{ipiq}\}$ is a function of the spread in mistuning. Chain C with the smallest spread in mistuning has most values in a range 0.85 to 1.0 and no negative values at all. Chain B still exhibits a significant peak around 0.9 to 0.95, but with greater spread down to around -0.2.

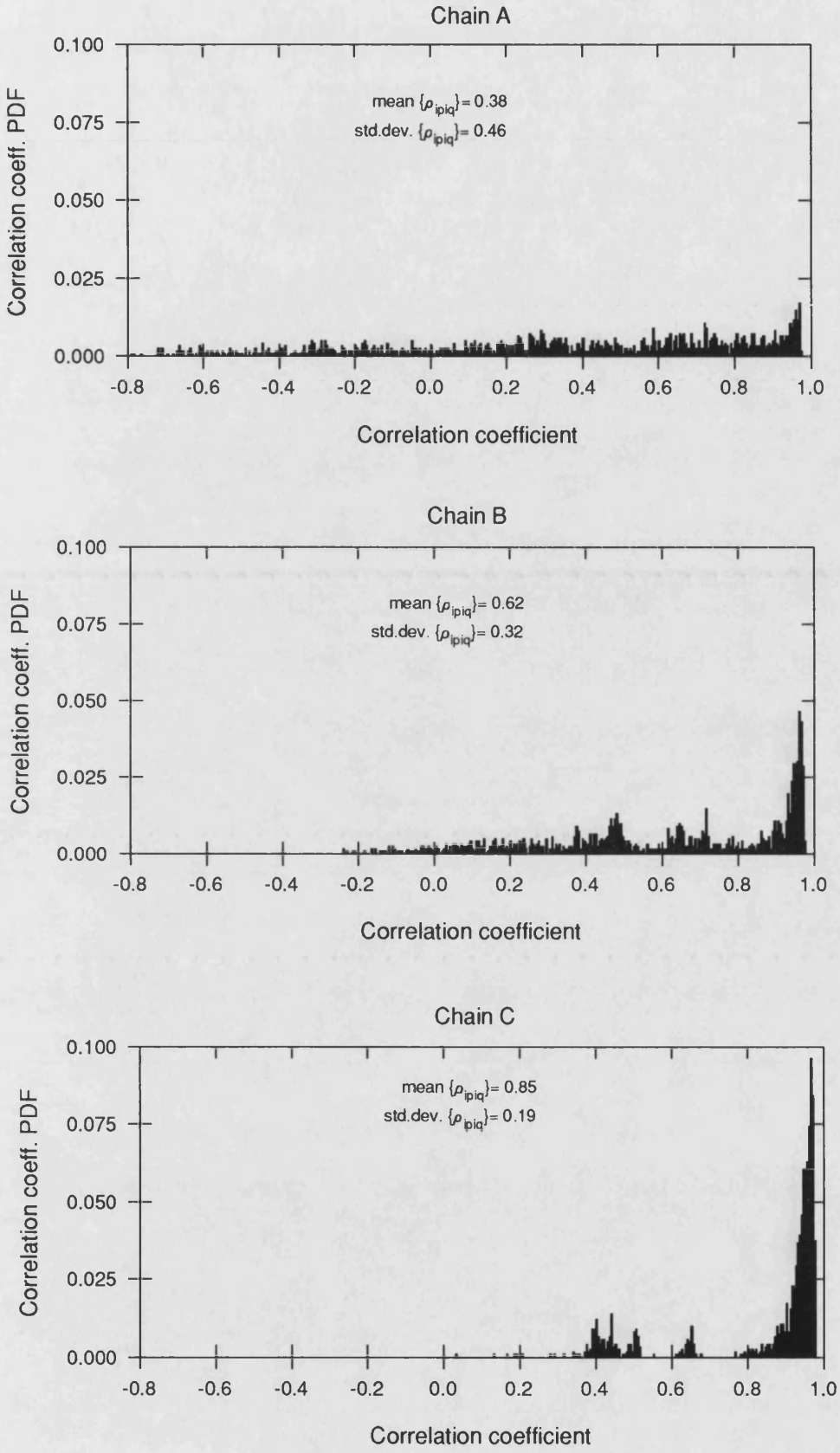

Figure 5.17: *Distribution of correlation coefficient for the modelled chains*

Chain A shows a small peak around 0.9 to 0.95, but has a substantial spread with a wide range of negative as well as positive values. Accumulation of jitter in the three chains was calculated using equation 5.78. The effective input jitter power spectral density $\{S_{il}(0)\}$ was determined from the variance of the jitter sequences calculated to determine the set of correlation coefficients by:

$$S_{il}(0) = \frac{\sigma_l^2}{\int_{-1/2T}^{1/2T} |H_l(f)|^2 df} \qquad (5.91)$$

The mean and standard deviations of the values of $S_{il}(0)$ for each chain is given in figure 5.18 where the jitter power spectral densities at the end of each chain are given. For comparison, the power spectral denisties for entirely systematic (all $\{\rho_{ipiq}\}$ = 1) and entirely random accumulation (all $\{\rho_{ipiq}\}$ = 0) accumulation for each chain is shown.

As shown by Chamzas [7], the systematic jitter power spectral density of a chain with jitter transfer functions that exhibit random variation about a mean still exhibit sharp nulls. With partial correlation of the pattern-dependent jitter injected at each repeater these nulls lose their sharpness with the reduction in mean correlation. The main lowpass lobe of the spectrum is reduced in amplitude and the sidelobe roll-off is also reduced. Even chain C with a mean $\{\rho_{ipiq}\}$ of 0.85 shows noticeable departure from entirely systematic accumulation away from the main lobe. However, since most of the spectral power is in the main lobe, the accumulation of r.m.s. jitter will be close to that of entirely systematic accumulation. The accumulation of r.m.s. pattern-dependent jitter for the three chains was calculated in the same way as presented earlier in this chapter and is plotted in figure 5.19 with entirely systematic and entirely random accumulation shown for comparison

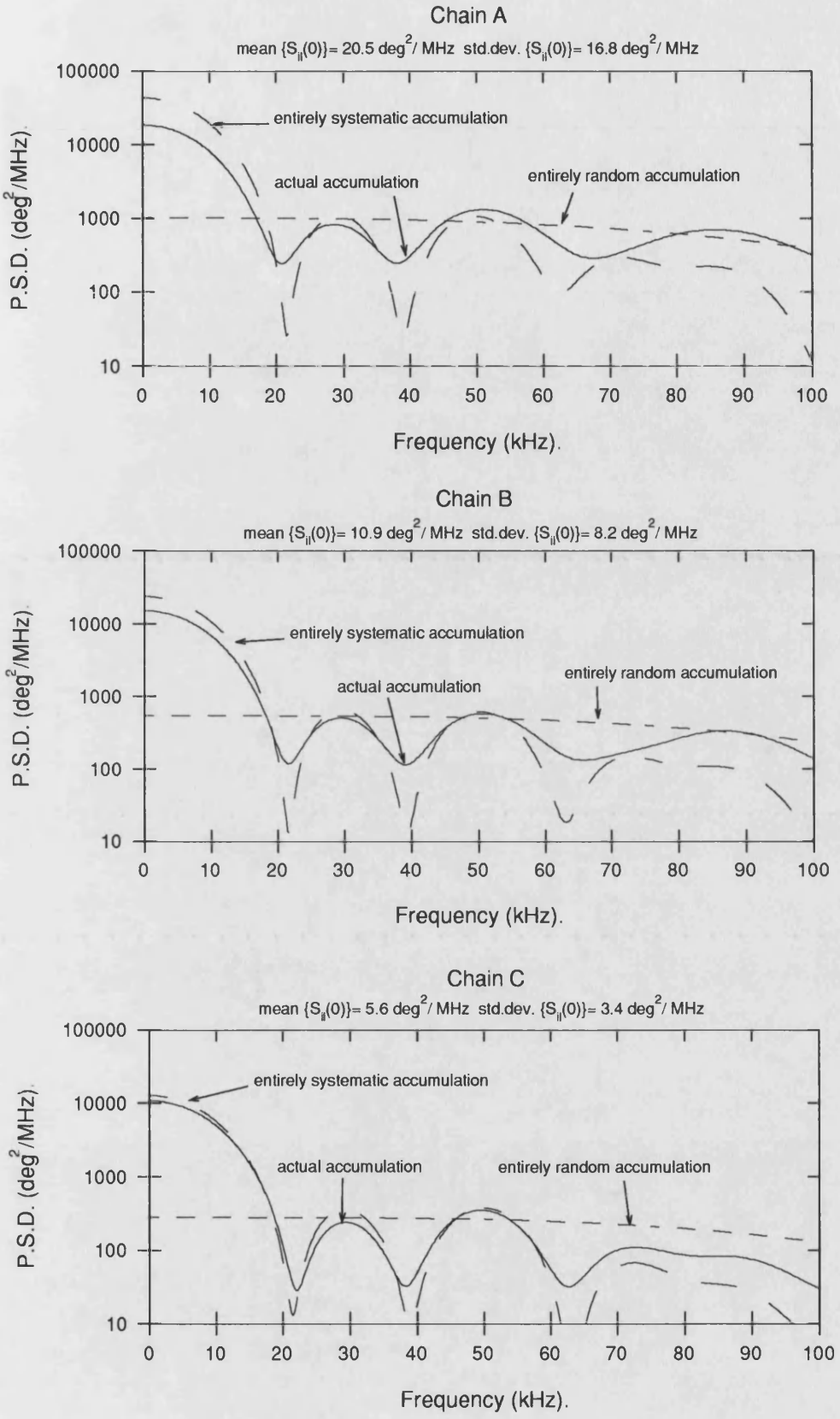

Figure 5.18: *Jitter power spectral densities after 50 repeaters*

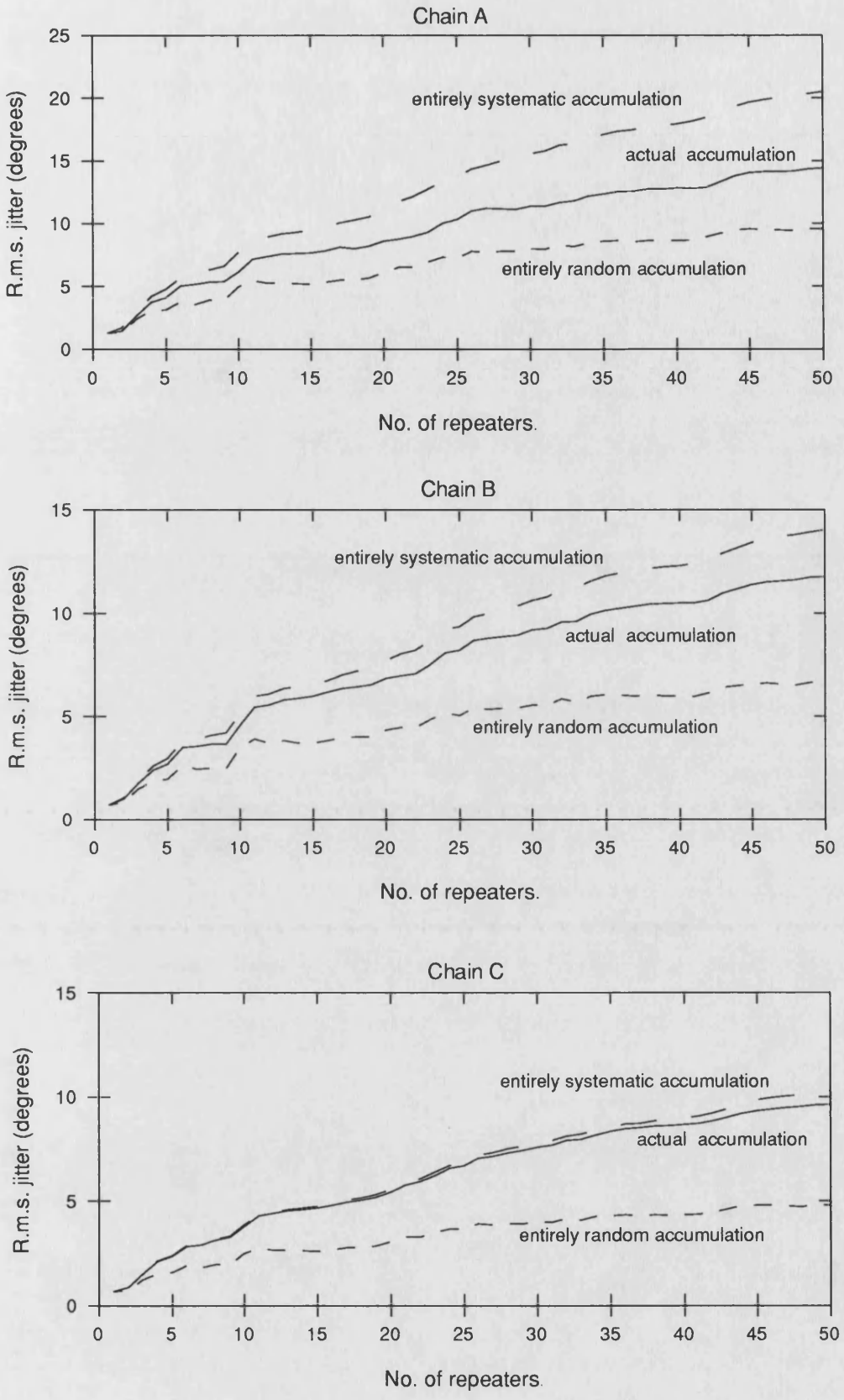

Figure 5.19: *Accumulation of pattern-dependent jitter in a 50 repeater chain*

If all $\{\rho_{ipiq}\}$ can be replaced in an N repeater chain by an apparent average correlation coefficient $\bar{\rho}_N$ then equation 5.78 can be rewritten as:

$$S_N^{PD}(f) = \sum_{l=1}^{N} S_{il}^{PD}(0) \prod_{m=l}^{N} |H_m(f)|^2$$

$$+ 2\bar{\rho}_N \,\mathrm{Re}\left\{ \sum_{p=1}^{N} \sqrt{S_{ip}^{PD}(0)} \left(\prod_{s=p}^{N} |H_s(f)|^2 \sum_{q=1}^{p-1} \sqrt{S_{iq}^{PD}(0)} \prod_{r=q}^{p-1} H_r(f) \right) \right\} \qquad (5.92)$$

If $S_N^{PDS}(f)$ is the jitter power spectral density of entirely correlated pattern-dependent jitter and $S_N^{PDR}(f)$ that of entirely uncorrelated pattern-dependent jitter, then the above equation can be written as:

$$S_N^{PD}(f) = (1-\bar{\rho}_N) S_N^{PDR}(f) + \bar{\rho}_N S_N^{PDS}(f) \qquad (5.93)$$

So the average correlation of pattern-dependent jitter can be determined from:

$$\bar{\rho}_N = \frac{S_N^{PD}(0) - S_N^{PDR}(0)}{S_N^{PDS}(0) - S_N^{PDR}(0)} \qquad (5.94)$$

This is plotted for the three chains studied in figure 5.20. By considering the various jitter power spectral densities at zero frequency, the apparent average correlation coefficient $\bar{\rho}_N$ is related to the individual coefficients $\{\rho_{ipiq}\}$ by:

$$\bar{\rho}_N = \frac{\sum_{p=1}^{N} \left(\sqrt{S_{ip}^{PD}(0)} \sum_{q=1}^{p-1} \rho_{ipiq} \sqrt{S_{iq}^{PD}(0)} \right)}{\sum_{p=1}^{N} \left(\sqrt{S_{ip}^{PD}(0)} \sum_{q=1}^{p-1} \sqrt{S_{iq}^{PD}(0)} \right)} \qquad (5.95)$$

This is not equal to the mean of $\{\rho_{ipiq}\}$, but as N increases, $\bar{\rho}_N$ becomes a good approximation as demonstrated in figure 5.20 when compared to the mean values of $\{\rho_{ipiq}\}$ given in figure 5.17.

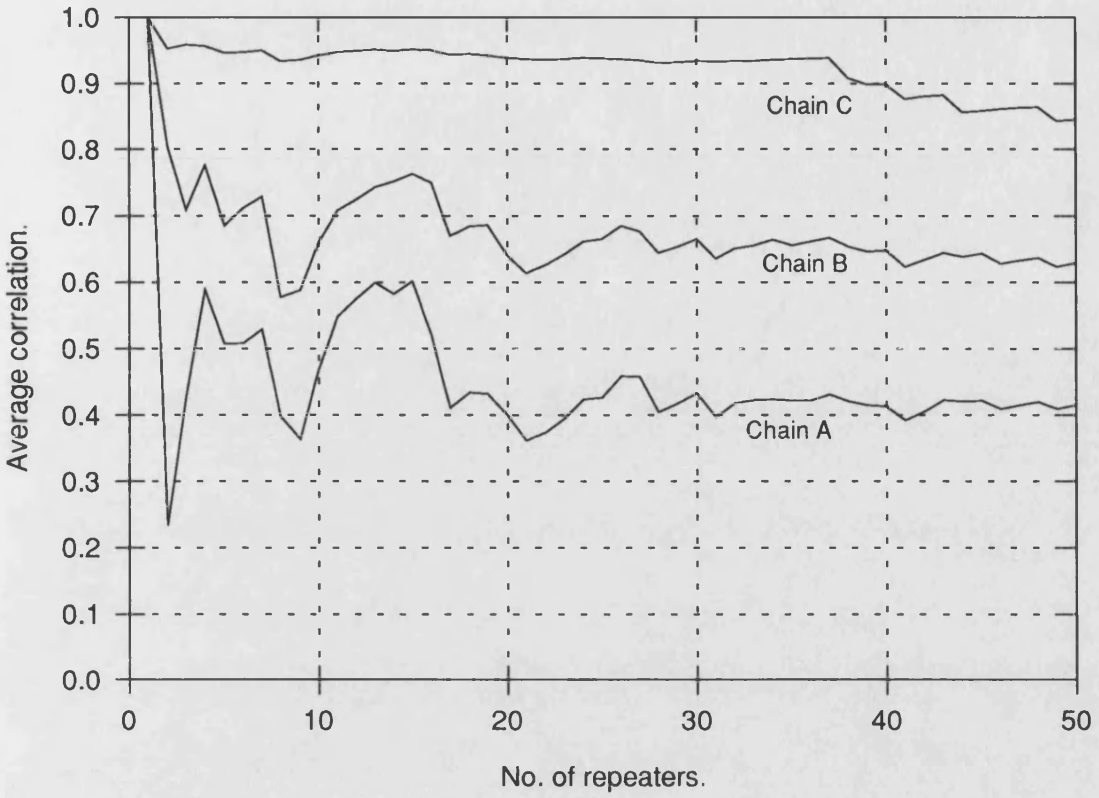

Figure 5.20: *Variation of average correlation along the three chains*

Since the pattern-dependent jitter generated at a single repeater typically has an injected (flat) jitter power spectral density an order of magnitude greater than that of noise-dependent jitter (for example, Trischitta [16]), the random accumulation of the un-correlated component of the pattern-dependent jitter is likely to exceed that of the noise-dependent jitter for a large range of partial jitter correlation. The sensitivity of random jitter to jitter peaking was discussed earlier - in figure 5.21 the normalised growth of pattern-dependent jitter k_C, is plotted for jitter peaking of 0, 0.1 and 0.2dB of a second order response as earlier, but with variation in the apparent average correlation coefficient. The normalised growth is defined as:

$$k_C = \frac{\sigma_N^{PD}}{\sigma_1^{PD}} = \frac{\int_{-1/2T}^{1/2T} S_N^{PD}(f)df}{\int_{-1/2T}^{1/2T} S_1^{PD}(f)df} \qquad (5.96)$$

Equal injected jitter power spectral density at each repeater is assumed, though by its very nature this is not the case in a real chain exhibiting partial correlation. However, for long chains this value would represent the average injected jitter and the onset and magnitude of exponential jitter growth as demonstrated would occur at the same magnitude and rate as in figure 5.21.

Evidence of the partial accumulation of pattern-dependent jitter exists in results published by several authors. Trischitta, Sannuti and Chamzas [17] describe a circulating loop experiment to simulate a long chain with a few repeaters by passing the same data stream repeatedly around a closed loop of repeaters. Their six-repeater loop exhibits poor correlation and by comparison with figure 5.21, it is estimated that the simulated chain of 100 to 200 repeaters exhibits an apparent mean correlation, $\overline{\rho}_N$, of around 0.5. The six repeaters chosen may not be a particularly representative sample of the total number of repeaters that would be in the actual chain and thus the result is significantly distorted. The 21-repeater loop also exhibits incomplete correlation of injected jitter but to a far lesser extent. Again, comparison with figure 5.21 (all repeaters have 0dB peaking) yields an estimate of the apparent mean correlation, $\overline{\rho}_N$, of about 0.8.

Trischitta and Sannuti report another jitter accumulation example [16] that clearly exhibits incomplete correlation of pattern-dependent jitter, this time with an estimated apparent mean correlation of about 0.56. Even the early work of Byrne et al. [6] shows a small degree of incomplete correlation in the measured jitter power spectral densities and the jitter accumulation reported (though

masked by log-log scaling). This does demonstrate that for long-haul digital links and local area networks, both of which contain large numbers of cascaded repeaters, that significant sensitivity of jitter accumulation to manufacturing tolerances of repeater timing extraction circuits exists beyond that of jitter transfer function peaking alone as previously thought.

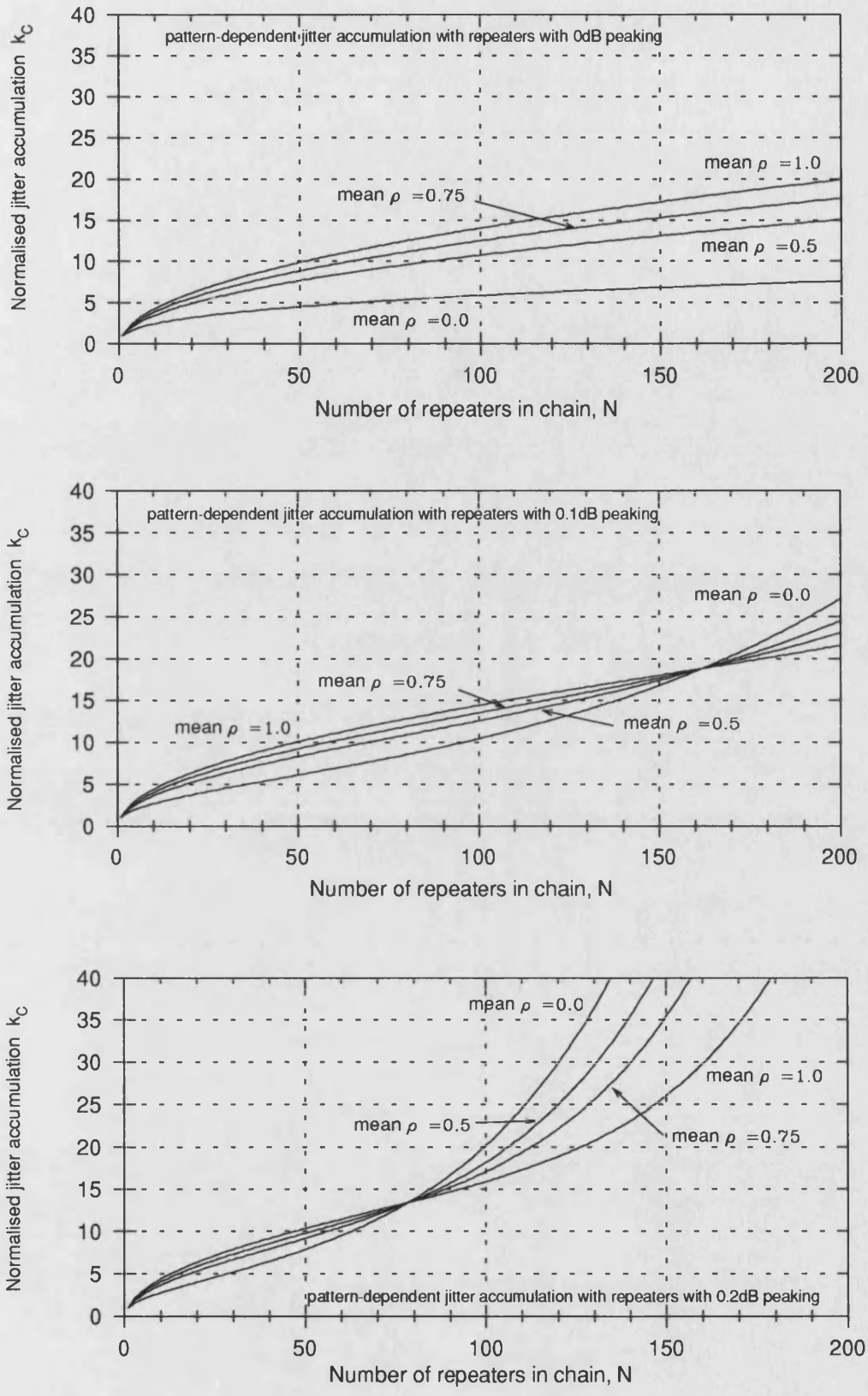

Figure 5.21: *The effects of jitter peaking on the accumulation of partially-correlated pattern-dependent jitter*

5.9. Effects of accumulating jitter on synchronous transmitters and coverage scheme performance

The architecture of a synchronous transmitter that could be entirely phase-locked to the recovered clock of a self-timed digital transmission system was introduced in chapter 4. A phase noise transfer model was also given allowing the output phase noise of the transmitter to be calculated and the ability of the phase-lock circuitry to maintain locked assessed, if the power spectral density of the input phase noise to the transmitter is known.

This chapter has presented a detailed model for predicting the accumulation of jitter, particularly the dominant pattern-dependent jitter, for a chain of repeaters. The simplest form of digital transmission system for a coverage scheme based on this technique is to connect all transmitters in the scheme by repeatered line, thus applying the phase noise model of the synchronous transmitter to the model for jitter accumulation, system performance can be predicted.

Both a V.H.F. and a U.H.F. transmitter will be considered with output frequencies of around 100MHz and 500MHz respectively as these are representative of the typical frequencies at which synchronous coverage schemes may be used in private mobile radio schemes. With reference to the phase noise model of chapter 4, a channel spacing of 25kHz is assumed and thus N_1 is 16. For an output frequency at V.H.F., M = 10 and N_2 = 4000 is assumed (actual output of 110.8MHz) and at U.H.F., M = 25 and N_2 = 20000 (actual output of 510.8MHz). In both cases, the R.F. multiplication M can be achieved by two frequency multiplier stages and the V.C.X.O. frequency is kept to 10MHz in the V.H.F. transmitter and 20MHz in the U.H.F. transmitter.

The 2.048Mbit/s P.C.M. input transmitter architecture is considered first since this is the primary 32-channel mulitplexed data rate and hence allows a choice of

voice channels to be broadcast with ample provision for signalling and control for dynamic or remote control of delay equalisation for audio path matching.

The use of passive timing recovery by second order resonators (SAW filters are not used at data rates as low as 2.048Mbit/s) allows the simplest repeater design. Byrne et al. [6] report measurements on a American standard 1.544Mbit/s repeatered line employing such circuits with Q factors around 100. The average injected jitter in this practical chain was 0.44×10^{-4} deg^2/Hz. Referring this figure to a symbol rate of 2.048Mbit/s (i.e. multiply by a factor of 1.544/2.048) and assuming a Q of 100, the growth in output phase noise and loop phase errors is shown in figure 5.22 as determined by applying the partial correlation model of jitter growth and the transmitter phase transfer model.

With both loop natural frequencies set to 10Hz (small noise bandwidth without excessively slow lock acquisition time) both loops maintain lock over the entire chain with a minimum margin for the static error of the second loop of around 0.2 radians. Poor correlation of pattern-dependent jitter may spread the jitter power spectral density into the frequency range of the loop phase error transfer functions, but since the loop bandwidths are a good deal smaller than the main lobe of the jitter power spectral density and thus the reduction in the amplitude of this lobe due to an average correlation of 0.5 is for more significant and reduces the growth of phase errors.

The second graph of figure 5.22 where the first loop natural frequency is increased to 100Hz demonstrates that this loop performs an important filtering effect on the input phase noise due to timing jitter so that the phase noise at the input to the second loop does not result in excess phase error. With this increase in natural frequency the second loop phase error rises quickly to exceed the lock limit. In both cases the first loop phase error is a fraction of the second loop phase error and much less critical to lock performance. The V.H.F. transmitter locked to

a 2.048Mbit/s transmission line would have a common first loop and has a smaller multiplication ratio on the second loop thus phase is not nearly as critical.

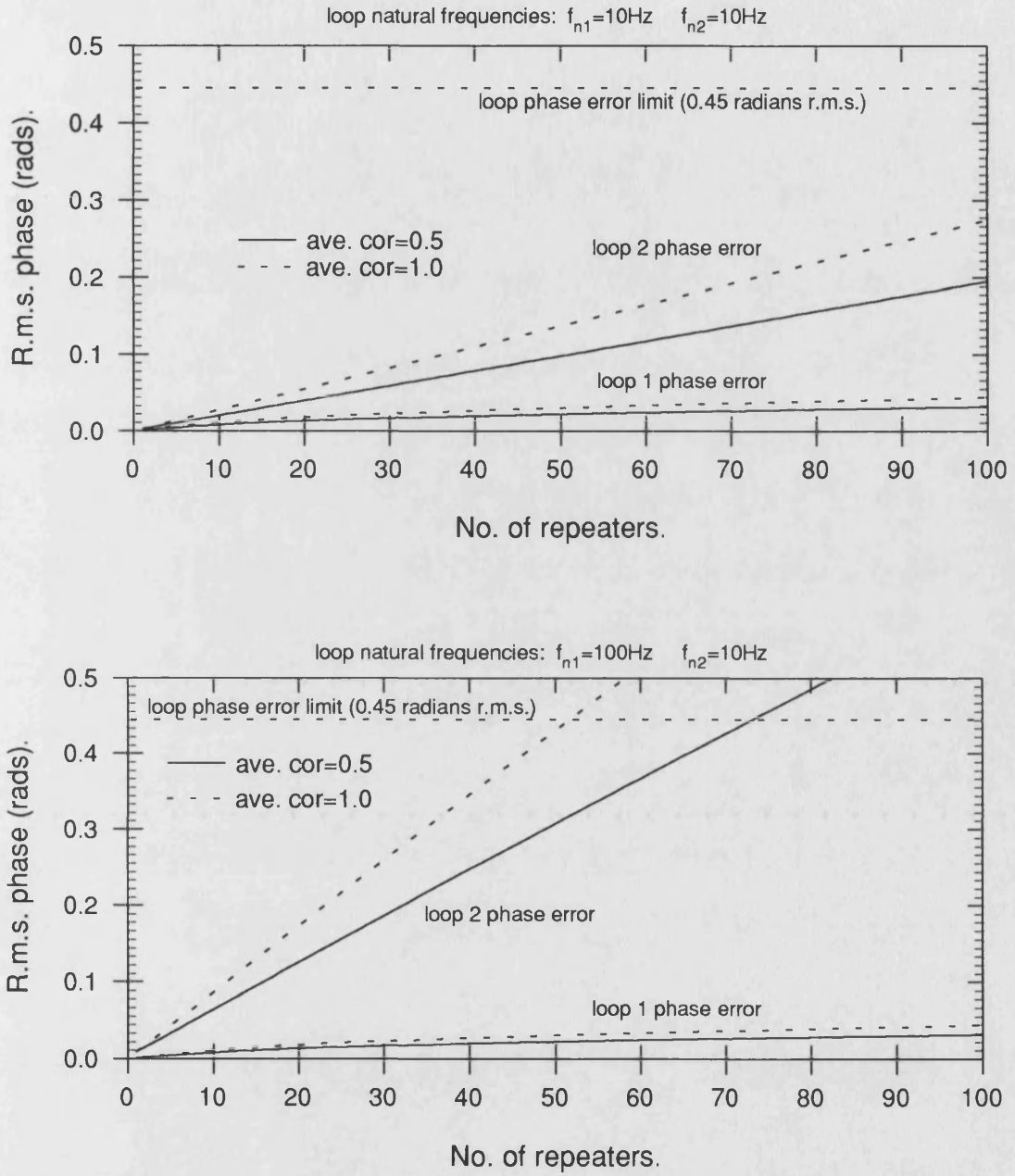

Figure 5.22: *Growth of transmitter phase lock loop errors due to accumulating pattern-dependent jitter*

Using 192kbit/s transmission with the same timing extraction, the second loop phase error exceeds the lock limit within 5 repeaters of the beginning of the chain with 10Hz loop natural frequencies. Even reduction to 1Hz in both loops only postpones this by another 5 repeaters. Increase of Q to 2000 (only realisable by PLL extraction) extends the length of chain to a total of 15 or so repeaters. Only extreme care in transmission system and repeater design, manufacture and maintenance would allow operation over longer repeater chains and thus it must be concluded that it is impractical to use bit rates as low as this for synchronisation, particularly in U.H.F. schemes.

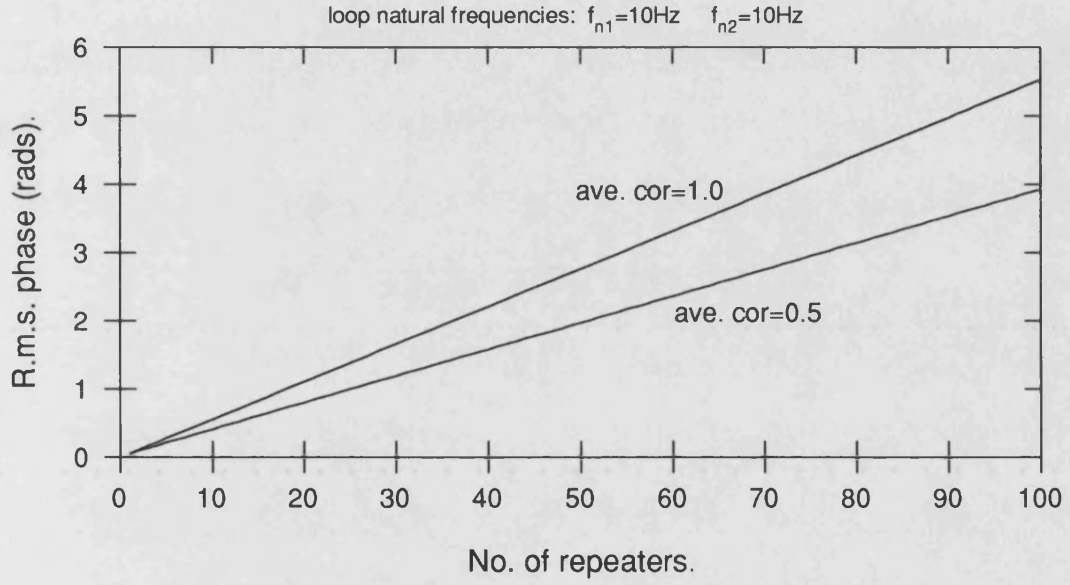

500MHz transmitter synchronised by 2.048Mbit/s transmission with tuned circuit timing extraction (Q=100)

Figure 5.23: *Growth of transmitter output phase noise due to accumulating pattern-dependent jitter*

The relative stability of the carrier phase of each transmitter covering a service area will affect performance in areas of coverage overlap as discussed in chapter 2. Time-varying phase difference between two carriers produces significant distortion in areas of near equal signal strength in F.M. schemes (e.g. carrier

offsets in quasi-synchronous F.M.) since every time the instantaneous phase difference passes through π radians, a carrier null occurs. The relative carrier phase stability between two transmitters is given by the standard deviation of the time-varying difference between the phase noise due to accumulating jitter of each transmitter. Fixed phase differences will occur due to the delays of digital transmission and circuits used for carrier frequency generation, but these are indistinguishable from differences in propagation delays from two sites.

If Δ_m is the instantaneous phase difference between two transmitters connected to different points of a repeatered line with m repaeters between them, then its standard deviation $\sigma_{\Delta m}$ can be determined from the integration of its power spectral density $S_{\Delta m}(f)$. The simplest form of its power spectral density can be obtained assuming completely correlated pattern-dependent jitter and is given by (see equation 5.35):

$$S_{\Delta m}(f) = S_{i1}(0)\left|H_{TX}(f)\right|^2\left|\sum_{n=N+1}^{N+m} H^n(f)\right|^2 \qquad (5.97)$$

where $H_{TX}(f)$ is the transmitter phase transfer function, N is the number of repeaters up to the first transmitter (including its own timing extraction) and m is the number of repeaters between first and second transmitter (including timing extraction of the second repeater). For the case of the U.H.F. transmitter synchronised to a 2.048Mbit/s line using bandpass filter timing extraction, the bandwidth of the synchronous transmitter is sufficiently smaller than the repeater phase transfer function $H(f)$, that the summation term of equation 5.97 is constant with N (up to 100 repeaters) and thus so is $\sigma_{\Delta m}$ which is approximately equal to the r.m.s. output noise of the m^{th} repeater and can be obtained from figure 5.23. This yields figures of around 0.27 and 0.55 radians r.m.s. for m=5 and 10 repeaters respectively (and thus approximate maximum transmitter separations of 5 and 10 miles for this type of line - typical of the

separation between transmitters that may be intended to give synchronous coverage of a common area). Potentially, these phase differences may have any mean value at the mobile and may result in "fading" similar to that of quasi-synchronous schemes. However, the magnitude of this relative phase variation is less than 0.1 wavelengths r.m.s. which might easily arise from the movement of masts and antennas in the wind at U.H.F. frequencies and is unlikely to cause significant degradation of the field in the areas of near equal signal strength in regions of coverage overlap between two transmitters locked to different points along a repeatered line.

5.10. Conclusions

This chapter has considered the generation and propagation of timing jitter in digital transmission lines employing self-timed repeaters and the effects of accumulating jitter on the synchronous transmitter presented in chapter 4.

Regardless of the form of timing extraction filter used (tuned circuit, phase lock loop or surface acoustic wave filter), timing jitter may be fundamentally divided into two types by its source, i.e. noise-dependent jitter resulting from additive channel noise and pattern-dependent jitter resulting from the random nature of the digital stream and imperfections in the timing recovery process.

With the increase in use of SAW filters for timing extraction in high bit rate optical fibre systems, a direct simulation of the timing recovery process to calculate jitter in passive timing extraction was developed allowing all parameters of a repeater employing passive timing extraction to be varied to examine their effect. This overcomes the limitations of mathematical analyses of other authors which are confined to particular non-linearities, timing filter transfer functions and pulse shapes. Also, since it allows the calculation of actual jitter sequences rather than just give measures such as variance and power spectral density, it allows considerably easier calculation of the cross-correlation of the jitter produced by repeaters with differing parameters as required in the accumulation analysis. The simulation technique was verified against the published analyses for tuned circuit timing extraction for variation in Q-factor, trigger threshold, mistuning and additive channel noise and gave the characteristic jitter power spectral densities for these imperfections.

Perfect pulse shape equalisation and zero amplitude-to-phase conversion (no trigger threshold offset in bandpass extraction or static phase tracking errors in a PLL) results in pattern-dependent jitter with a power spectral density that goes to zero at zero frequency. However, with all repeater imperfections present in

practice, both pattern-dependent and noise-dependent jitter exhibit a lowpass power spectral density that is flat at zero frequency. The lowpass nature of the spectrum results from the jitter transfer function of the timing extraction filter. The jitter transfer function of a PLL is simply its phase transfer function whereas a transformation to baseband of a bandpass filter transfer function is required to give the jitter transfer functions of tuned circuit and SAW filter timing extraction. This leads to Chapman's jitter model of a digital repeater for analysis of jitter accumulation. The jitter generated by the repeater is modelled as a gaussian additive jitter source at the input to the jitter transfer function of the repeater which filters the sum of the injected jitter and the jitter already present on the incoming digital stream. This model is used to compute the power spectral density of the jitter after a chain of repeaters and thus determine the accumulation of r.m.s. jitter. The simplest form of the model assumes identical repeater transfer functions and levels of noise-dependent and pattern-dependent jitter.

Conventional analyses assume that the pattern-dependent jitter is completely correlated from repeater to repeater and accumulates systematically, and that noise-dependent jitter is completely uncorrelated from repeater to repeater and accumulates randomly. The systematic jitter thus accumulates significantly faster by its very nature and since its power spectral density at a single repeater is typically greater by an order of magnitude, noise-dependent jitter does not accumulate significantly. However, the presence of jitter peaking in the transfer functions of a chain has undesirable results causing exponential runaway of the accumulating jitter and is most severe on randomly accumulating jitter. Peaking results from poor damping of a PLL (damping factor less than 4), passband ripple or mistuning in bandpass timing extraction and peaking of more than 0.1dB is undesirable.

However, even if the assumptions of identical transfer functions and levels of injected jitter are lifted, accumulation of jitter in chains of repeaters has been shown to depart significantly from theory (generally under-accumulating), particularly in chains of optical fibre repeaters employing SAW filter timing extraction. The assumption of complete correlation of the injected jitter at each repeater is not necessarily valid and was discarded inorder to develop a more accurate model of jitter accumulation.

By employing an established model for the transfer function of a SAW filter in the developed simulation, the variation in correlation coefficient between the jitter produced by two optical fibre repeaters was determined for variation in principle parameters: mistuning, Q-factor and trigger threshold offset. Holding other parameters constant, differing trigger threshold offsets can reduce correlation to around 0.6, but variation in SAW Q-factor has little effect on correlation, it remaining near unity. This would be expected from Chapman's model since this should only change the jitter transfer function, not the injected jitter. However, mistuning gives the most dramatic results since opposite mistunings give large negative correlation coefficients as might be expected intuitively.

The spread in correlations between each repeater in a chain was calculated for three 50-repeater chains with random scatter in the principle parameters representative of manufacturing tolerances with each chain having successively higher standard deviation of mistuning since this is the parameter with the greatest potential effect on correlation. With a standard deviation of 0.01 in the SAW mistuning factor no negative correlation was observed and most correlation coefficients were slightly less than unity. However, with a standard deviation of 0.05, there was a significant spread of values over the entire range from -0.8 to 1.0.

Expressions have been derived for the power spectral density of accumulating jitter in a chain of repeaters in terms of the injected jitter power spectral densities (assumed white since this is the cases experienced in practice, but the theory may be modified to include any shape of the power spectral density) and jitter transfer functions of each repeater and the correlation coefficients of the jitter injected at each repeater with all others in the chain. Using this theory, the jitter power spectral density and hence the accumulation of pattern-dependent jitter in the three chains of repeaters whose correlation coefficients had been determined was calculated. The jitter power spectral densities and the rates of accumulation showed good agreement with published measured results. The characteristic nulls of the pattern-dependent jitter power spectral density are progressively made less sharp and less deep as the spread in correlation coefficients increased.

The expressions for jitter power spectral density can be simplified by assuming the correlation coefficient to be the same between all repeaters in the chain. By calculating the apparent average correlation coefficient along the chain, it was shown that as the chain increases in length, the apparent average correlation coefficient approaches closely the mean of the set of actual correlation coefficients - 0.85, 0.62 and 0.46 in the three chains studied.

Since the remainder of the pattern-dependent jitter that does not accumulate systematically must accumulate randomly, the constraints on jitter peaking are more important since the pattern-dependent jitter is significantly larger than the noise-dependent jitter. The variation in accumulation of pattern-dependent jitter in chains exhibiting jitter peaking with apparent average correlation was determined and shows the increased potential for exponential growth in jitter with reduction in apparent average correlation.

One of the principle drawbacks of quasi-synchronous F.M. schemes was the

requirement of have expensive, high-precision oscillators in each transmitter requiring careful alignment and maintenance to set the carrier frequency. Using the jitter accumulation model it has been shown that providing the source of a 2.048Mbit/s P.C.M. transmission line has sufficient long term frequency stability (see chapter 4), then transmitters of the kind presented in chapter 4 can be phase-locked (without excessive requirement on P.L.L. bandwidth and thus oscillator stability - simple crystal control is sufficient) to that line and inexpensive, moderate Q-factor bandpass timing extraction may be employed in line repeaters. The accumulation of timing jitter over even a long repeatered line does not prevent phase lock of transmitter loops and the relative phase stability of transmitters locked to different parts of the line experiencing different levels of jitter is not likely to be sufficient to cause degradation of synchronous coverage performance. Lower bit rate transmission such as the "2B+D" rate of 192kbit/s is likely to cause transmitter locking failures due to excessive loop tracking errors and is hence impractical for this use.

5.11. References

[1] Takasaki, Y., "*Digital Transmission Design and Jitter Analysis*" Artech House 1991 ISBN 0-89006-503-9.

[2] Nyquist, H., "*Certain topics in telegraph transmission theory*" A.I.E.E. Trans., vol. 47 April 1928, pp. 617-644.

[3] Gardner, W. A., Franks, L.E. "*Characterisation of cyclostationary random signal processes*" I.E.E.E. Trans. on Information Theory vol. IT-21 no.1, Jan. 1975 pp.4-14.

[4] Takasaki, Y., "*Optimising pulse shaping for baseband digital transmission*" I.E.E.E. Trans Comms. vol. COM-20 no. 5, Oct. 1972, pp.877-884.

[5] Brooks R. M., Jessop A., "*Line coding for optical fibre systems*" Int. J.

Electrons. vol. 55 no.1, July 1983 pp.81-120.

[6] Byrne, C.J. et al., "*Systematic jitter in a chain of digital regenerators*" Bell Syst. Technical Journal, vol. 42, Nov. 1963, pp.2679-2714.

[7] Chamzas, C. "*Accumulation of jitter: a stocastic model*" AT&T Technical Journal vol. 64, no.1, Jan. 1985, pp. 43-76.

[8] Crochiere, R.E., Rabiner, L.R. *"Multirate Digital Signal Processing"* 1983 Prentice-Hall Inc. New Jersey ISBN 0-13-605162-6.

[9] Gardner, F. M. "*Phase lock techniques*" 1979 John Wiley & Sons, Inc. New York ISBN 0-471-04294-3

[10] Rosenberg, R. L., Chamzas, C., Fishman, D. A., "*Timing recovery with SAW transversal filters in the regenerators of undersea long-haul fiber transmission systems*" I.E.E.E. Journal of Lightwave Technology vol. LT-2 No.6 Dec. 1984 pp. 917-925.

[11] C.C.I.T.T., 1988 Blue Book - Volume IV, Fascicle IV.4 *Recommendation O.151.*

[12] Oppenheim A. V., Shafer R. W., "*Digital signal processing*" 1975 Prentice-Hall Inc., New Jersey.

[13] Mengali U., Pirani G., "*Jitter accumulation in PAM systems*" I.E.E.E. Trans. on Communications, vol. COM-28, no.8, August 1980 pp.1173-1183.

[14] Franks L. E., Bubrouski J. P., "*Statistical properties of timing jitter in a PAM timing recovery scheme*" I.E.E.E. Trans. on Communications, vol. COM-22, no.7, July 1974 pp.913-920.

[15] Roza E., "*Analysis of phase-locked timing extraction circuits for pulse code transmission*" I.E.E.E. Trans. on Communications, vol. COM-22, no.9, September 1974 pp.1236-1249.

[16] Trischitta P. R., Sannuti P., "*The accumulation of pattern-dependent jitter for a chain of fiber optic regenerators*" I.E.E.E. Trans. on Communications, vol. COM-36, no.6 June 1988 pp. 761-765.

[17] Trischitta P. R., Sannuti P., Chamzas C., "*A circulating loop experimental technique to simulate the jitter accumulation of a chain of fibre optic regenerators*" I.E.E.E. Trans. on Communications, vol. COM-36, no.2 February 1988 pp. 205-213.

[18] Manley J. M., "*An generation and accumulation of timing noise in PCM systems - an experimental and theoretical study*" Bell Syst. Tech. J., vol. 48, March 1969 pp. 541-613.

Chapter 6:
Conclusions and Further Work

Co-channel radiation of identical signals from a number of geographically-separated transmitters could improve the extent and intensity of coverage in a mobile radio scheme with maximum spectral-efficiency. A single channel could be used to cover a large area or improve the quality of coverage (i.e. increased mean and reduced variance of field strength within the coverage area) by arranging a number of transmitters to cover a common area. The later is particularly effective for providing handportable coverage in urban areas where the adverse effects of buildings on propagation severely limit the continuity of coverage that a single transmitter can achieve. Further, the effects of Rayleigh fading can be reduced since the fading amplitude envelopes due to each transmitter are uncorrelated and hence simultaneous fades from all transmitters covering the area are very unlikely.

In practice, radiation of identical signals from remote transmitters is impossible to achieve. Conventional "quasi-synchronous" area coverage schemes use analogue landlines to convey the modulating audio to each transmitter and high stability oscillators at each transmitter to set the output carrier frequency. The equalisation of modulation and carrier frequency can not be achieved and maintained exactly; since the oscillators are prone to drift with time and the analogue landlines each have time and frequency-dependent transmission characteristics that can only be equalised to within set tolerances.

F.M. "quasi-synchronous" schemes are more prone than A.M. schemes to distortion in areas of coverage overlap due to the imperfect matching of radiated signals. Co-channel F.M. distortion results from two mechanisms; the high level of audio output noise when the instantaneous signal strength drops below the receiver threshold, and the intermodulation distortion of the instantaneous phase

of the resultant field. The greatest distortion occurs in both cases when the mean signal strength from each transmitter is similar, a widespread occurrence in an intensive area coverage system and so acceptable performance under these conditions is essential. Both distortion effects are functions of the difference in the instantaneous phase of the F.M. output of the two transmitters. The difference in instantaneous phase arises from carrier frequency offset and/or mismatch in the modulation of the two transmitted signals. Both effects seriously degrade received speech quality and in practice it is found that carrier offsets must be controlled to less than 2Hz and analogue landlines must be equalised to better than 2dB in amplitude and 50μs in delay across the audio bandwidth used.

Digital transmission of modulating audio to remote sites allows exact amplitude matching and accurate delay equalisation that is easily implemented across the entire audio range with simple digital circuitry. A novel all-digital modulation technique has been presented that converts digital samples of the modulating signal to convention phase modulation (suitable preprocessing of the audio gives a frequency modulated output). This precise phase modulator is easily implemented in digital circuitry and gives identically repeatable performance at each transmitter. The effects of the inherent sampling, quantisation and zero-order hold of the modulated phase limit the quality of the received signal and have been analysed and quantified, but do not have any effect on co-channel operation as they are identical for each modulator. Sampling of the modulated phase of an angle-modulated signal results in replicas of the ideal continuous phase spectrum spaced at integer multiples of the sampling frequency either side of the carrier frequency. Bandpass filtering can remove the post-modulation alias components providing the sampling frequency is greater than the *modulated* signal bandwidth (whereas the sampling frequency for transmission of the audio is set at twice the *un-modulated* signal bandwidth). Since F.M. is a non-linear modulation type, the required bandwidth of the modulated signal is function of

not only the modulating signal bandwidth, but the frequency deviation also. Carson's rule gives accurate estimates of F.M. bandwidth only for very low and very high deviations. Even 2.5kHz deviation narrowband mobile radio systems exhibit some bandwidth expansion, so sampling frequency constraints have been developed using statistical bounds on the spectral distribution of power in an F.M. signal modulated by band-limited gaussian modulation. Blachman's 2nd and 4th moments of spectrum give around 1% in-band alias distortion power for a 3.4kHz bandwidth modulating signal sampled at 8kHz and a frequency deviation 2.5kHz. Since this is the deviation used for 12.5kHz channel spacing narrowband F.M. systems, suitable crystal filters exist to perform the required post-modulation anti-alias filtering. The baseband bandwidth and sampling frequency are standard for digital telephony transmission and thus using these constraints, greater deviations are not directly possible without increase in distortion power. However, post-modulation frequency multiplication may be used to increase deviation.

The zero-order hold of the modulated phase results in a $sinx/x$ type spectral envelope imposed on the ideal spectrum and centred on the carrier frequency. Over much of the range of half the sampling frequency either side of the carrier, the effect is not significant, but at the extremities a drop in the spectrum amplitude of 4dB exists. This results in amplitude and phase distortion of the ideal signal after anti-alias filtering.. The amplitude distortion is only severe for deviations in excess of those allowed by the sampling frequency constraints and may be removed by hard-limiting. The distortion in the received audio due to the phase distortion is calculated by numerical techniques (by Fast Fourier Transform) and is shown to be small and spectral equalisation is not performed.

Receiver output distortion due to quantisation of the modulated phase has been quantified. If the resolution of the modulator is sufficiently high such that phase

errors are small (at least 100 steps in 2π radians), the phase can be treated as broadband white noise accompanying the desired modulated signal. As with additive channel noise, the quantisation distortion in the F.M. receiver output has a parabolic power spectral density and thus pre-emphasis/de-emphasis at the transmitter and receiver improves the signal to quantisation distortion ratio (SQNR) at the receiver output. Again as with additive channel noise, the bandwidth expansion that accompanies increased deviation gives a demodulation gain in SQNR, but this is also limited by sampling rate. An 8-bit modulator at 2.5kHz deviation and 8kHz sampling achieves an SQNR of over 65dB with pre-emphasis/de-emphasis. This is the limit in performance possible using a 64kbit/s digital transmission channel for the modulating audio.

The only variability left between transmitters is the transmission parameters of post-modulation circuitry. The I.F. crystal filters used for anti-alias filtering are the most significant devices and from the measured transmission characteristics of three typical devices of the same type, differential characteristics were determined and for both amplitude and delay they can be modelled as the sum of approximately symmetric passband ripple of two "wavelengths", one short with respect to the filter bandwidth and one long. The co-channel distortion of receiver output due to one ideal transmitter and one with differential I.F. characteristics was calculated by F.F.T. techniques for a range of amplitude and delay ripples of both wavelengths. The short wavelength delay ripple results in the greatest distortion, but in the worst case analysis this is still considerably less severe than that experienced due to modulation misequalisation in conventional "quasi-synchronous" schemes.

A V.H.F. transmitter based on the precise phase modulator has been constructed and tested with sinusoidal and speech signals to verify its predicted performance. A synchronous architecture was used were all frequencies were derived from, and

synchronous with, a reference input of 2.048MHz and intended for the recovered clock of a CCITT recommended 30 channel multiplex 2048kbit/s digital trunk line.

In order to determine the phase lock performance of a synchronous transmitter, the power spectral density of jitter in the recovered P.C.M. clock is required. Several authors have previously derived forms for the jitter power spectral density in self-timed digital repeaters, but most are restricted by simplifying assumptions to allow tractable mathematical analysis. A direct simulation approach has been adopted here to allow free choice of system parameters and quantify the power spectral density. Two forms of timing extraction filter have been considered, bandpass filter (either both tuned resonator and surface acoustic wave filter) and phase-lock loop. Jitter may be classified by source or accumulation behaviour. The two principle sources of timing jitter are channel noise dependent and digital pattern dependent

The classification of jitter by accumulation behaviour gives two types, random and systematic jitter. Random jitter is entirely uncorrelated with the jitter of any other timing extraction process in a digital network and systematic jitter is entirely correlated with similar components in the jitter of any other timing extraction process. Traditional models of jitter accumulation in a chain of digital repeaters use Chapman's linear time-invariant model of the repeater timing extraction filter jitter transfer function preceded by a jitter source representing the jitter injected at that repeater that adds to the input jitter. By assuming, complete correlation (systematic jitter) of the pattern-dependent jitter and complete uncorrelation (random jitter) of the noise-dependent jitter injected at each repeater, it can be shown that without peaking in the jitter transfer functions of each repeater that pattern-dependent jitter accumulates faster and that with jitter peaking, random jitter growth becomes more rapidly exponential

in long repeater chains. Since noise-dependent jitter is smaller in magnitude though this reduces the seriousness of this effect.

However, as reported by a number of authors, this model has been shown to significantly depart from measured results, particularly in high bit rate optical fibre systems using surface acoustic wave filters. A partial correlation model has been proposed that more accurately describes the accumulation of pattern-dependent jitter. Using the direct jitter simulation developed to calculate jitter power spectral density with jitterless input P.C.M., the variation of the correlation coefficient between the systematic jitter injected at two repeaters can be determined. The case of optical fibre repeaters using surface acoustic wave timing extraction filters has been examined as application of the model, and the dependence of pattern-dependent jitter correlation with variation of key parameters such as filter Q-factor, mistuning and timing threshold offset. Filter Q has little effect on the correlation which remains almost unity as expected from Chapman's model since it should only change the jitter transfer function. Timing threshold offset variation reduces the correlation, but remains positive. The most significant result is that opposite polarity mistuning yields large negative correlations that will reduce the accumulation of jitter in a chain. By calculating correlation coefficient sets for repeaters forming a chain with random scatter in parameters due to manufacturing tolerances, the developed theory was used to show that the apparent average correlation coefficient of the injected jitter in a chain approaches the mean of the set of correlation coefficients. Hence significant numbers of negative correlation coefficients substantially reduce the mean correlation and the accumulation of pattern-dependent jitter.

However, the pattern-dependent jitter that no longer accumulates systematically now accumulates randomly and will in general be greater than the noise-dependent jitter. Calculating the variation of pattern-dependent jitter

accumulation in the presence of jitter peaking as the apparent average correlation coefficient is reduced shows acceleration of exponential jitter growth which imposes tighter constraints on the permitted jitter peaking in a chain.

The simplest form of coverage scheme based on the technique proposed is that where a single repeatered transmission line links the synchronous transmitters. The long-term stability of the transmitter carrier frequencies are all determined by the stability of the clock of the P.C.M. source, but the lock performance depends on the accumulating jitter. It has been shown that inexpensive 2.048Mbit/s digital transmission lines using metallic media and moderate Q-factor bandpass filter timing recovery in repeaters may be used without transmitter lock problems on even long (100 repeater) chains. Relative phase instability between transmitters locked to different points of the repeatered line (and hence experiencing different amounts of jitter) is also shown to be unlikely to cause significant degradation in areas of coverage overlap. Substantial instability is only likely between transmitters locked to parts of the line that are too far apart that they are likely to be serving the same coverage area. The use of low bit rate lines (192kbit/s) is impractical due to transmitter phase lock failures that will occur due to excessive loop tracking errors after only a handful of repeaters.

There are two principal areas with scope for further work beyond that presented in this thesis. Firstly, a synchronous area coverage scheme, with three or more transmitters of the type described in Chapter 4, could be implemented and the received distortion in areas of coverage overlap examined. The effects of relative carrier phase instability due to accumulated jitter between transmitters and mismatch in transmitter filter characteristics could then be practically verified and possibly quantified.

Secondly, the effects of pulse misequalisation in PCM repeaters on the

correlation of the pattern-dependent jitter has not been investigated. Quantification of the variation of correlation coefficient with pulse shaping for both passive and phase-lock extraction would allow greater confidence in manufacturing repeater chains having high correlation of pattern-dependent jitter and thus reduced risk of exponential growth of randomly accumulating jitter.

Appendix A:

CALCULATION OF DISTORTION IN THE OUTPUT OF AN IDEAL F.M. RECEIVER BY THE FAST FOURIER TRANSFORM

A.1 Determination of Received Phase

The output of an ideal F.M. receiver is proportional to the time-differential of the received phase of the incoming signal. In the situations considered in this thesis, the received signal can be subject to amplitude variations $a(t)$, as well as phase variations $\phi(t)$, and thus the incoming signal is of the form:

$$e(t) = a(t)\cos(2\pi f_o t + \phi(t)) \qquad (A.1)$$

where f_o is the carrier frequency. An ideal receiver removes the amplitude fluctuations $a(t)$ by hard-limiting and the audio output is:

$$e_{af}(t) = \frac{d}{dt}\{\phi(t)\} \qquad (A.2)$$

assuming a demodulator constant of $1 V rad^{-1} s$. To calculate the audio output of an ideal F.M. receiver $e_{af}(t)$, the received signal is split into components that are in-phase and quadrature to the carrier, i.e.:

$$e(t) = I(t)\cos 2\pi f_o t + Q(t)\sin 2\pi f_o t \qquad (A.3)$$

so that:

$$e_{af}(t) = \frac{d}{dt}\left\{\frac{Q(t)}{I(t)}\right\} \qquad (A.4)$$

However, calculation of the above by conventional means yields errors in the result if at any time $|\phi(t)| \leq \pi/2$, since the inverse tangent function can only return values in the range $-\pi/2$ to $\pi/2$ due to the periodicity of the tangent

function. This anomally can be overcome by processing the calculated phase values after evaluation. Since the phase $\phi(t)$ in the cases under consideration is continuous and smoothly varying, any discontinuities of magnitude greater than $\pi/2$ in adjacent phase samples is taken to indicate a transition where the actual value of $\phi(t)$ has exceeded $\pi/2$ or a multiple thereof. This can be corrected for by adding a factor for the accumulated phase to the instantaneous phase. For a negative discontinuity where $\phi(n)$ is the n^{th} phase sample:

$$\phi(n) - \phi(n-1) \leq -\frac{\pi}{2} \qquad (A.5)$$

then the accumulated phase is incremented by π radians since $\phi(t)$, the actual phase, is still increasing. Similarly, for a positive phase discontinuity, i.e.:

$$\phi(n) - \phi(n-1) \geq \frac{\pi}{2} \qquad (A.6)$$

the accumulated phase is decremented by π radians since $\phi(t)$ is still decreasing. However, adjacent sample differences of this size are also possible if the signal analyzed contains components with sufficiently high instantaneous time differentials. This would lead to erroneous increments in the phase accumulation. The rate of change of phase, $\dot{\phi}$ required to achieve this is:

$$\dot{\phi} = \frac{\pi}{2} f_s \qquad (A.7)$$

where f_s is the frequency at which the simulated phase is sampled. Consider a sinusoidally varying phase $\psi(t)$, where:

$$\psi(t) = \beta \sin 2\pi f t \qquad (A.8)$$

then:

$$\dot{\psi}(t) = 2\pi\beta f \cos 2\pi f t \qquad (A.9)$$

and thus the maximum value is:

$$\dot{\psi}_{max} = 2\pi\beta f \qquad (A.10)$$

For no erroneous phase accumulation:

$$\dot{\psi}_{max} < \dot{\phi} \qquad (A.11)$$

and since βf is the frequency deviation Δf:

$$\Delta f < \frac{f_s}{4} \qquad (A.12)$$

For undistorted audio, the highest frequency examined is *3.4kHz* and the sampling frequency used is *50kHz*, so:

$$\Delta f < 12.5kHz \qquad (A.13)$$

So since the range of interest is Δf up to *5kHz*, considerable harmonic distortion would be required to give sufficiently large signals at high frequencies to cause an erroneous decision. Further, any erroneous phase accumulation would result in a phase discontinuity that would give rise to audio distortion values in excess of *100%* and would easily be identified if they occured.

This processing may lead to some ambiguity in the absolute instaneous value of the received phase (since the first value of $\phi[n]$ is not necessarily in the range $-\pi/2$ to $\pi/2$) but this is irrelevent since the phase is differentiated to obtain the differentiationfinal output and thus waveform continuity is essential: the mean (or d.c.) value is lost in differentiation. Differentiation is achieved by a *256* point F.I.R. (Finite Impulse Response) differentiator designed using the signal processing package *DaDISP* which yielded an exellcent approximation to an ideal differentiator.

A.2 Audio distortion factor and the Discrete Fourier Transform

In order to assess the effect of imperfections in generation and reception of F.M. signals a sinusoidal test tone is often used as a modulating signal, and the output from an ideal receiver is calculated. The expressions that result are highly

complex and exact algebraic answers are unobtainable, though in most cases it is clear that the output will consist of a component at the modulating frequency and a series of harmonics of that frequency whose amplitudes tend to reduce with increasing harmonic order until negligible. Thus the output from an ideal receiver is of the form:

$$e_{af}(t) = \sum_{p=1}^{P} a_p \cos(2\pi p f_m t + \varphi_p) \qquad (A.14)$$

where there P is the number of significant harmonics of the fundamental frequency f_m, phase ϕ_p and amplitude a_p. The audio distortion factor of the signal $e_{af}(t)$ is then defined as:

$$D.F. = 100\sqrt{\frac{\sum_{p=2}^{P} a_p^2}{a_1^2}}\,\% \qquad (A.15)$$

where a_1 is the amplitude of the fundamental. Isolation of the amplitude of each harmonic from the complex generating equations for some of the signals of interest is impractical directly, though if the Fourier transform of these expressions could be obtained then it would obviously be a periodic line spectrum. The amplitudes of the lines would give the harmonic amplitudes and thus the distortion factor could be calculated, i.e.:

$$E_{af}(f) = \boldsymbol{F}\{e_{af}(t)\} = \sum_{p=1}^{P} \frac{a_p e^{j\frac{\varphi_p f}{p f_m}}}{2}(\delta(f - p f_m) + \delta(f + p f_m)) \qquad (A.16)$$

where $\boldsymbol{F}$ denotes the Fourier transform. However, to obtain the above equation from any expression, the continuous-time Fourier transform is required. However, the complexity of the continuous-time expressions prohibit direct transform and computer calculation of the signal cannot be continuous or extend over all time as the infinite limits of the transform integral require. If the

conventional transform is reduce to a discrete-time transform $E_{af}(f)$ of N sample points taken every T_s seconds, then:

$$E_{af}(f) = \sum_{n=0}^{N-1} e_{af}[n] e^{-j2\pi f n T_s} \qquad (A.17)$$

This still requires a continuous frequency variable f, where a computer implementation of the transform can only calculate a finite number of points at discrete values of frequency. This results in the commonly-known Discrete Frequency Transform, or *D.F.T.* :

$$E_{af}[k] = \sum_{n=0}^{N-1} e_{af}[n] e^{-j2\pi k n/N} \qquad (A.18)$$

where $E_{af}[k]$ is at frequency kf_s/N, f_s is the sampling frequency which is chosen such that the amplitude of any harmonic beyond $f_s/2$ is negligible, thus avoiding aliasing by observing the Nyquist criterion. Now, if the distorted signal is sampled, the resulting signal $e_{af}[n]$ is:

$$e_{af}[n] = \sum_{p=1}^{P} a_p \cos(2\pi p q\, n/N + \varphi_p) \qquad (A.19)$$

where:

$$q = N \frac{f_m}{f_s} \qquad (A.20)$$

Thus the D.F.T. of $e_{af}[n]$ is:

$$E_{af}[k] = \sum_{n=0}^{N-1} \left(\sum_{p=1}^{P} a_p \cos(2\pi p q\, n/N + \varphi_p) e^{j2\pi k n/N} \right) \qquad (A.21)$$

or:

$$E_{af}[k] = \sum_{p=1}^{P} \left(\sum_{n=0}^{N-1} a_p \cos(2\pi p q\, n/N + \varphi_p) e^{j2\pi k n/N} \right) \qquad (A.22)$$

The D.F.T. of a single sinusoid does not give a spectral line at the frequency of

interest, but results in the D.F.T. of the function that truncates the time series $e_{af}[n]$: in the above case a function $w[n]$ where:

$$\begin{aligned} w[n] &= 1 \quad 0 \le n < N \\ &= 0 \quad elsewhere \end{aligned} \tag{A.23}$$

The D.F.T. of $w[n]$ is centred on the frequency of the sinusoid and is an approximation to an impulse function, but consists of a main lobe spread across a number of discrete frequencies near the frequency of the sampled sinusoid, and a spread of the remaining signal across the entire spectrum or *leakage*. Thus the magnitude of the D.F.T. of a harmonic series is:

$$\left|E_{af}[k]\right| = \frac{1}{2}\sum_{p=1}^{P} a_p \left|W'[k-pq]\right| + \left|W'[k+pq]\right| \tag{A.24}$$

By applying a time-window function to the signal samples the amount of leakage across the spectrum is reduced and the amount of signal in the main lobe increases so that only the $N/2$ positive frequency values of the D.F.T. are of interest due to the symmetry of the spectrum, i.e.:

$$\left|E_{af}[k]\right| = \frac{1}{2}\sum_{p=1}^{P} a_p \left|W'[k-pq]\right| \tag{A.25}$$

where $W'[k]$ is the D.F.T. of the time-window function. If the power in a discrete signal is approximated by:

$$P \approx \frac{1}{N}\sum_{n=0}^{N-1} e_{af}^2[n] \tag{A.26}$$

then from the discrete form of *Parseval's Theorem*, i.e.:

$$\sum_{n=0}^{N-1} \left|e_{af}[n]\right|^2 = \frac{1}{N}\sum_{k=0}^{N-1} \left|E_{af}[k]\right|^2 \tag{A.27}$$

then the power can be written as:

$$P \approx \frac{1}{N^2}\sum_{k=0}^{N-1} \left|E_{af}[k]\right|^2 \tag{A.28}$$

which due to the symmetry of the D.F.T. is:

$$P \approx \frac{2}{N^2} \sum_{k=0}^{N/2-1} \left| E_{af}[k] \right|^2 \qquad (A.29)$$

If the window function applied is such that the main lobe of the D.F.T. of the window contains nearly all of the spectral power and the leakage across the rest of the spectrum is minimal, then the power of a single sinusoid can be assessed by summing the square of D.F.T. coefficients in the main lobe only, i.e. the c most significant points either side of the maximum component of the main lobe $E_{af}[k_{max}]$. In practical situations, the fundamental component of the signal will be the highest (otherwise the distortion factor is *>100%*) and so the maximum D.F.T. coefficient can be assumed to be the peak of the main lobe due to the fundamental. Thus the power in the fundamental is:

$$P_1 = \frac{2}{N^2} \sum_{k=-c}^{c} \left| E_{af}[k_{\max} + k] \right|^2 \qquad (A.30)$$

The total power in the signal is:

$$P_T = \frac{2}{N^2} \sum_{k=0}^{N/2-1} \left| E_{af}[k] \right|^2 \qquad (A.31)$$

and the distortion power is the difference of P_T and P_1, so the distortion factor is:

$$D.F. = 100 \left(\frac{P_T - P_1}{P_1} \right)^{0.5} \% \qquad (A.32)$$

or:

$$D.F. = 100 \left(\frac{\sum_{k=0}^{N/2-1} \left| E_{af}[k] \right|^2 + \sum_{m=-c}^{c} \left| E_{af}[k_{\max} + m] \right|^2}{\sum_{m=-c}^{c} \left| E_{af}[k_{\max} + m] \right|^2} \right)^{0.5} \% \qquad (A.33)$$

A.3 Implementation of D.F.T. distortion analysis

The range of fundamental audio frequencies of interest is the communications bandwidth *300Hz* to *3400Hz* so a sampling frequency of *50kHz* can be used and still include all harmonics of these frequencies to *25kHz* before aliasing occurs. However, in the application of interest, the audio output of an F.M. receiver will be subject to post-demodulation lowpass filtering and no harmonics will be present in the ideal receiver output beyond the cut-off of this filtering. This effect can be incorporated into the calculation by truncating the summation of total output signal power to the discrete frequencies representing the range, say *0* to *3500Hz*, i.e.:

$$D.F. = 100\left(\frac{\sum_{k=0}^{K}\left|E_{af}[k]\right|^2 + \sum_{m=-c}^{c}\left|E_{af}[k_{\max}+m]\right|^2}{\sum_{m=-c}^{c}\left|E_{af}[k_{\max}+m]\right|^2}\right)^{0.5} \%$$ *(A.34)*

where K is the nearest discrete frequency corresponding to *3500Hz*. The D.F.T. is implemented in its fast form: the F.F.T. and so the discrete frequency k^{th} is:

$$f_k = \frac{kf_s}{N}$$ *(A.35)*

where N is the total number of points and f_s the sampling frequency, so:

$$K = \text{int}\left[\frac{3500N}{50000}\right]$$ *(A.36)*

Since the number of points in the time record of the signal $e_{af}[n]$ sets the frequency resolution of the F.F.T., it must be chosen in order to ensure that there is sufficient separation between the main lobes of the harmonics of low frequency fundamentals otherwise overlap will cause errors in the result. The width of the main lobe ($2c$ points) is thus required and is dependent on the window. The window used is a four-term raised-cosine window [1] of the form:

$$w[n] = \sum_{k=0}^{3} w_k \cos(2\pi kn/N) \qquad (A.37)$$

where:

$$w_0 = 0.3635819 \;\; w_1 = -0.4891775 \;\; w_2 = 0.1365995 \;\; w_3 = -0.0106411 \qquad (A.38)$$

The spectrum of this window is shown in figure A.1.

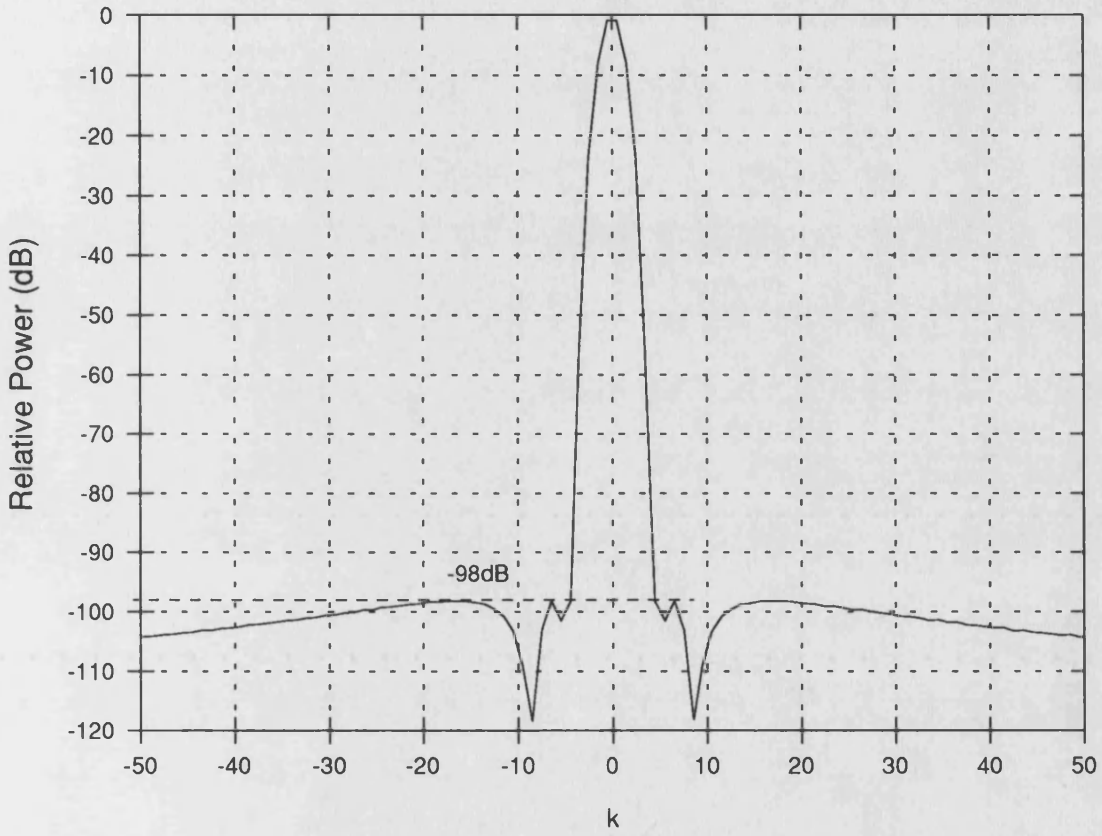

Figure A.1: *D.F.T. of the four-term window used in distortion analysis*

Suppression of leakage components by the window described is such that the highest sidelobe is *-98dB* relative to the main lobe reducing the effect of leakage on the result to a minimum. The main lobe extends over around *6* points either side of the peak which corresponds to a lobe width of *70Hz* at *50kHz* sampling and an *8192* point transform. This gives adaquate spacing between harmonics

for a minimum modulating frequency of *300Hz*.

A.4 References

1. Nutall A. H., "*Some Windows with Very Good Sidelobe Behaviour*" I.E.E.E. Transactions on Acoustics, Speech and Signal Processing, Vol. ASSP-29 No.1 February 1981 pp. 84-91.

Appendix B:
CIRCUIT DIAGRAMS

List of drawings Page

Audio preprocessing *B.2*
Analogue to digital conversion *B.3*
Precise Phase Modulator *B.4*
I.F. filtering for 25kHz channel spacing *B.5*
Frequency synthesizer *B.6*
I.F. L.O. multiplier strip *B.7*
V.C.X.O. P.L.L. *B.8*
R.F. L.O. multiplier strip *B.9*
R.F. amplification and filtering *B.10*

[B.2]

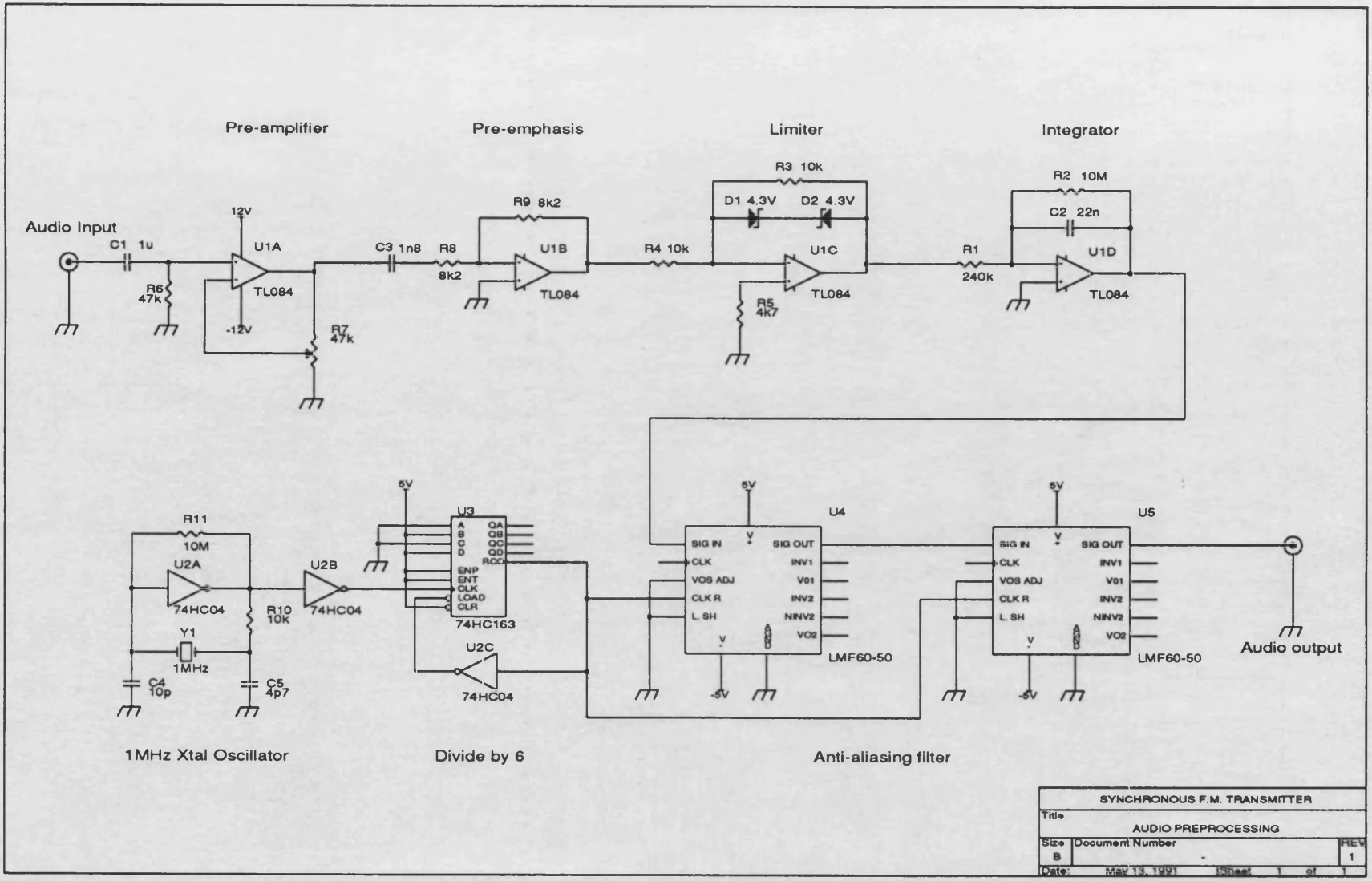
Pre-amplifier
Pre-emphasis
Limiter
Integrator
Audio Input
C1 1u
12V
U1A
TL084
-12V
R6 47k
R7 47k
C3 1n8
R8 8k2
R9 8k2
U1B
TL084
R4 10k
R3 10k
D1 4.3V
D2 4.3V
U1C
TL084
R5 4k7
R1 240k
R2 10M
C2 22n
U1D
TL084
5V
U3
74HC163
R11 10M
U2A
74HC04
R10 10k
U2B
74HC04
Y1 1MHz
C4 10p
C5 4p7
U2C
74HC04
U4
SIG IN
CLK
VOS ADJ
CLK R
L. SH
SIG OUT
INV1
V01
INV2
NINV2
VO2
LMF60-50
-5V
U5
LMF60-50
Audio output
1MHz Xtal Oscillator
Divide by 6
Anti-aliasing filter
SYNCHRONOUS F.M. TRANSMITTER
Title
AUDIO PREPROCESSING
Size B
Document Number
REV 1
Date: May 13, 1991
Sheet 1 of 1

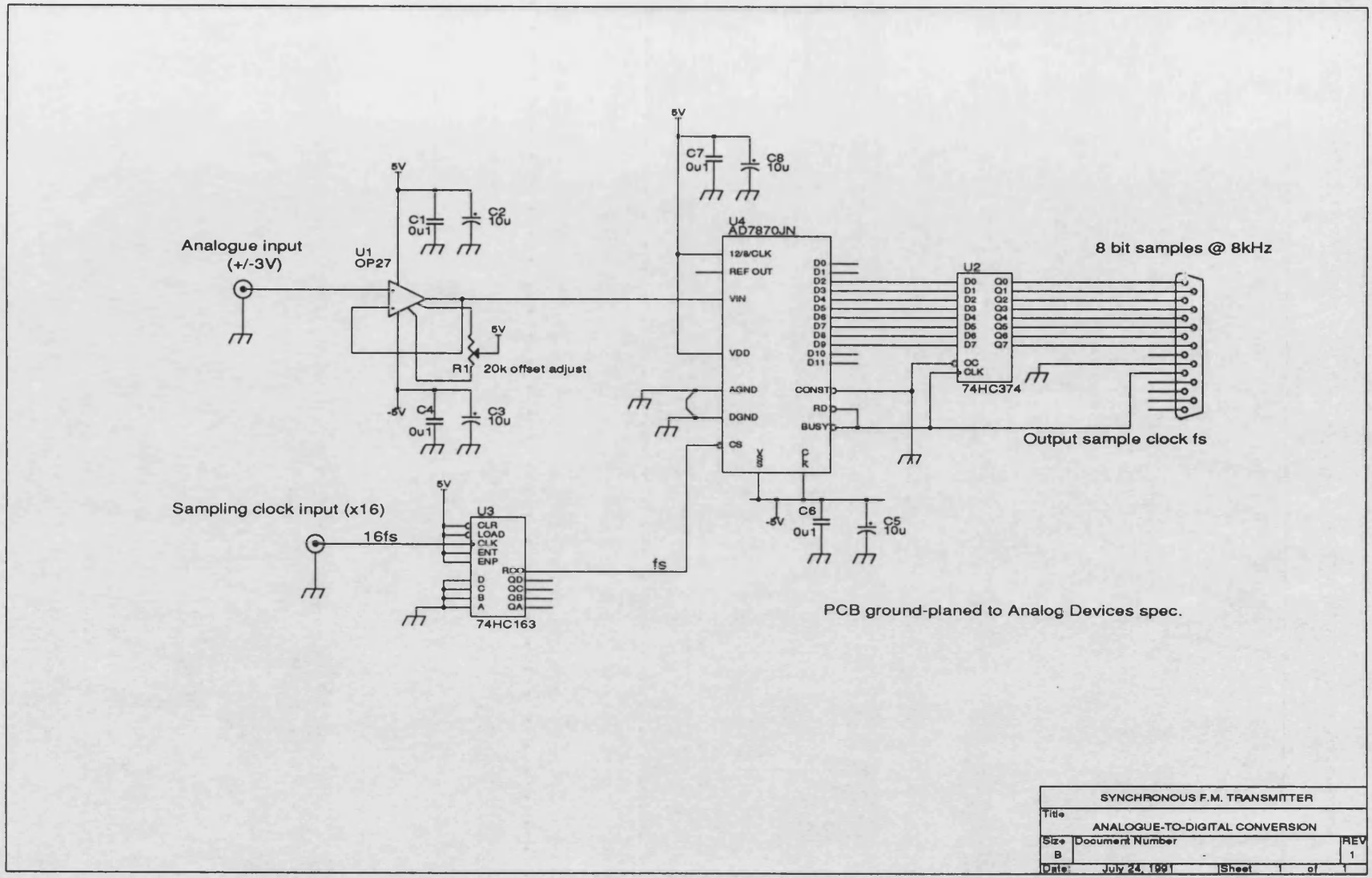
Analogue input
(+/-3V)
U1
OP27
5V
C1
0u1
C2
10u
-5V
C4
0u1
C3
10u
R1
20k offset adjust
U4
AD7870JN
12/8/CLK
REF OUT
VIN
VDD
AGND
DGND
CS
D0
D1
D2
D3
D4
D5
D6
D7
D8
D9
D10
D11
CONST
RD
BUSY
C7
0u1
C8
10u
C6
0u1
C5
10u
U2
74HC374
OC
CLK
8 bit samples @ 8kHz
Output sample clock fs
Sampling clock input (x16)
16fs
U3
CLR
LOAD
CLK
ENT
ENP
RCO
D
C
B
A
QD
QC
QB
QA
74HC163
fs
PCB ground-planed to Analog Devices spec.
SYNCHRONOUS F.M. TRANSMITTER
Title
ANALOGUE-TO-DIGITAL CONVERSION
Size
B
Document Number
REV
1
Date:
July 24, 1991
Sheet
1
of
1

[B.4]

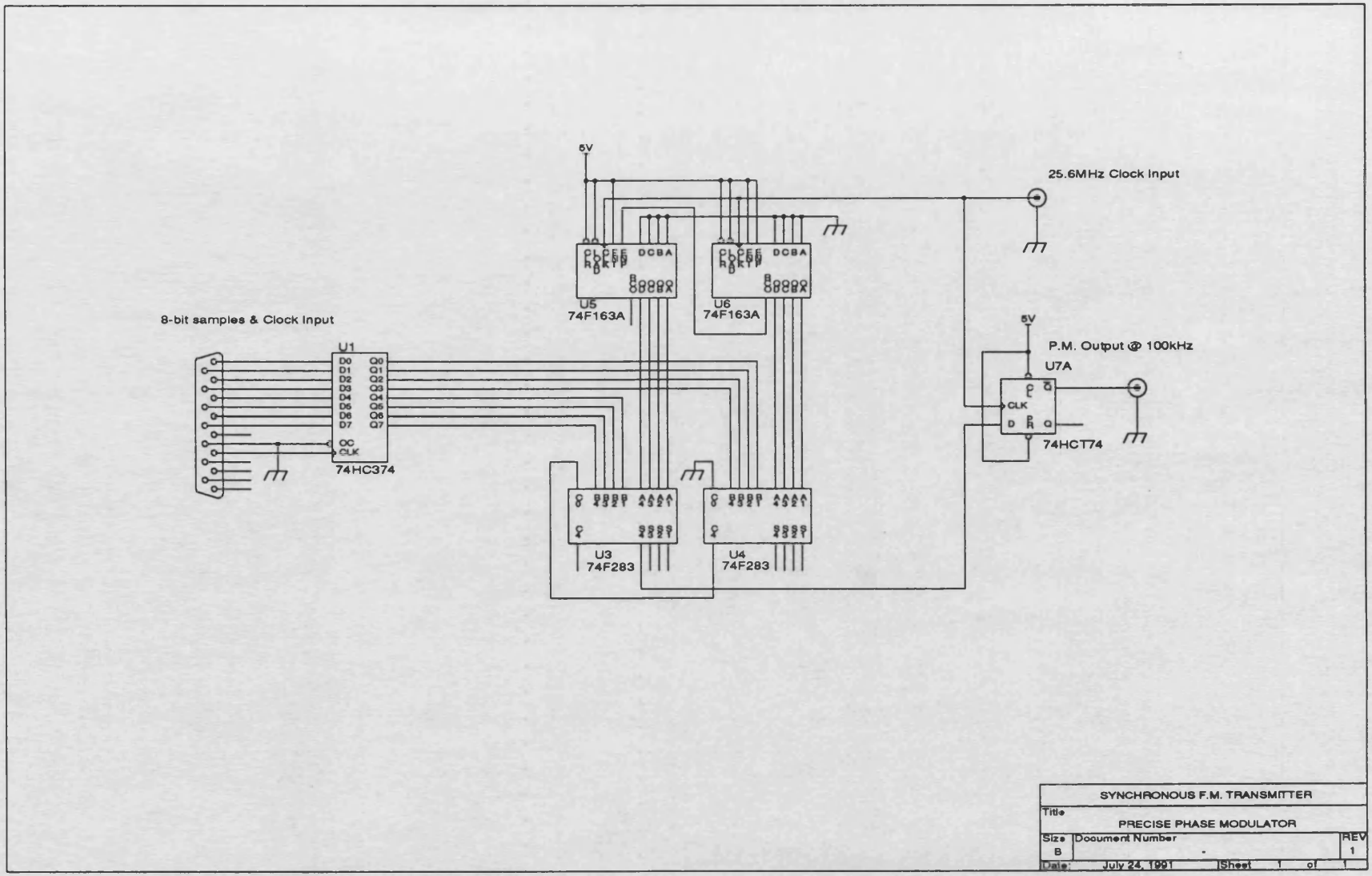
5V
25.6MHz Clock Input
8-bit samples & Clock Input
U1
74HC374
U5
74F163A
U6
74F163A
U3
74F283
U4
74F283
5V
P.M. Output @ 100kHz
U7A
74HCT74
SYNCHRONOUS F.M. TRANSMITTER
PRECISE PHASE MODULATOR
Size B
Document Number
REV 1
Date: July 24, 1991
Sheet 1 of 1

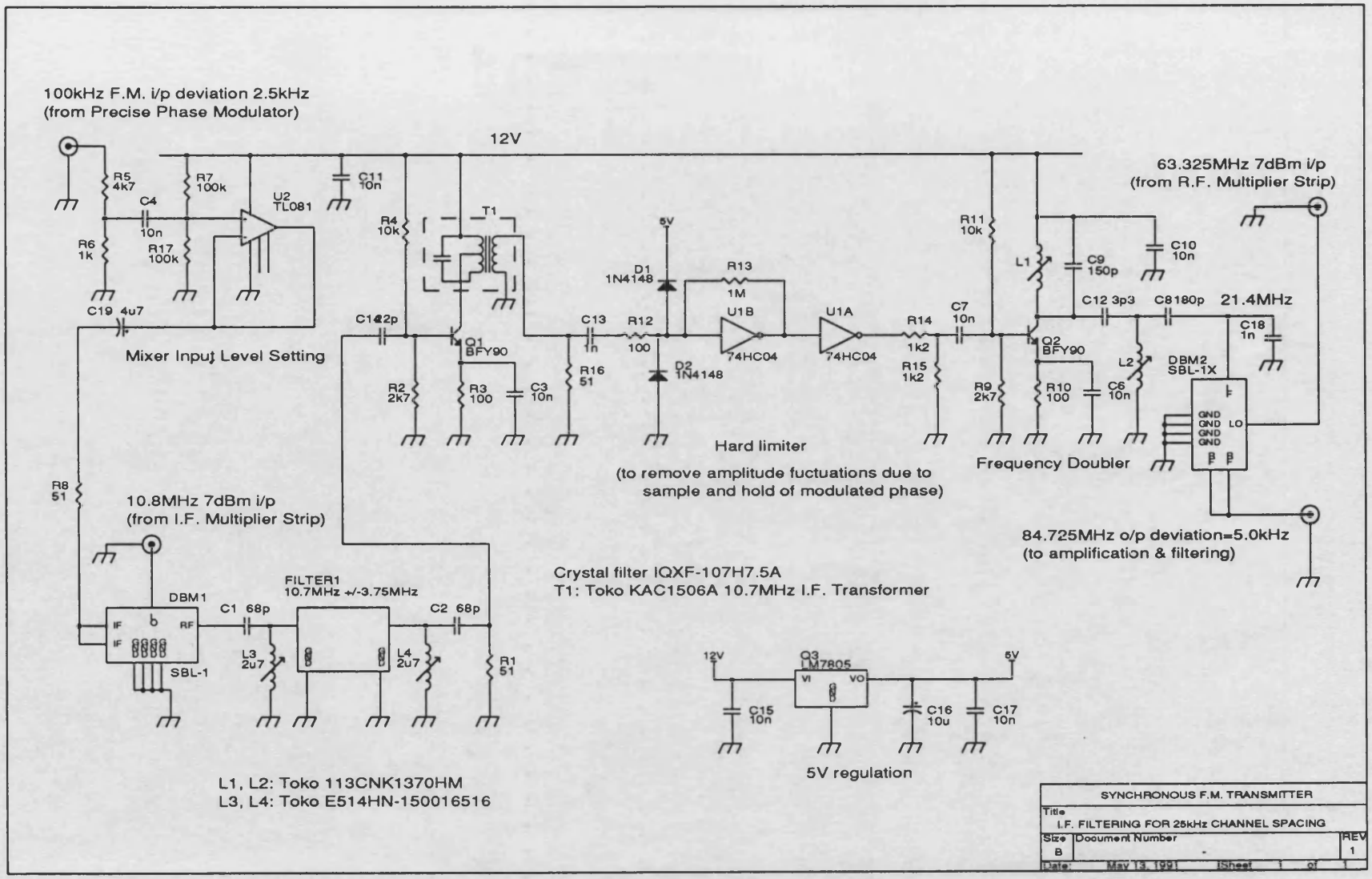
100kHz F.M. i/p deviation 2.5kHz
(from Precise Phase Modulator)
12V
63.325MHz 7dBm i/p
(from R.F. Multiplier Strip)
R5 4k7
R7 100k
C4 10n
U2 TL081
C11 10n
R6 1k
R17 100k
C19 4u7
Mixer Input Level Setting
R4 10k
T1
C14 22p
Q1 BFY90
R2 2k7
R3 100
C3 10n
C13 1n
R16 51
5V
D1 1N4148
R13 1M
R12 100
U1B 74HC04
D2 1N4148
U1A 74HC04
R14 1k2
R15 1k2
C7 10n
R11 10k
R9 2k7
Q2 BFY90
R10 100
C6 10n
L1
C9 150p
C10 10n
C12 3p3
C8 180p
21.4MHz
C18 1n
L2
DBM2 SBL-1X
GND GND GND GND LO
Hard limiter
(to remove amplitude fuctuations due to
sample and hold of modulated phase)
Frequency Doubler
84.725MHz o/p deviation=5.0kHz
(to amplification & filtering)
R8 51
10.8MHz 7dBm i/p
(from I.F. Multiplier Strip)
DBM1
IF RF IF
SBL-1
FILTER1
10.7MHz +/-3.75MHz
C1 68p
C2 68p
L3 2u7
L4 2u7
R1 51
Crystal filter IQXF-107H7.5A
T1: Toko KAC1506A 10.7MHz I.F. Transformer
12V
Q3 LM7805
VI VO
5V
C15 10n
C16 10u
C17 10n
5V regulation
L1, L2: Toko 113CNK1370HM
L3, L4: Toko E514HN-150016516
SYNCHRONOUS F.M. TRANSMITTER
Title
I.F. FILTERING FOR 25kHz CHANNEL SPACING
Size B
Document Number
REV 1
Date: May 13, 1991
Sheet 1 of 1

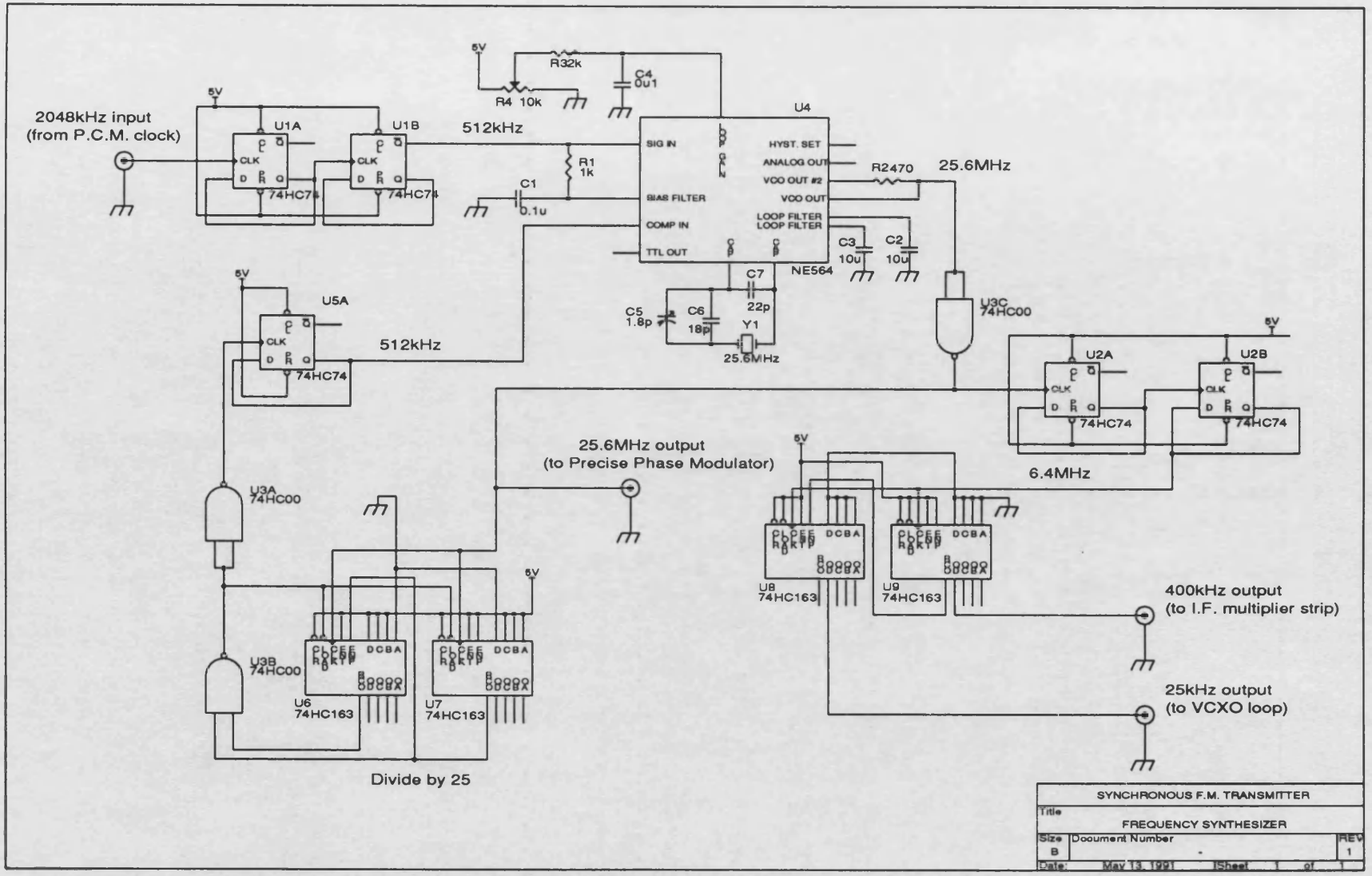
2048kHz input
(from P.C.M. clock)
5V
U1A
U1B
74HC74
512kHz
R32k
R4 10k
C4
0u1
U4
SIG IN
BIAS FILTER
COMP IN
TTL OUT
HYST. SET
ANALOG OUT
VCO OUT #2
VCO OUT
LOOP FILTER
LOOP FILTER
NE564
R1
1k
C1
0.1u
R2470
25.6MHz
C3
10u
C2
10u
C7
22p
C5
1.8p
C6
18p
Y1
25.6MHz
U5A
512kHz
U3C
74HC00
U2A
U2B
74HC74
6.4MHz
25.6MHz output
(to Precise Phase Modulator)
U3A
74HC00
U3B
74HC00
U6
74HC163
U7
74HC163
U8
74HC163
U9
74HC163
400kHz output
(to I.F. multiplier strip)
25kHz output
(to VCXO loop)
Divide by 25
SYNCHRONOUS F.M. TRANSMITTER
Title
FREQUENCY SYNTHESIZER
Size
B
Document Number
REV
1
Date: May 13, 1991
Sheet 1 of 1

[B.7]

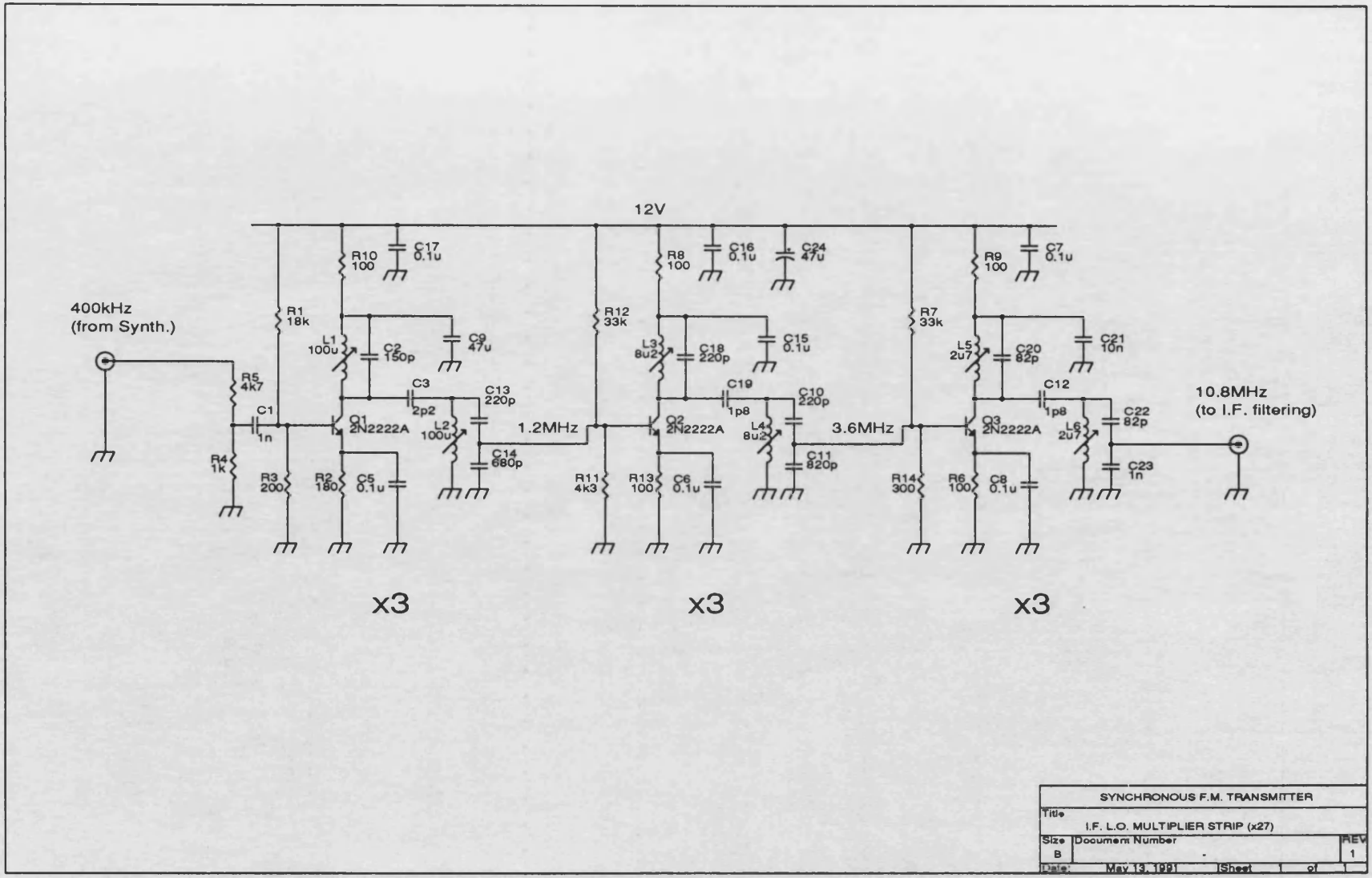
12V
400kHz
(from Synth.)
R1 18k
R10 100
C17 0.1u
L1 100u
C2 150p
C9 47u
R5 4k7
C1 1n
C3 2p2
C13 220p
Q1 2N2222A
L2 100u
C14 680p
R4 1k
R3 200
R2 180
C5 0.1u
1.2MHz
R12 33k
R8 100
C16 0.1u
C24 47u
L3 8u2
C18 220p
C15 0.1u
C19 1p8
C10 220p
Q2 2N2222A
L4 8u2
C11 820p
R11 4k3
R13 100
C6 0.1u
3.6MHz
R7 33k
R9 100
C7 0.1u
L5 2u7
C20 82p
C21 10n
C12 1p8
Q3 2N2222A
L6 2u7
C22 82p
C23 1n
R14 300
R6 100
C8 0.1u
10.8MHz
(to I.F. filtering)
x3
x3
x3
SYNCHRONOUS F.M. TRANSMITTER
Title
I.F. L.O. MULTIPLIER STRIP (x27)
Size B
Document Number
REV 1
Date: May 13, 1991
Sheet 1 of

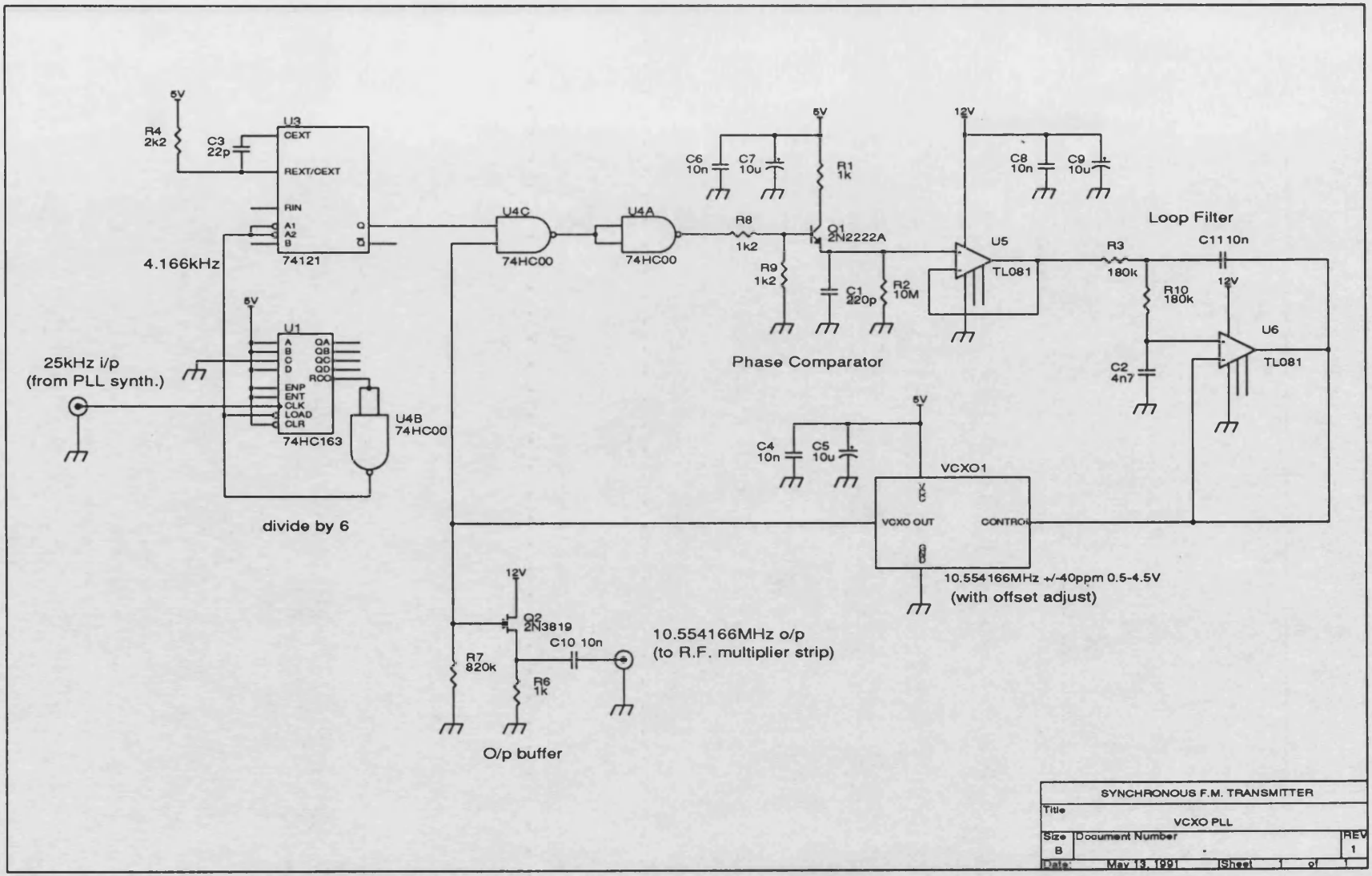
5V
R4
2k2
C3
22p
U3
CEXT
REXT/CEXT
RIN
A1
A2
B
Q
74121
4.166kHz
U4C
74HC00
U4A
74HC00
C6
10n
C7
10u
R1
1k
R8
1k2
Q1
2N2222A
R9
1k2
C1
220p
R2
10M
Phase Comparator
12V
C8
10n
C9
10u
U5
TL081
Loop Filter
R3
180k
C11 10n
R10
180k
U6
TL081
C2
4n7
25kHz i/p
(from PLL synth.)
U1
A
B
C
D
QA
QB
QC
QD
RCO
ENP
ENT
CLK
LOAD
CLR
74HC163
U4B
74HC00
divide by 6
C4
10n
C5
10u
VCXO1
VCC
VCXO OUT
CONTROL
GND
10.554166MHz +/-40ppm 0.5-4.5V
(with offset adjust)
Q2
2N3819
C10 10n
R7
820k
R6
1k
10.554166MHz o/p
(to R.F. multiplier strip)
O/p buffer
SYNCHRONOUS F.M. TRANSMITTER
Title
VCXO PLL
Size
B
Document Number
REV
1
Date:
May 13, 1991
Sheet
1
of
1

[B.8]

[B.9]

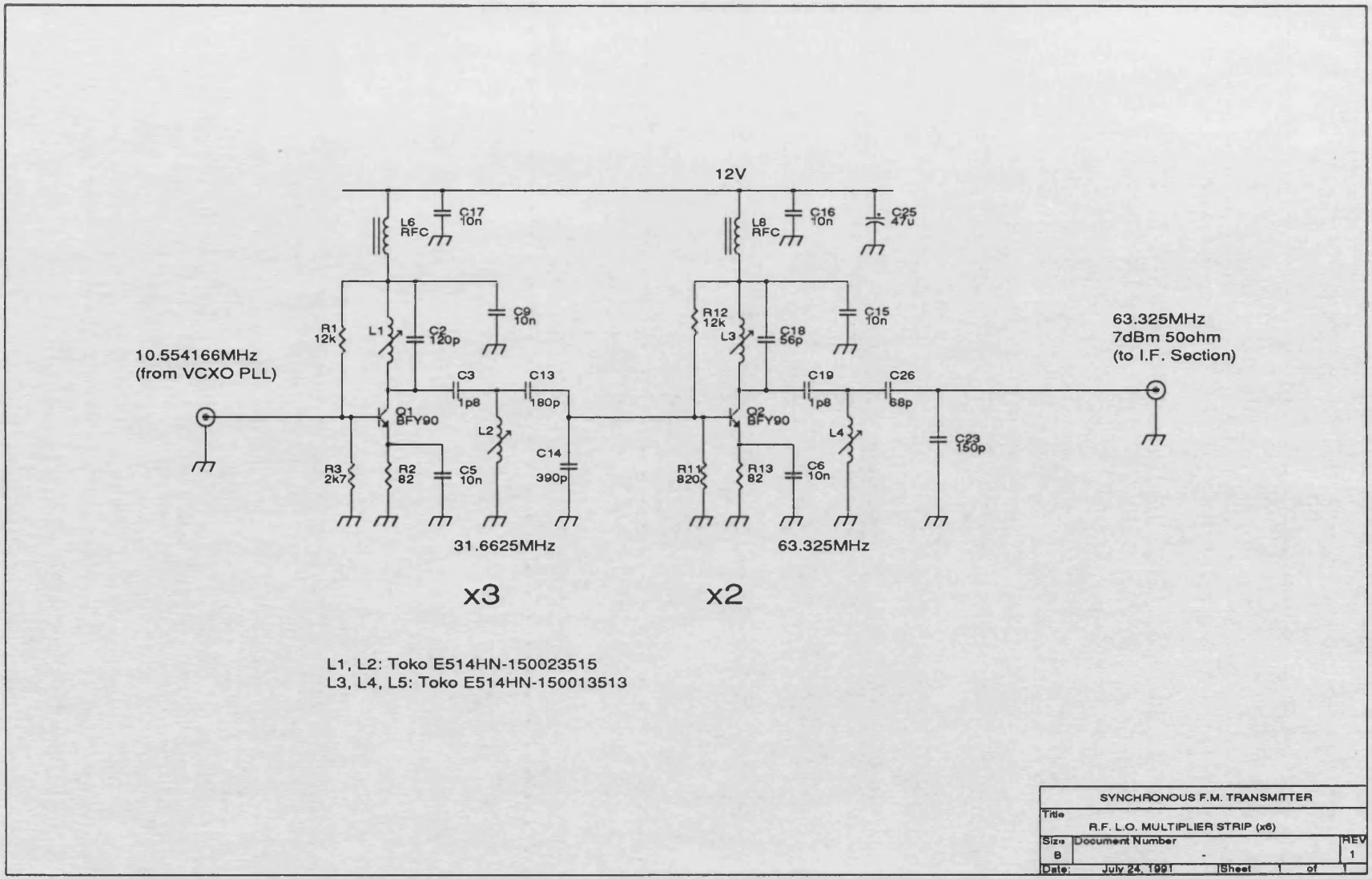
12V
L6 RFC
C17 10n
L8 RFC
C16 10n
C25 47u
R1 12k
L1
C2 120p
C9 10n
R12 12k
L3
C18 56p
C15 10n
10.554166MHz
(from VCXO PLL)
63.325MHz
7dBm 50ohm
(to I.F. Section)
C3 1p8
C13 180p
C19 1p8
C26 68p
Q1 BFY90
Q2 BFY90
L2
L4
C14 390p
C23 150p
R3 2k7
R2 82
C5 10n
R11 820
R13 82
C6 10n
31.6625MHz
63.325MHz
x3
x2
L1, L2: Toko E514HN-150023515
L3, L4, L5: Toko E514HN-150013513
SYNCHRONOUS F.M. TRANSMITTER
Title
R.F. L.O. MULTIPLIER STRIP (x6)
Size B
Document Number -
REV 1
Date: July 24, 1991
Sheet 1 of 1

[B.10]

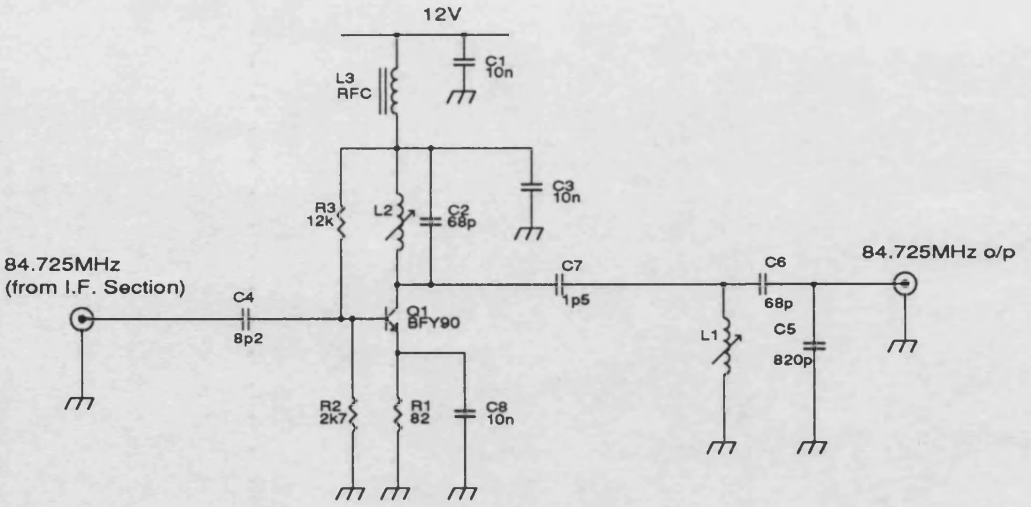

L1, L2: Toko E514HN-150025511

SYNCHRONOUS F.M. TRANSMITTER		
Title: R.F. AMPLIFICATION & FILTERING		
Size: B	Document Number: -	REV: 1
Date: July 24, 1991	Sheet 1 of 1	

Appendix C

The Bessel Function

The function is the Bessel function of the first kind, order n and argument β. Its generation and properties are described fully in [1]. It is shown below in figure C.1 for the first few values of integer n and arguments β up to 10 since in the situations examined in this thesis, these are the range of interest.

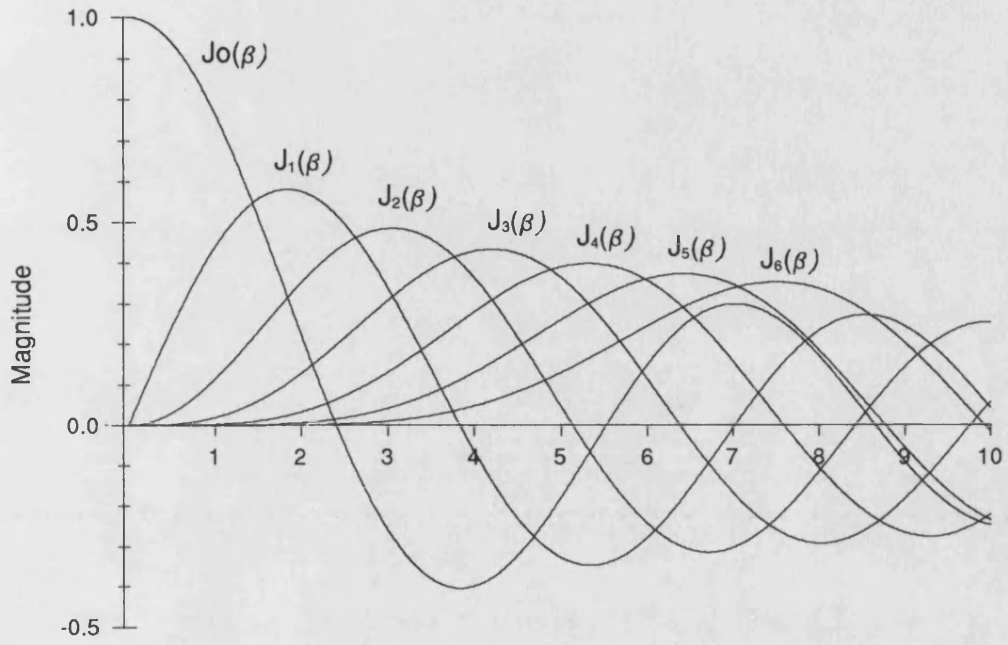

Figure C.1: *Synchronous F.M. area coverage scheme*

For modulator constant verification, the zeros, β_z of $J_n(\beta)$ for n = 0,1 are required. These are tabulated below.

	β_1	β_2	β_3
$J_o(\beta_z)=0$	2.405	5.520	8.654
$J_1(\beta_z)=0$	3.832	7.016	10.173

C.1 References

[1] Gradshteyn I.S., Ryzhik I.M., "*Tables of Integrals, Series and Products*" London: Academic Press, 1965 ISBN 0-12-294760-6.